CHANGES IN THE TURBULENT BOUNDARY LAYER STRUCTURE ASSOCIATED WITH NET DRAG REDUCTION BY OUTER LAYER MANIPULATORS

By

Nasser Rashidnia

A DISSERTATION

Submitted to
Michigan State University
in partial fulfillment of the requirements
for the degree of

DOCTOR OF PHILOSOPHY

Department of Mechanical Engineering

1985

ABSTRACT

CHANGES IN THE TURBULENT BOUNDARY LAYER STRUCTURE
ASSOCIATED WITH
NET DRAG REDUCTION BY OUTER LAYER MANIPULATORS

By

Nasser Rashidnia

A specially designed wind tunnel was used to examine the effects of tandemly-arranged parallel plate manipulators (TAPPMs) on turbulent boundary layer structure and the associated drag. Momentum balances and use of the velocity gradient near the wall were used to obtain the net drag and local skin friction changes. Measurements showed that local skin friction reductions were found from $20\delta_0$ to as far as $120\delta_0$.

Two sets of plates, identical except for thickness were used. Results with .003" plates produced a maximum net drag reduction of 10% at $58\delta_0$ using momentum balance. Downstream of this position the drag began to relax back to its unmanipulated level, and returned to normal by $100\delta_0$. The wall friction coefficient (obtained from mean velocity gradients near the wall referred to as the "C_{fn}") remained below normal. The net drag calculated from C_{fn}, taking the device drag into account, resulted in a 2% drag reduction at $120\delta_0$. The difference in the net drag results obtained from the two independent methods suggests difficulty detecting three-dimensional effects due to the wake of the TAPPM.

At $20\delta_0$, simultaneous laser sheet flow visualization and hot-wire anemometry were used to conditionally sample the u', v', and u'v' information of the large eddies in both manipulated, and normal boundary layers at $y/\delta = .4$ and .6. (The TAPPM was located at $y = .8\delta_0$). The Reynolds stress in the large eddies was significantly reduced at $20\delta_0$, but substantially recovered at $51\delta_0$. This was verified using spatially separated temporal correlations of u', v', and u'v' at the two locations.

The frequency of occurrence of the footprints of the bursting process was also measured using flow visualization from a sublayer slit. The mean frequency of occurrence of the "pockets" decreased when scaled with both outer and inner variables $u_{\tau n}$ (where $u_{\tau n}$ obtained from near wall mean velocity gradient was used), but increased when scaled with $u_{\tau\theta}$ (obtained from momentum balance).

The outward normal velocity of the inner region was significantly decreased at $20\delta_0$, while the thickness of the sublayer increased by 10-20% throughout the $130\delta_0$.

ACKNOWLEDGEMENTS

I would like to acknowledge the support of the NASA Langley Research Center (Contract NAG-1-302), grant monitor: Dr. D.M. Bushnell, and the support of AFOSR (Contract F49620-85-C-0002) for part of the last phase of the data acquisition of this experiment. I would also like to express gratitude to my advisor, R.E. Falco, for his advice and guidance throughout my graduate research studies. Many thanks is due to my committee members, in particular C.A. Petty and R.W. Bartholomew for their constructive comments and assistance. To Douglas Little for writing and modifying most of the computer programs and to Nancy Dawson for processing photos as well as their friendship, my deepest appreciation and thanks. The assistance of many students and technicians who contributed to the construction of the facility and many other areas of this project must not be forgotten. On a final note I would like to thank such colleagues as Mr. Kue Pan, C.C. Chu, and Marwan Zabdawi for their friendship and support.

Lastly, a special thanks to Jan Cilla-Rashidnia for all the moral support she provided. THANK YOU TO ALL.

TABLE OF CONTENTS

LIST OF FIGURES

LIST OF TABLES

LIST OF SYMBOLS

A	Coles (1968) "law of the wall" parameter = 5.61
B	Coles (1968) "law of the wall" constant = 5.0
C_{fa}	Skin friction coefficient = $\tau_w/(1/2\rho U^2\infty)$ where a=c ; τ_w is obtained from Clauser plot, a=n ; τ_w is obtained from $d\bar{U}/dy_w$, (Newtonian) a=θ ; τ_w is obtained from momentum balance
G	Equilibrium shape factor
h	Height of manipulator plates away from wall
H	Shape factor = δ_d/θ
k	Von Karman's constant = .41
l	Chord dimension of parallel plate manipulator
R_θ	Reynolds Number = $\rho U_\infty \theta/\mu$
s	Streamwise spacing between tandem manipulator plates
$R_{p'q'}$	Space-time correlation of functions p' and q' where p' is used as the reference function
TAPPM	Tandem arrayed parallel plate manipulator
T_B	Time period between wall burst events ("Pockets")
U	Streamwise velocity component = $\bar{U}$ + u'
u'	Fluctuating velocity component in the x direction
$\langle u' \rangle$	Ensemble averaged of u' in the large scale motions (LSM)
$\bar{U}$	Time-averaged mean of streamwise velocity component
U_∞	Time-averaged freestream velocity
u^+	$\bar{U}/u_\tau$
$u_{\tau a}$	Wall shear velocity = $(\tau_w/\rho)^{0.5}$ where a=c ; τ_w is obtained from Clauser plot, a=n ; τ_w is obtained from $d\bar{U}/dy_w$, (Newtonian, a=θ ; τ_w is obtained from momentum balance
u'v'	Fluctuating Reynolds shear stress
$\langle u'v' \rangle$	Ensemble average of u'v' in the large sale motions (LSM)
v'	Fluctuating velocity component in the y direction

$\langle v' \rangle$	Ensemble average of v' in the large scale motions (LSM)
x	Cartesian coordinate in streamwise direction; origin at leading edge of test plate
x_o	Downstream distance between leading edge of the test wall and turbulence manipulator
y	Cartesian coordinate taken normal to test wall (flat plate); origin at wall surface
y^+	$\rho u_\tau y/\mu$
z	Lateral cartesian coordinate taken parallel to flat plate; origin along test wall centerline
δ	Boundary layer thickness = y value where $\bar{U}$ equals 0.99 U_∞
δ_d	Displacement thickness = $\int_0^\delta \left[1 - \bar{U}/U_\infty\right] dy$
δ_o	Boundary layer thickness at the leading edge of upstream plate of the TAPPM
θ	Momentum thickness = $\int_0^\delta \bar{U}/U_\infty\left[1 - \bar{U}/U_\infty\right] dy$
Δ	Energy thickness = $\int_0^\delta \bar{U}/U_\infty\left[1 - (\bar{U}/U_\infty)^2\right] dy$
ξ	Distance downstream of manipulator where measurements were taken = $(x - x_o)/\delta_o$
π	Wake strength coefficient
ρ	Fluid density
τ	Non-dimensionalized time delay in temporal correlation calculations = $(t-t_o)U_\infty/\delta$
τ_w	Wall shear stress
μ	Dynamic viscosity

CHAPTER 1

INTRODUCTION

During the past twenty-five years, it has been known that fully-developed turbulent flows contain groups of coherent flow patterns and eddies imbedded essentially random fluctuations. The strength of these organized motions is large compared to that of the "random" fluctuations, but is still difficult to detect because of their unsteadiness and three-dimensional nature. Studies of the inherent eddy structures of two-dimensional boundary layer flows and the manner in which they react to distortions have been conducted under the direction of Dr. R. E. Falco at Michigan State University. These studies have identified two main types and scales of motions: the typical ("Falco") eddy, (on the order of 100 wall units) which appears throughout the layer, and the large-scale motion (LSM) eddy inclined at 33° on their upstream boundary (Falco, 1977) to the flow direction. The main differences between those motions seem to be scale, strength, and degree of organization. However, there is a high degree of order in the boundary layer structures. The interaction among these scales has been examined (Falco, 1983). Whatever the connection among these scales may be, they contain a large fraction of the turbulence energy, and thus are of interest to researchers.

Over the past two decades, interest has been growing in the manipulation of particular turbulent structures for technological

applications. These applications include turbulent drag reduction, separation delay, and reduction of noise and vibration (Bushnell, 1983). Moreover, the shortage of energy resources, and petroleum resources in particular. has increaswd efforts to improve the efficiency of transportation systems, among them aircraft. Thus research toward the development of techniques for reducing viscous drag on aerodynamic bodies has become more and more crucial. To illustrate the magnitude of the drag problem: "Typical values of skin friction drag range from 25% of the total drag for supersonic fighters to 50% for long-haul transports and 54% for general aviation executive jets." (Hefner et al.. 1979).

It has been shown that turbulence can be controlled through the manipulation of the large-scale structures. One method being used today to manipulate the production of turbulence of the turbulent boundary layer employes a pair of thin flat ribbons, or airfoil devices, placed in tandem in the outer layer. Net drag reductions of 7% and higher in smooth flat plate turbulent boundary layers have been reported. The Illinois Institute of Technology studies reports the highest net drag reductions, ranging from 10-28% with very slow relaxation (Plezniak and Nagib, 1985). Other studies have reported local skin friction reductions for about $55\delta_0$, but the 20-25% net reduction is far from being verified yet.

Most of the investigations have used only one method to measure the skin friction drag _ either indirect measurements from momentum balance, (e.g., IIT group since 1978, Anders, 1984 and 1985), or direct measurement using skin friction balance. The results generated by these

independent techniques have not to date been compared. In addition to skin friction balance measurements, Lemay et al. (1985) used a Preston tube to measure skin friction. However, the universality of the "law of the wall" might not hold in the manipulated turbulent boundary layers. Details of the turbulence structure changes due to the presence of the manipulators have not been reported yet. They did, however, show similar local wall-friction reduction and evolution in the manipulated boundary layers.

A number of recent investigations have made direct skin friction measurements. (Hefner et al., 1983; Westphal, 1986, Lynn and Screenivasan, 1985, Lemay et al., 1985, and Mumford and Savill, 1984) In visual studies using smoke-wires, it is difficult to see detailed motions in the eddy structures of flow and manner altered by the plates. Thus, flow visualization has been limited to a few studies. Still many speculations have been made without a proper visualization of the manipulated layers. It was seen as necessary add to the rsearch on skin friction drag by combining direct (mean velocity gradient near the wall) and indirect measurement (monentum balance). In addition to independent experiments (visualization and/or velocity measurements), simultaneous flow visualization and hot-wire anemometry for the study of structural changes due to the TAPPM was needed.

The present research was based on recent and ongoing developments in drag reduction techniques, and the manipulation of outer layer in the turbulent boundary layers (IIT, 1979 and NASA, 1979, in particular). In order to verify the net skin drag reduction obtained by Corke (1981), a high quality wind tunnel was designed and constructed. The tunnel has

17 m test section, and a unique no contraction inlet with a low turbulence intensity level of about .2% at the nominal speed of U_∞=3 mps. The tunnel's top wall is diverged to produce a near zero axial pressure gradient over the test wall. Using a pair of 0.003" thickness manipulator plates, a 10% net drag reduction up to 60 boundary layers downstream of the manipulators, as measured by momentum balance, was achieved. Using local C_{fn} measurements, the net drag decreased by 2% at $120\delta_o$. Several different flow visualization techniques were employed to observe the large eddy "breakup", and/or "supression" which has been claimed by both the NASA research team (since 1978) and the IIT group (since 1979). To date, however, the "breakup" of the structures has not been verified. The effect of tandemly-arranged parallel plate manipulators (TAPPMs) on outer layer structure of turbulent boundary layers was also explored. The goal of this research was to find answers to questions regarding mechanisms responsible for drag reduction and for changes in the turbulent boundary layer structure. Hot-wire anemometry and flow visualization techniques were employed both independently and simultaneously in this research. The simultaneous measurement technique was developed at the Turbulent Structure Laboratory at Michigan State University and has been used successfully there since 1977. The details of this method have been also explained by Lovett (1982). A modified side view visualization, similar to the experimental setup used by Signor (1982) was used in the last combined data acquisition part of the experiment. The present research made use of a twin-x-wire array probe. The x-array hot-wire sensors were mounted at $y = .6\delta_{local}$ (top x-wire No. 1), and $.4\delta_{local}$ (bottom x-wire No. 2) the highest $C_{f\theta}$ reduction

station and $20\delta_0$ downstream of the manipulator station. This made possible a detailed study of the net drag variations and the associated turbulence structure changes in the boundary layers. Changes in vertical and streamwise directions, along with the Reynolds stress of the large scale motions due to the TAPPM, were investigated. In addition, space-time correlations of fluctuating components, using the top x-array signals as reference (u'_1, v'_1, and $(u'v')_1$) at two stations were performed (ξ = 20 and ξ =51). Due to the importance of the wall turbulence on the skin drag, sublayer turbulent events were also investigated via visualization. On the basis of the above results of these investigarions, explanations of mechanisms possibly responsible for skin drag changes in manipulated turbulent boundary layers are offered.

CHAPTER 2

DESCRIPTION OF EXPERIMENTAL FACILITIES AND TECHNIQUES

2.1 Facilities

This chapter presents a discussion of the experimental apparatus used during during the various data collection stages and of the data reduction and analysis techniques employed.

2.1.1 Wind Tunnel

Preliminary studies in the low-speed boundary layer wind tunnel were performed at the Turbulence Structure Laboratory (TSL) at Michigan State University. These studies led to the design and construction of improved low turbulence intensity flow visualization wind tunnel, with a test section 56' long by 4' wide and nominally 2' high. This test section length allowes detailed flow studies using both probes and flow visualization to be made over a long enough distance to measure the relaxation effects of the devices. The top and one side wall are made of 3/8" plexiglass to allow visualization from both directions. The top wall is adjustable to produce different pressure gradients if necessary. For the present experiment, the top wall was diverged to produce the lowest pressure gradient possible. The divergence is 0.25 degree. The bottom and the second side wall are made from 3/4" thick plywood. These walls are sanded so that they are hydraulically smooth and painted black for background flow visualization purposes. The tunnel is of the

open-circuit suction type. It is positioned in the center of a 60' x 100' x 20' laboratory area, which acts as the return circuit for high-quality probe measurements. The suction is provided by a high-quality low-noise axial fan (Chicago Blower Corporation, 44½" diameter, W9, Class 1, 8.51 BHP, with a 10 HP, 1200 RPM TEFC 3/60/230-460, T-FRAME electric motor). The speed is kept constant using an Eaton Model 4000 eddy current speed controller. The fan is located between the exhaust section (8' long diffuser shape, which is connected with flexible joints to the end of the test section), and the final exchangeable radial diffuser. The abovementioned flexible joint reduces transmission of any possible vibrations from the fan assembly to the test section. For flow visualization experiments, the radial diffuser can be exchanged with an axial exhaust section when smoke flow visualization is performed. In this manner the wind tunnel exhausts into a last exit section that ultimately empties outside into the atmosphere, allowing the continuous flow of the smoke visualization marker (for further details of this technique see R.E Falco, 1980). This last exit section consists of a wind-baffled passage which was built outside the laboratory. It contains a 1/2" x 6" Hex-cell honeycomb, followed by a fine grid screen attached to one end of the exit section. This combination of honeycomb and screen in the exit section reduces the possible effects of atmospheric wind pressure variations on the flow in the test section. The tunnel is joined by means of bolts, nuts, washers, and BUNA-N rubber seals. This was done for ease of future extension or modification of the wind tunnel. The lower wall of the tunnel was used as the test plate. It was braced with

2" x 94" extra angle irons from the exterior of the tunnel, with spanwise bracing of 2 inch angle irons for every 4 feet of lengthwise direction to enable accurate adjustment and leveling of the test wall. This wall is carefully adjusted horizontally to a flatness within 0.001 inch per foot in both streamwise and spanwise directions. Figure 2.1 is a schematic of the wind tunnel.

2.1.2 Measurement Stations, Probe Support, Traverse Mechanism, and Positioning Instrument (Cathetometer)

Since the test wall was relatively long (56 feet), the test section downstream of the manipulators was divided into 10 stations. The distance between stations was non-uniform. The non-uniform spacing was based on results obtained through velocity measurement and flow visualization. After obtaining a large variation in boundary layer parameters from one measurement station to the next in a preliminary spacing, it was decided to further investigate the boundary layer parameters between the previously tested stations. The final positions between test stations represent the minimum number thought necessary to obtain accurate drag measurements. The distances of these stations from the leading edge of the test plate are shown in Figure 2.2. The boundary layer grew to approximately 10 inches at the last test station on the test wall. This thick boundary layer allowed hot-wire measurements as close as one wall unit ($y^+ = 1$). To this end, a two-stage traverse mechanism was designed. The traverse gear would only move the probe in y-direction. The first stage (one inch travel with 0.001 inch advance at a time if needed) was provided by a digital

micrometer with ±0.0001 inch accuracy. After the first inch travel of the probe away from the wall, the second stage of the traverse was provided by a larger traverse mechanism with 12 inch travel capacity and lower resolution. At this stage, the first micrometer was locked and the probe was moved higher by the second part of the mechanism up the center line of the tunnel into the freestream. All y (normal to the test plate) movements of the probe were done manually. In order to keep the direction of probe travel perpendicular to the test wall and uniform for all the stations, a liquid level was mounted onto the moving part of the traverse mechanism body and adjusted for each station. The traversing mechanism was mounted and rigidly fixed to 9" x 8"x 3/8" aluminum plates attached to the outside part of the test wall (floor of the wind tunnel) for each test station. The support of the probe was a 3/8"-diameter, 18"-long aluminium pipe. The pipe passed through a 3/8"-diameter hole in the test wall, and its lower end was fixed to the moving part of the mechanism. When a station was not in use, the holes were carefully plugged and sealed without leaving any unnecessary roughness on the test wall. The probe sensing part was always positioned 10 inches upstream of the supporting rod, in order to avoid any possible interference with the flow field under measurement.

A measurement of the closest position of the sensor to the test wall was carefully made using a short-range telescope (cathetometer). This instrument was used to find a reference point to compare the readings from the traverse mechanism and to obtain the actual distance of the probe from the wall. The cathetometer is capable of measuring the vertical distance within 0.01 mm with an error of ±0.001 mm. The

probe could thus be positioned, for all the stations of the test wall, as close as $y^+ = 1$ above the test wall surface. In addition, velocities in the sublayer portion of the turbulent boundary layer under survey could be measured.

2.1.3 Tunnel Inlet

In order to achieve high quality (two-dimensional), low turbulence intensity flow and to avoid Taylor-Görtler vortices on the test wall, it was decided not to use the traditional contraction for the inlet of the tunnel. Based on the low-velocity experiments proposed for this research, a high precision 4 mm Hex-cell honeycomb (Figures 2.3 and 2.4) along with a series of fine mesh aluminum screens sandwiched in one box with the same section area as the inlet of the test section (contraction area ratio 1:1) was constructed. A series of iterations with the distance and number of screen arrangements were made, and smoke-wire flow visualizations were conducted. This was followed by turbulence intensity measurements at varios downstream stations. The final configuration of the inlet was obtained after a period of 6 months. The tunnel inlet adjustments were based on the work of Loehrke and Nagib (1977), and of de Bray (1967). A range of turbulence intensities (0.15-0.25%) for velocities 5-20 fps were obtained. The final inlet configuration is shown in Figure 2.5. The turbulence intensity level at the nominal test velocity (3 m/sec.) at several stations is shown in Figure 2.6. As evident in this figure, the turbulence intensity is low and acceptable by the standards of other researchers in the field. Using this simple inlet configuration a large amount of space and design

and construction effort was saved. Other advantages of this unique inlet are avoiding possible Taylor-Görtler vortices (Smith, 1955, Schlichting, 1979), which are generated on the convex/concave curved surfaces of any contraction unit in traditional wind tunnels, and keeping the floor of the tunnel as the test wall, which reduces the effort of adding new parts and supports which would otherwise be excessive for a tunnel of this length. It also reduces the chance of new secondary flows due to the side or leading edge effects of a suspended test plate.

Two different screen arrangements were used for the experiments. First, a pack of 44 screens almost touching one another followed a precision hex-cell honeycomb with 3/16" cells that were 3" long (CYNAMID, BLOMINGDALE DEPARTMENT, HAVRE DE GRACE,MD.). Figure 2.3 shows the honeycomb and the carefully cut ends. This honeycomb was followed by a single screen of mesh size 0.04", 0.01" wire diameter placed immediately downstream (only for the second inlet configuration.) The second inlet configuration, which was used for the final experiments, is also a combination of 6 screens of the same quality used in the original inlet arrangement, but with different spacings between screens. This set of screens is followed by a honeycomb of the same precision with another screen placed downstream of it (Figure 2.5). Also note that this combination of screen-honeycomb-screen box is made modifiable in order to be able to either increase or decrease the number of screens for different turbulence intensity levels of the tunnel flow. The results of boundary layer flow measurements discussed below further confirm the excellent quality of this inlet design.

2.1.4 Exit Diffusers

Two different exit diffusers were employed at the end behind the tunnel fan; axial and radial diffusers. The axial diffuser was also used to discharge the smoke of filled air resulting from flow visualization into the atmosphere outside the laboratory building. The radial diffuser was used when highest quality probe measurements were required and flow visualization was not being performed. Each diffuser was mounted on a supporting structure with four rollers. This roller arrangement provided the convenience of exchanging the two diffusers with minimal effort. The radial diffuser, which had been tested on the Lagrangian Wind Tunnel (LWT) in Turbulece Structure Laboratory, has an area ratio of 2:1 (exit to inlet area). The axial diffuser also has a 2:1 area ratio (Figure 2.1).

2.2 Experimental Apparatus

Several different techniques and instrumentation units, and probes were utilized, during the experiments. They are described below.

2.2.1 Static Pressure Probes

In order to measure the variation of static pressure along the test wall, wall pressure taps were placed every 48 inches along the center line of the test wall. These pressure taps were designed according to Shaw's (1960) suggestion, and accurately machined from a 0.25"-diameter aluminum rod. The sensing hole of these taps had a 0.125" diameter. The taps were 1.5" long and were carefully mounted (every 48") flush

with the surface of the test wall. They extended outside the tunnel floor and connected to 0.25" inner diameter clear Tygon tubes of 24" long, with a plug at the end to prevent leaking when they were not in use. In addition, a 1/8"-diameter static L-shaped pressure probe (United Sensor PSC-12, 1/8", with four 1/32" holes) was mounted on a movable support. The probe was positioned one inch (= 8d) above the test wall surface and 12" upstream of its support. The probe was also used to measure the static pressure for streamwise pressure gradient and spanwise Preston tube experiments, as explained in Section 2.2.2. The results of these home made pressure taps were in excellent agreement with those of the L-shaped static pressure probe.

2.2.2 Traveling Preston Tube

In order to examine the two-dimensionality of the flow on the test wall the arrangement of a total pressure probe resting on the wall and the abovementioned L-shaped static pressure probe was used. This arrangement of pressure probes, which is a modified version of the well-known Preston tube (J.H. Preston, 1954) with V.C. Patel's (1965) design suggestion, was employed to measure the shear stress on the test wall. The measurements were conducted in spanwise direction of the test wall by moving the Preston tube, which was attached to a traversing mechanism with 36" traveling distance. The sensor part of the probe was 12" upstream of the support, thereby avoiding any disturbance in the measurement. A schematic of the probe appears in Figure 2.8. In order to calibrate the Preston tube, the shear stresses (τ_w), were estimated from the Clauser plot. This plot was graphed based on Coles' "law of

wall", several Reynolds numbers, and different stations along the center line of the test wall for the regular turbulent boundary layer. The present calibration data were plotted on the empirical calibration curve (refer to Figure 3.2). The relation in calibration was suggested by Preston; i.e., $\tau_w d^2\rho/4\mu^2 = F(dP_p d^2\rho/4\mu^2)$. The results of the above calculations were in excellent agreement with the curve-fit equation was suggested by Patel (1965). Therefore, the same curve-fit was used as the calibration reference in the present experiment. Further calculation procedure is discussed in Section 2.4.1.

2.2.3 Boundary Layer Manipulators and Tripping Device

The manipulator device used was a tandem-arranged parallel plate manipulator (referred to as TAPPM). The two TAPPM plates were very thin and of the same thickness. Two different thicknesses of plates were employed during this research. The first set of manipulators were 48" x 3" x 0.03" and the second set had a thickness of 0.003". The first set was made of stainless steel, shim stock, and the second set of manipulator plates were spring steel shim stock blue tempered (Type C-1095 from DE.STA.CO). These thin plates were secured between two blocks of steel which were used for holding the TAPPM plates at the desired height above the test wall. Tension in the TAPPM plates was provided through an adjustable arrangement from outside of the tunnel's vertical walls. In order to keep a uniform tension in the manipulator plates for different times in use, a strain gage was mounted at the far end of each of these thin plates. The strain in the plates under tension was measured by a VISHY electronic strain indicator. In this

manner tension in the plates could be monitored and kept under the same conditions for the entire experimental period. There was no evidence of any vibration of the TAPPMs. This was confirmed by steady still reflection observed from a light shining on the surface of the TAPPMs. The test was conducted for 5, 10.5, 15 fps freestream velocities in the tunnel. The non-dimensional geometry of these manipulators was similar to the configuration suggested by Corke (1981) (refer to Figure 2.2).

The boundary layer flow was tripped by placing a .0625" (1.588 mm) diameter threaded rod at x = 19.5" (49.5 cm) from the leading edge of the test wall. The leading edge referred to in this experiment is the point at which the test section is connected to the downstream of the honeycomb of the tunnel inlet. Note that all the streamwise distances referred to are from this reference point.

2.2.4 Hot-wire Anemometry and the Data Acquisition System

2.2.4.1 Single Probe Hot-wire

Most of the velocity profile measurements were conducted with a single wire, called a U-wire. The axis of this wire was in the z direction (refer to Figure 2.2 for the coordinate system used throughout this study). U-wires measured the streamwise component of velocity. They were used for near-wall mean velocity and intensity measurements and sometimes for overall velocity profiles. In every case the U-wire was calibrated before a measurement and this calibration was checked after a measurement.

2.2.4.2 Twin-x-wire Probe

A four-element hot-wire array was employed to measure velocity components. This array consisted of two single probes, each with a two element 'x' wire . The two 'x' wire probes were independently mounted on a 3/8"-diameter aluminum rod using similar fixtures which allowed for the adjustment of 'x' wire number one with respect to 'x' wire number two, which was held stationary. These fixtures were mounted to the traverse mechanism, allowing adjustment in the normal direction to the test wall.

Tungsten wire with a diameter of 5 microns was used as the sensing element of the probe. The probes were fabricated in the Turbulence Structure Laboratory at Michigan State University. The twin-x-wire probe is shown in Figure 2.9. Each 'x' wire probe was in x-y plane from which the streamwise velocity component 'u', the component in the y direction 'v', and hence the product of the fluctuating portion of the velocities (the Reynolds Stress '$\overline{u'v'}$') could then be determined.

The 'x' probes were used at two stations downstream of the TAPPM location. The geometry of their relative positions is shown in Figure 2.9. The four element hot-wire probe was operated using four DISA type 55M10 constant temperature standard bridge anemometers. The four anemometer signals were digitized by a 12 bit analog-to-digital (A/D) converter and stored on a RL02 disc connected to a DEC PDP11/23 microcomputer. The four anemometer signals were simultaneously sampled and then digitized. Simultaneous hot-wire and flow visualization technique is discussed in detail by Falco (1980), Lovett (1982), and Signor (1982). For this experiment a more powerful laser light source

was used from a Copper Vapor Laser with 40 watts power. Note that this laser power is five times more powerful than the Argon Ion laser used by the three researchers mentioned above. Thus, the flow visualization was clearer and provided better resolution, enabling more accurate visual information to be obtained.

2.2.5 Flat Pitot-tube

The first part of the velocity survey was conducted using a flat Pitot-tube, shown in Figure 2.10. The pitot-tube was constructed in at the TSL shop and refined to a standard finish by the author. A wall static pressure tap was used as a reference pressure. This was usually located near the tip of the total pressure tube at the particular location of the velocity collection station. The results were also checked against a United Sensor Pitot static tube (PSC-12, 1/4"). The test results were extremely consistent. Therefore, the total pressure tube was used for velocity profile survey along the center line of the test wall. The total pressure tube was mounted on the same traverse mechanism used for hot-wire anemometry. Several Pitot tube displacement corrections were applied to the data near the wall. Little difference was found; therefore no correction in Pitot static tube measurements was made. The results of velocity profile survey in the regular turbulent boundary layer were confirmed by the good quality of the total pressure sensor. (Refer to velocity profiles of the first part of experiment with the .003" thickness TAPPM device in Section 3.2.)

2.2.6 Flow Visualization

2.2.6.1 Smoke Fog

The Volume flow marking techinque provides good detail within the turbulence, but requires a wind tunnel that is "open" return. A laser sheet of light was used for definition of the side view of the flow field. The boundary layer was visualized by introducing a fog of oil droplets (average droplet diameter was approximately 5 μ) into the flow. The droplets were introduced into the flow through a row of holes which spanned the tunnel width (located at x = 13.5"). A small overpressure was used so that the laminar boundary layer above the holes remained stable. The laminar boundary layer with the oil fog in the lower part close to the wall was then tripped. The turbulent boundary layer resulting from this process was almost completely filled with the oil fog, hereafter referred to as smoke. This visualization technique and its use with hot-wire anemometry is explained in detail by Falco (1980). The side view of the flow, along with the counter (LED clock) representing the numbers of the digitized data of the hot-wire array in the flow, was recorded by a high-speed 16 mm movie on 7250 Kodak film to be used in the conditional sampling of the large-eddy scales in both regular and manipulated turbulent boundary layers.

2.2.6.2 Smoke-Wire

This technique is also well-known (refer to Corke et al (1977) for a complete description of the technique). A stainless steel wire of .04 mm diameter was used, with a variable DC power supply which was controlled manually. Three 1000-watt floodlights were used as the light source, with a 16 mm Red Lake Locam movie camera and Kodak 7250 Video News Films to record the visualization data at two stations (x = 210" ,and x = 520").

2.2.6.3 Titanium Tetrachloride (TiC14)

Titanium tetrachloride (TiC14) is very difficult to use because it is extremely corrosive to metals and dangerous to laboratory personnel when given off. Its use in transient flow visualization, however, is of value. TiC14 three types of experiments: 1) to observe the possible separation of flow on the surface of the TAPPMs, 2) to provide evidence of the coherence of the TAPPM wakes, and 3) to study the mass transport and lift-up of the fluid from the sublayer into the outer region of the boundary layer downstream of the TAPPM device. The use and safety aspects of the technique are discussed by Freymuth et al. (1983).

2.3 Experimental Procedure

All three phases of the experimental procedure, including the tunnel preparation, are discussed in this section.

2.3.1 Visual Data Acquisition

After the main structure of the wind tunnel was built, a series of smoke fog flow visualization tests were conducted in order to check possible leaks. The first step was to run the tunnel fan at a very low speed, which produced a steady one foot/sec. freestream velocity in the test section. The boundary layer that developed over the entire length of the test wall (56 feet) was laminar. This could be seen by observing the smoke, which stayed stable and attached to the test wall from x = 13.5" where it was introduced into the boundary layer, up to the end of the test section (x = 672"). During this experiment no serious leaks were detected. At higher speeds up to 20 ft/sec, smoke was used to detect possible leaks close to the joints of the sections from outside the tunnel. Observation of the flow through the clear plexiglass walls of the test section made this detection procedure possible. This technique was used until all the leaks were sealed. The inlet configuration (Figure 2.4) was used on the tunnel during this phase of the work. Based on a rough estimate of turbulence intensity (0.8%) by hot-wire anemometry, the tunnel was used for the next task. This was to examine the pressure gradient, the two-dimensionality of the flow, and eventually the velocity survey of the test wall.

2.3.1.1 Tunnel Preparation Visualization

It was later found that the turbulence intensity level could still be improved by removal and rearrangement of the screens in the inlet box frame. The screen box, 6 inches in length, was replaced by one 30 inches in length. This allowed flexibility in the rearrangement of

screens so that the number of screens and the distance between screens could be altered easily. A series of smoke-wire visualizations for each arrangement was conducted. For each modification, a series of still 35 millimeter photos was taken and studied. It took a period of over six months to obtain a reasonable improvement in the turbulence intensity of the flow in the freestream region. The final configuration is shown in Figure 2.5. The mesh and cell size of the screens and honeycomb is provided in Section 2.1.3. An example of the smoke-wire visualization of the freestream and the boundary layer flow at station A ($x \simeq 240''$) is provided in Figure 2.7.

A very interesting phenomenon was observed near the center line of the tunnel when a continuous smoke was introduced into the tunnel's core region. Careful real-time visual observation of the smoke streaklines showed a jumping of these lines, which left the impression that a new problem in the tunnel was encountered. Note that this could not be detected by the 35mm still photos. The high-speed films were taken at two stations ($x = 240''$ and $x = 520''$). For $U_\infty = 10.5$ ft./sec., the 16mm film framing at 100 frames/sec. showed that passage of "large eddies" in the bottom and the top wall boundary layers of the tunnel were responsible for this phenomenon. When a large eddy was in view on the bottom wall boundary layer, a bending was observed in the streaklines in the potential region of the flow. This distortion had a finite amplitude at the centerline of the tunnel. This phenomenon was amplified when a valley between two large eddies on the top boundary layer was present. This result was more clearly seen in the 16mm films taken at $x = 520''$ station. The reason was that the boundary layers of

both the top and the bottom were relatively thicker at this station (boundary layer thickness, δ = 8" at x = 520"). The amplitude of this wave shape in streak lines was measured and was on the order of 0.01-0.02 boundary layer thickness. Figure 2.15 shows an example of the phenomenon. Thus, the apparent unsteadiness was not due to the wind tunnel fan, but to the passage of the large eddies in the turbulent boundary layer.

2.3.1.2 TAPPM Wake and Wall-Layer Visualization

As discussed in Section 3.3.1 below, the results of the velocity profile survey in the relaxation region of the skin drag created a suspicion that the flow around the TAPPM's was separated. To obtain a difinitive answer regarding the separation around these plates, a series of flow visualizations using TiC14 as the flow marker was conducted. The visualization experiment was performed at three spanwise locations on both plate surfaces of the TAPPM for U_∞ = 5, 10.5, 15 fps. The snapshots of this experiment did not show any evidence of separation (see Figure 2.17).

A series of TAPPM wake and wall layer flow visualizations at station A were conducted. This part of the visualization experiment resulted in very conclusive findings in terms of the correlation of drag reduction and the structure changes in the turbulent boundary layer which were studied in this research.

A volume of 2 cc TiC14 was applied, using a 5cc syringe for each 39-frame roll of film taken (the syringes were plugged after each application, so they were not used again), over a region that always

started at the same x-position. For each case (manipulated and regular boundary layer) snapshots were taken. The time between each snapshot was 0.5 second. Each time a fresh strip (of fixed length and width 70 cm by 1 cm) was laid on the test wall under similar visualization conditions, an estimate of the difference in mass transport from sublayer region into the outer region for the two cases of manipulated and regular turbulent boundary layers could be obtained. The experiments were recorded on 35mm films (Kodak Tri-X pan, ISO 400) and later were quantized on the film analyzer. The difference in the level of sublayer fluid lifted up and ingested into the outer layer confirmed the changes in C_f for the two boundary layer cases. Figure 2.11 gives the dimensions and the geometry of the region under investigation in this experiment. The portion of the films of the flow field which was quantized appears in the central portion of the view. After a series of similar trials, the last rolls of film, which contained 39 frames in each case, were selected for final data acquisition and analysis. 26 data points (y values) were measured from each frame. These values were the highest points that the sublayer fluid reached into the outer region. The distance between the two points selected to measure y values (from wall surface to the top boundary of the marker) was based on the smallest sized structures observed in the flow in this region. In this manner each eddy structure seen in the flow, on the average, had two y values in the data obtained from these films. In each case, 1014 y-values were recorded. These values were statistically analyzed using a TSL program called RATHIS, which created an equal interval histogram and used the mean and standard deviation of the sample to fit a

theoretical distribution over the histogram. The histogram and the theoretical distribution were plotted using a routine called RATPLT on the TSL computer. Final results of this part of the experiment will be discussed in Section 3.3.1.

2.3.1.3 Wall Layer "Pocket Module" Event Visualization

In order to study the changes of the interaction phenomenon in the region close to the wall, via visualization, the station (x = 340" (8.64 m)) where the local skin friction $C_{f\theta}$ (based on the momentum balance calculation) had the largest change by manipulation of the boundary layer, a visualization setup was used. For further information on this technique, refer to Falco (1980) and Lovett (1982). This experiment consisted of smoke introduction through a tangential slit in the test wall, providing a dense sheet of smoke on the wall in the x-z plane to mark the occurrence of the "pockets". The tangential slit was 12 in. (30.5 cm) long in the z-direction, with a 0.07" (1.18 mm) gap in the y direction and an injection angle of 9 degrees. The smoke was injected at this station so that smoke was only highly concentrated in the regions of the boundary layer very close to the test wall surface. As the turbulent motions entered fluid from regions above the wall, the region containing the smoke would show the "footprint" of the interactions of smoke-free fluid coming from above the wall region. This footprint is referred to by Falco (1980) as the "pocket module", (also refer to Lovett, 1982). These footprints were illuminated using two 300-watt floodlights mounted above the tunnel and shining on the test wall. They were photographed using the Locam 16 mm high-speed

movie camera (500 frames/sec.). Because of the narrow depth of field of the f/.95 lens, determination of the correct y plane to focus on for the sharpest image of the pocket was accomplished by trial and error.

2.3.2 Mean Velocity and Combined Hot-wire and Laser Visual Data Acquisition Systems

The first mean velocity profile data with the first TAPPM device (TAPPM No. 1, 48" x 3" x 0.03", in Experiment I) were collected using the flat Pitot-tube probe discussed in Section 2.2.5. This probe was made of a 3/8" diameter copper tube. The static probe part of this Pitot-tube was chosen to be a wall static pressure tap nearest to the tip of the total pressure probe. A schematic of this probe appears in Figure 2.10. The velocity profile voltages collected for this part of the experiment with TAPPM No. 1 were manually recorded from a digital voltmeter. Using Bernoulli's equation, the corresponding velocities were calculated in fps. These velocity profile data were later manually typed in a pre-formatted file processed on the TSL computer to obtain the mean velocity profiles and their integral parameters. This program and procedure is discussed below. The steps in processing and plotting the various graphs of these profiles are shown in Figure 2.12.

An MKS Baratron .01 TORR resolution pressure transducer was used for pressure readings. Pressure related to voltages were averaged by a DISA integrator on the 100 second range; i.e., for each y position of the Pitot-tube probe, the pressure transducer signal was time averaged over a 100 second period. The instantaneous signals were monitored on an oscilloscope. Final averaged voltages were recorded from the TSI

digital voltmeter, and converted to velocities via the Bernoulli's equation. They were then interactively typed into a data file to be processed by a computer command file program called CALANL. The function this program performs is shown in Figure 2.12.

The next set of velocity profiles was obtained using a single hot-wire probe. This time, the second TAPPM (48" x 3" x 0.003") was used to manipulate the turbulent boundary layer. This was done in order to obtain accurate information close to the wall, as well as turbulence intensities.

The final mean velocity profile and rms fluctuations data were obtained using a constant temperature DISA hot-wire anemometer. Two TSI digital voltmeters were used to record the mean and rms fluctuations of the velocity profiles. The hot-wire was calibrated in the same wind tunnel before and after each velocity profile data collection. The hot-wire calibration consisted of collecting simultaneous average voltages from the hot-wire and pressure readings from the pressure transducer. The final velocity profile and respective hot-wire calibration data were collected using the two TSI digital voltmeters, a single hot-wire probe with a DISA 55M10 constant temperature anemometer, an MKS Baratron model 146H-0.1 pressure transducer, and a Keithly digital voltmeter.

The experiments using the twin-x-wire probe array and the array combined with simultaneous visual data collection were the most involved of the above experiments. The signals from the twin-x-wire probe were digitized using a simultaneous sample and holds, a 125 KHz analog to digital converter (hereafter referred to as "the A/D"), and a PDP-11/23

Dec computer, using the RT-11 operating system. The computer had an RL02 disk drive for mass storage (hereafter referred to as "the data acquisition computer"). The MKS Baratron pressure transducer (mentioned above) was used for calibration. A Plasma Kinetic 40 Watt Copper Vapor laser was used to produce a sheet of light parallel to the flow, normal to the wall, and in the plane of the probe array. Mellors Groit cylindrical lenses and mirrors were used to produce the laser sheet, which was 1/8" thick. Figure 2.16 is a schematic of the optical arrangement used for this part of the experiment. A digital counter (hereafter referred to as "the LED clock", or "counter") triggered by the computer registered a change for every digitized data point. This was recorded on the 16mm film simultaneously with the visualized boundary layer. In addition, the hot-wire probe data was recorded by data acquisition computer and stored on the RL02 disk. Each realization took 4.91 seconds which was separated into three portions, and later saved in three separate data files. For each portion the LED clock was reset by the computer and indicated the changes in each separate portion of hot-wire data. The total time of data recording for each final case (regular or manipulated boundary layer) was 49.1 seconds.

The following equipment was used to record the structures in the flow passing the probe when the twin-x-wire was in use; 1) four DISA 55M10 constant anemometers, 2) the MKS Baratron pressure transducer and two TSI digital voltmeters, 3) the Keithly digital voltmeter, 4) the smoke generator, and 5) the Redlake Locam high-speed movie camera with the same lens at f/.95 and 16mm Kodak 7250 film. The two x-wire probes were calibrated using the standard TSL procedure (see Lovett, 1982).

Two computers, an LSI-11/23 with 1.0 MB memory running RSX-11M, and a Digital Equipment Corporation VAX running VMS, Version 4.0 system were used for processing the data collected in this part of the experiment. A diagram of the main instrumentation and computer network appears in Figure 2.14.

2.4 Data Reduction and Analysis

Several techniques and experimental procedures were involved in this research. The order of performance of the experiments is outline below.

2.4.1 Streamwise Pressure Gradient and Skin Friction Data

A high quality flow facility was required for the main experiments involved in all phases of this research. A zero pressure gradient in the stream direction on the test wall was the first goal in building the wind tunnel facility. It was hoped to eventually develop a two-dimensional turbulent boundary layer along almost the entire length of the test wall. To this end, a series of pressure measurements in streamwise and spanwise directions was conducted. The streamwise pressure measurements were conducted by recording the pressure difference between a reference static pressure wall tap located at x = 25.5 in. (0.65 m) downstream of the leading edge of the test wall and other static pressure taps located 48 in. apart along the center line of the test wall. Each measurement was taken for a period of 100 seconds and was time-averaged with the DISA integrator (described

above). The same measurements were conducted using the United Sensor L-shaped static pressure probe. The results were very close. No significant differences in the pressure readings were observed. Thus the quality of information from the 1/8" static pressure taps was confirmed. These pressure readings were substituted into Bernoulli's equation and finally non-dimensionalized to obtain $dCp/dx = 2dp/\rho U_\infty^2$ per foot. The streamwise pressure gradient of the flow in the tunnel will be discussed in Section 3.1.1.

Spanwise skin friction variation measurements were conducted using the movable Preston tube (Preston, 1954) described above. The pressure readings were again time-averaged by the DISA integrator for 100 second periods. This information was substituted into Patel's 1965 calibration. The calibration held for total pressure tubes with $d/D = 0.6$, where d is the inner diameter and D is the outer diameter of the total pressure tube used in the Preston tube probe. The diameter D was selected smaller than the height of the highest point of the log-linear region of the inner law velocity profile from the test wall. In other words, the diameter of the total head tube was always less than the thickness of the logarithmic layer of the boundary layers ($D < 0.1\delta$) under survey (refer to Preston, 1954). Therefore, based on the calibration results, the suggested equation, $x^* = \log_{10}(\rho dPd^2/4\mu^2)$ which in this research resulted basically in the number $4.4 < x^* < 4.7$ for several stations under investigation, and the following equation which was also used for this range of measurements: $y^* = 0.8287 - .1381x^* + 0.1437(x^*)^2 - 0.006(x^*)^3$, where y^* is defined as $\log_{10}(\tau_w d^2\rho/4\mu^2)$, the shear stress at the wall and the local skin friction coefficient C_f were

obtained.

2.4.2 Mean Velocity Profile Data

Mean velocity profile data for the thicker TAPPM (the first set of boundary layer velocity profiles) was calculated by hand from measured voltages using Bernoulli's equation. Further non-dimensionalization and plotting of the results were performed on the TSL computer operated under the RSX-11M system. The mean and rms of velocity profile data of the thinner TAPPM experiment were processed using calibration and data reduction algorithms of the TSL. The single hot-wire was calibrated before and after the actual velocity profile data acquisition period, which was usually about 4 hours when data was collected with digital voltmeters. The temperature variations during this period were less than $\pm 0.3^{\circ}C$. When the data was digitized by the A/D, it took one hour to collect data for each complete velocity profile, which consisted of 50 probe positions. In this manner, potential variations of probe calibration over the course of the measurements could be accounted for. No noticeable variations due to drifting were obtained throughout the course of the experiments. Both sets of velocity profiles were analyzed and processed in the same manner, using a number of computer programs which are summarized in Figure 2.12. A listing of the programs and command files (only those written particularly for this experiment) involved in processing the data is presented in Appendix A. The boundary layer parameters from velocity profiles were determined from both sets of data to obtain the net skin drag and wall friction coefficient, C_f, and their variations along the center line of the test

wall for the regular and manipulated boundary layers. Each profile consisted of 50 discrete data points, spaced normal to the test wall so as to result in high resolution near the wall and at the outer edge (to enable the sublayer edge and the overall boundary layer thickness to be accurately defined.) In spite of this approach, the velocity profiles were smoothed by hand using the following procedure. The data was plotted (y vs $\bar{U}$) by computer on a large sheet of graph paper, approximately 32 cm by 150 cm. Then, using a large french curve, sets of 5 to 10 points at a time were fitted on a curved line. In cases of a bad fit of a point to the curve, the velocity of that particular point was changed to fit the smooth curve. In cases where a deviation from a smooth curve in the velocity profile was observed, the relative velocity difference was not more than 1% at that particular position. The smoothed profile was replotted and the data processing was continued on the computer. Profiles were taken at streamwise stations, shown in Figure 2.2.

The data from each profile was used to plot a series of plots, which are described as follows: (1) y vs $\bar{U}$ coordinates for the first portion of the data points which were very close to the surface of the test wall (0.0 to 0.1" (2.54 mm)). There were, on average, 10 data points in this graph which could normally be fitted on a straight line. This line, for most of the profiles, would pass through the origin of the axis (y vs $\bar{U}$). In some cases, the line did not pass through zero (origin), and the error in reading the y value was not more than ±0.002". The error was corrected for y values of the particular velocity profile data and the graph was replotted. The slope of this

line was used to obtain the shear stress at the wall. The friction velocity and other parameters obtained by this method will hereafter be referred to by a subscript "n", such as friction velocity $u_{\tau n}$, local skin friction coefficient C_{fn}, and so forth. (2) The second plot showed y vs $\overline{U}$ for all of the velocity profile data. (3) Consequently, two Clauser plots were printed out. These two plots were used to obtain an estimate of the C_f. One was based on Coles's "law of the wall" ($u^+ = 5.61\log_{10}y^+ + 5.0$) parameters (see Coles, 1968) and the other was based on Patel's "law of the wall" ($u^+ = 5.51\log_{10}y^+ + 5.45$) parameters (see Patel, 1969). Based on the validity of Coles information in turbulent boundary layers, the final estimate of C_f was based on the Coles "law of the wall" parameters. These parameters were used to obtain the Clauser plot and to estimate the skin friction coefficient for the particular velocity profile being processed (For further details of the method, refer to Clauser, 1954).

(4) At this point of velocity profile data processing, the information regarding slope at the wall and the C_{fc} from the Clauser plot were interactively typed into the TSL computer. The processing was automatically continued. This complete velocity profile processing and plotting routine was performed by a command file, referred to as CALANL. Its position in the data processing is shown in Figure 2.12. The responsibility of CALANL (for programs involved, see Appendix A) was to process and plot the data in a relatively automatic manner. The subprograms in CALANL are as follows:

VELPRO- can either calculate velocities from a calibrated single hot-wire or bypass this part and continue to process the data for Clauser plot.

MULPLT- plots data in desired format.

VELPR3- calculates the boundary layer profile parameters: freestream velocity U_∞, boundary layer thickness δ ($y = \delta$ at $0.99U_\infty$), displacement thickness δ_d, momentum thickness θ, shape factor H, Reynolds number based on the momentum thickness R_θ, energy thickness Δ, Cole's wake coefficient (π) based on C_{fn} and C_{fc}, and friction velocity based on C_{fn} and C_{fc} (estimated from the Clauser plot). In addition, this program non-dimensionalizes the velocity profile data to obtain the rest of the plots explained in Figure 2.12. All the above information is stored in one master data file.

Once this part of the velocity profile survey and analysis for both regular and manipulated boundary layers was accomplished, a plot representing the momentum thickness (θ) vs distance from the test wall leading edge x was made using the calculated θ. This was in order to obtain two main results: (a) $C_{f\theta} = 2d\theta/dx$. This relation is obtained from the von Karman integral equation (Schlichting, 1979) ($d\theta/dx$ was obtained by a graphical differentiation of the θ curve plotted against x), provided that the pressure gradient along the x-direction in the boundary layer is equal to zero ($dp/dx = 0$). Finally, the $C_{f\theta}$ and C_{fc} were used in reprocessing the entire velocity profile data in the final non-dimensionalization, presented in Chapter 3. (b) The variation of the net drag of the manipulated with respect to regular boundary layer from:

$$\text{Net Drag Ratio} = (\theta_x - \theta_o)_{man.}/(\theta_x - \theta_o)_{reg.}$$

where θ_o and θ_x are momentum thicknesses of the boundary layers at TAPPM and x-station locations where corresponding net drag is calculated respectively. This relationship is also the result of the von Karman

integral equation, which represents a non-dimensional form of the net drag of the boundary layer flow on a flat plate of x length.

The results from the above equations led to the observation of crucial changes and the relaxation of the drag which developed downstream of the TAPPM device. Furthermore, these results were the key factors leading to the third phase of the experiments performed at stations where interesting changes in the structures of the flow were expected. This phase attempted to determine what structural changes result from the insertion of the TAPPMs into the boundary layer flow.

This phase of the experiment involved flow visualization, hot-wire array anemometry, and simultaneous visualization and hot-wire measurements. Details of the experimental procedure, data processing, and analysis will be provided in the following sections of this chapter.

2.4.3 Twin-x-wire Probe Data Processing and Analysis

The results of skin friction changes calculated from the momentum balance in both the regular and manipulated boundary layers were used to guide the study of structural changes. Structural measurements were made in the boundary layers at two stations (x = 240" and x = 340"). The data were collected with the twin-x-wire array both alone and simultaneously with visual data (only at x = 240"). These were processed on the TSL computer and in part on the MSU Engineering Computer Facility VAX-11/75, using VMS 4.0 operating system. The x-wire array data which were collected by the data acquisition computer system were transferred to the TSL computer and were processed from "raw" form (bits per millivolt) to velocities with the CONVOL program. CONVOL uses

calibration information in Collis and Williams' (1959) parameter form and outputs the results of each wire, whether slant or straight, as velocities (if U-wire) or as pseudo-velocities (if a slant wire). The pseudo-velocities needed to be converted into u and v components. At the same time, a correction was made to compensate for possible errors in the angles of the x-wires. Two coefficients, CP and CN were obtained via a calibration procedure detailed by Lovett (1982). These were obtained from a separate program called CPCN, and were used as inputs to the TSL program VEL4 to account for the probe angle error corrections. In addition to data file names, VEL4 program requires the following information to process the data: sampling rate of the A/D, number of columns in the data files, format of the data files, and CP and CN values for both x-wires used in the array. The processed output files from VEL4 contain 12 columns of numbers, of which the 6 columns that contain the fluctuating components of velocities and Reynolds stresses (i.e., fluctuation = total - mean) are of interest in this experiment (the others are for storage of velocity gradient information). The fluctuating quantities which were examined in this experiment are u'_1, v'_1, $u'_1v'_1$, u'_2, v'_2, and $u'_2v'_2$ (subscript 1 refers to the top x-array probe located at $y = 0.6\delta$ and subscript 2 refers to the lower x-array at $y = 0.4\delta$ in the twin-x-wire probe). Due to possible signal noise interference with A/D, a 5-point moving average smoothing routine was used in VEL4. The smoothing process of the data which was performed by VEL4 is actually the same as that used by Signor (1982) in his data processing programs.

In order to obtain a visual sense of the velocity and Reynolds

stress variations calculated in VEL4, the long-time records of these fluctuating quantities were plotted using a program called TIMPLT which was developed at TSL. TIMPLT is capable of plotting as many as 8 long-time series records of data for comparison purposes on the same plotting axis. These plots were studied to enhance and verify the visual data obtained from films taken in the simultaneous visual and x-array probe data. This technique has been developed and successfully used over the past several years in turbulence studies at TSL.

The fluctuating velocities were further processed to obtain space-time correlations. A program called CORRELATE3 was used to process the data. Due to the massive amount of data recorded in this experiment, a faster processing computer with a larger memory than the TSL computer was of great value in performing the correlation calculations. To this end, the data were processed by the VAX-11/750 VMS system of the Engineering Computer Facility at MSU. The purpose of the space-time correlation analysis was to study the structural changes in the boundary layer flow resulting from the application of the TAPPM device.

The data for this part of the experiment were collected at two stations ($x = 240''$ and $x = 340''$; $\xi \simeq 20$ and $\xi \simeq 51$, respectively). Since the space-time correlations at $\xi = 51$ did not show significant changes due to TAPPMs, it was decided to conduct simultaneous visualization and probe data acquisition only at $\xi \simeq 20$. These results will be discussed in the following chapter.

In order to obtain information about changes in the large-eddies of the boundary layers studied in this experiment, space-time correlation

analysis of such flows was necessary. This was accomplished by processing the fluctuating velocities obtained with the twin-x-wire probe. The fluctuating velocities and the Reynolds shear stresses used in the analysis were u'_1, v'_1, u'_2, v'_2, $(u'v')_1$, and $(u'v')_2$, respectively. The correlations which were computed were $R_{u'_1u'_2}$, $R_{v'_1v'_2}$, $R_{u'_1v'_2}$, and $R_{(u'v')_1(u'v')_2}$. As evident, the reference is the top x-wire probe (referred to as number 1.)

The space-time correlation calculation for p' and q' functions is defined as:

$$R_{p'q'} = \overline{p'(X_0,Y_0,Z_0,t_0)q'(X,Y,Z,t)}$$

where the overbar represents time-average of the function. Subscript p' of R represents the reference signal, which in this experiment is defined as the velocity (or Reynolds stress) fluctuation at the top x-wire array position, and q' represents the velocity (or Reynolds stress) fluctuation at the lower x-wire array position. If functions p' and q' are statistically homogeneous in space and stationary in time, the correlation depends only on the difference in the coordinates $X_2 - X_1$, $Y_2 - Y_1$, $Z_2 - Z_1$, and $t_2 - t_1$. In the case of zero pressure gradients, such as the condition in this experiment, the homogeneity with respect to Z and stationarity with respect to t is expected. In the zero pressure gradient case the growth of the boundary layer thickness is slow, as has been shown. One may therefore scale the coordinates with the local value of boundary layer thickness. Although y/δ is held constant, there is no homogeneity along the y coordinate itself. The space coordinates in this experiment for the two stations under survey were non-dimensionalized by the respective local boundary

layer thickness and were kept constant as: $X_2 - X_1 = 0.5\delta$, $Y_2 - Y_1 = 0.2\delta$, $Z_2 - Z_1 = 0.0$, and finally the time $\tau = (t - t_0)U_\infty/\delta$, which was the only variable in the correlation computation process for both stations.

The flow field for this experiment was stationary in time. Thus based on Taylor's hypothesis for the stationary flow conditions one can express:

$$R_{p'q'}(X_0, t) \simeq R_{p'q'}(X, t_0)$$

The validity of this relationship is well supported and documented by Favre (1965). Based on the above discussion, the correlations $R_{u'_1u'_2}$, $R_{v'_1v'_2}$, $R_{u'_1v'_2}$, and $R_{(u'v')_1(u'v')_2}$ have been calculated and normalized once by their respective rms values of the signals, and again by the freestream velocity (U_∞). The results of this analysis will be discussed in the next chapter.

The program CORRELATE3 for processing data from this experiment requires the output velocity files of the VEL4, the number of columns in the data file, the columns of velocity fluctuations to be processed for correlation, the sampling window size (the number of points before and after the moving reference), the correlation step size, and the name of the output file for each data take. The data sets for each case of the experiment were (ensemble) averaged by the CORAVG program and plotted using the MULPLT.

2.4.4 Conditional Sampling of Probe Data with the Aid of Film Data

An understanding of the large-eddy structural changes due to the TAPPM device was the main goal of this research. To gain some physical

insight into the correlation of skin friction drag reduction obtained in experiments boundary layer manipulators (TAPPMs) and large-eddy alterations, one must have strong evidence of the changes in the large-eddies. This allows one to explain the mechanisms possibly responsible for the final solution of this drag reduction puzzle. Many unsuccessful attempts relied mainly on probe data and a few inaccurate visualizations to explain the large-eddy structure changes in the manipulated boundary layers. Utilizing the unique TSL facility and experimental techniques avoided in this experiment the problem of vagueness of visual techniques used by others. The study of the films from the high-speed movies of both regular and manipulated boundary layers, combined with probe data, were therefore crucial to the final goals of this experimental program.

The process of conditionally sampling the probe data to the large eddies using the films was as follows: The digital clock read-out appeared in the bottom portion of the frames. Those moments in which the probe entered and left the large-eddies were recorded. Each pair of recorded numbers represented the probe data numbers to be conditionally sampled out from the long-time record of the data takes. Each data take period was 4.91 seconds. The rate of sampling was 5 KHz. Using these number pairs, it was visually possible to look at the plots of the probe data to observe the fluctuating velocities and the Reynolds stresses inside the sampled large-eddies. This is actually one of the most active techniques available at TSL for the study of the structure of turbulence. For further details of this technique refer to Falco (1983). Due to clearer visibility of the large-eddies boundaries at the

position of the top x-wire in the hot-wire array ($y/\delta = 0.6$), only the number pairs for this x-wire were recorded to be used in the conditional sampling process of the data. Figure 2.18 displays an example of the event of a large-eddy passage by the probe. The number which is printed in reverse on the lower portion of the picture represents the point number stored in this data take.

The criteria for choosing the large-eddies to be sampled were: (1) shape, (2) size, (3) observability of the sharp gradient of smoke concentration and the valleys (non-turbulent regions upstream and downstream of the large-eddies) as the eddies convected over the field of view.

The quantitative signals obtained from the probe were selectively sampled in this manner, based on the visualization. Then these samples for regular and manipulated boundary layers were ensemble-averaged separately for each case. The ensemble-averaged signals were then normalized by different boundary layer flow characteristic parameters, and plotted by TIMPLT. The ensemble averaged signals of u', v', and u'v' give an excellent representation of the flow dynamics inside the large-eddies (refer to Falco, 1977,1982).

The long-time records of the fluctuating signals, plotted by TIMPLT, were of excellent help in the sampling process of the data, which visually confirmed the accuracy of this technique. However, the final objective of this investigation was to determine the effects of the TAPPMs on the large-eddy structures, and to examine whether these eddies "break up", as the NASA Langley research team (1972-present)

claim. This as well as the interaction of the wake of the TAPPMs with other structures in the boundary layer, will be examined in the following chapters.

CHAPTER 3

RESULTS

In this chapter the results of the documentation of flow facility, the mean velocity profile survey, and the integral parameters of these velocity profiles will be discussed first. Next the results of flow visualization, x-array hot-wire anemometry both alone and combined with simultaneous laser sheet flow visualization along with space-time correlations will be discussed. Finally, an analysis of the results for both cases of regular and manipulated turbulent boundary layers will be presented.

3.1 Flow Field Conditions

Section 3.1 focuses on the flow conditions required for the experiment. The conditions required were constant pressure along the test section (zero pressure gradient), a two-dimensional boundary layer flow with a low-level turbulence intensity wind tunnel, a long flat test wall to investigate skin friction drag, and structural development in both the regular and manipulated boundary layers.

3.1.1 Pressure Gradient Along the Centerline of the Test Wall

Figure 3.1 shows the results of the pressure measurements in a non-dimensional form along the x-axis of the test wall. The differential pressure coefficient defined as dC_p/dx, where $C_p = dP/\rho U_\infty^2$,

dP = (downstream static pressure - upstream static pressure), and dx = $x_2 - x_1$, was used to obtain the information plotted in Figure 3.1. It was observed that the coefficient, which is calculated at different streamwise stations, is on average less than ±0.001 per ft about mean value of -0.002. This value is considered very low for a pressure gradient that is experimentally obtained. Murlis (1975) considers a 0.02 value for this coefficient a negligible pressure gradient. Thus, in this experiment the value -0.002, which is one order of magnitude less than the low pressure gradient obtained by other researchers, should clearly be considered negligible. The pressure gradient measurement was conducted for both regular and manipulated boundary layers. The results indicated no difference between them. Thus, the zero pressure gradient condition required for this experiment was satisfactorily met. The small variation in this coefficient was due to the slightly bowed top of the 8 ft tunnel sections. The first point at x = 49.5" had the lowest value. This was possibly due to the presence of the tripping device, which was located 6" upstream of the first wall pressure tap. One can see that the low value is relaxed to the average value farther downstream of the trip. The last point has a somewhat higher dC_p/dx value than the rest of the points, and is the result of the presence of the diffuser 24" downstream of the last wall pressure tap.

3.1.2 Two-dimensionality of the Boundary Layer

The two-dimensionality of the flow on the test wall was examined using the traveling Preston tube. The results of this experiment for

two inlet configurations with two tripping devices are shown in Figures 3.2-3.5. Figure 3.2 shows the variation of the skin friction in spanwise direction at several stations when the boundary layer was tripped with grit 36 sandpaper as suggested by Corke (1981). The sandpaper was 30 cm wide in the flow direction and cemented to the test wall. It protruded 0.8 mm above the wall. The upstream edge of the sandpaper was located 10 cm downstream of the leading edge of the test wall. Figure 3.3 shows an improvement of this variation using a 0.0625" threaded rod at x = 19.5". Figure 3.4 shows further improvement of the skin friction variation from 10.3% to 4.6%. This was accomplished through the use of the second inlet configuration, which was discussed in Section 2.1.3. A point of interest here is that the low C_f variations resulted from the lower freestream turbulent intensity (from 0.8% to 0.2%). This change also demonstrates the effect of freestream turbulence on the skin friction variation and other integral parameters (such as θ, δ_d etc...) in the boundary layers on the test wall and on the two-dimensionality of the flow in question in the second boundary layer velocity profile survey case.

3.1.3 Turbulence Intensity of the Wind Tunnel

As explained above, two inlets were used in order to achieve a good quality flow. The streamwise turbulence intensity levels of both cases are shown in Figure 2.6. The higher intensity was used when the first set of TAPPM devices were examined (Experiment I) in the test section. Turbulence intensity was improved when the screen and honeycomb arrangements were altered. This improvement was from approximately 0.8

to a lower value of 0.2%, which was sufficient for the present experiment.

3.1.4 Smoke Flow Visualization of the Laminar Flow on the Test Wall

Before the velocity profile survey on the test wall, the tunnel fan was run at one fps and smoke was introduced into the boundary layer at x = 13.5" downstream of the leading edge of the test wall. The flow stayed laminar on the entire length (17 m) of the test wall. This was an excellent demonstration of the good quality of the flow facility, particularly with respect to three dimensionality at the beginning of the experimental program.

3.2 Mean Velocity Profiles

In order to obtain an estimate of skin friction drag in regular and manipulated turbulent boundary layers, a series of velocity profiles was obtained. With the first TAPPM device (TAPPM thickness = 0.03"), the velocity profile data was obtained using the Pitot probe, which is explained in Chapter 2. The velocity profile data were obtained for both regular and manipulated boundary layers (hereafter referred to as 'Experiment I'). The second sets of velocity profile survey were conducted using a single hot-wire probe (hereafter referred to as 'Experiment II'), and the .003" thickness TAPPM device for manipulated boundary layer in position. These velocity profiles were then processed and used to obtain the integral parameters of the turbulent boundary layers and the skin friction drag variation along the test wall for both

experiments.

3.2.1 Mean Velocity Profile and Integral Parameters in Experiment I

Each boundary layer profile for the first TAPPM device experiment were made up of 30-34 data points. These profiles were taken at several stations, shown in Figure 2.2. The Reynolds numbers, R_θ in this experiment, ranged from 1434 to 5648. The data processing procedure is explained in Chapter 2. Figures 3.6 to 3.10 show the non-dimensional mean velocity profiles in Experiment I for regular boundary layers at different stations. Figure 3.6 shows y/θ vs $\bar{U}/U_\infty$. This figure represents the similarity of profiles in the fully developed turbulent boundary layer required for manipulation in the next step of the velocity profile survey aimed at reduction of skin friction drag downstream of TAPPM over the test wall. Figure 3.7 shows the Clauser plot of velocity profiles, from which C_{fc}'s were estimated for the regular boundary layer case. This figure represents $\bar{U}/U_\infty$ vs Rey, where Rey = $\rho y U_\infty/\mu$. The straight lines plotted in this figure represent various C_{fc} uniformly ranged (with 0.00025 between two consecutive lines) from 0.00100 to 0.00575. It is observed that the data in the log region usually fit a straight line. From this line, based on its location, corresponding C_{fc} of the particular velocity profile were obtained. The C_{fc} was found to be in close agreement with $C_{f\theta}$, calculated from the momentum integral equation for the two-dimensional regular turbulent boundary layers. Figure 3.44 shows $C_{f\theta}/C_{fc}$ vs ξ, where $\xi = (x-x_o)/\delta_o$, and confirms the closeness of local skin friction coefficients from the two different methods at various stations. The

difference between the two methods was, at worst, lower than ±4% at few stations.

Figure 3.8 is a representation of the wall-unit non-dimensional velocity profiles, i.e. u^+ vs y^+. Note that the friction velocities which have been used in the non-dimensionalization were obtained by the momentum balance method, referred to as $u_{\tau\theta}$. They were used to non-dimensionalize the rest of the velocity profiles, unless otherwise stated. The solid straight line, Coles "law of the wall", $u^+ = 5.61\log_{10}(y^+) + 5.0)$, and $u^+ = y^+$ of the viscous-sublayer are also shown in this figure. The figure shows that the log law region is consistent with the log law empirical formulation suggested by Coles. The momentum balance method, which has been used by other researchers with similar manipulators (NASA Langley, and IIT research teams), was also used in the skin friction drag calculation of this experiment.

In order to demonstrate the equilibrium condition of the boundary layers as suggested by Clauser (1954), Figure 3.9 adopted from Rotta (1962) is presented. This figure shows $(U_\infty - \overline{U})/u_\tau$ vs $yu_\tau/\delta_d U_\infty$. The present results are highly consistent with the pipe flow data obtained by Clauser for constant pressure condition. Figure 3.10 shows the wake function W vs y/δ. For comparison purposes, the wake function, $W = 2\sin^2(\pi y/2\delta)$ suggested by Coles (1968) is also plotted in the same figure.

In Experiment I with manipulators in position, a similar non-dimensionalization procedure was used. Corresponding velocity profiles are presented in Figures 3.11-3.15 in the order mentioned above. The data in Figure 3.11 nearly collapses on each other, except

for the first two stations (A, and B) downstream of the TAPPM. This is the effect of the manipulator's wake, which is positioned at $0.8\delta_o$. It is obvious that the skin friction coefficients, C_{fc}, estimated from Figure 3.12 (Clauser plot), no longer agree with the $C_{f\theta}$. Notice that the data fits straight lines at various stations, i.e., the log region has not deviated from a straight line. But one cannot use the information from this plot to infer the local skin friction coefficient. This is because the Clauser plot is only devised based on regular boundary layer conditions. Using the calculated θ from the velocity profiles at various stations for both regular and the manipulated boundary layers, Figure 3.16, θ vs x, was constructed. It used to obtain $C_{f\theta}$ and $u_{\tau\theta}$, which were finally used to normalize the velocity profile data of this section. The momentum thickness at station A ($\xi \simeq 24$) was significantly increased. This increase was due to the skin drag which the TAPPM's presence added to the regular boundary layer drag. As one moves farther downstream, θ stays higher than its regular boundary layer counter part, yet it has a lower gradient leading to the lower local skin friction coefficient up to station E (at $\xi \simeq 86.4$), where the resulting net drag is zero. After this station the momentum thickness overshot, produced a higher drag, and again relaxed back at ξ values higher than 150 farther downstream. The result of the net drag variation deduced from this process in a non-dimensional form is presented in Figure 3.44.

Figure 3.13 (u^+ vs y^+) shows the velocity profiles non-dimensionalized by the inner layer parameter $u_{\tau\theta}$. The deviation from Coles log law can be attributed to the momentum thickness gradients

(obtained from Figure 3.16) at various stations. In contrast to Corke's (1981) results, no unique universal log law line for the manipulated boundary layer mean velocity profiles was obtained, due to the curve fit to Θ vs x. Notice that the parameters A and B (refer to equation $u^+ = A\log_{10}(y^+) + B$) are obtained by fitting straight lines through the data in the log region. This line fit was normally covered by data at $30 < y^+ < 500$. Parameters A and B (at various stations) are shown in Figure 3.17.

When Figure 3.14 (manipulated boundary layer) is compared to Figure 3.9 (regular boundary layer), the data from the stations with reduced skin friction coefficient ($\xi < 80$), and farther downstream profiles ($\xi > 80$) where skin friction coefficient decreased for the second time, no longer fit the curve of the regular boundary layer. This phenomenon can be interpreted as boundary layer flow in an adverse pressure gradient. This is similar to the pipe flow results by Clauser (1954), which showed lower skin friction for corresponding mean velocity profiles.

The wake law profiles in the manipulated boundary layer are somewhat scattered around the Coles wake function law. There is a trend of low skin friction profiles ($\xi < 70$) positioned above, high skin friction profiles ($\xi > 80$) below, and profiles with the same $C_{f\Theta}$ values of their corresponding regular boundary layer collapsed on the Coles wake function curve. Thus, the wake profiles in the manipulated boundary layer do significantly change.

3.2.2 Mean Velocity Profile and Integral Parameters in Experiment II

Since no net drag reduction occurred in Experiment I (refer to

Figure 3.44), it was decided to use the thinner manipulators (t = 0.003"; t/δ_0 = 0.00095) based on the Anders et al. (1984). Each velocity profile in Experiment II was made up of 50 discrete data points. These profiles were taken at several stations (refer to Figure 2.2). The data processing procedure is explained in Chapter 2. Table 3.2 contains some of integral characteristics of the boundary layers in Experiment II. Figures 3.18 to 3.25 show the non-dimensionalized velocity profiles in Experiment II for regular boundary layers at various stations. Figure 3.18 shows y/Θ vs $\overline{U}/U_\infty$. Figure 3.19 displays the Clauser plot of velocity profiles from which C_{fc} were estimated for the regular boundary layer case. This figure represents $\overline{U}/U_\infty$ vs Rey, where Rey = $\rho y U_\infty/\mu$. The straight lines plotted in this figure represent various C_{fc} uniformly ranged (with 0.00025 between two consecutive lines) from 0.00100 to 0.00575, as used in Experiment I. Information (C_{fc}) from this figure is used in the results to be presented in Section 3.2.3 for a comparison with momentum balance and skin friction coefficient results obtained from the slope of the mean velocity close to wall (for "Newtonian fluid"). Figure 3.20 is a representation of the wall-unit non-dimensional mean velocity profiles (u^+ vs y^+). A solid straight line, Coles "law of the wall", $u^+ = 5.61\log_{10}(y^+) + 5.0)$, and $u^+ = y^+$, viscous-sublayer region are also plotted in the same figure. It is clear that the regular boundary results in this figure, all fit the solid line in the "log law" region to a large extent. This is a good representation of the fully-developed turbulent boundary layer in the unmanipulated case.

The equilibrium condition of the boundary layer is also shown in

Figure 3.21. This figure shows $(U_\infty - \bar{U})/u_\tau$ vs $yu_\tau/\delta_d U_\infty$. Figure 3.22 displayes the wake function W vs y/δ. For comparison purposes the wake function $W = 2\sin^2(\pi y/2\delta)$, suggested by Coles (1968), is also plotted in the same figure. Figures 3.23 to 3.26 show the non-dimensional streamwise component of fluctuating mean velocity profiles at different stations. Figure 3.23 of this group shows $rms(u')/u_\tau$ vs y^+. Figure 3.24 shows $rms(u')/U_\infty$ vs y/θ for the mean velocity profile, and Figure 3.25 shows close to wall data normalized in the same way as in Figure 3.24. Due to the thick boundary layer in this experiment, velocities very near the surface of the wall could be measured using the single hot-wire probe. The probe could reach as low as one wall unit ($y^+ = 1$) close to the wall (refer to Figures 3.20, 3.26, and 3.27). This can also be seen in Figure 3.27, which shows the dimensional mean velocities close to the wall in the regular boundary layer at various stations. It is important to note that each profile has at least 10 points which fit a straight line passing through the origin (y = 0.0 and U = 0.0 in Figure 3.27). This confirms the linearity condition in the sublayer region of the mean velocity profiles. These results were also used to obtain the thickness of the sublayer region. Notice that the resulting local skin friction coefficients from the slope of the velocity profiles are different from both Clauser C_{fc} and from $C_{f\theta}$ presented in this experiment. Details of the discrepancies between local skin friction coefficients obtained by different methods are discussed in chapter 4.

In Experiment II, with manipulators in position, a similar non-dimensionalization procedure was used. Corresponding velocity profiles are presented in Figures 3.28-3.36 in the same order as for the

regular boundary layer case discussed above. In Figure 3.28, velocity profiles are non-dimensionalized by the outer parameters (Θ and U_∞). This figure shows y/Θ vs $\overline{U}/U_\infty$ at various stations. Only two profiles of stations A (ξ = 19.3) and B (ξ = 34.81) show the effect of wake of the manipulator plates. Figure 3.29 diplays the data plotted in the Clauser plot. This figure is presented here to demonstrate the inadequacy of the Clauser plot method for the manipulated boundary layer. Results of local skin friction coefficients obtained from this figure are discussed in the following section.

Using the friction velocity obtained via the momentum balance method, Figure 3.30 (u^+ vs y^+) results. The trend of the profiles position in this figure follows the variation of $C_{f\Theta}$ at different stations. Notice that the parameters A and B (refer to equation $u^+ = A\log_{10}(y^+) + B$) are obtained by fitting a straight line through the data in the log region. This line fit was normally located at $30 < y^+ < 500$. Parameters A and B at (various stations) are shown in Figure 3.39. $C_{f\Theta}$ results are also discussed in the following section.

The equilibrium condition of the boundary layer is also shown in Figure 3.31. This figure shows $(U_\infty - \overline{U})/u_\tau$ vs $yu_\tau/\delta_d U_\infty$. Similar to Experiment I, this figure shows that at stations where the skin friction drag is reduced, the profiles demonstrate a deviation from the other profiles, leading to a pressure gradient-like effect in the manipulated boundary layer (Clauser 1954). The wake function of the manipulated case is shown in Figure 3.32. In this figure, there is a large profile deviation from the Coles wake function. This reflects the presence of the manipulators in place, demonstrating a significant change in the

wake region.

Figures 3.33 to 3.36 show the non-dimensionalized streamwise component of the fluctuating velocities at different stations. Figure 3.33 of this group shows $rms(u')/u_\tau$ vs y^+. At low skin friction stations, there is higher $rms(u')/u_\tau$ in the inner region (also refer to Figure 3.36), and lower $rms(u')/u_\tau$ in the outer region of the manipulated boundary layer, in comparison to their corresponding regular boundary layers. Figures 3.34 and 3.35 show the same effect when the rms(u'), and y are non-dimensionalized by the outer region parameters U_∞ and θ. Figure 3.37 shows the dimensional mean velocity profiles close to wall in the manipulated boundary layer at various stations. Similar to regular boundary layer, each profile has 10 points which fit a straight line passing through the origin (y = 0.0 and U = 0.0 in Figure 3.37). This confirms the linearity condition in the sublayer region of the mean velocity profiles. Notice that the resulting local skin friction coefficients from the slope of the velocity profiles are different from Clauser C_{fc} and $C_{f\theta}$ presented in this experiment. Details of the local skin friction coefficient results obtained through different methods are presented in the following section. Furthermore, using the calculated θ from the velocity profiles at various stations for both regular and manipulated boundary layers, Figure 3.38 (θ vs x) was constructed. It was then used to obtain $C_{f\theta}$ and $u_{\tau\theta}$, which were finally used to normalize the velocity profile data in this experiment. This figure shows that at station A (ξ = 19.3), θ overshoots (due to device drag) and then relaxes back (with a lower θ gradient than the regular boundary layer). This θ gradient stays low, even after θ

reaches values less than those of the regular boundary layer. This reflects a net skin drag reduction (lower θ). At about station D ($\xi > 60$), the momentum thickness gradient increases sharply, and after $\xi \simeq 94$ it levels off with the regular boundary layer to almost no net drag reduction.

The results of Figures 3.37 and 3.27 were also used to obtain the thickness of the sublayer region. Individual near-wall velocity profiles for regular and manipulated boundary layers appear in Figures 3.42 and 3.43. Streamwise sublayer thickness variation for both regular and manipulated boundary layers are shown in Figure 3.40 (dimensional). In dimensional form, the manipulated boundary layer has, on average, a 17% thicker sublayer. For reference, the streamwise variation of ratio of the non-dimensional sublayer thickness (normalized by $u_{\tau n}$ obtained from the slope of the mean velocity profile near the wall) is shown in Figure 3.41. Overall, this indicates a similar increase in sublayer thickness. On the other hand, when the sublayer thickness is normalized by $u_{\tau\theta}$ (obtained from the momentum balance), it must show sharp variations, as seen in $C_{f\theta}$ vs ξ.

3.2.3 Skin Friction and Net Drag Results of Experiment I

Using the information from Figure 3.16 (θ vs x), the local skin friction coefficient $C_{f\theta}$ (by a graphical differentiation; $C_{f\theta} = 2d\theta/dx$) and the non-dimensional net drag $(\theta_x - \theta_{x_o})_{Man.}/(\theta_x - \theta_{x_o})_{Reg.}$ along the centerline of the test wall were calculated. These parameters combined with the results discussed above were used to obtain Figures 3.44 to 3.47. Figure 3.44 shows $C_{f\theta}/C_{fc}$ vs ξ, which is an example of high

consistency between momentum balance $C_{f\theta}$ and the Clauser C_{fc} results in the regular boundary layer.

The net drag result in Experiment I is shown in Figure 3.45 $(\theta_x - \theta_{x_o})_{Man.}/(\theta_x - \theta_{x_o})_{Reg.}$ vs ξ. The net drag increase is at its highest value at $\xi \simeq 25$. This is reduced to zero at $\xi \simeq 80$, and again increased to higher values (10%) at stations farther downstream. Thus no net skin drag reduction was obtained in Experiment I. However, it is concluded that if there are to be beneficial effects of TAPPMs, these will be limited to $\xi \simeq 80$ (Rashidnia and Falco, 1983). Figure 3.46 is a replot of the same result in addition to the streamwise normalized local skin friction variation $(C_{f\theta})_{Man.}/(C_{f\theta})_{Reg.}$ vs ξ. At $\xi < 80$, where net drag has increased, the local skin friction is reduced, $(C_{f\theta})_{Man.}/(C_{f\theta})_{Reg.} < 1.0$. The two curves cross ($\xi \simeq 80$) and the ratio $(C_{f\theta})_{Man.}/(C_{f\theta})_{Reg.}$ stays above 1.0. As a result of the sharp increase in gradient of θ in the range of $80 < \xi < 120$, $(C_{f\theta})_{Man.}/(C_{f\theta})_{Reg.}$ increases and reaches its peak ($\simeq 1.4$). In addition, net drag increases from zero to 10% in the same distance range. Then net drag tends to relax back to regular boundary layer very slowly, while the ratio $(C_{f\theta})_{Man.}/(C_{f\theta})_{Reg.}$ sharply decreases to about 0.7 at $\xi = 188.4$.

In Experiment I, the slope of the mean velocity profile near the wall was obtained by a single hot-wire probe at two stations $\xi \simeq 44$ (a decreased local skin friction station) and at $\xi \simeq 121$ (an increased local skin friction station). The result is shown in Figure 3.47 for comparison with momentum balance $C_{f\theta}$% changes. The magnitude of changes in these two methods is not the same, yet they demonstrate similar trends of local skin friction variations.

3.2.4 Skin Friction and Net Drag Results of Experiment II

Using the information from Figure 3.38 (θ vs x) local skin friction coefficient $C_{f\theta}$ (by a graphical differentiation; $C_{f\theta} = 2d\theta/dx$ similar to Experiment I) and the non-dimensional net drag $(\theta_x - \theta_{x_0})_{Man.}/(\theta_x - \theta_{x_0})_{Reg.}$ along the centerline of the test wall were calculated. These parameters combined with previously explained results, were used to obtain Figures 3.48 to 3.53. Figure 3.48 shows $C_{f\theta}/C_{fc}$ vs ξ, which is an example of consistency between momentum balance $C_{f\theta}$ and the Clauser C_{fc} results with the same percentage variation obtained in Experiment I.

The non-dimensional net skin drag result in Experiment II is shown in Figure 3.49 $(\theta_x - \theta_{x_0})_{Man.}/(\theta_x - \theta_{x_0})_{Reg.}$ vs ξ). The net drag was at its highest value at $\xi \simeq 20$. This was reduced to zero at $\xi \simeq 45$, and reached its minimum at $\xi = 58.2$; i.e., a 10% net drag reduction resulted. This net reduction relaxed back to normal boundary layer drag at $\xi \simeq 94$, and remained at its normal value (zero net drag change). However, in Experiment II, a net drag of 10% was obtained. This is only up to 60 boundary layer thicknesses downstream of the manipulator. Figure 3.50 is a replot of the same result, in addition to the streamwise normalized local skin friction variation, $(C_{f\theta})_{Man.}/(C_{f\theta})_{Reg.}$ vs ξ. In the range of $\xi < 45$, where no net drag reduction is obtained, there is still a significant reduction in the local skin friction coefficient $C_{f\theta}$ ($\simeq$ 45%); i.e., $(C_{f\theta})_{Man.}/(C_{f\theta})_{Reg.} \simeq 0.55$. At ξ =58.2, where the maximum net drag reduction is achieved, the local skin friction reaches its regular boundary layer value. The peak of the $C_{f\theta}$ increase is reached at $\xi \simeq 66$, where the momentum thickness gradient has its maximum in the manipulated boundary layer. The two curves meet

again at $\xi \simeq 93$, where net skin drag and local skin friction coefficient changes are almost nonexistent. This condition (ratio $(C_{f\theta})_{Man.}/(C_{f\theta})_{Reg.} \simeq 1$) follows to the last measuring station.

In Experiment II, the near-wall slope of the mean velocity profile was obtained by a single hot-wire probe at several stations. Figure 3.52 shows the streamwise percentage local skin friction coefficient variation $((C_{fn})_{Man.} - (C_{fn})_{Reg.})/(C_{fn})_{Reg.}$ vs ξ. For comparison, similar parameters obtained from the momentum balance method $((C_{f\theta})_{Man.} - (C_{f\theta})_{Reg.})/(C_{f\theta})_{Reg.}$ are also plotted in Figure 3.51. This figure does not show a general correlation between the two curves, except in the local wall-skin friction ($\xi < 50$), where both methods show different level of reduction in the manipulated boundary layers. The difference between the above independent techniques in the local skin friction coefficient amounts to 50% in upto $50\delta_o$. Figure 3.53 shows the ratio $(C_{f\theta})_{Man.}/(C_{fn})_{Man.}$ vs ξ. This indicates that the C_{fn} obtained from the slope of the mean velocity profile near the wall is not consistent with the $C_{f\theta}$ obtained from the momentum balance method.

3.3 Flow Visualization Results

This section consists solely of visualization results obtained with the second TAPPM configuration, unless otherwise specified.

3.3.1 Flow Visualization on Manipulator Plates

The results of boundary layer drag relaxation (refer to Figures 3.49 and 3.50) cast some doubt on the possibility of flow separation around the TAPPM plates. Careful flow visualization around the manipulator plates was conducted and checked, and no evidence of any sort of flow separation was observed. An example of this check is given in Figure 2.17. During the process of separation detection, further flow visualization was conducted downstream of the plates. Figure 3.54 presents an example of the manipulated boundary layer, with the wake of plates present along with the rest of the layer structures. These pictures necessitated a study of the plates' wake by themselves. A combination of wake and wall region flow visualization around $\xi = 20$ sparked new evidence of wake interaction with wall region flow. As many as 200 snapshots of this experiment were taken. A study of two cases (upstream plate alone and both plates in place) indicated that when two plates were in place the structures in the wake of the plates were coherent for longer downstream distances than the one-plate case. The mixing of wall region flow and wake structure was also reduced around $\xi = 20$. This is shown in Figures 3.55(a) and 3.55(b). Figure 3.55(a) shows the one-plate case, and 3.55(b) shows two plates in place.

It was then decided to obtain quantitative results regarding the flow marker (TiCl4) normal distance rise at this station ($\xi \simeq 20$). To this end, a number of rolls of film were taken from this region. Under similar visualization conditions, the last two rolls with 39 frames of film were used for the final analysis. Figure 3.56 presents an example of the film used to measure the normal values of the marker lifted up

into the wall region. The y values obtained from similar films were statistically analyzed. The experimental setup appears in Figure 2.11. The results of this analysis are presented in Figure 3.57. The mean value of y^+, averaged around $\pm 3.3\delta_0$, shows a 25% reduction in the manipulated case. Table 3.1 displays the mean characteristics of the boundary layers at $\xi = 19.3$ in this experiment. It is also interesting to note that the flow marker (TiCl4), which was originally painted on the test wall surface, travelled in the normal direction upto $y^+ \simeq 240$ in the regular case and $y^+ \simeq 180$ in the manipulated boundary layer. It covered a large portion of the logarithmic region within a range of 6 boundary layer thicknesses to the leading edge of the flow marker on the wall.

3.3.2 Sublayer "Bursting" Results From Falco "Pocket" Flow Modules

The results of the interaction of "typical eddies" with the sublayer flow leading to the "pocket" module were obtained at the station ($\xi = 51$) where the maximum $C_{f\theta}$ reduction occurred. Using this information, along with the duration of experiment and the frame rate of the movies, a calculation of the burst rate of wall events in both regular and manipulated boundary layers was possible. Figure 3.58 gives an example of the "footprints" of this interaction (referred to as the "pocket module"). This sublayer structure was originally observed by Falco (1974), and is one of the strongest bits of evidence of turbulence production structure in the turbulent boundary layers. It was found that the frequency of occurrence of footprints of the bursting process was significantly changed. This frequency increased (from 0.6905 to

1.033) when scaled with outer variables ($T_B U_\infty/\delta$), but decreased (from 29.670 to 21.699) when scaled on inner variables ($\rho T_B u_{\tau\theta}^2/\mu$).

When the period T_B was normalized by $u_{\tau n}$ (obtained from mean velocity gradient at the wall) and μ/ρ, a 28% increase in $\rho T_B u_{\tau n}^2/\mu$ was obtained.

3.4 Correlation of Fluctuating Component Results

Based on the skin friction results and wall bursting results obtained through "pocket" flow module visualization at station C (ξ = 51), it was decided to do a space-time correlation analysis of the fluctuating components obtained from twin-x-wire array. A similar correlation analysis was conducted at station A (ξ = 20). These results were obtained for both regular and manipulated boundary layers.

3.4.1 Correlation of Fluctuating Components Normalized with Their Respective RMS Values

Results of the analysis on u', v', and u'v', when normalized with their respective rms values, are presented as follows. Figures 3.59 to 3.62 represent the results at ξ = 51, and Figures 3.63 to 3.66 show similar results at ξ = 20. Notice that all the peaks in these figures are shifted to the right side of τ = 0, where $\tau = (t - t_0)U_\infty/\delta_{Reg.}$. This is the result of the streamwise separation ($0.5\delta_{local}$) of the two x-wire arrays.

Figure 3.59 shows the rms normalized correlation of vertical velocity components at .6δ and .4δ ($R_{v'_1 v'_2}/\mathrm{rms}(v'_1)\mathrm{rms}(v'_2)$ vs τ).

Signals of the top x-array (subscript 1) are used as the reference in the correlation calculation. Note that the peak values for both cases were positive. There was a little change in the peak of the normal fluctuations (8.75% reduction). No other significant differences are indicated in this figure.

Figure 3.60 shows the rms normalized correlation of streamwise fluctuations for both regular and manipulated boundary layers ($R_{u'_1u'_2}/\text{rms}(u'_1)\text{rms}(u'_2)$ vs τ). When there is a 10.8% reduction in this correlation, the peak is narrowed a small amount. Therefore, a relatively small change appears in the large-scale motions (LSMs), as a result of the presence of the TAPPM's wake on the manipulated boundary layer. At about one δ_{local} to left of the peak, the correlation is closer to the zero value. This may be a sign of alteration of the flow in the valleys between the two consecutive LSMs at this station. At the same station, cross correlation of the signals, $R_{u'_1v'_2}$ with a negative peak, hardly shows a peak value change in Figure 3.61 ($R_{u'_1v'_2}/\text{rms}(u'_1)\text{rms}(v'_2)$ vs τ). This correlation on the left-hand side of the peak shows a minor positive correlation in the manipulated case, which could be an indication of the manipulator's wake.

A correlation reduction of 9.4% occurred in the peak of Reynolds stress signature ($R_{(u'v')_1(u'v')_2}/\text{rms}((u'v')_1)\text{rms}((u'v')_2)$ vs τ). This reduction was of the same order as the normal and streamwise components previously indicated. Figure 3.62 shows the correlations with positive peaks.

In the rms normalized form at station C (ξ = 51), results of temporal correlations did not reveal significant changes. It was

therefore, proper to conduct the same analysis on the data obtained at ξ = 20, where the effect of the manipulator was expected to be more active. Using the same procedure applied to the data at ξ = 51, Figures 3.63 to 3.66 were obtained. Figure 3.63 indicates a 6.4% reduction, not noticeable, in the peak of normal velocity correlations. Streamwise fluctuating temporal correlations are significantly changed. Figure 3.64 ($R_{u'_1u'_2}/rms(u'_1)rms(u'_2)$ vs τ) indicates a similar result, along with a 30% narrower peak in the manipulated than the regular boundary layer case.

The cross-correlation at this station ($R_{u'_1v'_2}/rms(u'_1)rms(v'_2)$ vs τ, at ξ = 20), shows a 13% reduction and a 25% narrower peak. This is shown in Figure 3.65. This effect is more pronounced in the Reynolds stress correlation ($R_{(u'v')_1(u'v')_2}/rms((u'v')_1)rms((u'v')_2)$ vs τ, in Figure 3.66, which indicates a 48% lower and 30% narrower peak when compared with the regular boundary case.

3.4.2 Correlation of Fluctuating Components Normalized with Freestream Velocity (U_∞)

Although the traditional normalization in space-time correlation showed the presence of some structures in both regular and manipulated boundary layers, it was not easy to observe a clear picture of flow alterations due to the TAPPM. For reference, the aforementioned fluctuating correlations were non-dimensionalized with the freestream velocity (U_∞), which was held constant for all cases.

Results of this analysis on u', v', and u'v' are presented as follows. Figures 3.67 to 3.70 represent the results at ξ = 51, and

Figures 3.71 to 3.74 show similar results at $\xi = 20$. Notice that all the peaks are again shifted to the right-hand side of $\tau = 0$, as was the case in Section 3.4.1. This was explained as the result of streamwise separation of the x-wire arrays.

Figure 3.67 shows the correlation of vertical velocity components at .6δ and .4δ ($R_{v'_1v'_2}/U_\infty^2$ vs τ). The subscripts used were similar to those in the previous section, as explained above. There are no significant differences in the temporal correlations at station C.

Figure 3.68 ($R_{u'_1u'_2}/U_\infty^2$ vs τ) shows the correlation of streamwise fluctuations for both regular and manipulated boundary layers. A small amount of correlation reduction is observed in the peak value shown in Figure 3.68. In general, no significant change is indicated in that correlation. At the same station, cross-correlation of the signals $R_{u'_1v'_2}/U_\infty^2$ with a negative peak, shows little peak value change in Figure 3.69 ($R_{u'_1v'_2}/U_\infty^2$ vs τ). The only apparent change in the correlation at this station ($\xi = 51$) is shown in Figure 3.70 for Reynolds stresses, with a 7.5% peak increase and a 30% peak width increase. The average Reynolds stress correlation farther outside the peak also stayed above the regular boundary layer. Thus, the correlation functions, when normalized by the freestream velocity at station C ($\xi = 51$), again showed no significant change.

Similar normalization was applied to the signatures at station A ($\xi = 20$). Figures 3.71 to 3.74 present these results. Figure 3.71 ($R_{v'_1v'_2}/U_\infty^2$ vs τ) shows a 48% reduction in the peak correlation of normal fluctuating velocities. A 60% reduction in the streamwise correlation of u' signals (Figure 3.72, $R_{u'_1u'_2}/U_\infty^2$ vs τ) was obtained.

This is a major difference that was not so obvious in the rms normalized correlations in the previous section. Cross-correlation results at this station are shown in Figure 3.73 ($R_{u'_1v'_2}/U_\infty^2$ vs τ). This figure shows a 54% reduction in peak value, which has narrowed the same amount in width. It is interesting to note that the correlation function is very close to zero for the most part at values $\tau < 0$ for the manipulated boundary layer, in comparison to the regular case with a positive value of 0.00004 in a relatively long range negative τ ($-0.6 > \tau > -2.0$).

The most striking change in the entire correlation occurred in the Reynolds stress signatures (Figure 3.74, $R_{(u'v')_1(u'v')_2}/U_\infty^4$ vs τ). The major changes in these correlation results are an 84% reduction in peak and a 97.2% reduction for the rest of this correlation function. It is clearly evident that this result demonstrates the fact that there is hardly any correlation between the two Reynolds stresses at .6δ and .4δ. In other words, in addition to the results in previous figures, one might be convinced that u' and v' signals are decoupled a great deal. This will be further explored in the conditionally sampled results of the large-scale motions, presented in the following section.

3.5 Conditionally Sampled Large-Scale Motions (LSMs)

This section is devoted to a description of the results of the conditionally sampled large-scale motions (LSMs) and the ensemble averaged data of these structures' signatures for both regular and manipulated boundary layers. These were obtained by simultaneous hot-wire anemometry and laser flow visualization performed at station A

(ξ = 20). Note that three signals, u', v', and u'v', are discussed here. Note also that based on better visibility of the top x-wire array, the data were sampled with signals of the probe, which was located at y=0.6δ. The lower x-wire array was located at .4δ and was .5δ downstream of the top array. In order to find the upstream and the downstream border of the signals related to the averaged LSMs passing by the probe located at y=.4δ, a simple geometrical analysis on an ideal LSM was performed. To this end, a sketch of the side view of a LSM was plotted, and using the suggested 33° angle (Falco, 1974) of the upstream side of an ideal large eddy structure and the average convective velocity of a typical LSM at the probe position, the approximate location of front and back of the averaged scales was estimated. A schematic of the LSM used for the above procedure is shown in Figure 3.75.

In order to demonstrate the changes in motions in the large-eddy structures when the turbulent boundary layer was manipulated, the abovementioned signals from both cases were conditionally sampled. The method of sampling from movies is explained in Chapter 2. The sampled data were then averaged and plotted, mainly to observe the dynamics of the flow inside the bulges (refer to Falco, 1977 for details of this technique) and outside the bulges in the "valleys". Ideally, a large eddy in the turbulent boundary layer is assumed to look from a side view like the structure shown in Figure 3.75, with the flow moving from right to left. The fluctuating velocity and Reynolds shear stress signals, when normalized by friction velocity $u_{\tau\theta}$ (see Tennekes and Lumley, 1972), are shown in Figure 3.76 with separate horizontal axes. The two

vertical axes in the middle portion of the signals represent the boundaries (upstream = right-hand side, and downstream = left-hand side) of the large eddies sampled in this experiment. Therefore, the distance between these two vertical axes represents a normalized streamwise length of the LSMs at the probe location. The signals outside these two lines indicate the average activity of the flow upstream and downstream of the LSMs in this experiment. For comparison, signals of the top x-wire probe for both regular and manipulated boundary layers are shown in the same figure. Figure 3.77 shows similar signals obtained with the lower x-wire probe located at y = .4δ (and .5δ downstream of the top x-wire array).

A comparison of the ensemble-averaged signals when normalized by u_τ both at .6δ and .4δ indicates a significant reduction in the transfer of low momentum fluid into the high momentum fluid region when the manipulators were present. The distribution of $\langle u' \rangle$ and $\langle v' \rangle$ signatures inside the LSMs show more symmetry in the manipulated layer when compared to the unmanipulated case. In the same configuration, the Reynolds stress signals show an increase both upstream and downstream of the LSMs, with a reduction inside the LSMs at y=.6δ.

Figure 3.76 indicates a 100% increase of wallward normal motion in the upstream boundary and a small increase in the downstream boundary, with a large percentage increase of upflow in the downstream portion of the LSMs. The ensemble-averaged streamwise velocity at .6δ changes are as follows: a 13% increase in the upstream portion with no change at this boundary and a 25% decrease in the upstream valley of the LSMs. A 15% increase in boundary, with no change in the downstream portion of

the average LSM is indicated in Figure 3.77. The Reynolds stress $\langle u'v' \rangle_1$ associated with the above sweeps show a 20% increase in the upstream boundar, along with a 16% reduction in the upstream portion of the average LSM, as indicated in this figure. The signal inside the average LSM is flat, indicating no signature with the LSM. A sharp negative Reynolds stress peak at the downstream boundary of the LSM is too complicated to explain here. It is unclear why this sharp Reynolds stress persists at this part of the manipulated LSM. Further investigation is needed.

The ensemble-averaged signatures of LSMs at .4δ, normalized with the $u_{\tau\theta}$, are shown in Figure 3.77. The changes at this y location are very significant, and reflect an even stronger effect of the manipulators on the flow dynamics closer to the wall. The most dramatic change occurred in the Reynolds stress signal, with a 30% reduction of the entire signal (refer to Figure 3.77). The strong change of wallward normal motion $\langle v' \rangle_2$ near the downstream boundary of the LSM corresponds to a 37% reduction. On average, no change in the central portion of the LSM appears in the same figure. This, combined with a 37.5% reduction in the streamwise velocity $\langle u' \rangle_2$ in the same region of the large eddy, caused a reduction of the Reynolds stress inside these large motions. The downstream boundary of the LSM shows a 75% reduction in the streamwise velocity. An overall result marks a total of 30% reduction in the long time average Reynolds stress in the signature shown in Figure 3.77.

A comparison of the ensemble-averaged signals, when normalized by the freestream velocity (U_∞) inside the large scale motions (LSMs) both

at .6δ and .4δ, indicates the same picture, but with somewhat large shifting in the Reynolds shear stress signals.

Figure 3.78 shows a 29% and 50% increase of wallward normal motion in the upstream portion and boundary, and a 15% increase in the downstream portion, along with no change in this boundary of the LSM's. The ensemble-averaged streamwise velocity at .6δ changes are as follows: a 30% increase in upstream portion with no change in this boundary, and a 27% decrease in the upstream valley of the LSM. The unchanged downstream portion and boundary of the average LSM is indicated in Figure 3.78. The Reynolds stress $\langle u'v' \rangle_1$ associated with the above sweeps show a 35% reduction in the upstream boundary, along with a 50% reduction inside the average LSM as indicated in this figure. A 10% Reynolds stress reduction in the downstream boundary of the average LSM, along with a 39% reduction in the overall long time average inside and outside of these scales, is important to note. Notice that the signal demonstrates a flat signature for a good portion of the average LSM. Although no significant change occurs at the boundary, the downstream portion shows a sharp negative peak. This is the same peak mentioned earlier in the $u_{\tau\theta}$ normalized signals which is difficult to understand.

The ensemble-averaged signatures of LSMs at y = .4δ, normalized with the freestream velocity, are shown in Figure 3.79. Similar changes to those found in .6δ, but with higher magnitudes, are also observed in these signals. The most dramatic change occurred in the Reynolds stress signal, with a 60% reduction in the entire length of ensemble-averaged signal at .4δ; inside and outside the averaged LSM (refer to Figure 3.79). The strong change of the wallward normal motion $\langle v' \rangle_2$ in the

downstream boundary of the LSM indicates a 48% reduction. An average of 35.5% decrease in the central portion of the LSM is shown in the same figure. This, combined with a 37.5% reduction in the streamwise velocity $\langle u' \rangle_2$ in the same region of the large eddy, resulted in the loss of the Reynolds stress signal inside these large motions. The downstream boundary of the scale shows a 75% reduction in the streamwise velocity. This marks a total of 60% reduction in the overall Reynolds stress in the signature shown in Figure 3.79.

When the signals were normalized by their respective rms values, they appeared similar to the comparisons with $u_{\tau\theta}$. These signals are shown in Figures 3.80 and 3.81. In addition, for reference purposes, the signals were normalized by the friction velocities ($u_{\tau n}$), which were obtained from the slope of the mean velocity near the wall in each case. These results are presented in Figures 3.82 and 3.83. They appeared similar to the comparison with U_∞.

It is therefore also shown here that the conditionally sampled data are consistent with the space-time correlation results at $20\delta_0$.

3.6 Accuracy

In this section a brief discussion of the maximum errors resulting from instrumentation and calculation will be presented. Errors resulting from the conditional sampling (670 samples in each case) technique have not been calculated. The errors due to sampling, however, are assumed to be small. This assumption is based on a comparison with similar results in regular boundary layers obtained by

Falco (1983) from his LSMs. It appears that Falco's ensemble-averaged signals at $y = .75\delta_{local}$ are in consistent with the signatures obtained at $y = .6\delta_{local}$ in this experiment. Notice that the sample size in the present experiment was one order of magnitude larger. It has been shown that the ensemble-averaged signatures in LSMs do not depend on R_θ over a range of $730 < R_\theta < 3116$. This was substantiated for $R_\theta = 2542$ in the present experiment.

The A/D was tested with a 3.75-volt input. The output was 3.75 ± .002 volts, or ± .006% in converted anemometer voltages. This error converts to 1.1% and .6% error in the streamwise and normal velocity components, respectively. The pressure transducer contributed a maximum of 1% error to the freestream velocity. The error of the A/D due to sampling rate is about .01%, which is negligible. The errors due to the calibration curve (using the Collis and Willams parameters) were .002% in velocity form. The sum of the above errors is at most 2.4 and 1.9 for the streamwise (u') and normal (v') velocity components respectively. This amounts to a 2% error for components. Based on the above error in u' and v', the error in u'v' was estimated to be less than 4%.

The error in local skin friction measurements obtained from the slope of the mean velocity profiles at the wall was calculated. The error bars on the most important factors which influence the measurement of the slope of the mean velocity profile at the wall were determined as follows:

1) measurement of probe position 3.% change in C_{fn};

2) hot-wire wall effects for the insulating test wall showed up

only below $y^+ \simeq 2$ (in excellent agreement with the work of Bhatia el al, 1982), and hence did not affect the measurements in this experiment;

3) the accuracy of the calibration from day to day of a burned-in hot-wire resulted in ± 1.5% changes in C_{fn}; temperature changes during a run, ± .2%; and the accuracy of the curve fit, ± .3%. Thus, the overall measurement accuracy of the wall slope technique is estimated to be ± 3.5%. In an attempt to eliminate the effect of changes in wire calibration in the C_{fn} calculation, a procedure was devised in which a calibration is made when a profile was taken. The wire was recalibrated after the profile data was taken. Minute changes in the calibration constants were always noted. However, this procedure reduced the overall error by another 0.5% to $\simeq$ ±3% at the expense of much time and effort.

CHAPTER 4

DISCUSSION

In Chapter 3 flow conditions and the consequences of manipulating the outer layer flow structures in turbulent boundary layers were presented. In this chapter these results will be examined and interrelated in order to demonstrate this effect of the manipulation on the physical mechanisms involved in the associated drag reduction and relaxation to the normal (unmanipulated) boundary layer situation. To this end, it is appropriate to place emphasis on the detailed study of large scale motion alterations and the role of the TAPPM wake in interrupting the interaction of outer layer fluid with near-wall layer fluid. Based on the difference between the values of $u_{\tau\theta}$ and $u_{\tau n}$, it is helpful to discuss the effect of each separarately. In cases of correlation, they are referred to accordingly. This analysis is an attempt to correlate the detail structural changes in large eddy geometry and the dynamics which resulted from the presence of the TAPPM in the boundary layer. Results of other investigations will be referred to whenever appropriate. This will corroborate the conclusions drawn in the present discussion.

4.1 Flow Condition and Time-Averaged Integral Characteristics of Regular and Manipulated Boundary Layers Based on the Momentum Balance Analysis

The two major changes in Experiment II namely _ freestream turbulence level and thickness of the TAPPM plates _ played an important

role in changing the net drag reduction from zero in Experiment I to 10% at ξ = 58.23 in Experiment II. The lower turbulence intensity (refer to Figure 2.6) is the key to the improved two-dimensionality of the turbulent boundary layers (Bradshaw, 1965) developed on the test wall (refer to Figure 3.4). This plus reduction in thickness of the plates suggested by other investigators (Corke, 1981; Hefner et al., 1983; Anders et al., 1984; Plesniak et al., 1984), resulted in the successful net drag reduction mentioned above. It was shown that any beneficial effects of the TAPPMs occur at downstream distances greater than 50-80δ_o (Rashidnia and Falco, 1983). This proved to be the case for a second time in the present experiments, resulting in a 10% net drag reduction at $\xi \simeq 60$. Similar trends of local skin friction reduction, overshoot, and relaxation were obtained by Anders et al (1984). Figure 4.1 shows the streamwise variation of $C_{f\theta}$ vs ξ. However, assuming a two-dimensional flow in the manipulated boundary layers, which might have suffered from some three-dimensional effects (difficult to avoid), skin drag results in different laboratories do not seem to show a unified trend. One may therefore speculate that when the TAPPM is in place, the development of the manipulated boundary layer is susceptible to three-dimensional flow caused by some kind of very small irregularity (e.g. angle of attack, spanwise and/or streamwise ripples, burrs at upstream/downstream edges of the plates) in the device which, in turn, develops a separation around itself. The skin friction drag evolution for similar flow conditions of several investigators has been also discussed by Anders (1985). It is thus necessary to examine the skin drag directly measured by different independent techniques available

today (e.g., Westphal, 1985; Lemay et al., 1985; Mumford and Savill, 1984; Lynn and Screenivasan, 1985). The visualization results presented in Chapter 2 (refer to Figure 2.18), did not show separation. (Note, however, that the resolution of this technique is not high enough to detect long thin separation regions of thickness the order of a few thousandths of an inch). It is of interest to note that the spanwise C_f results from Preston tube measurements indicated rather similar percentage variations in their peaks about their averages in the manipulated case. (They were not presented here because of their dependence on the universal law of the wall).

Using the momentum balance, present results indicate a $C_{f\theta}$ reduction comparable to other investigators for up to about $51\delta_o$ (Corke, 1981; Bertelrud et al., 1982; Anders et al., 1984). Figure 4.1 show even higher reduction, up to 45%, in local skin friction coefficient. This plus the results of the visualization experiment indicate that the sublayer fluid moved 25% less distance into the outer layer region (reduced from $y^+_{Reg.} = 240$ to $y^+_{Man.} = 179$, over a range of $\pm 3.3\delta_o$ around $\xi \simeq 20$). In addition, burst frequency in absolute value was reduced at $\xi \simeq 51$. It therefore justified the maximum $C_{f\theta}$ reduction in the region. On the other hand, it was shown that the sublayer thickness increased from 15-20% (refer to Figure 3.40) over the major downstream distance of the test wall after the TAPPM in the manipulated boundary layers. The increase in sublayer thickness was hypothesized by Corke (1981), but not supported with data. Corke's estimate was that sublayer thickness increased by 17%. From the present experimental results, it is now strongly evident for the first time, that the sublayer thickness in the

manipulated boundary layers does indeed increase (refer to Figures 3.40 and 3.41). This is consistent with the drag-reducing effects of riblets (Walsh, 1980 and 1982) which in fact increase the thickness of the sublayer. In the case of the TAPPM, the sublayer thickens for at least the first $50-60\delta_o$. This in turn makes the interaction of typical eddies with a thick sublayer somewhat less chaotic (Falco, 1983), leading to local skin friction reduction. The Typical Eddy/wall interactions with a thick sublayer are labeled type 1 and type 2 (as described by Falco). Type 1 was visually observed in a vortex ring/moving wall interaction experiment in the TSL which involved a rearrangement of sublayer fluid without the break-up of the typical eddy (in this case the vortex ring; also see Liang, 1984). In type 2, this interaction lifts the sublayer fluid up into the logarithmic region without the breakup of the Typical Eddy itself. However, the thickened sublayer does not appear to be the main physical mechanism behind the reduced skin drag. Otherwise, the relaxation to the normal situation after $\xi \simeq 75$ (obtained from the momentum balance) would not have occurred (refer to Figure 3.49).

The footprint (wall event) of the typical eddy is called the "pocket" flow module (Falco, 1980), showed that this interaction was weakened at $\xi = 51$ when TAPPMs were present. The wall event mean period T_B, when scaled with inner layer variables (u_τ and μ/ρ) over a range of Reynolds numbers ($738 < R_\theta < 4000$), has been shown by Falco (1983) to be $\rho T_B u_{\tau\theta}^2/\mu \simeq 30$ in regular boundary layers. Results of a similar experiment in the normal boundary layer (using $u_{\tau\theta}$ for non-dimensionalization of the burst period) confirms this number ($T_B^+ = 29.67$) at $R_\theta = 3495$. Similar normalization in the manipulated case

indicated $T_B^+ = 21.7$. The reduction of the inner wall normalized burst rate implies more wall interaction at this station, although in absolute value the number of wall events was reduced by 40%. On the other hand, when these mean periods were scaled with the outer layer variables (U_∞ and δ_{local}), they indicated 50% fewer bursts ("pockets"), consistent with the maximum skin friction reduction at this station. This conclusion takes into account Rao's (Rao et al., 1971) outer-layer scaling results, from which he concluded that the wall bursts scale with outer-layer parameters. Overall, interpreting these results in terms of the skin friction changes obtained from the momentum balance does not lead to a constant picture.

4.2 Large Eddy Characteristic Changes Associated with Drag Reduction in Manipulated Boundary Layers

A comparison of fluctuating components in boundary layers indicated that distinct changes occurred in the LSMs when TAPPMs were present. Temporal correlations at $\xi = 20$ were significantly modified. The reduction of streamwise velocity components inside and outside the large-scale motions, represented by ensemble-averaged signals at both $y = .4\delta$ and $.6\delta$ with the x-wire arrays, confirmed the reduction of the rms of the same signal in the fluctuating velocity profile results. These results are presented in Figures 3.33 and 3.34 from the independent measurement in Experiment II. Farther downstream, at $\xi = 51$, the correlations returned closer to their normal boundary layer level. This indicates that the LSMs regained most of their strength. The downstream relaxation of fluctuating components were also investigated by

Guezenenec et al. (1985). Their results showed that at $\xi = 45$ (close to station C in the present experiment) u', v' and u'v' had a small amount of overrelaxation. This, interestingly, supports the mean velocity and space-time correlation results at $\xi \simeq 51$. There is, however, a significant difference in the net drag reduction and its relaxation farther downstream. The IIT research team's net drag results (in particular, refer to Plesniak, 1984) did not show a sharp relaxation to normal boundary layers when the manipulators were present. Thus there is a significant difference in the net drag reduction and its relaxation results between the present results and the ongoing experiments at IIT. It is therefore concluded in accord with Hefner et al. (1983), that the resultant relaxation disturbances become significant by the order of 50-80 boundary layer thicknesses downstream of the manipulators. This conclusion refers the three-dimensional effects discussed earlier, and suggests the development length needed before they become important.

A detailed study of the ensemble-averaged signals in the LSMs indicate a significant reduction in the sweeps at .4δ in their upstream and downstream portions, and large reduction in the Reynolds stress inside bulges at both heights (.4 and .6δ) when the TAPPM was in place. Despite these large signal changes, it is not hypothesized that the large scale motions lose their identity. The ensemble-averaged u' and v' signals are almost identical to those of Falco's (1977 and 1983) results in the unmanipulated boundary layers. These signals, in general, did not lose their unique dynamic characteristics, when compared to their regular boundary layer counterpart (see Falco, 1977),

indicating their intact coherent structure at $\xi = 20$ in the manipulated case. However, there is a phase shift in $\langle v' \rangle$ with respect to $\langle u' \rangle$, which reflects the diminished correlation between u' and v', thereby reducing $\langle u'v' \rangle$. Visual data from movies also supports this conclusion.

In addition to the thick sublayer mechanism previously discussed, many mechanisms have been hypothesizes to be responsible for skin drag reduction in the manipulated boundary layers. These claims have not, however, been supported by data. Based on the sublayer flow visualization, and in light of the large-scale motions data at $\xi \simeq 20$, and to the wall event visualiation at $\xi \simeq 51$, following it is concluded here: a strong inhibition in the interaction of the inner and outer layer flow structures is another important mechanism responsible for the skin drag reduction in manipulated boundary layers. This has been further supported by the evidence that the wake of the manipulator plates maintains a strong coherence at $\xi = 20$, but by $\xi = 51$ is distributed throughout the turbulent boundary layer and reaches the wall. In other words, the relaxation of the skin friction drag in the manipulated boundary layer to normal conditions by about $60\delta_o$ is essentially unavoidable, unless the TAPPM is redesigned to generate a stronger, coherent wake, three-dimensionalities are created in the flow to prevent the relaxation. Alternatively, a second TAPPM may be placed upstream of the relaxation region.

4.3 Characteristics of Regular and Manipulated Boundary Layers Seen from the Perspective of the Wall-Friction Velocity ($u_{\tau n}$) Obtained by Local Means

The results of skin friction measurements obtained from the mean velocity gradients near the wall indicated a 15% to 25% lower local skin friction than that of the Clauser plot counterparts in the regular boundary layers. However, they were reduced in the manipulated case. The change in C_{fn} is shown in Figure 4.2. For comparative purposes, results obtained by other inestigators are displayed in the same figure. Note that they were obtained through different measurement techniques (both used a skin friction balance). All the results indicate lower skin drag in the manipulated boundary layers with a gradually lower relaxation pattern. A 2% net drag reduction was obtained when the C_{fn} were used in a simple drag analysis. The formulation is shown in Appendix B. Notice that a linear extrapolation was made to estimate the Θ at the trailing edge of the second plate of the TAPPM and to calculate the device drag. The resultant net drag from momentum balance and the local skin friction integration are shown in Figure 4.3.

It is more likely that direct measurements are not biased by the three-dimensional effects mentioned above. This is in agreement with the thickened sublayer results achieved in the present experiment. Furthermore, the wall event ("pocket" module flow) period in absolute value, T_B, in wall-unit normalized ($\rho T_B u_{\tau n}^2/\mu$), and in outer-layer-unit non-dimensionalized ($\rho T_B U_\infty^2/\mu$) form all indicate 38%, 28%, and 55% increases respectively. The longer periods between the wall events indicate that fewer pockets are forming, which is consistent with a thicker sublayer. They also indicate and slightly reduced strength of

the large-scale motions at this station, where C_{fn} is reduced 5%. Thus the difference in momentum balance results and direct skin drag measurements seems to support the suggestion that downstream three-dimensionality develops in the manipulated boundary layer. Further investigation is needed in order to answer this question.

CHAPTER 5

CONCLUSIONS

The results and conclusions presented in the previous chapters address several interrelated subjects of this experimental investigation. First, the objective of the flow facility design, construction, and performance was to develop a thick two-dimensional boundary layer (up to 10") low freestream turbulence intensity flow visualization wind tunnel, with high-quality hot-wire measurements. Next, net drag reduction in the manipulated boundary layers was obtained. This confirmed the ongoing research activities of others in the field, yet revealed sharp skin drag relaxation to unmanipulated case. Last, the detailed investigation of structural changes which were presented in the space-time correlations and the conditionally ensemble-averaged large scale motions were discussed.

The major findings of the three phases of this experimental project may be summarized as follows:

1) A high-quality flow wind tunnel with a unique (no-contraction) inlet, long enough to study the relaxation of manipulated turbulent boundary layers, was constructed. It appears possible to expand the improvements on this type of inlet configuration to achieve a wind tunnel with a low turbulence intensity and higher velocities, while avoiding a high cost contraction. This also reduces the possibility of generating streamwise Görtler vortices on the test wall.

2) Two sets of very thin tandemly-arranged parallel plate manipulators (TAPPMs), were used in an attempt to reproduce the results of other net drag reduction investigations and to study the downstream evolution of the drag changes. It was found that the thickness of the manipulator plates was of importance to both the skin friction change and the device drag. Also, the experiment with thinner plates (.003") resulted in a 10% net drag reduction only at $58.23\delta_0$ downstream of the TAPPM, which relaxed by $100\delta_0$. In each of the two separate experiments (I and II), a similar drag evolution was obtained, although the thick plates (.03") did not reduce the net drag. The local skin friction coefficient ($C_{f\theta}$) was reduced 30-45% for up to $50-85\delta_0$ downstream of manipulators in both experiments. The local skin friction obtained from mean velocity gradient near the wall was reduced by 10-20%, but did not show a sharp overrelaxation as it did when calculated from the momentum balance. A 2% net drag result was obtained from C_{fn}, taking the device drag into consideration, but no overrelaxation was shown.

3) No separation of flow was detected (to within the order of a few thousandths of an inch) over the manipulator plate surfaces. A laminar boundary layer was developed on both plates which were parallel to the test wall in the experiments.

4) The Coles constant in the "law of the wall" also underwent a sequence of changes. It increased in the $C_{f\theta}$ reduction range

region, then decreased, and finally relaxed back to the normal value (B = 5.) after $90\delta_0$.

5) The "law of the wake" portion of the mean velocity profiles also incurred some changes, which were similar to the variations in the Coles constant B.

6) The sublayer thickness increased 15-20% throughout the length of the test wall for the manipulated layers.

7) The burst frequency in the sublayer decreased by a 38% in absolute value, and by 55% when normalized by outer layer variables. It increased by 27% when normalized by the inner variables (μ/ρ, $u_{\tau\theta}$). When the burst frequency was non-dimensionalized by $u_{\tau n}$, it reduced by 28%.

8) The outward normal distance that the sublayer fluid travelled into the logarithmic region decreased 30% or 11.4% around the region of $\xi \simeq 20$ when it was normalized by $u_{\tau\theta}$ or $u_{\tau n}$ respectively.

9) The dynamics of the large-scale motions changed, but LSMs did not lose their uniqueness in geometry and the flow patterns within. The Reynolds stress of the LSMs was reduced significantly, although it increased in the "valleys".

10) The space-time correlations changed at $\xi = 20$, with significant reductions in the Reynolds stress and the streamwise components of temporal correlations. The large-eddy motions regained most of their strength by $51\delta_0$ downstream of the manipulators.

In summary, when all the information presented above are combined, it becomes clear that the TAPPM acts as a passive suppressor of the large-scale motions up to about $60\delta_0$. In that same downstream distance, TAPPMs interrupt interactions of the scales from the outer region with the inner-region-scale motions. In contrast to Corke's (1981) "aging", and NASA group's "break up" of the large eddies speculation, the large-scale motions neither "break up" nor do they lose their strength, but reappear after that distance ($60\delta_0$).

FIGURES

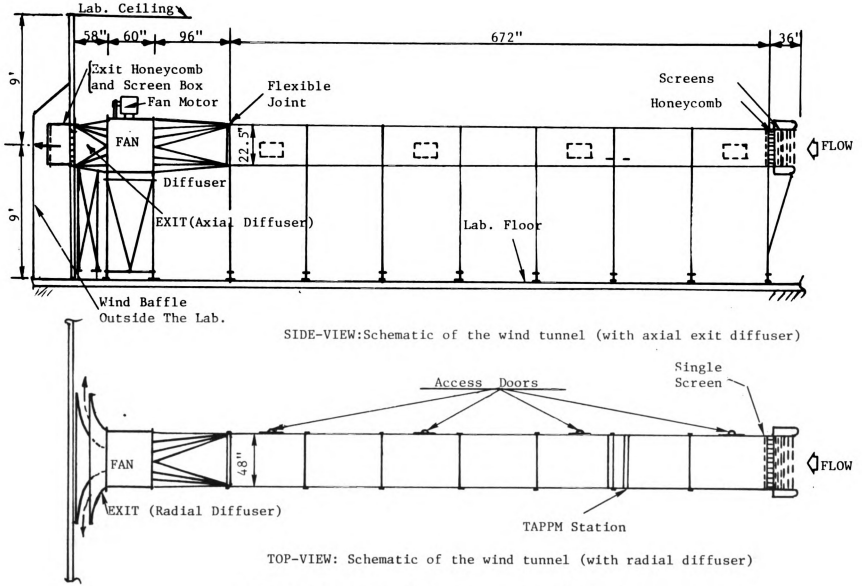

Figure 2.1 Schematic of the low-speed wind tunnel

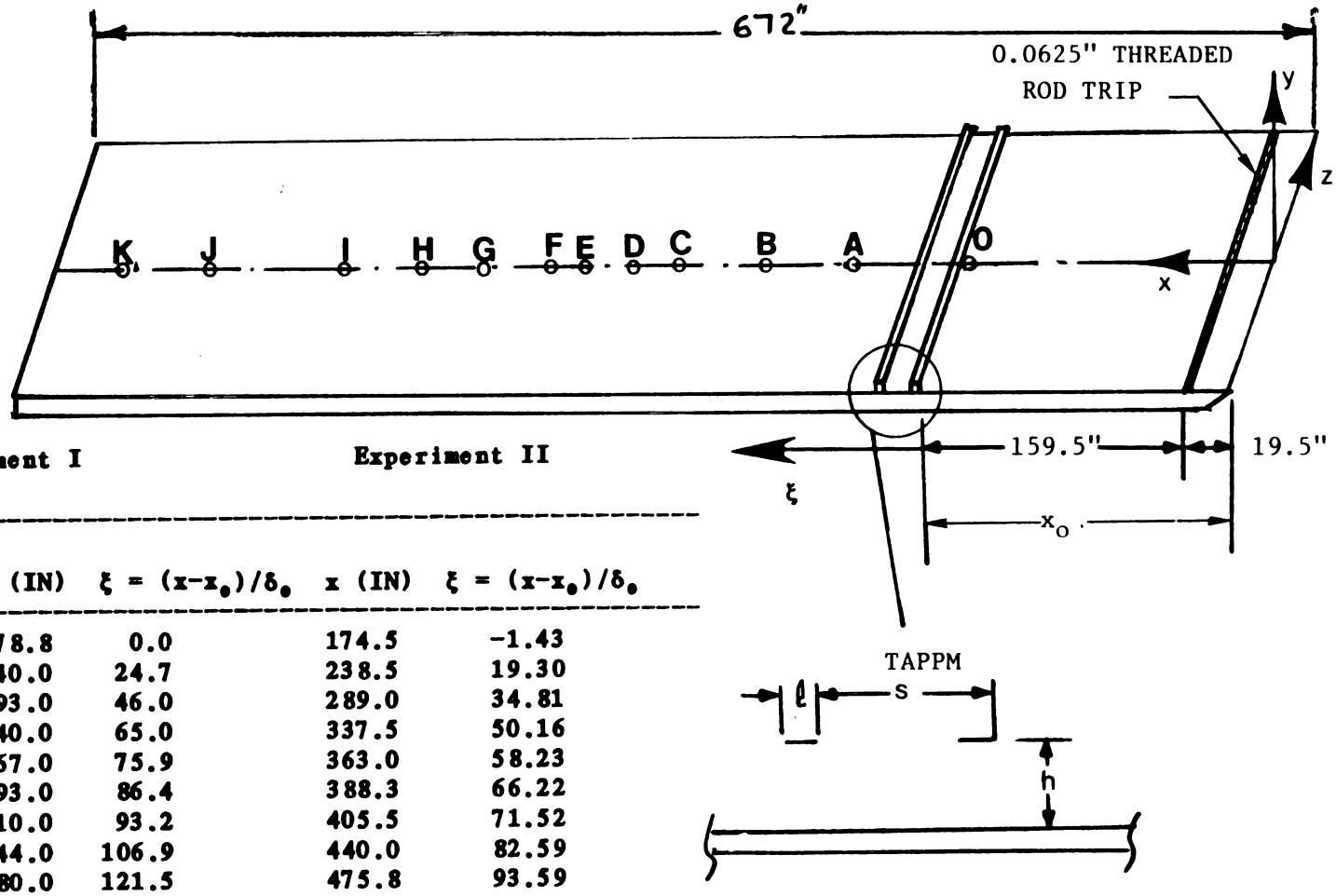

STATION	Experiment I x (IN)	Experiment I $\xi = (x-x_o)/\delta_o$	Experiment II x (IN)	Experiment II $\xi = (x-x_o)/\delta_o$
0	178.8	0.0	174.5	-1.43
A	240.0	24.7	238.5	19.30
B	293.0	46.0	289.0	34.81
C	340.0	65.0	337.5	50.16
D	367.0	75.9	363.0	58.23
E	393.0	86.4	388.3	66.22
F	410.0	93.2	405.5	71.52
G	444.0	106.9	440.0	82.59
H	480.0	121.5	475.8	93.59
I	521.0	138.0	516.8	106.88
J	594.0	167.4	594.3	131.41
K	646.0	188.4	642.0	146.52

EXPERIMENT I, $h = 0.8\delta_o$, $\ell = 1.21\delta_o$, $S = 7.74\delta_o$, $t = 0.0121\delta_o$, $R_{\theta_o} = 1450$
EXPERIMENT II, $h = 0.8\delta_o$, $\ell = 0.95\delta_o$, $S = 6.1\delta_o$, $t = 0.00095\delta_o$, $R_{\theta_o} = 2150$

Figure 2.2 Schematic of boundary layer test wall showing the TAPPM and measurement stations.

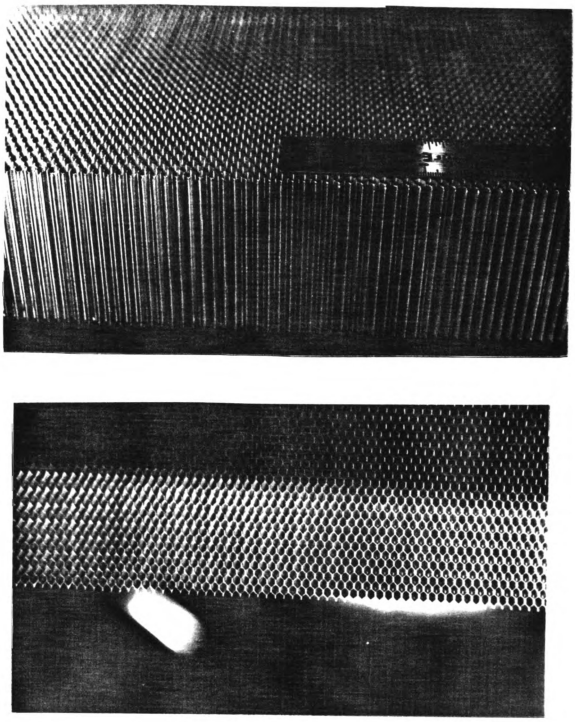

Figure 2.3 Honeycomb; Top picture shows the cell size, Bottom picture shows the uniformity of the lower edge of cells that rest on the lower side of the honeycomb box flush with the surface of the test wall at the leading edge.

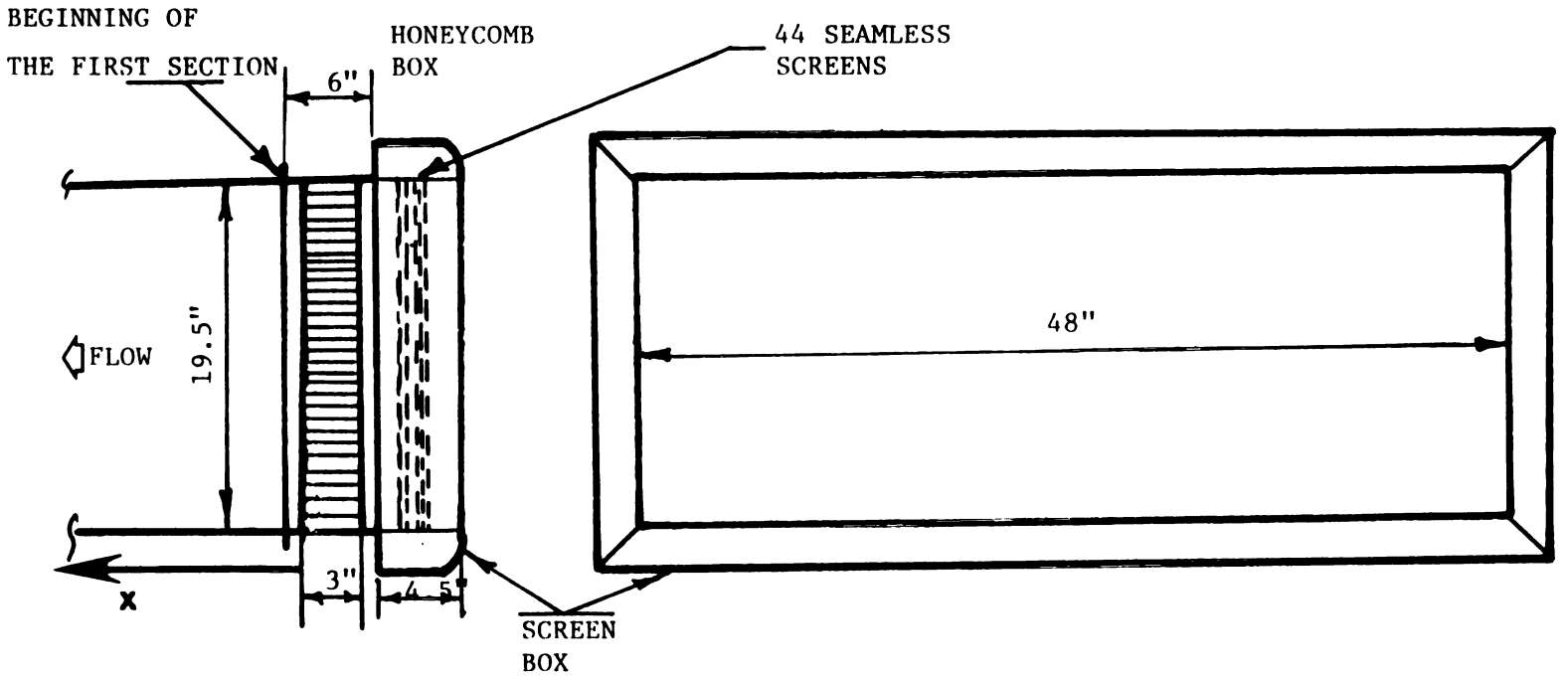

Figure 2.4 Schematic of honeycomb-screen arrangement used for experiment I.

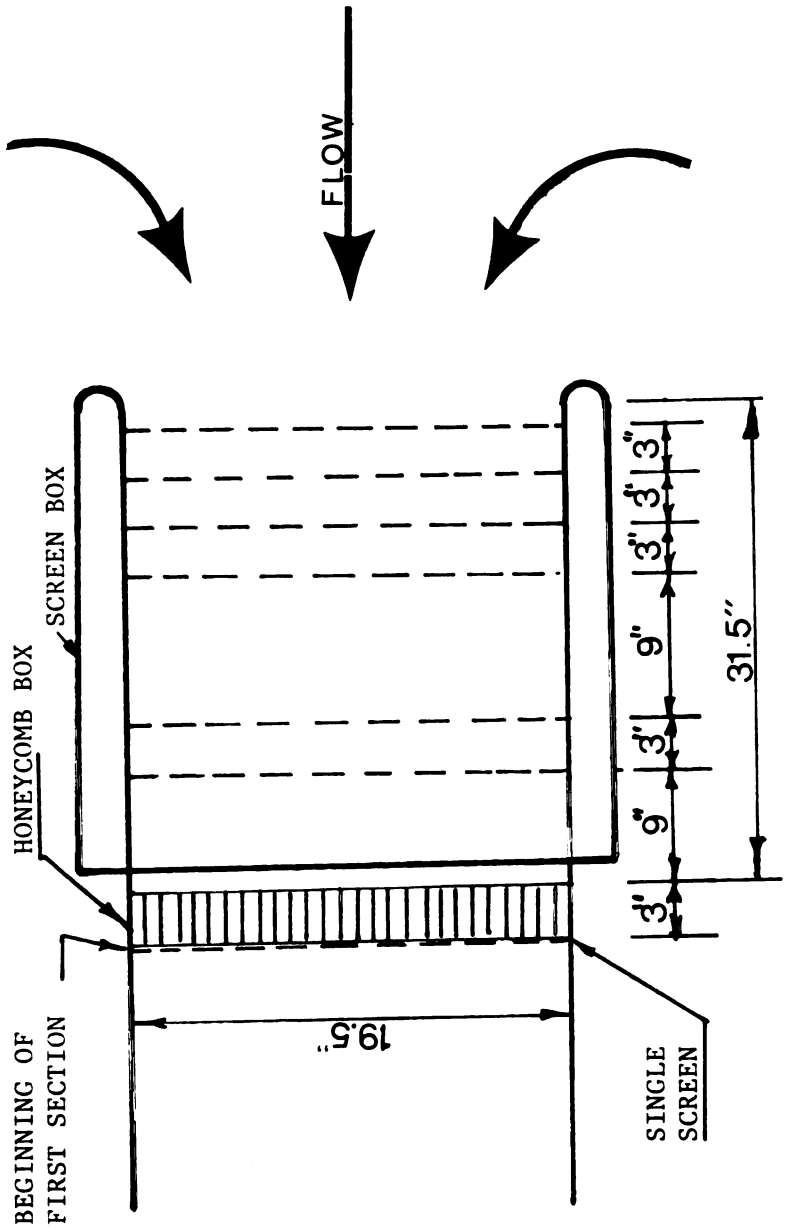

Figure 2.5 Schematic of honeycomb-screen arrangement used for experiment II.

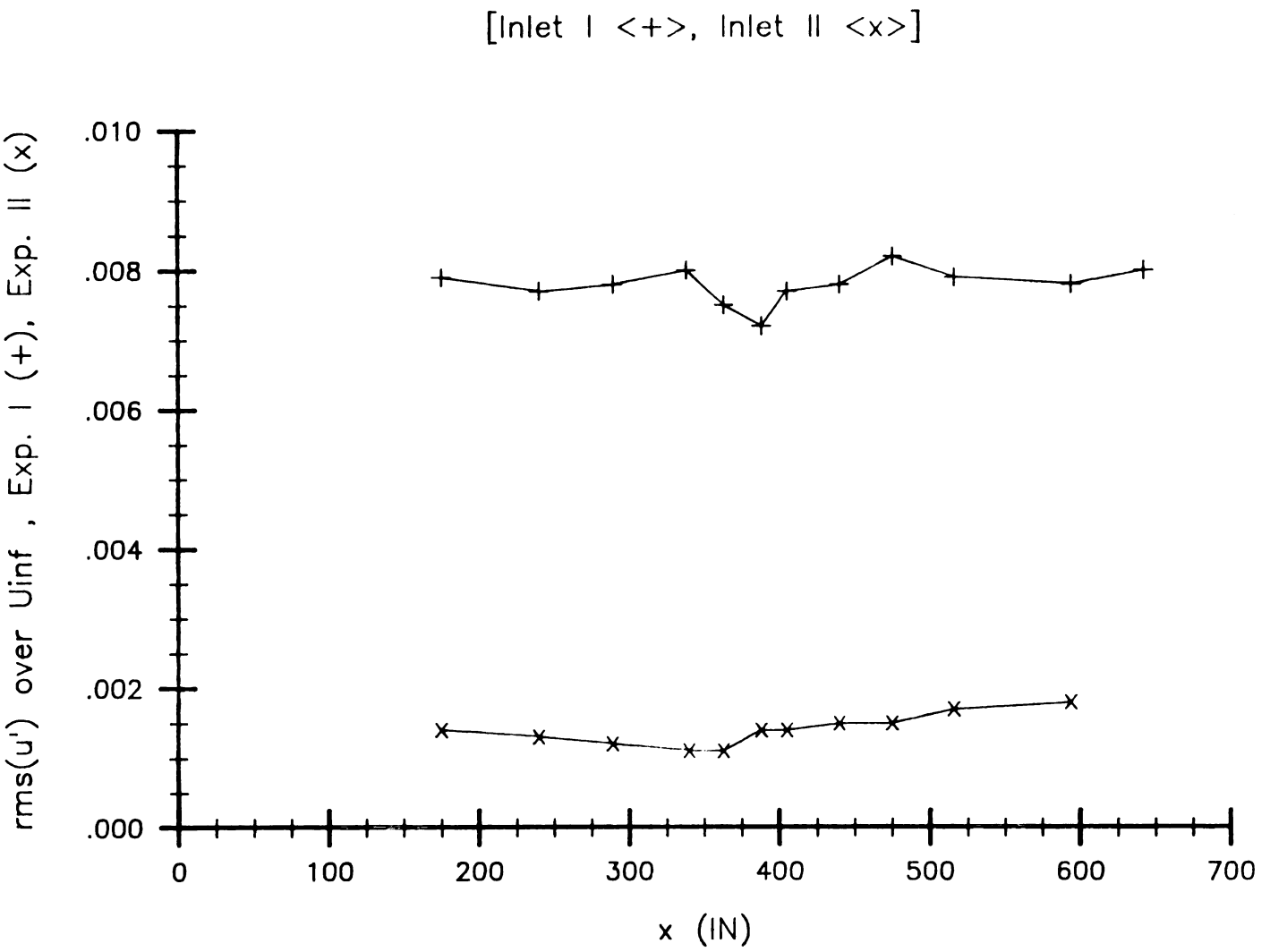

Figure 2.6 Variation of freestream turbulent intensity rms(u')/U_∞ versus x for both experiments: I (+), II (x).

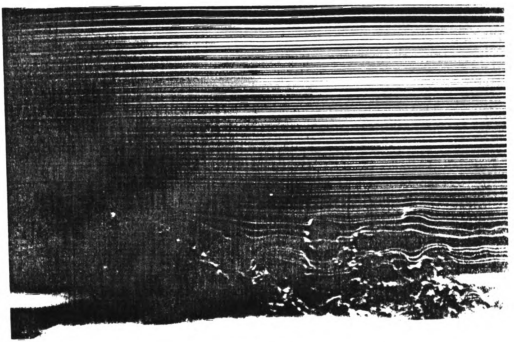

Figure 2.7 A snap-shot of the freestream and the boundary layer smoke-wire flow visualization around x = 210", (flow is from right to left).

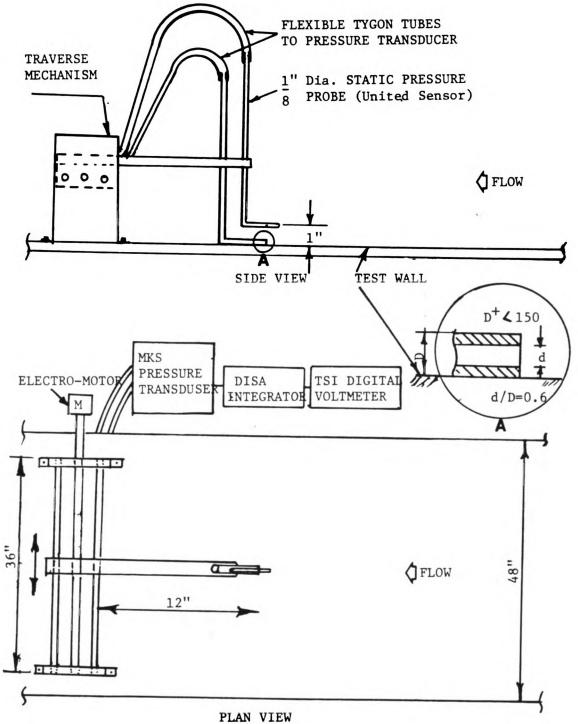

Figure 2.8 Schematic of the movable (modified) Preston tube probe.

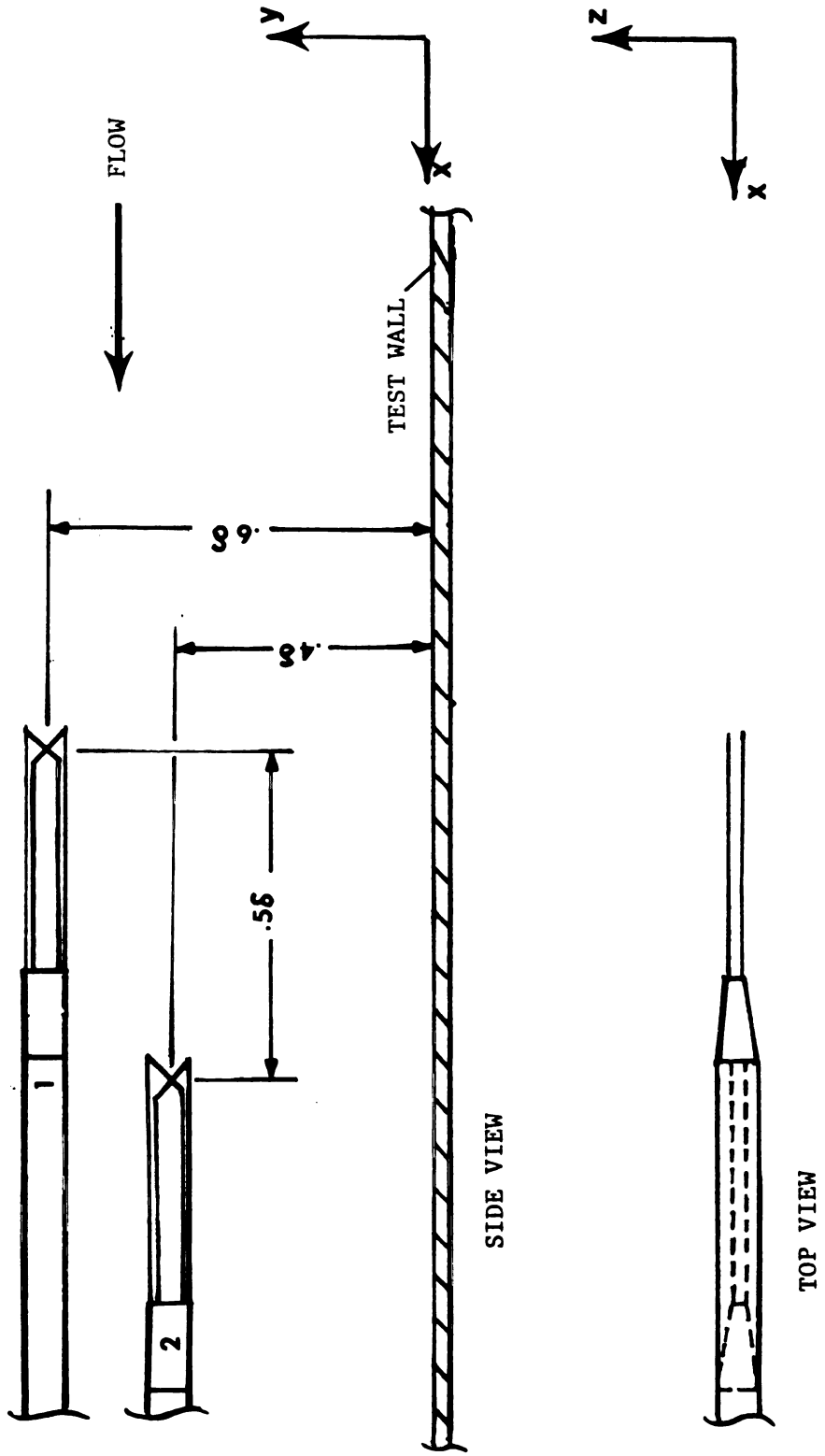

Figure 2.9 Schematic of twin-x-wire array probe.

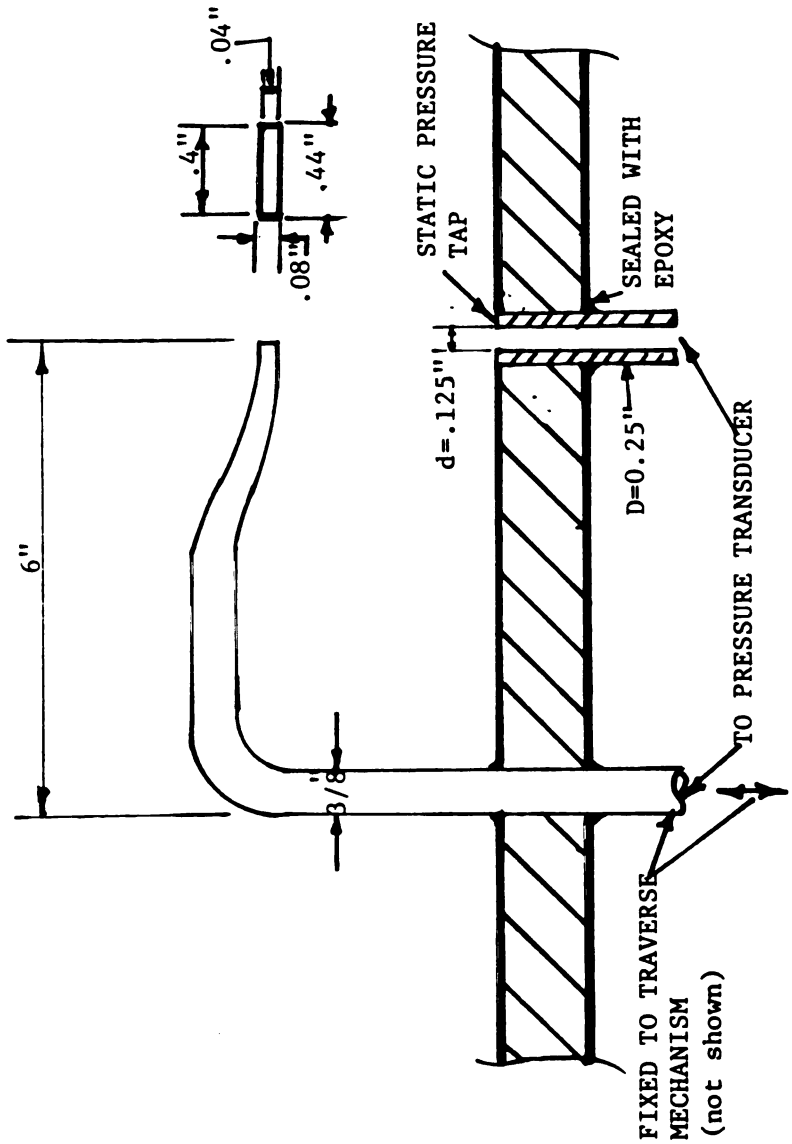

Figure 2.10 Schematic of Pitot static tube used in velocity profile survey in experiment I.

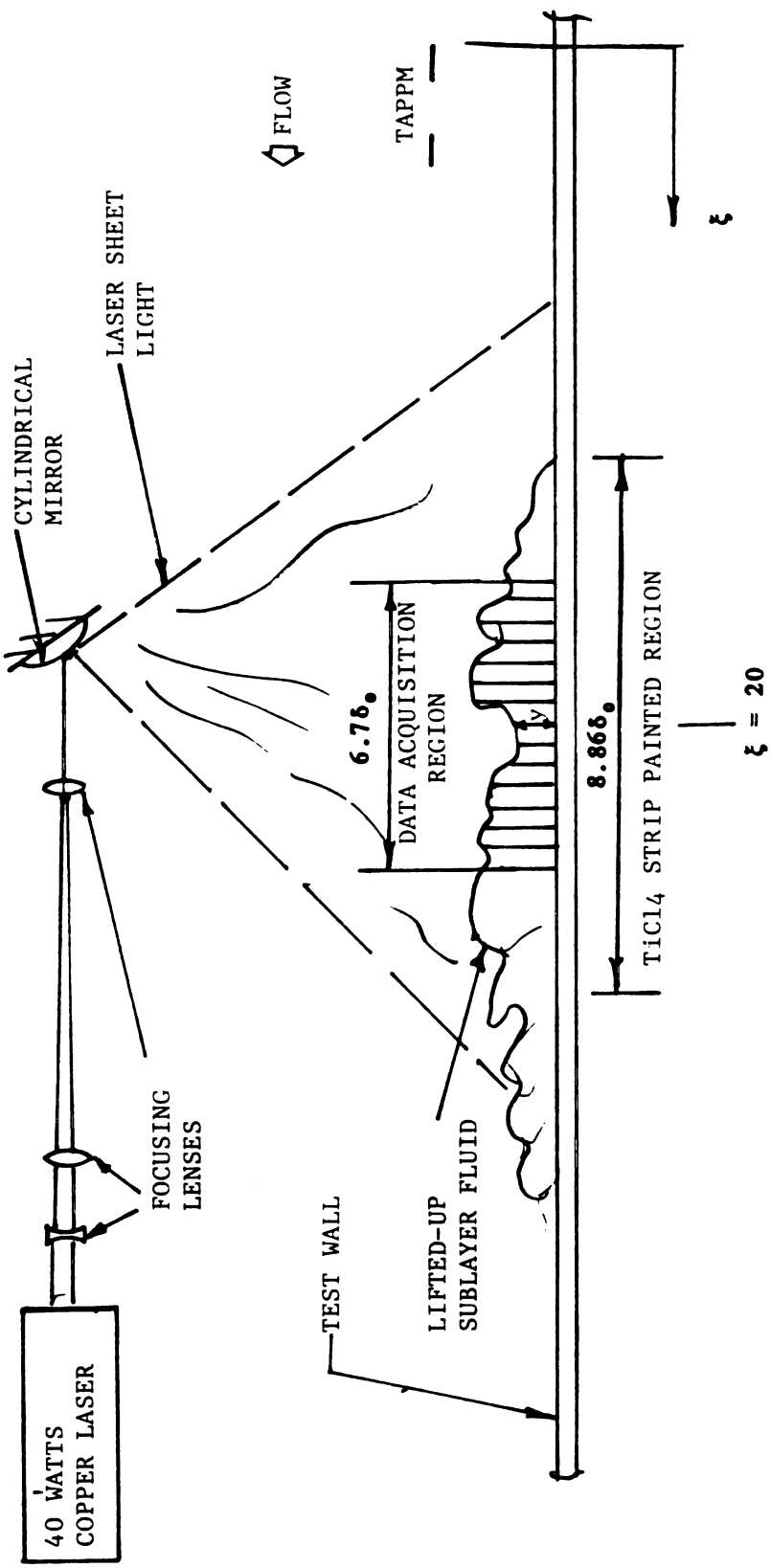

Figure 2.11 Schematic side view of laser optics and data acquisition streamwise region of inner wall flow visualization with Titanium tetrachloride ($TiCl_4$) flow marker.

CALIBRATION PROGRAMS

Data Acquisition

ALEX2	computer and A/D synchronization
RUNTST	collects u-wire and pressure trasducer calibration data

Data Reduction

CONVOL	converts bits/millivolt to voltages

Data Analysis

CAL1WIRE	determines Collis and Williams parameters
MULPLT	plots calibration data for a visual check of the result

MEAN VELOCITY PROFILE PROGRAMS

Data Acquisition

ALEX2	computer and A/D synchronization
RUNTST	collects velocity profile data

Data Reduction

CONVOL	converts bits/mollivolt to voltages (mean and fluctuations) and merges with probe positions in one data file

Data Analysis in Batch Form:

CALANL — command file for analysis and plotting programs

VELPRO — converts voltages to velocities and processes the velocity profile for four plots

MULPLT — plots the output of VELPRO as follows:

1) mean velocity profile close to the wall in the sublayer region (y vs U) for velociy slope estimation at the wall
2) y vs U of the entire velocity profile
3) Clauser plot to obtain C_{fC} based on Coles "law of the wall" parameters

VELPR3 — analyses the data and calculates the boundary layer velocity profile parameters, non-dimensionalizes the velocity profile based on two different estimations of the wall shear stress ($d\overline{U}/dy$ at wall ($C_{\tau n}$), and C_{fC} or $d\theta/dx$), and finally stores them with the rest of the information in one master data file

MULPLT — plots the output file of VELPR3:

4) y/θ vs $\overline{U}/U_\infty$
5) u^+ vs Y_+ based on both $u_{\tau\theta}$ and $u_{\tau C}$
6) $(U_\infty - \overline{U})/u_\tau$ vs $yu_\tau/\delta_d U_\infty$
7) Wake part of the velocity profile vs y/δ
8) $rms(u')/u_\tau$ vs y^+, also for near wall region
9) $rms(u')/U_\infty$ vs y/θ, also for near wall region

Figure 2.12 Velocity profile and calibration data acquisition, reduction, and analysis program sequence

CALIBRATION PROGRAMS

Data Acquisition

ALEX2	computer and A/D synchronization
RUNTST	collects twin-x-wire and pressure trasducer calibration data

Data Reduction

CONVOL	converts bits/millivolt to voltages

Data Analysis

CALFIT	determines Collis and Williams parameters
MULPLT	plots calibration data for a visual check of the result

TWIN-X-WIRE PROBE PROGRAMS

Data Acquisition

ALEX2	computer and A/D synchronization
RUNTST	collects twin-x-wire probe data

Data Reduction

CONVOL	converts bits/mollivolt to velocities
CPCN	calculates the CP and CN parameters for the x-wires
VEL4	calculates the long time record of fluctuating quantities
TIMPLT	plots long time records of fluctuating quantities
CORRELATE3	computes space-time correlations of fluctuating quantities
CORAVG	averages the space-time correlation output files of CORRELATE3
MULPLT	plots the space-time correlations
ENSMBL	selects, scales and averges the segments of the data records produced by VEL4 which correspond to large eddies striking the twin-x-wire arrey probe
NORMALIZE	non-dimensionalizes the long records of data

Figure 2.13 Twin-x-wire probe calibration, data acquisition, reduction, and analysis program sequence

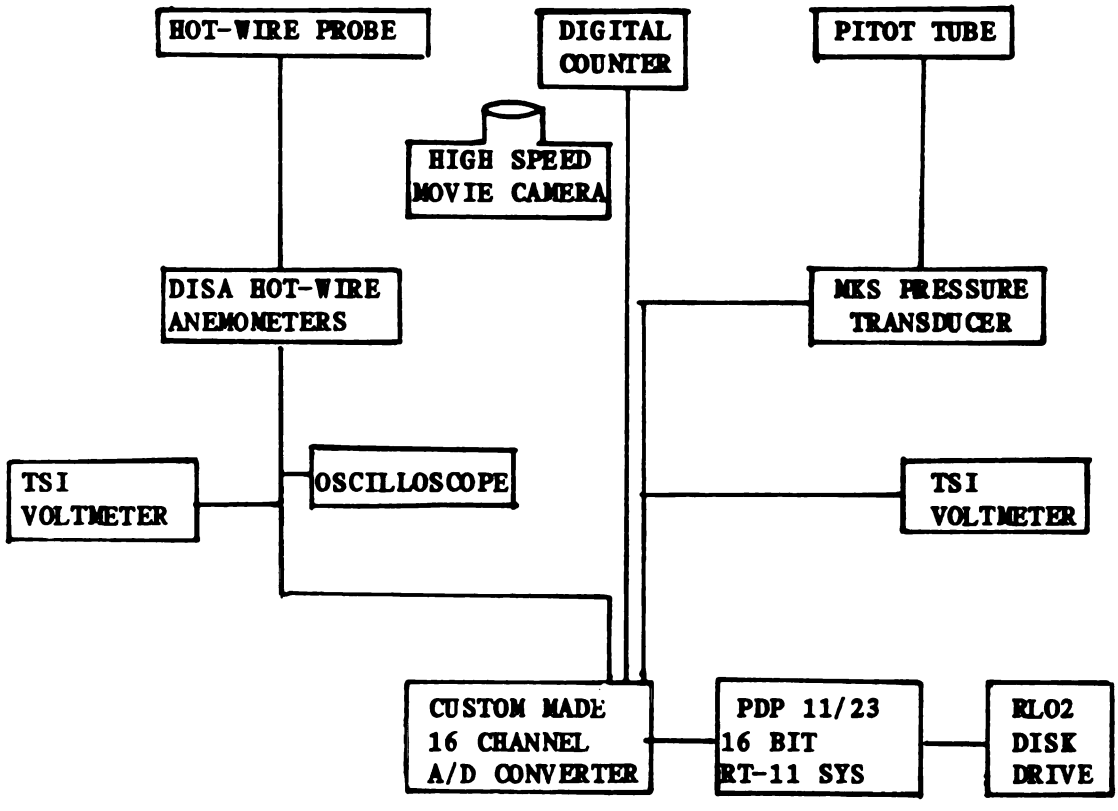

Arrangement of instruments used for hot-wire anemometry and simultaneous visual data acquisition.

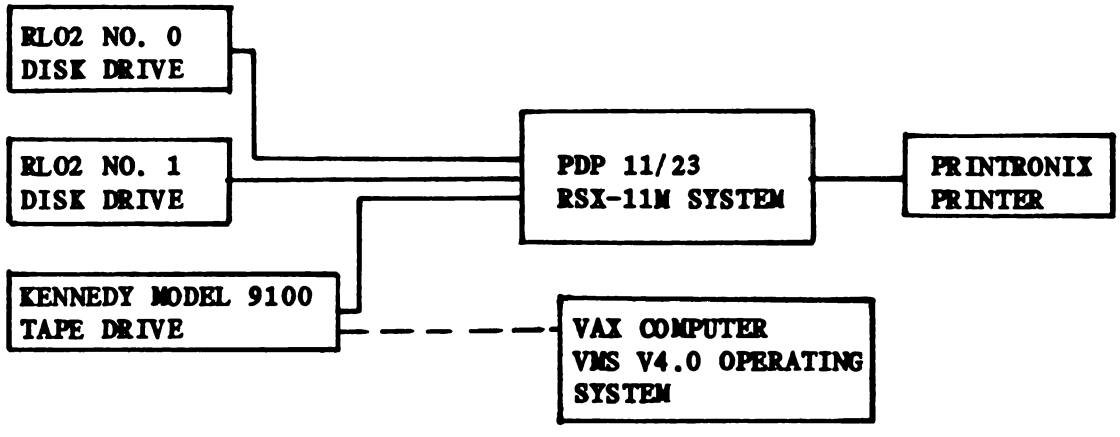

Figure 2.14 Block diagram of data acquisition and processing system.

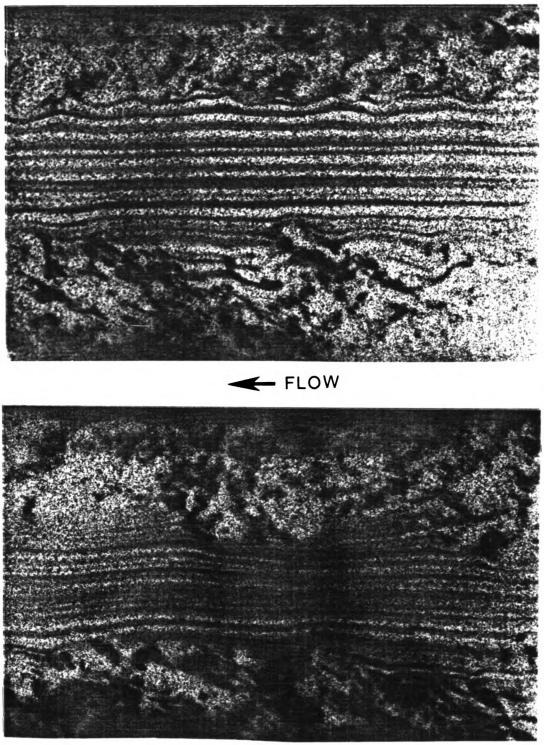

Figure 2.15 Smoke-wire flow visualization with high-speed movie camera at x = 520" (13.2m); straight streaklines (top); wavy streaklines in the freestream flow due to passage of large scale motions.

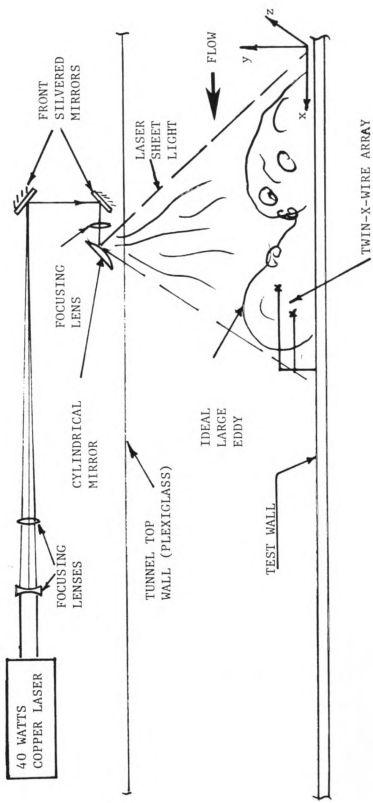

Figure 2.16 Schematic of laser optics and x-wire array probe arrangement used in simultaneous visualization and anemometry at 205$_\theta$.

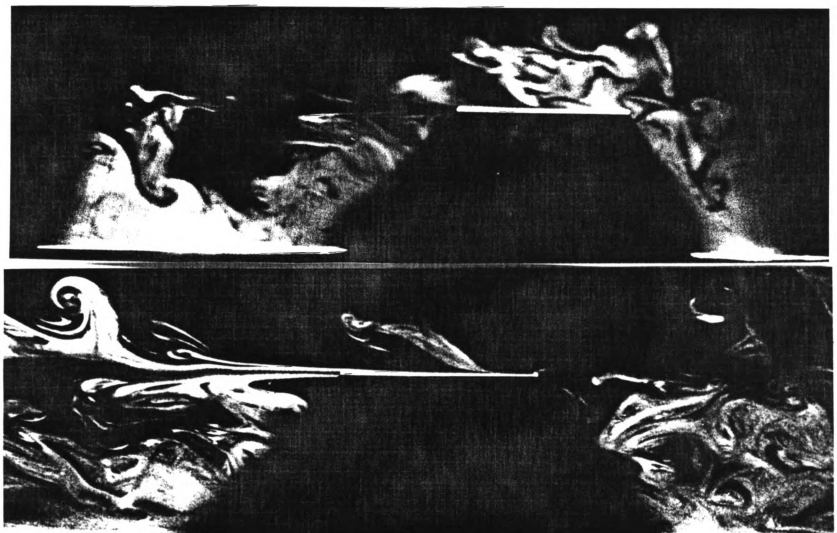

Figure 2.17 Smoke flow visualization around the downstream plate of TAPPM device ($h = .8\delta_o$) at $z = 0$ (top); $z = 30.5$cm in the turbulent boundary layer.

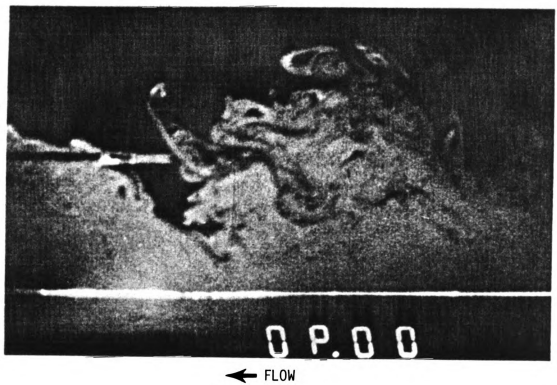

Figure 2.18 An example of a large eddy structure striking the probe in a turbulent boundary layer.

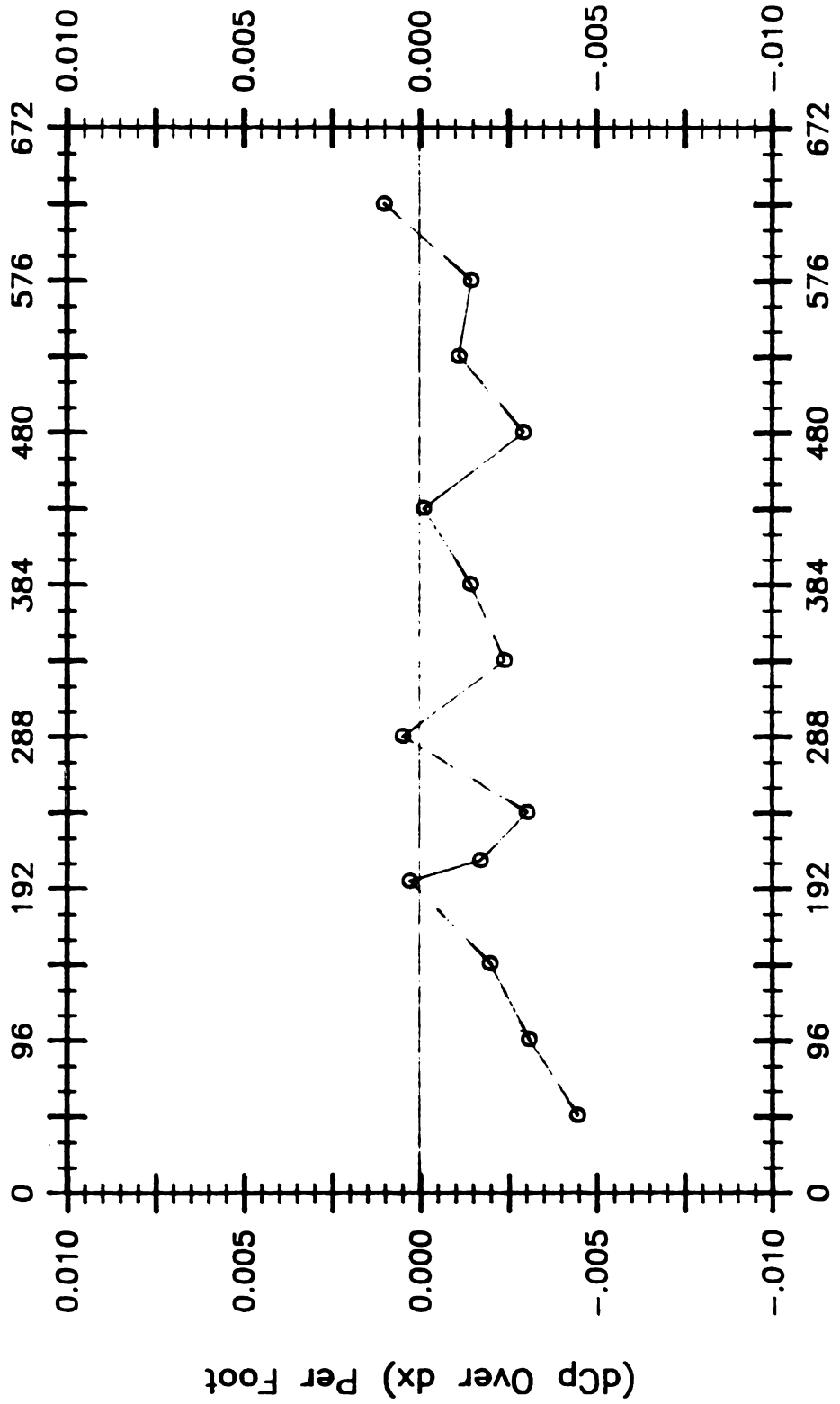

Figure 3.1 Variation of differential pressure gradient dC_p/dx per foot vs x.

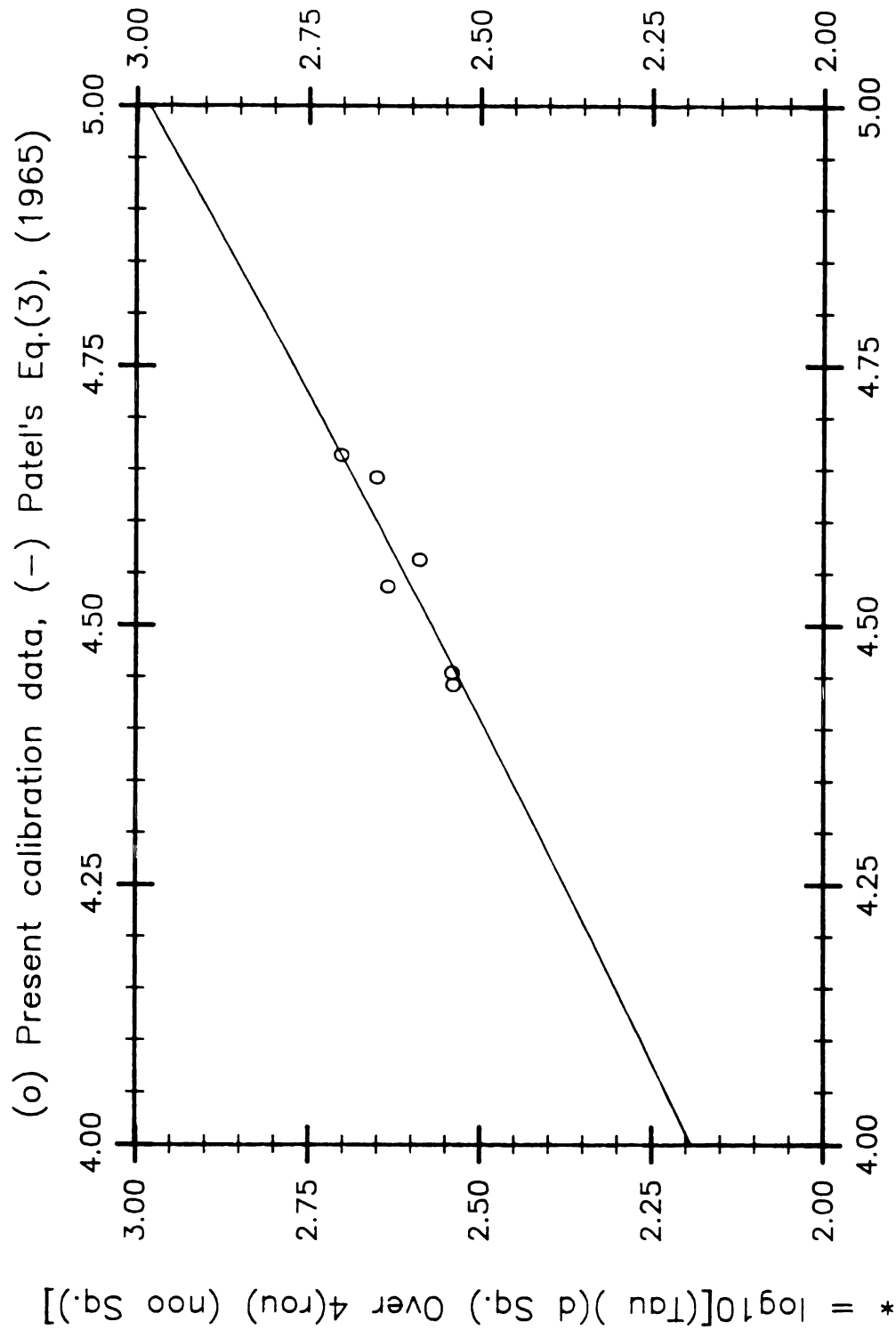

Figure 3.2 Preston tube calibration data (o), compared to Patel's (1965) empirical relation: $y^* = 0.8287 - 0.1381x^* + 0.1437x^{*2} - 0.0060x^{*3}$ (solid line).

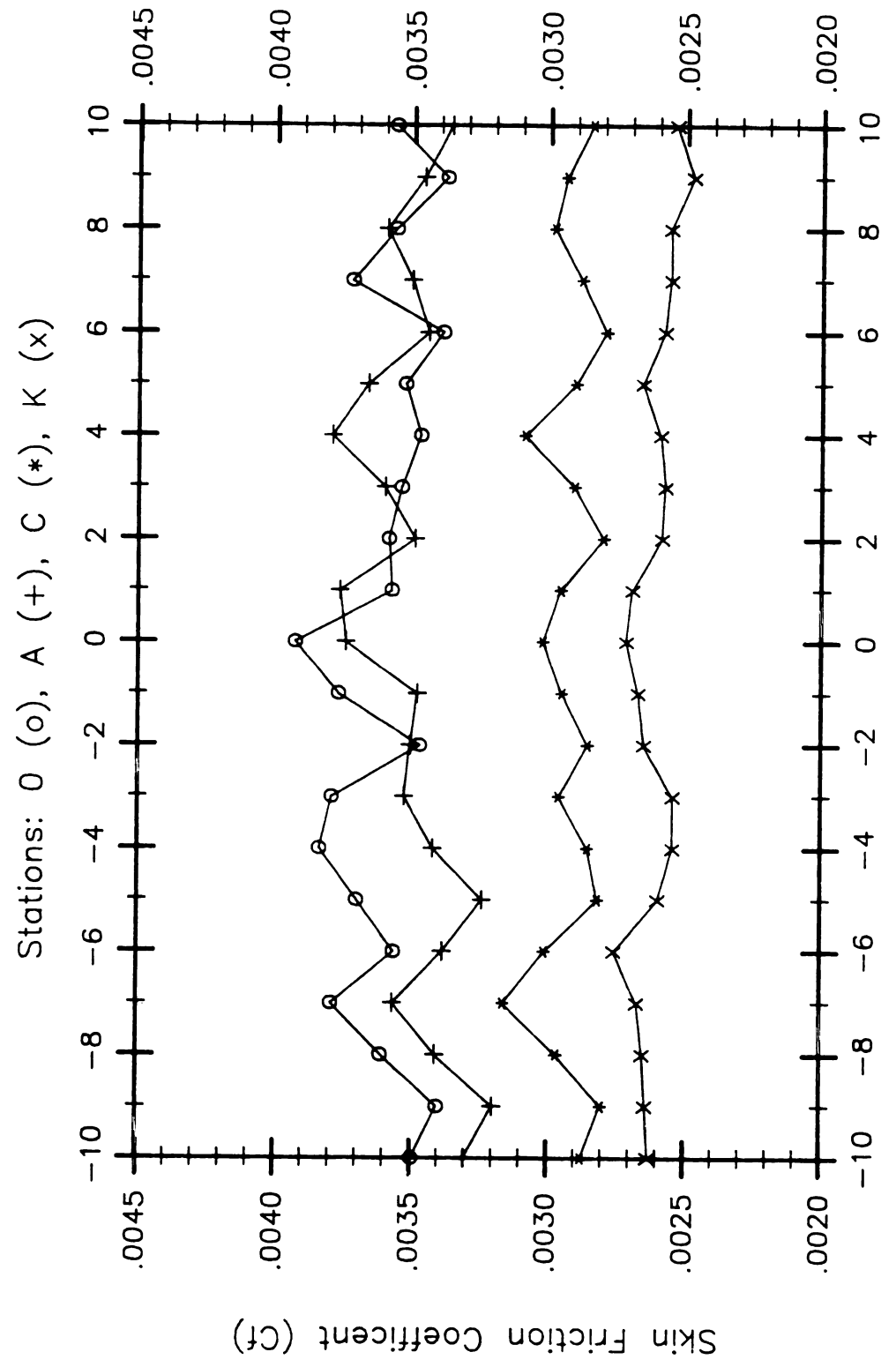

Figure 3.3 Spanwise variation of the local skin friction measured by Preston tube at different streamwise stations; 0 (o), A (+), C (*), and K (x), with a sand paper (36 grit) tripping device and inlet No. 1 configuration.

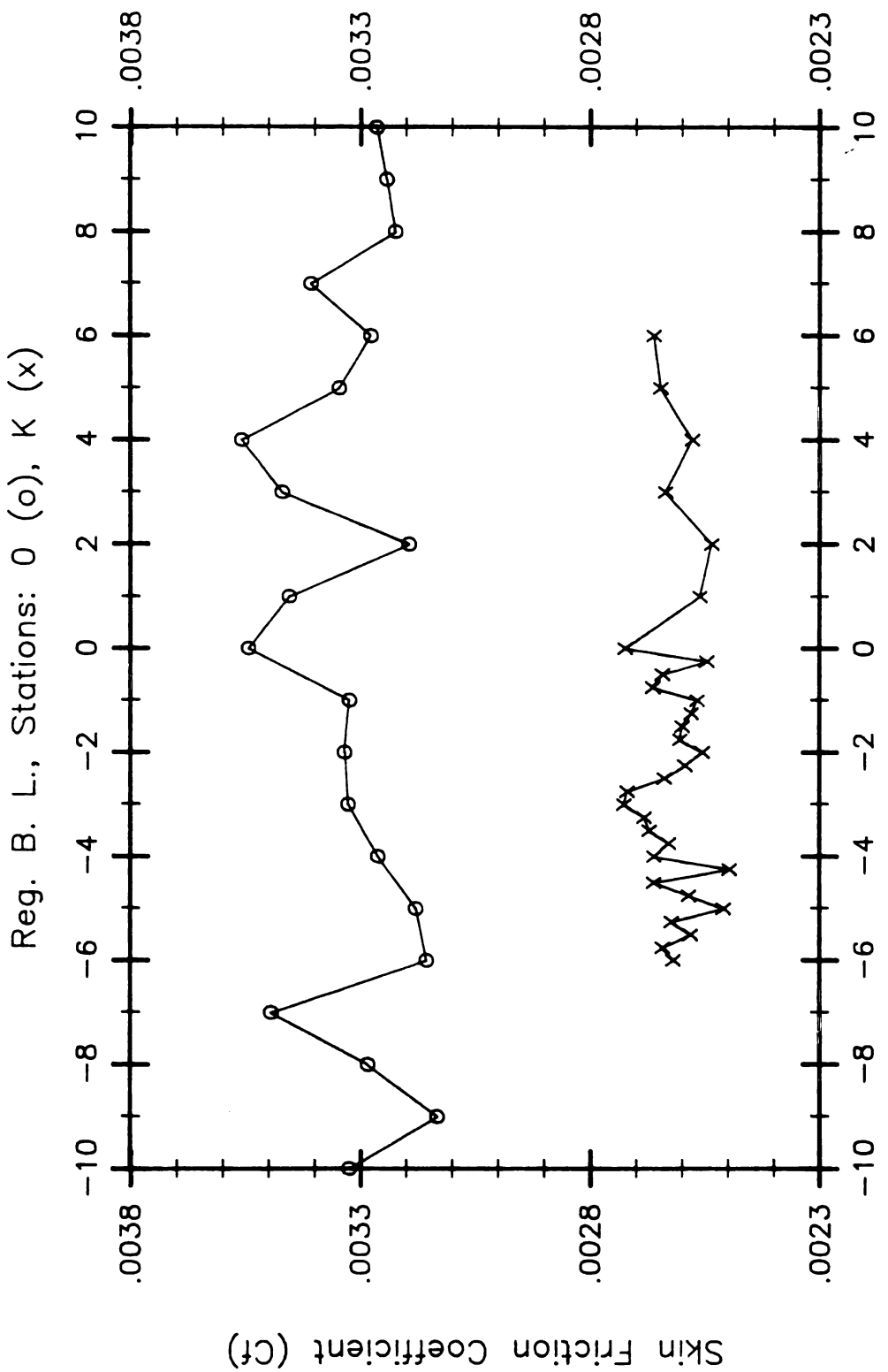

Figure 3.4 Spanwise variation of the local skin friction measured by Preston tube at different streamwise stations; 0 (o), and K (x), with a 1/16" threaded rod tripping device for inlet No. 1 configuration.

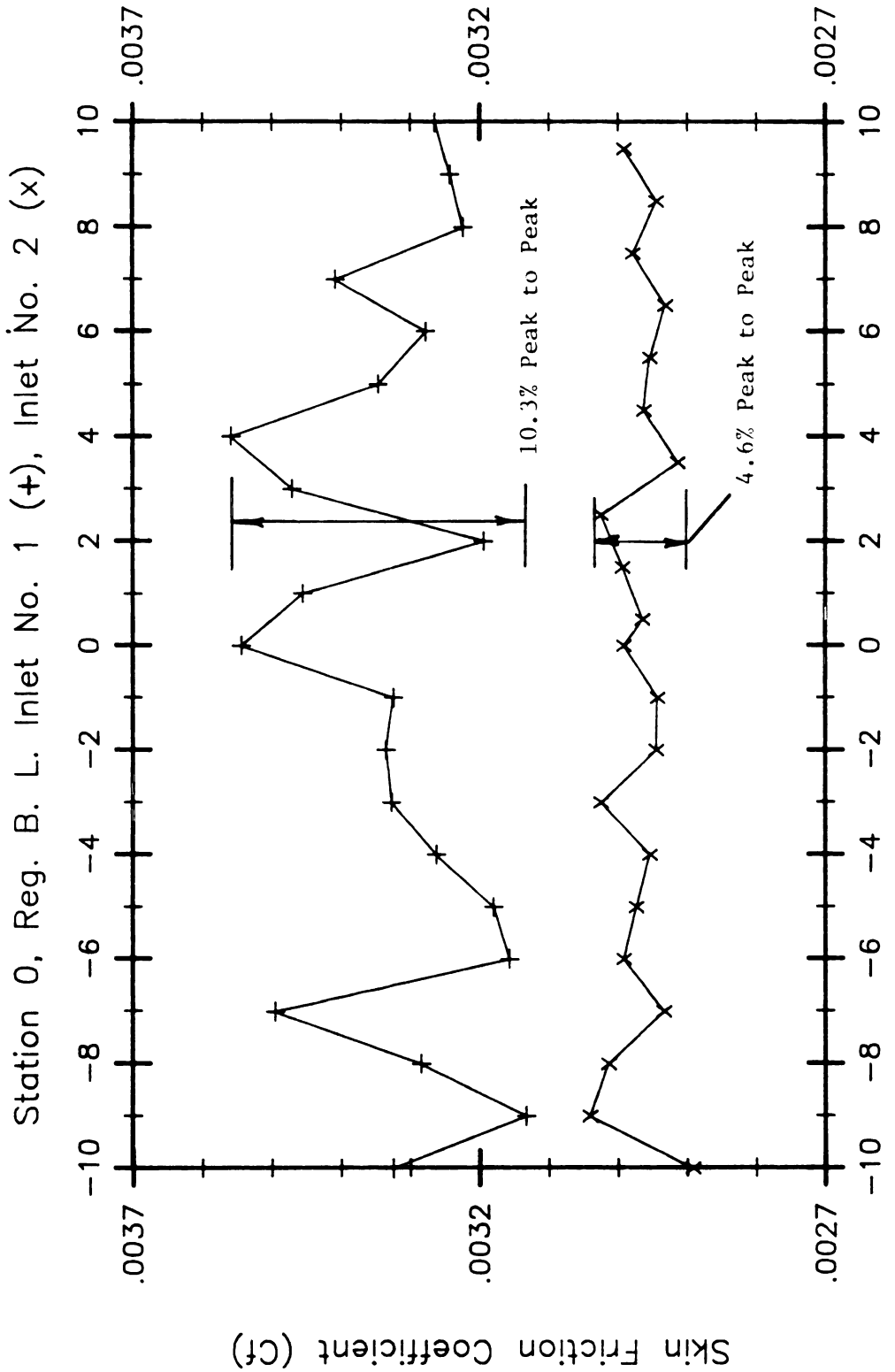

Figure 3.5 Comparison of spanwise variation of the local skin friction measured by Preston tube at station 0 (x = 179") with a 1/16" threaded rod tripping device (at x = 13.5") for inlet No. 1 (+) and inlet No. 2 (x) configurations.

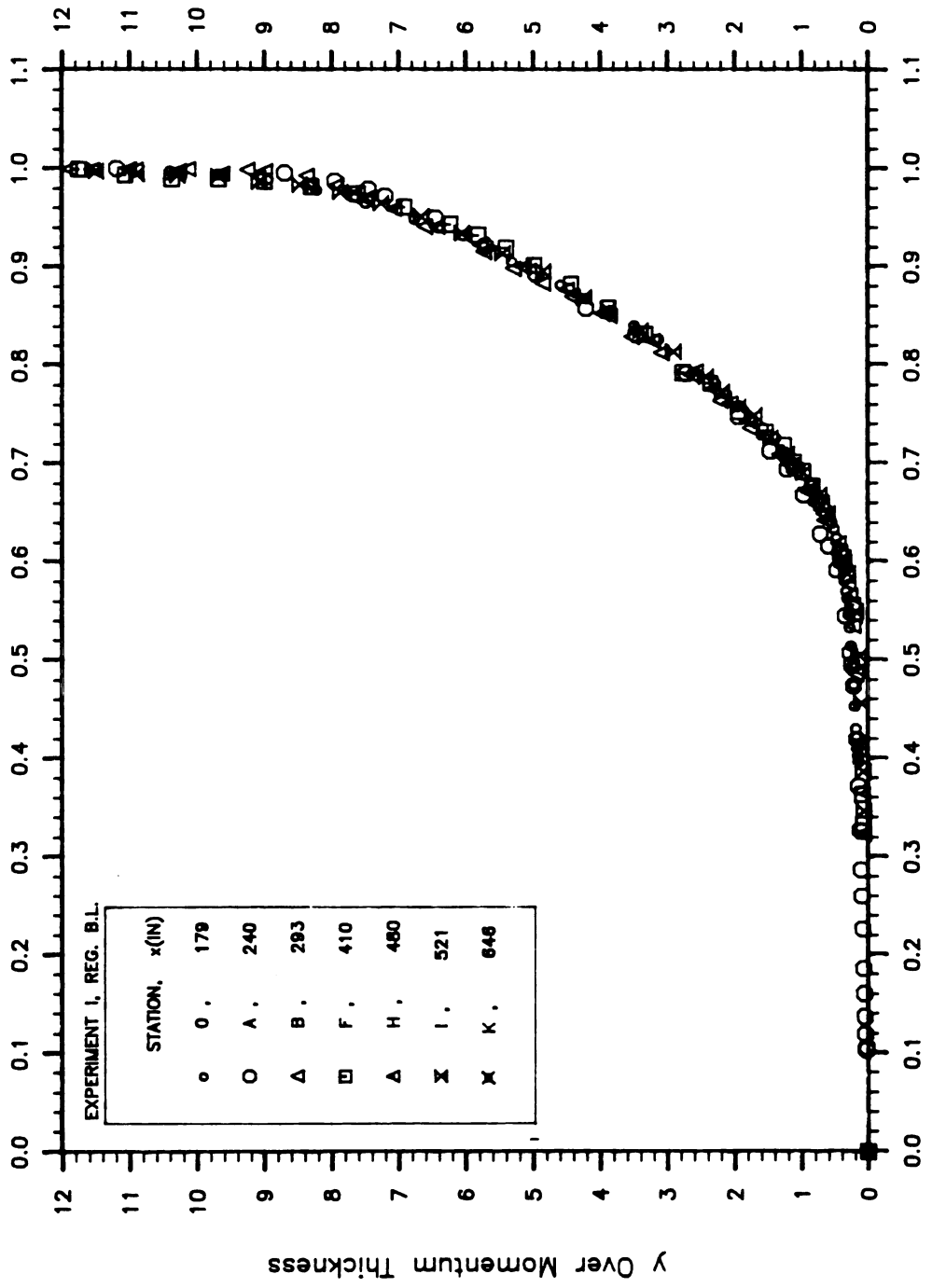

Figure 3.6 Non-dimensional mean velocity profiles (y/θ vs $\bar{U}/U_\infty$) at various streamwise stations in regular boundary layer from experiment I.

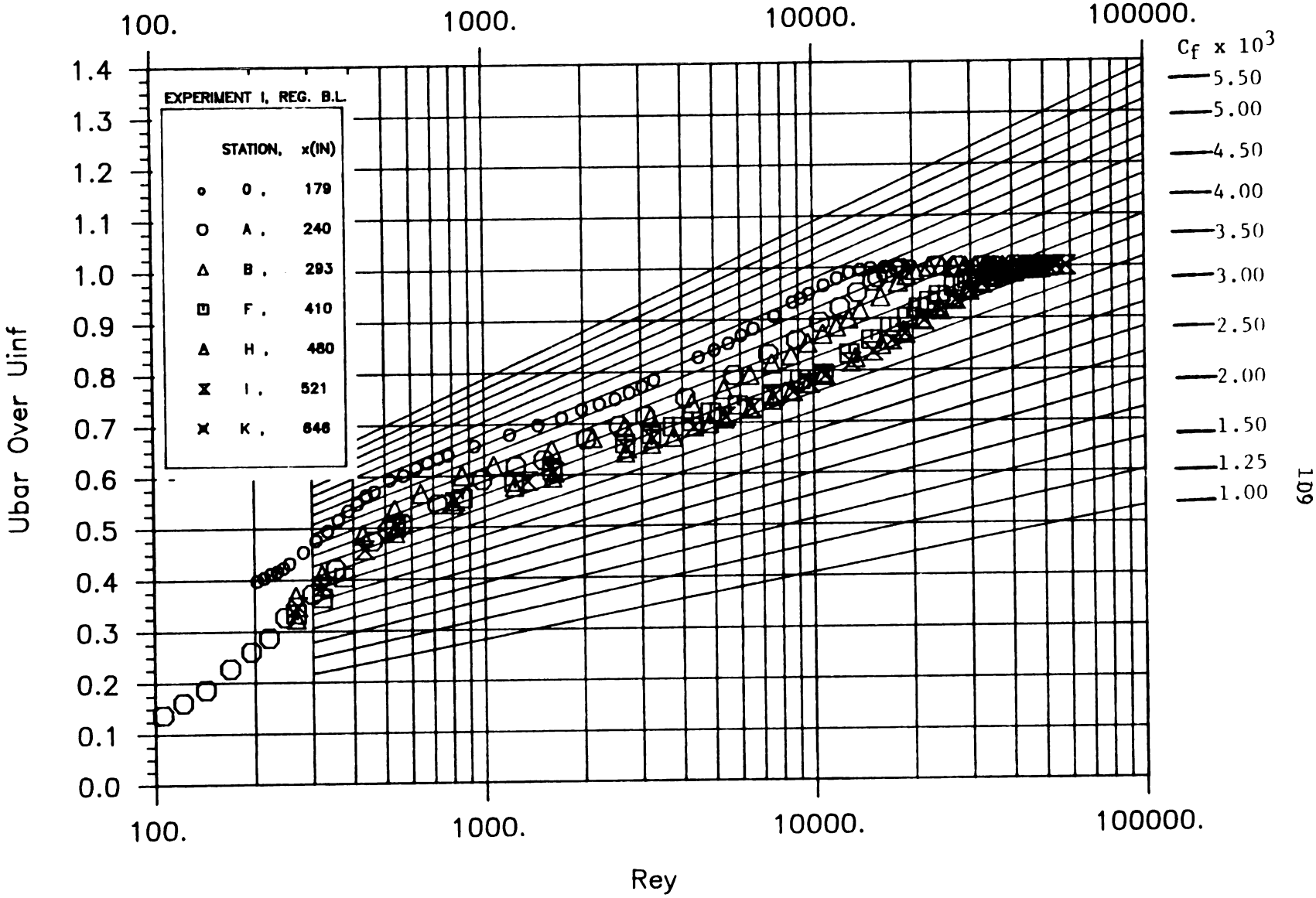

Figure 3.7 Clauser plot for mean velocity profiles ($\bar{U}/U_\infty$ vs $\rho U_\infty y/\mu$) at various streamwise stations in regular boundary layer from experiment I.

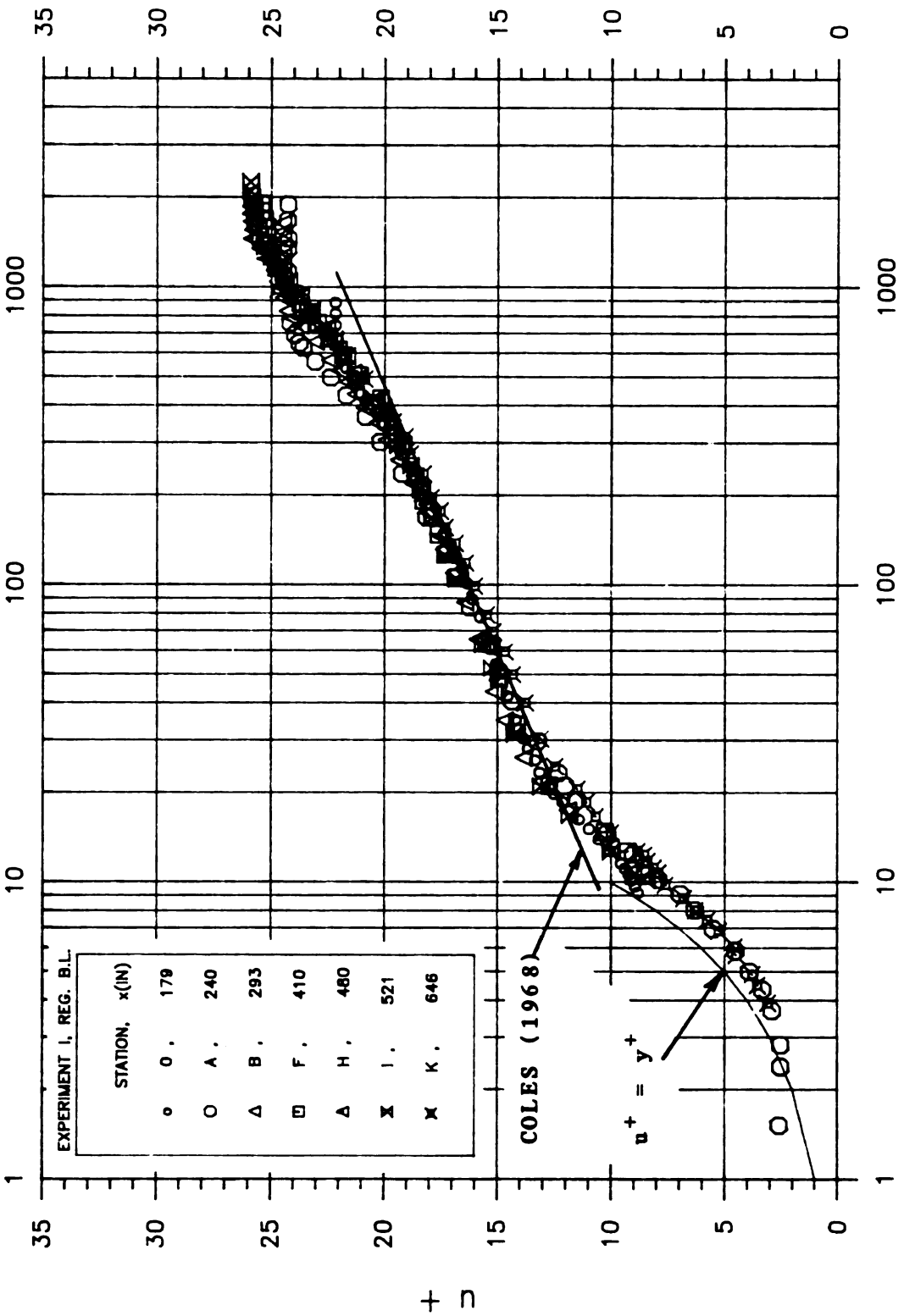

Figure 3.8 Wall-unit nom-dimensionalized mean velocity profiles ($\bar{U}/u_{\tau_0}$ vs $\rho y u_{\tau_0}/\mu$) at various streamwise stations in regular boundary layer from experiment I.

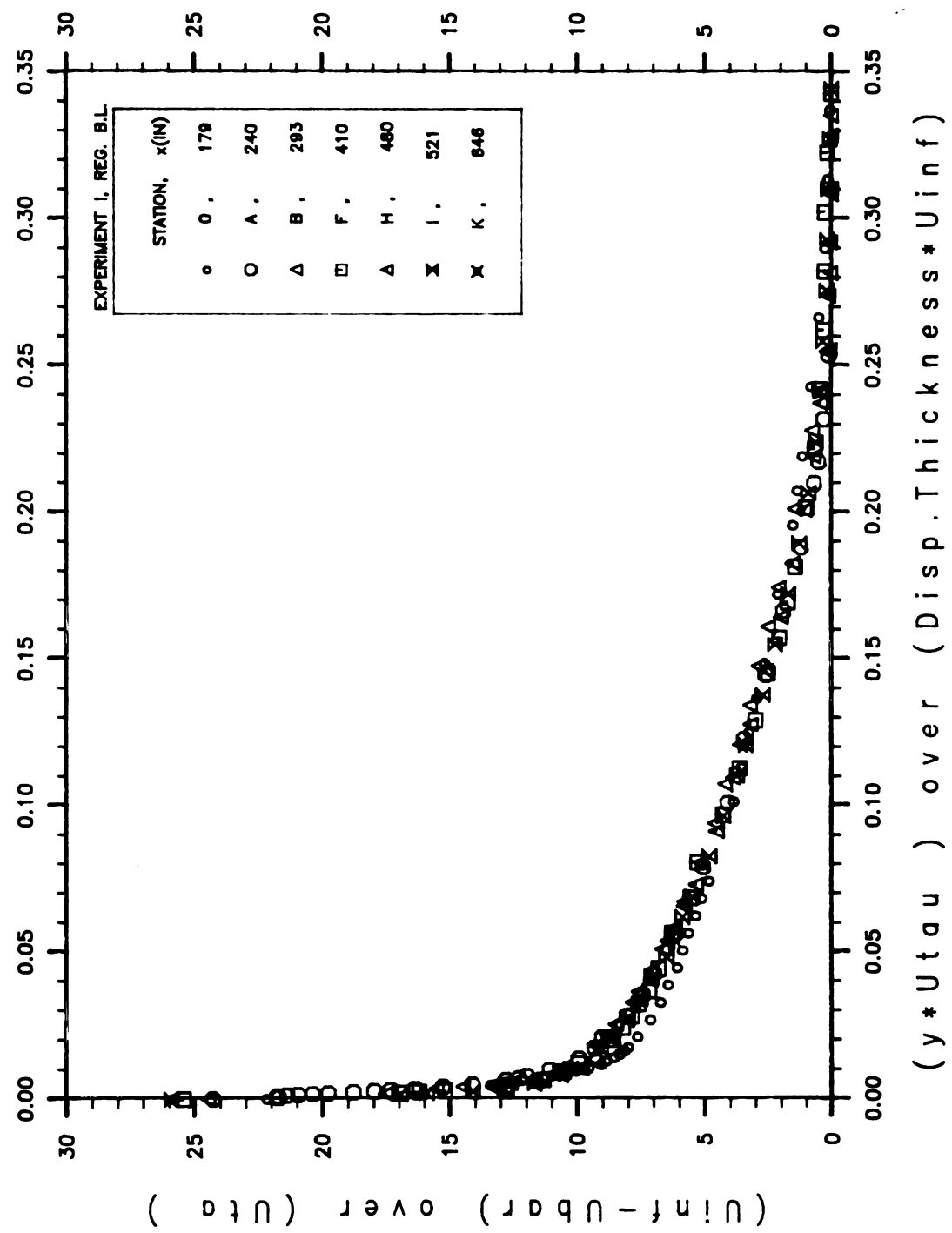

Figure 3.9 Variation of $(U_\infty - \bar{U})/u_\tau\theta$ vs $(yu_\tau\theta/\delta_d U_\infty)$ at various streamwise stations in regular boundary layer from experiment I.

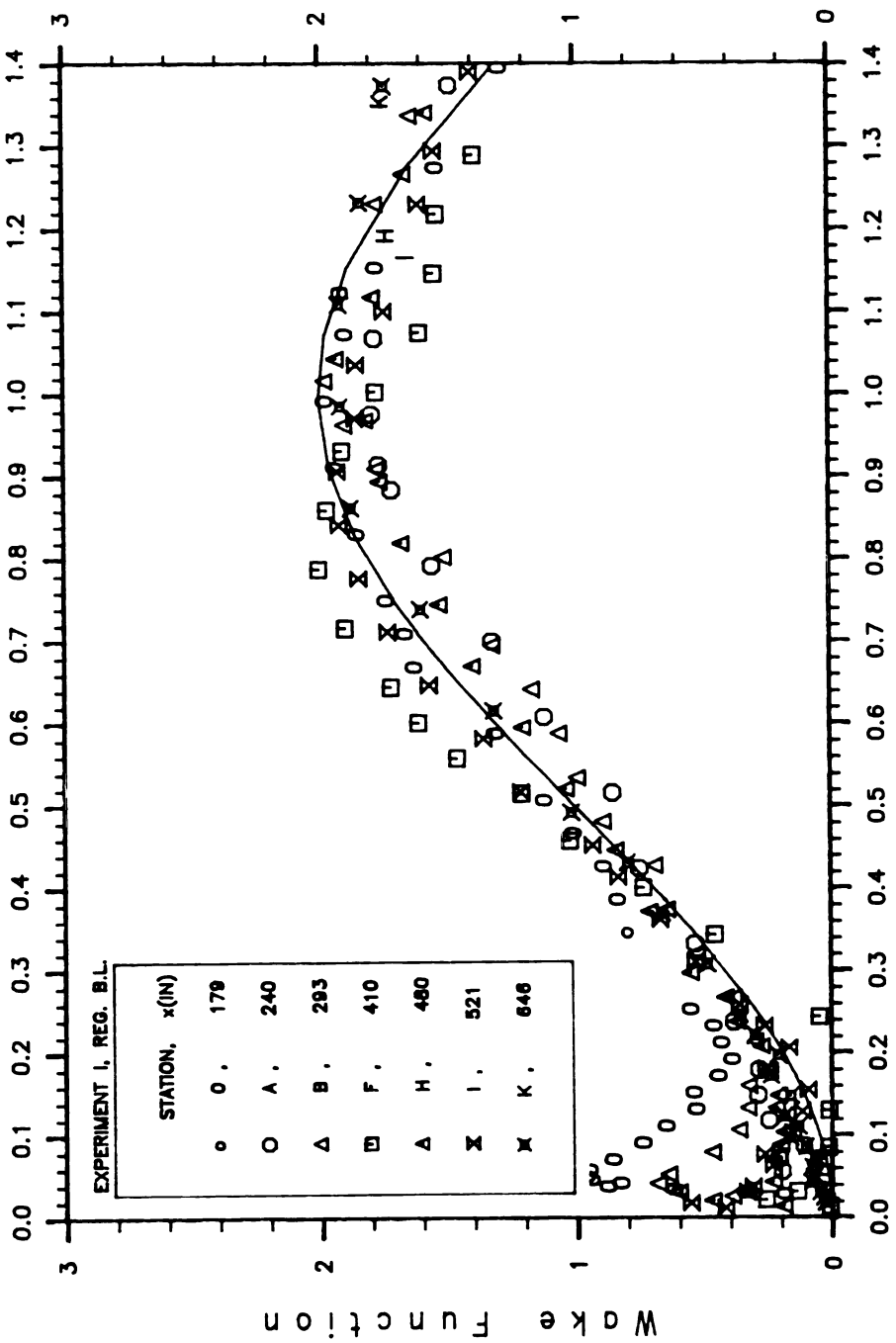

Figure 3.10 Wake function profiles (W vs y/δ) at various streamwise stations in regular boundary layer from experiment I. (Solid line : $W = 2\mathrm{Sin}^2(\pi y/2\delta)$)

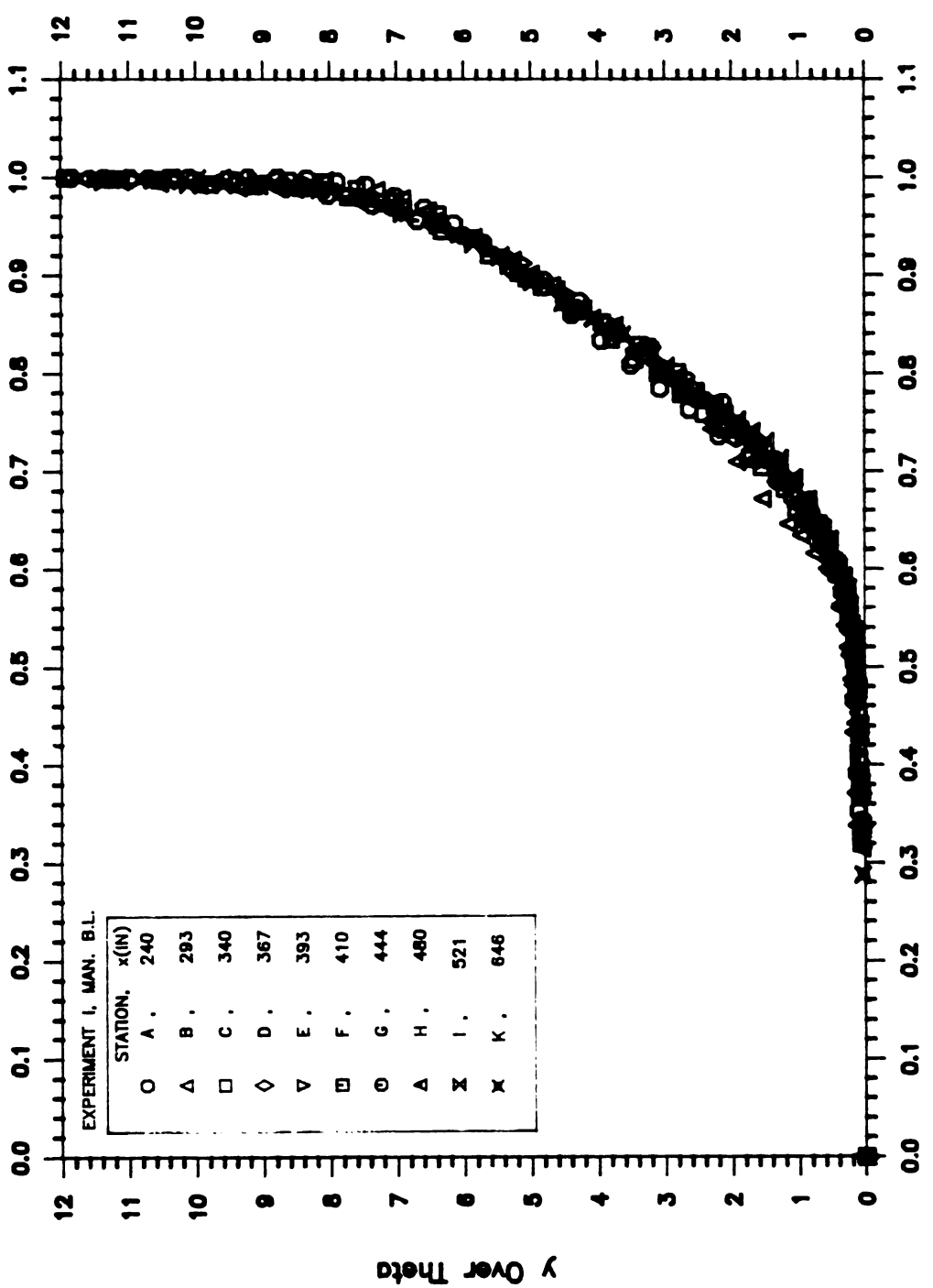

Figure 3.11 Non-dimensional mean velocity profiles (y/θ vs $\bar{U}/U_\infty$) at various streamwise stations in manipulated boundary layer from experiment I.

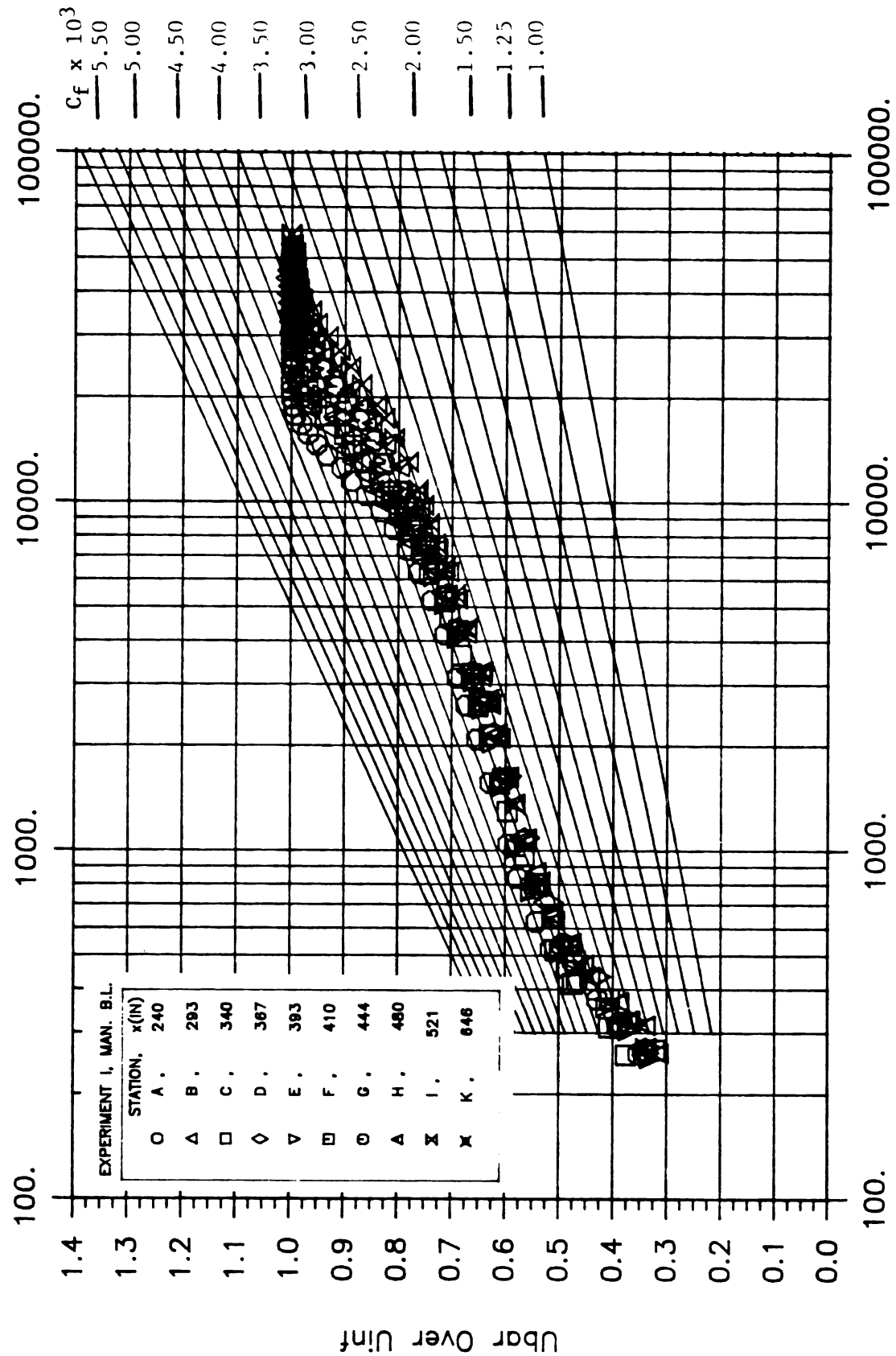

Figure 3.12 Clauser plot for mean velocity profiles ($\bar{U}/U_\infty$ vs $\rho U_\infty y/\mu$) at various streamwise stations in manipulated boundary layer from experiment I.

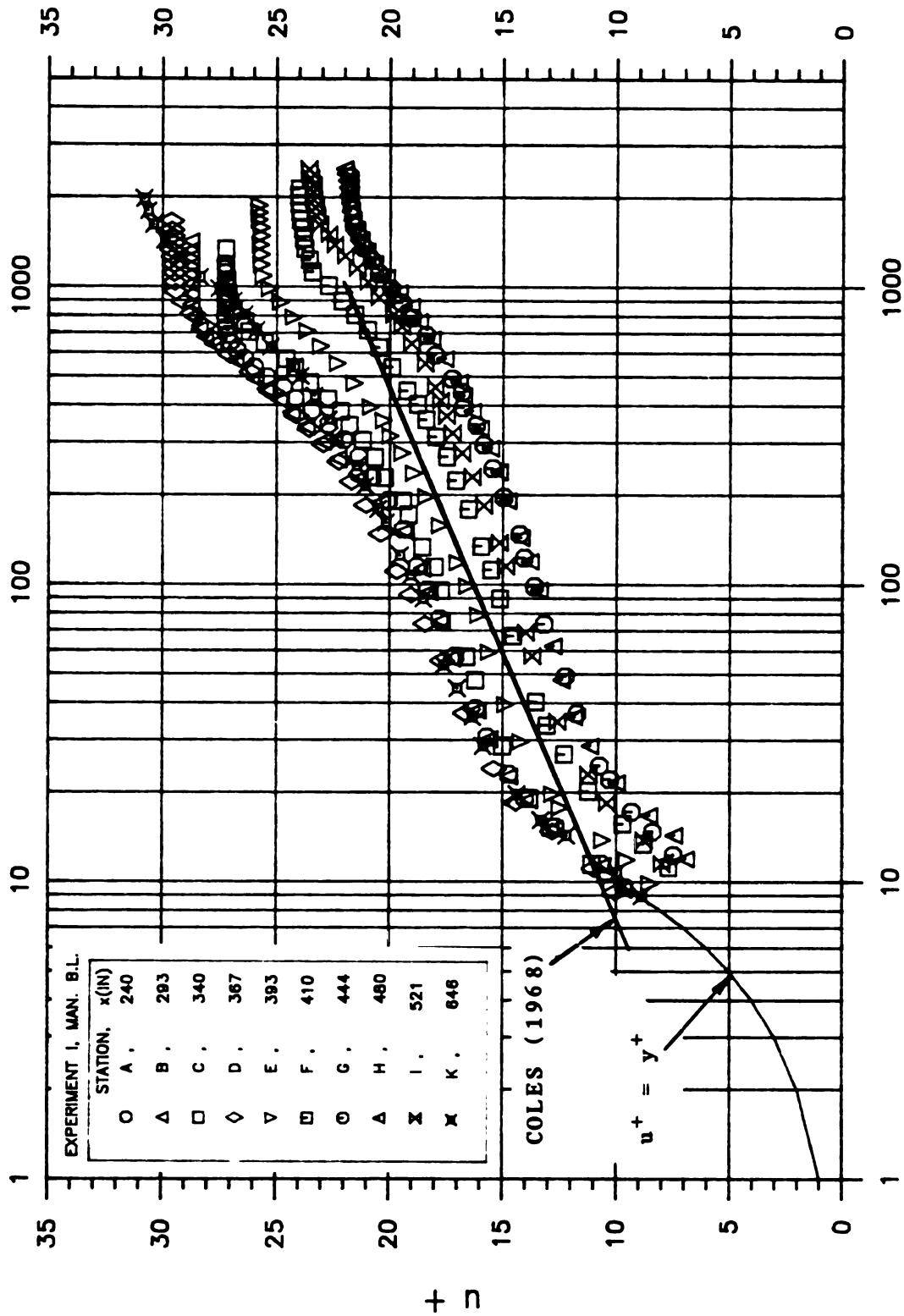

Figure 3.13 Wall-unit non-dimensionalized mean velocity profiles ($\bar{U}/u_{\tau\theta}$ vs $\rho y u_{\tau\theta}/\mu$) at various streamwise stations in manipulated boundary layer from experiment I.

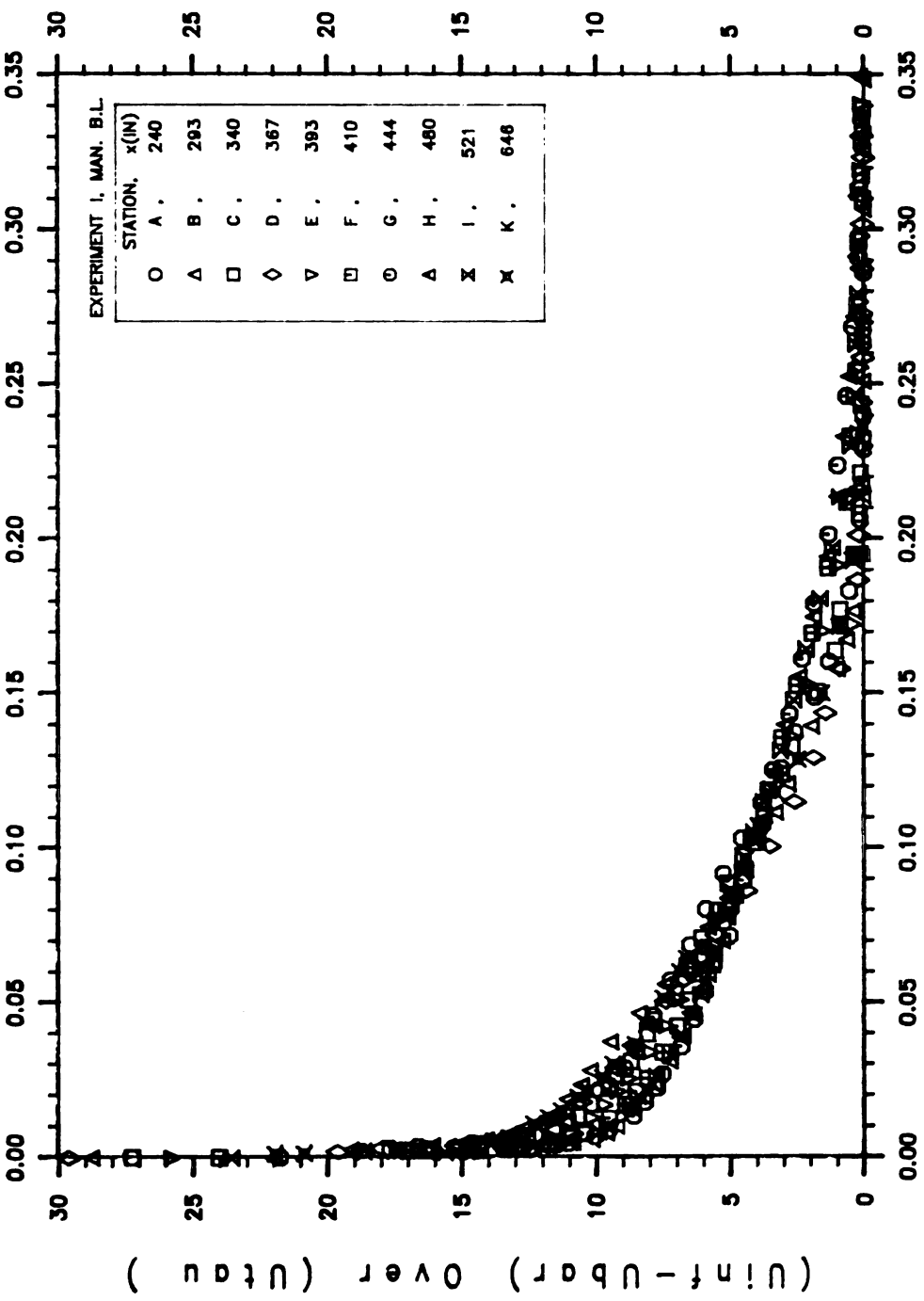

Figure 3.14 Variation of $(U_\infty - \bar{U})/u_{\tau\theta}$ vs $(yu_{\tau\theta}/\delta_d U_\infty)$ at various streamwise stations in manipulated boundary layer from experiment I.

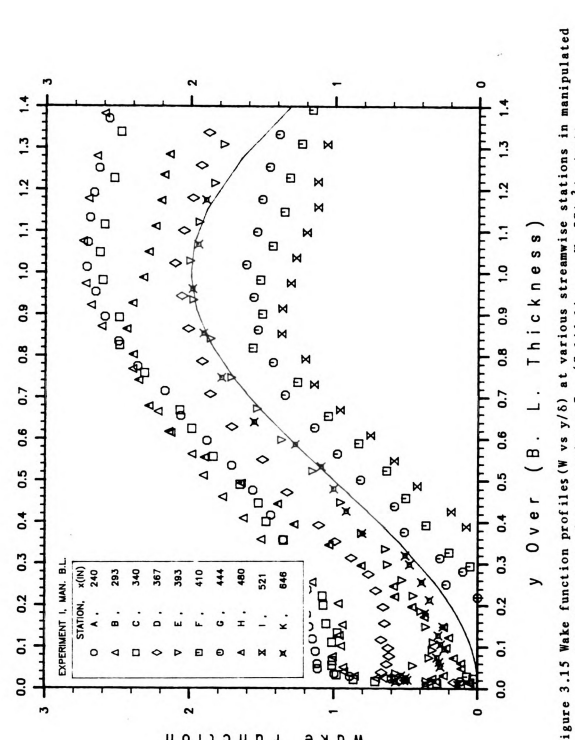

Figure 3.15 Wake function profiles(W vs y/δ) at various streamwise stations in manipulated boundary layer from experiment I. (Solid line : $W=2\mathrm{Sin}^2(\pi y/2\delta)$)

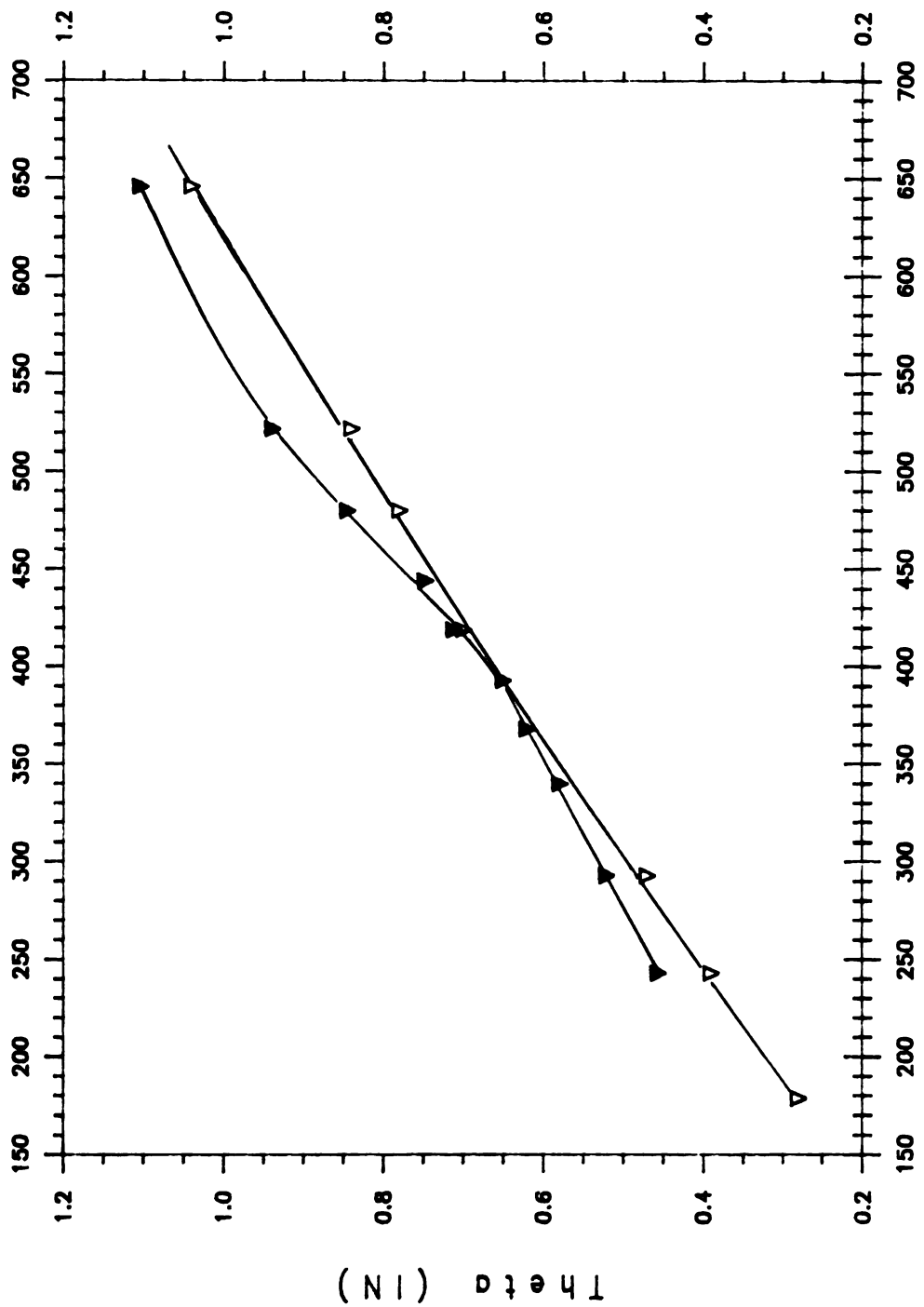

Figure 3.16 Comparison of streamwise momentum thickness distributions (θ (In.) vs x (In.)) for regular (open) and manipulated (filled) boundary layers from experiment I.

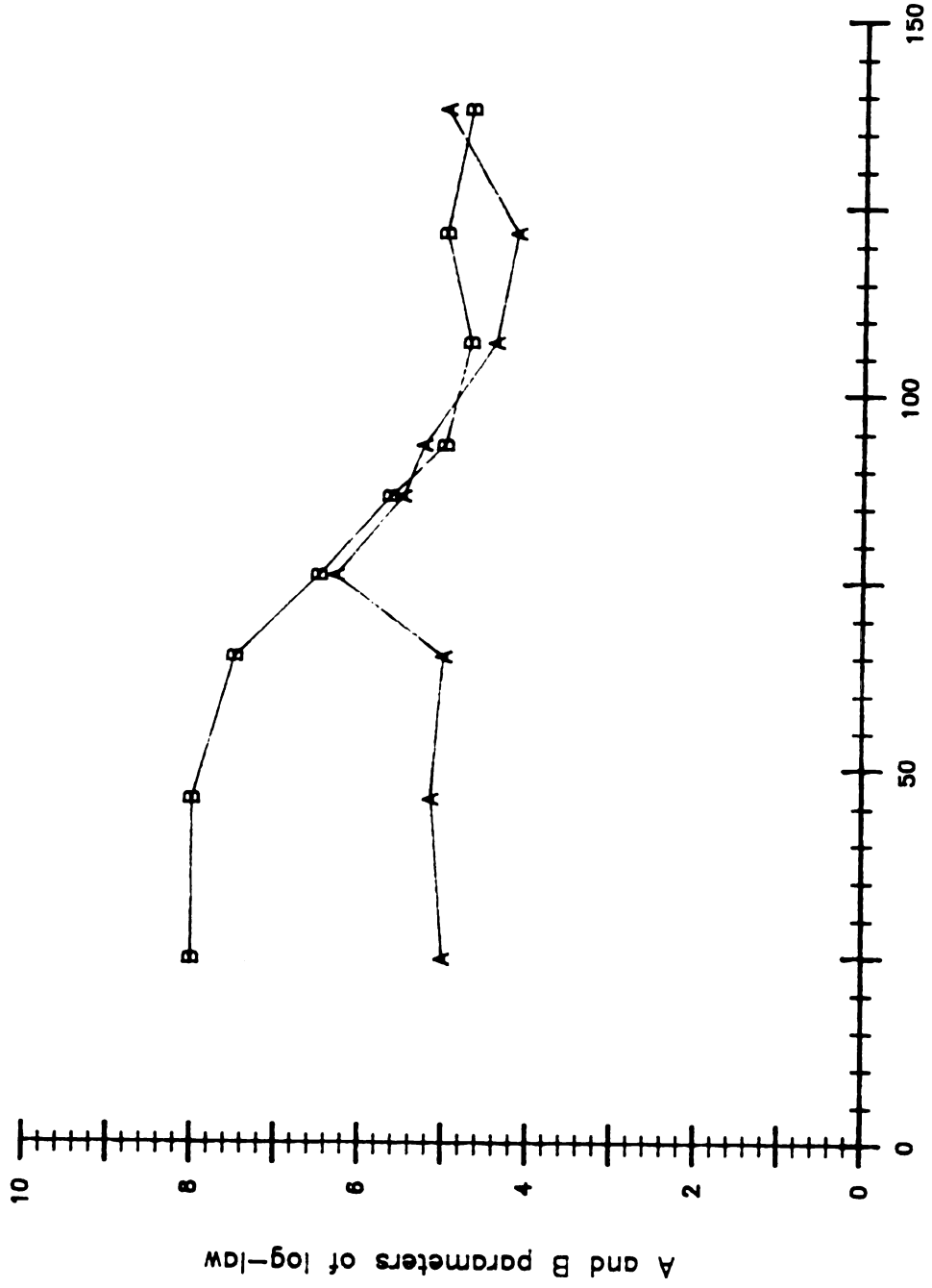

Figure 3.17 Streamwise variation of "law of the wall" ($u^+ = A\log_{10}(y^+) + B$) parameters (A and B) in manipulated boundary layers from experiment I.

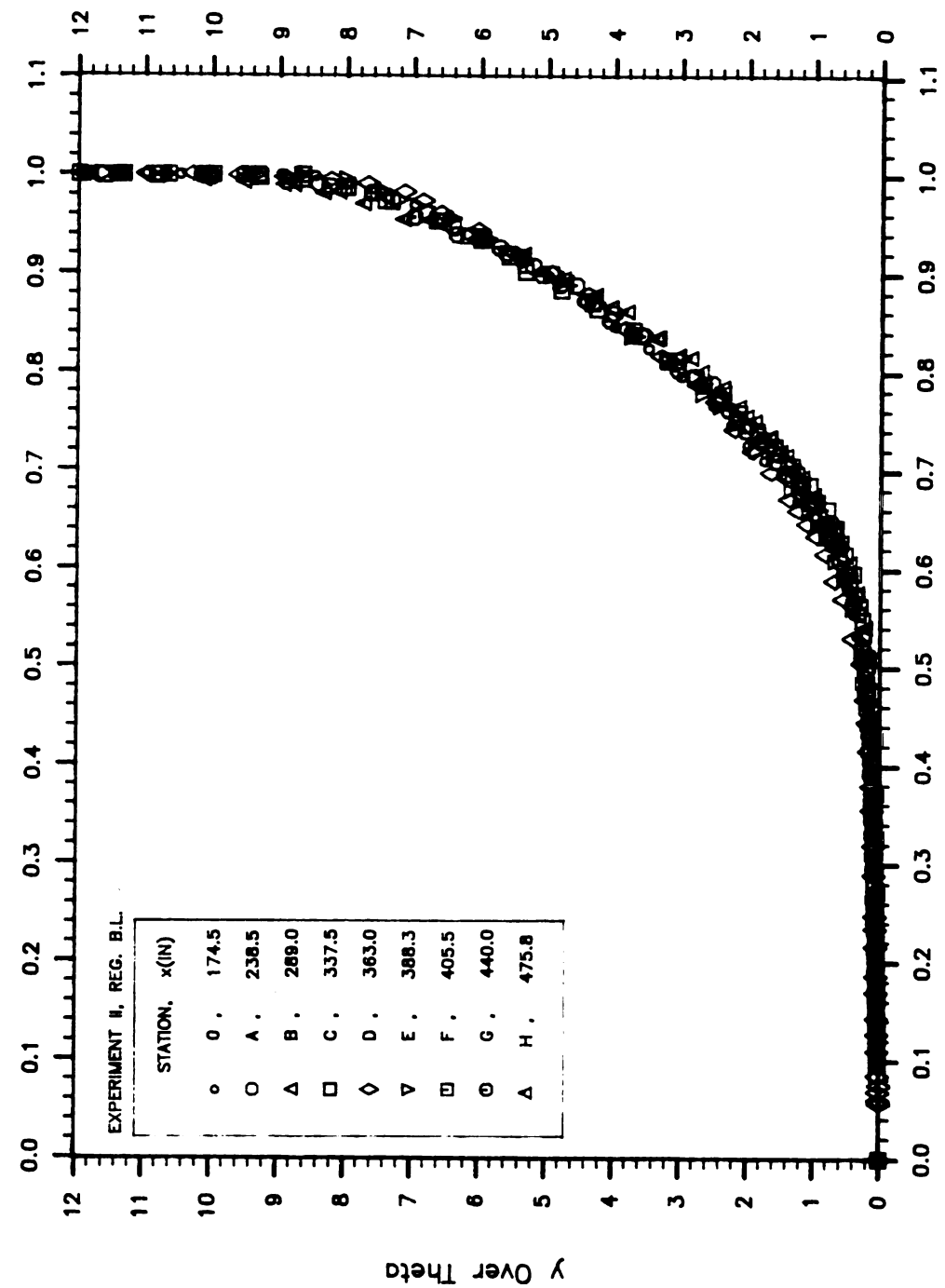

Figure 3.18 Non-dimensional mean velocity profiles (y/θ vs $\bar{U}/U_\infty$) at various streamwise stations in regular boundary layer from experiment II.

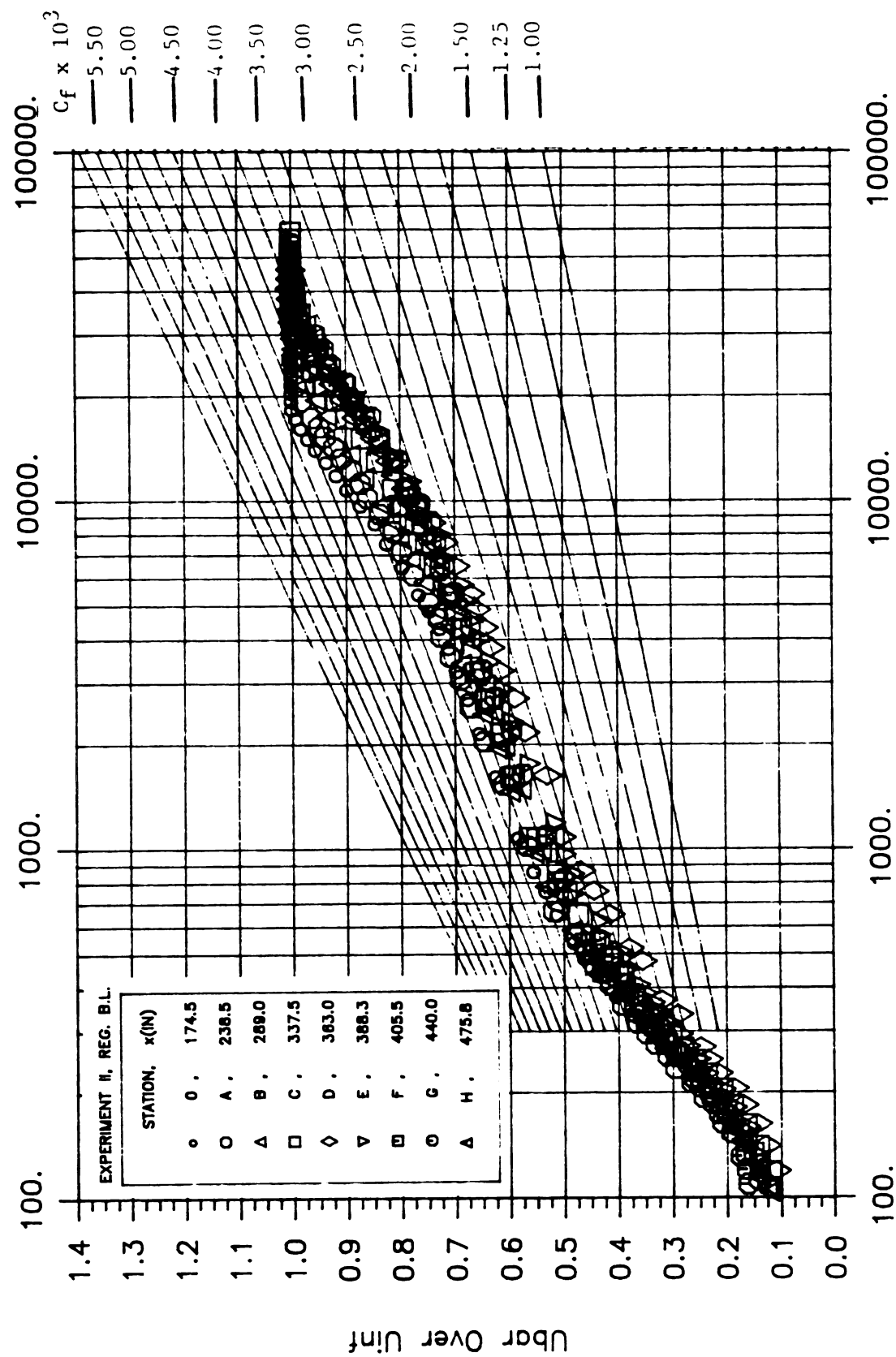

Figure 3.19 Clauser plot for mean velocity profiles ($\bar{U}/U_\infty$ vs $\rho U_\infty y/\mu$) at various streamwise stations in regular boundary layer from experiment II.

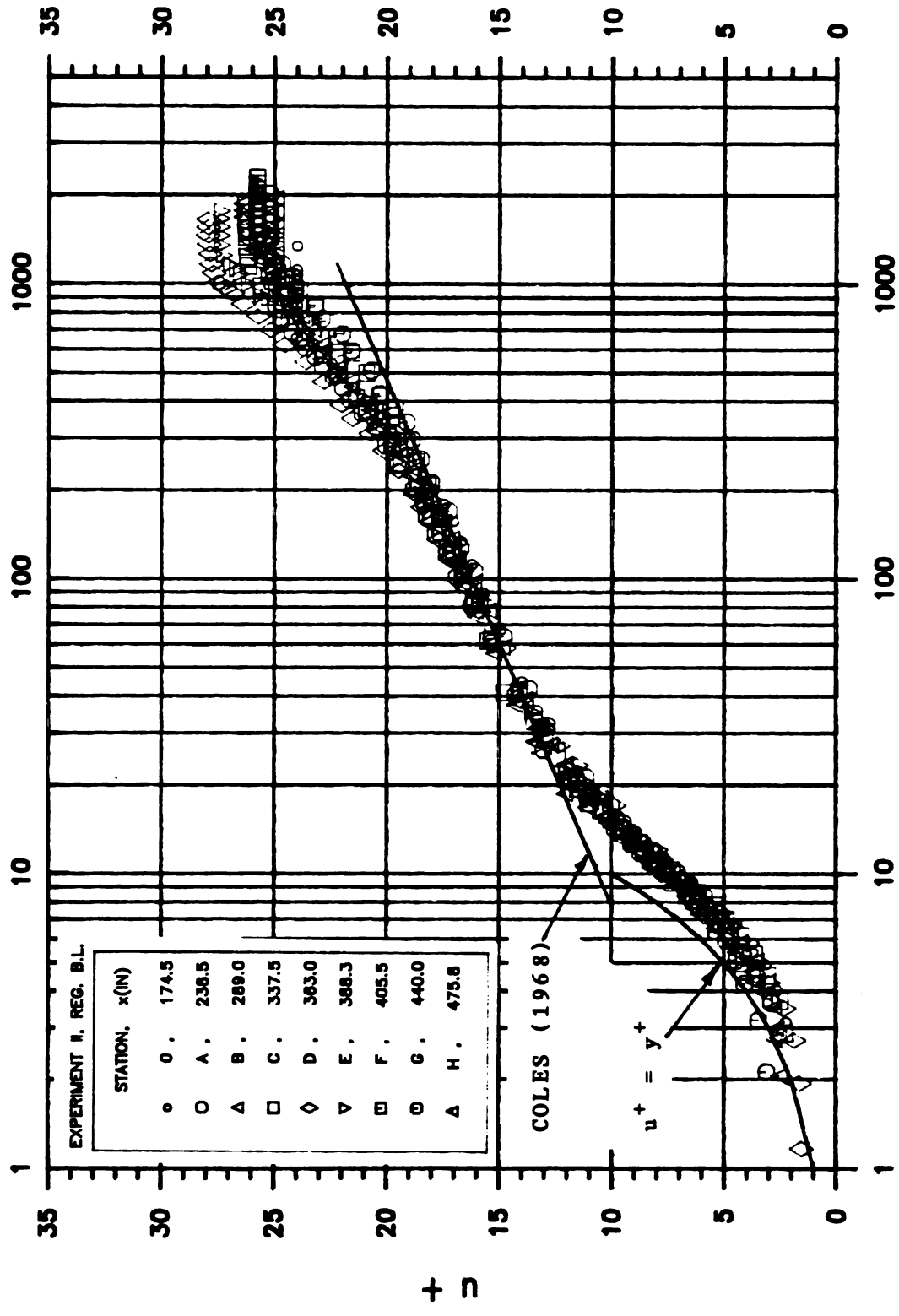

Figure 3.20 Wall-unit non-dimensionalized mean velocity profiles ($\bar{U}/u_{\tau\theta}$ vs $\rho y u_{\tau\theta}/\mu$) at various streamwise stations in regular boundary layer from experiment II.

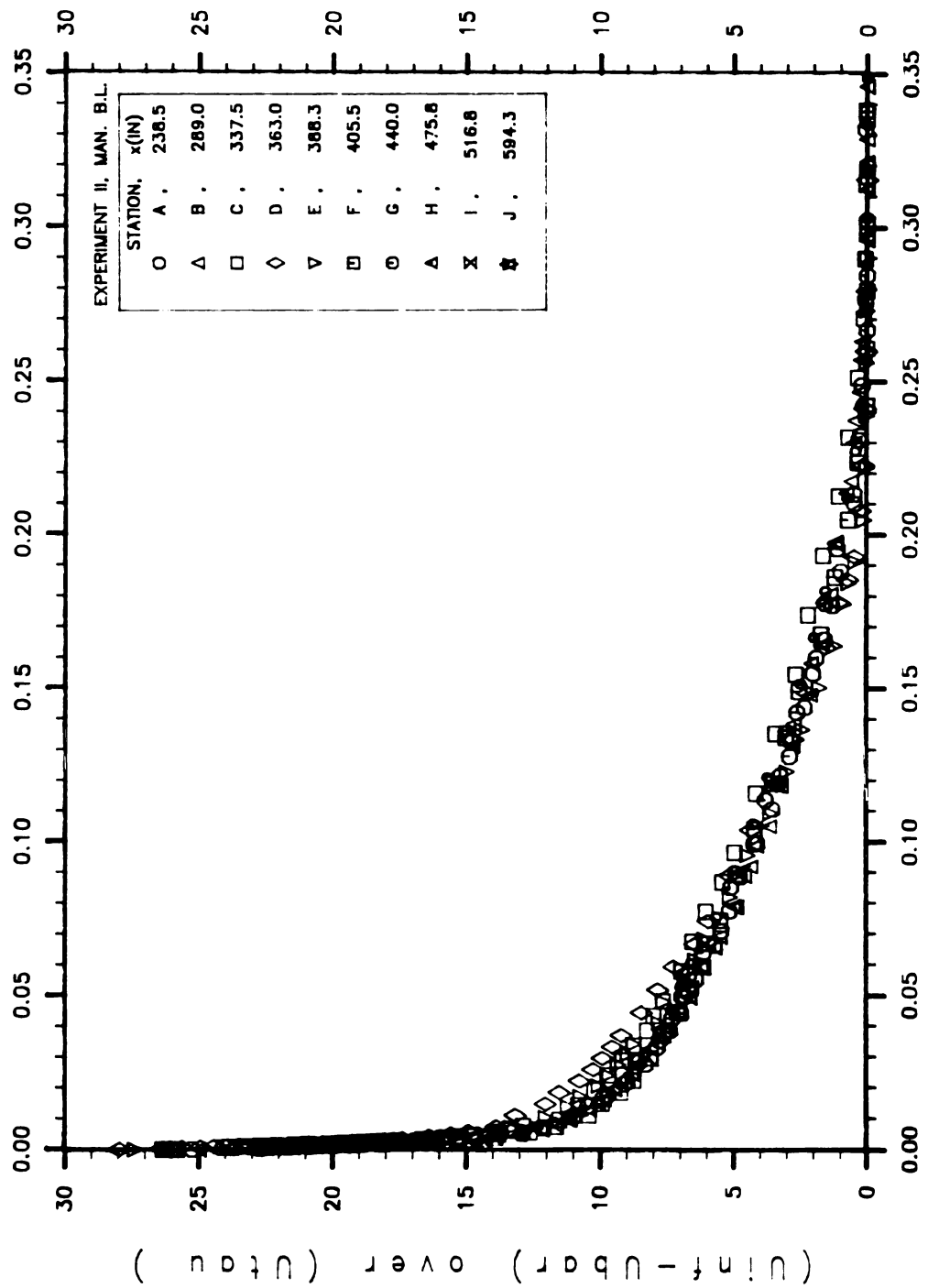

Figure 3.21 Variation of $(U_\infty - \bar{U})/u_{\tau\theta}$ vs $(yu_{\tau\theta}/\delta_d U_\infty)$ at various streamwise stations in regular boundary layer from experiment II.

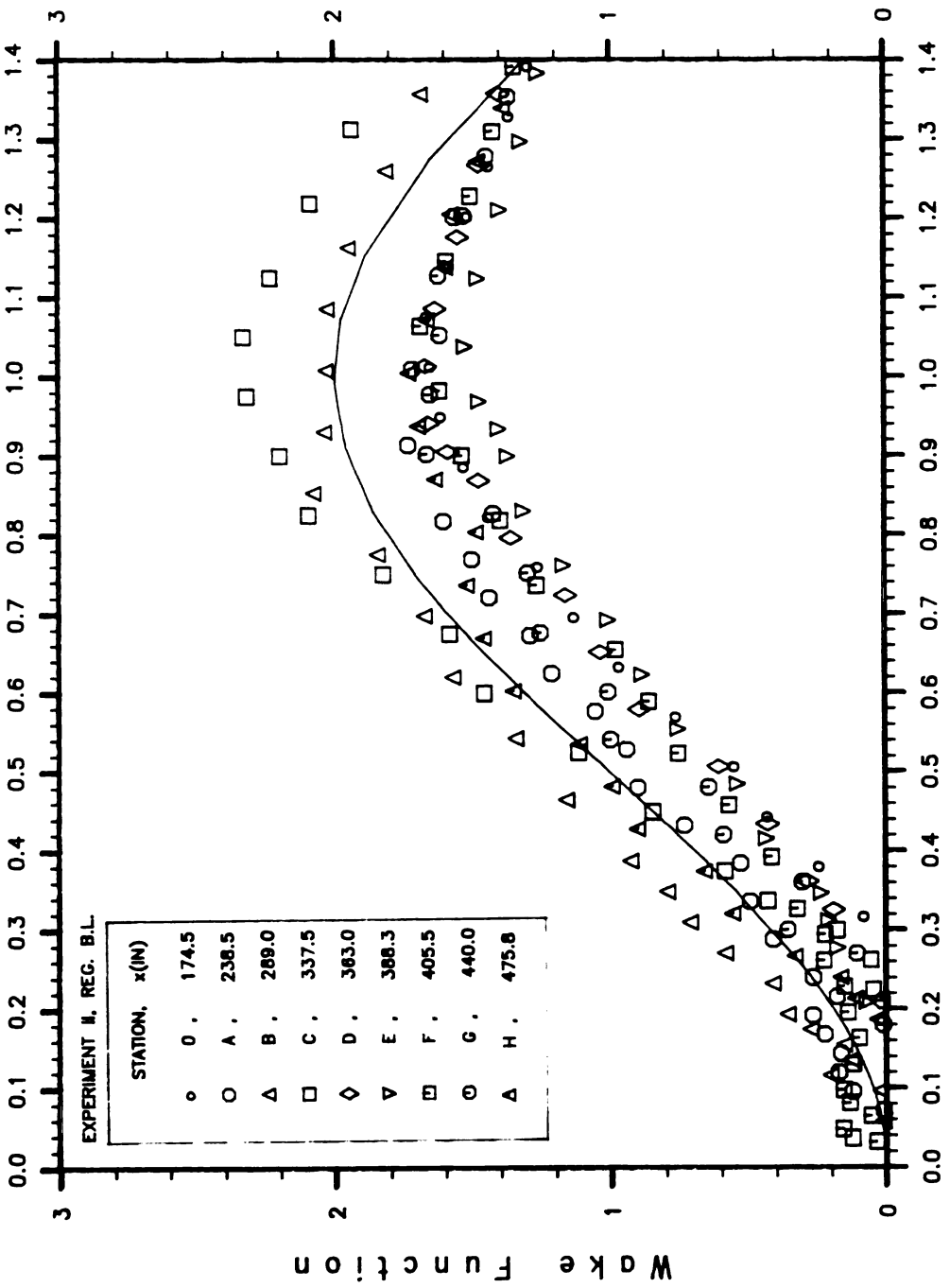

Figure 3.22 Wake function profile (W vs y/δ) at various streamwise stations in regular boundary layer from experiment II. (Solid line : $W = 2\sin^2(\pi y/2\delta)$)

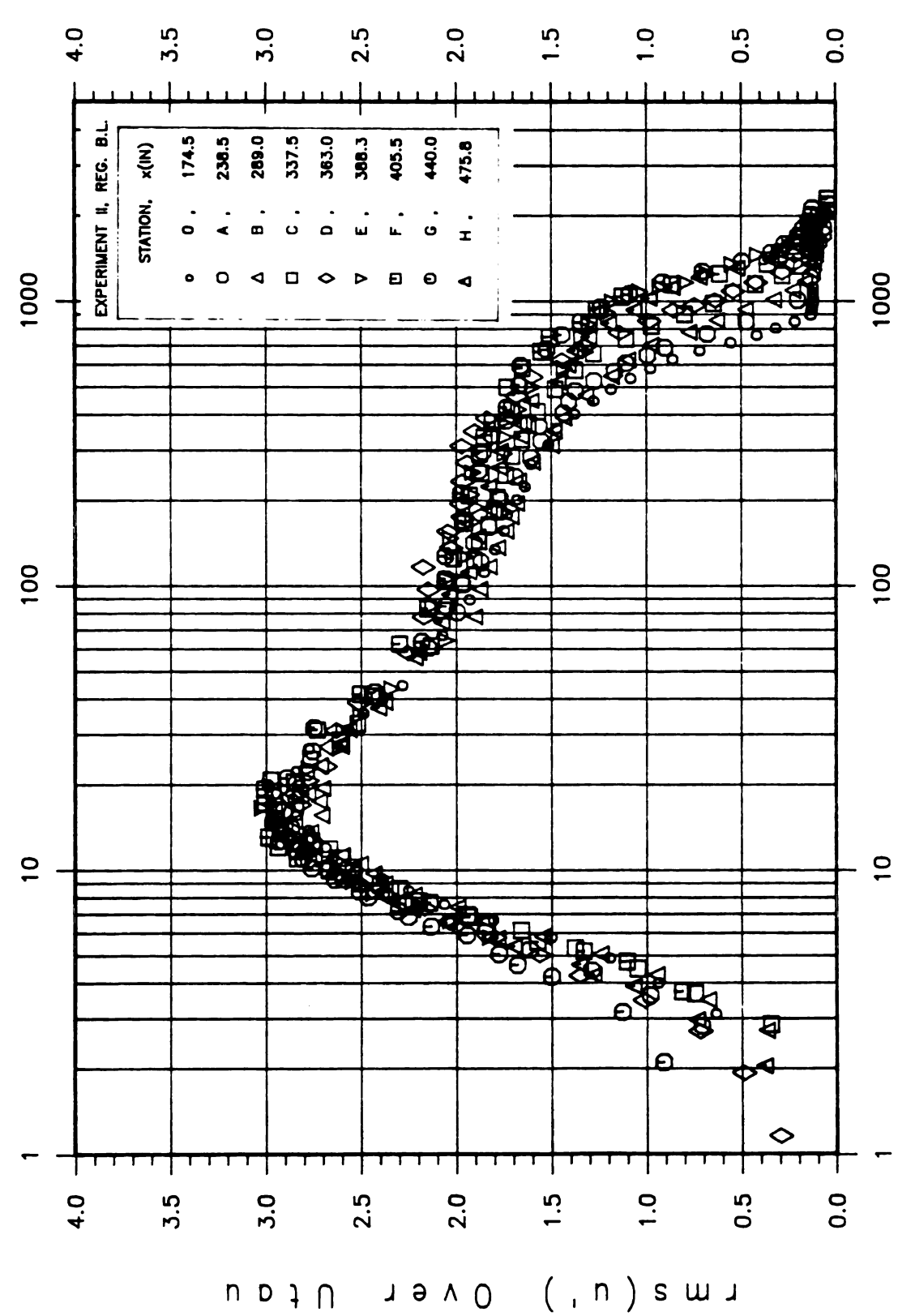

Figure 3.23 Wall-unit non-dimensionalized fluctuating velocity profile (rms(u')/$u_{\tau\theta}$ vs $\rho y u_{\tau\theta}/\mu$) at various streamwise stations in regular boundary layer from experiment II.

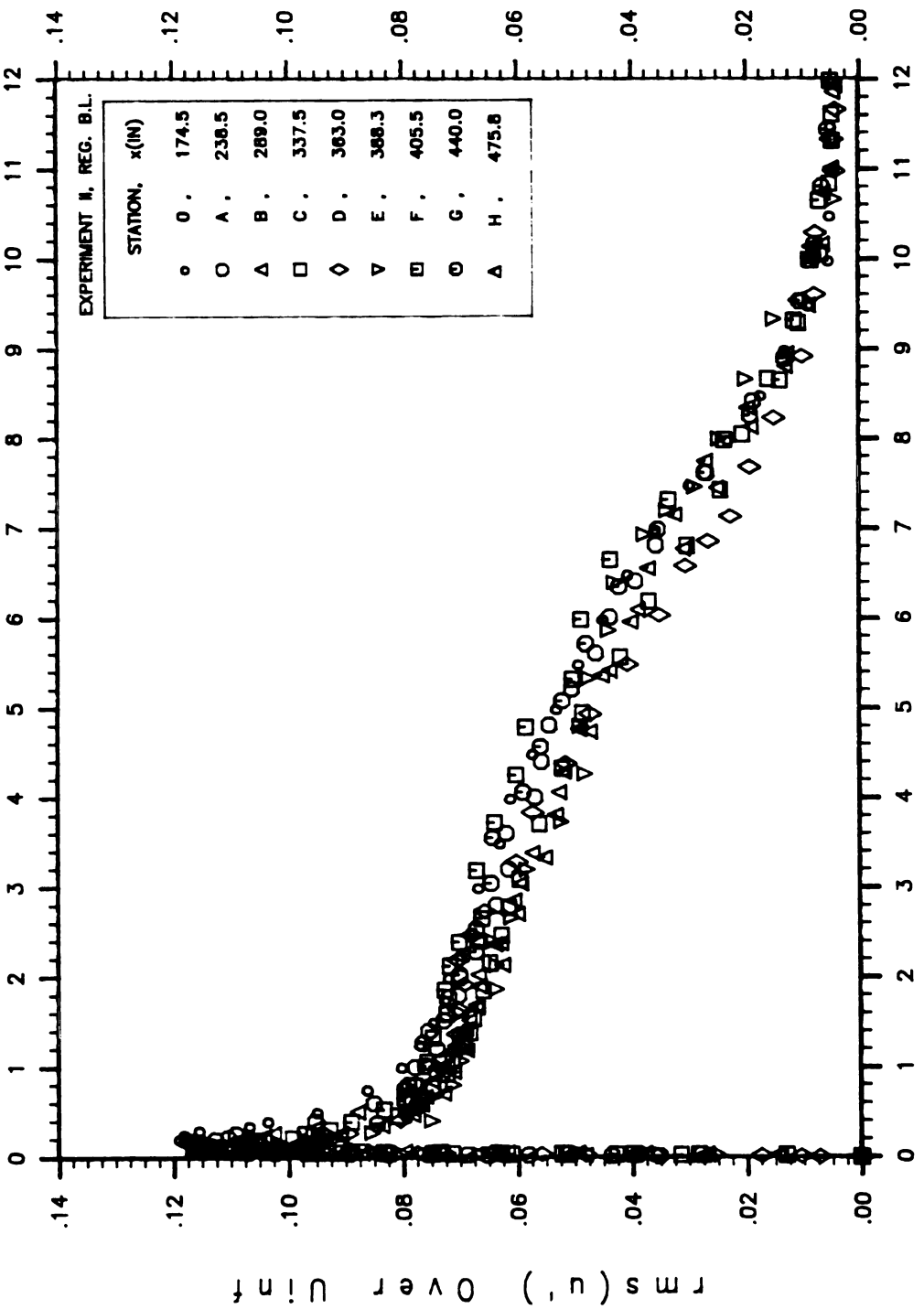

Figure 3.24 Variation of rms(u')/U_∞ vs y/θ at various streamwise stations in regular boundary layer from experiment II.

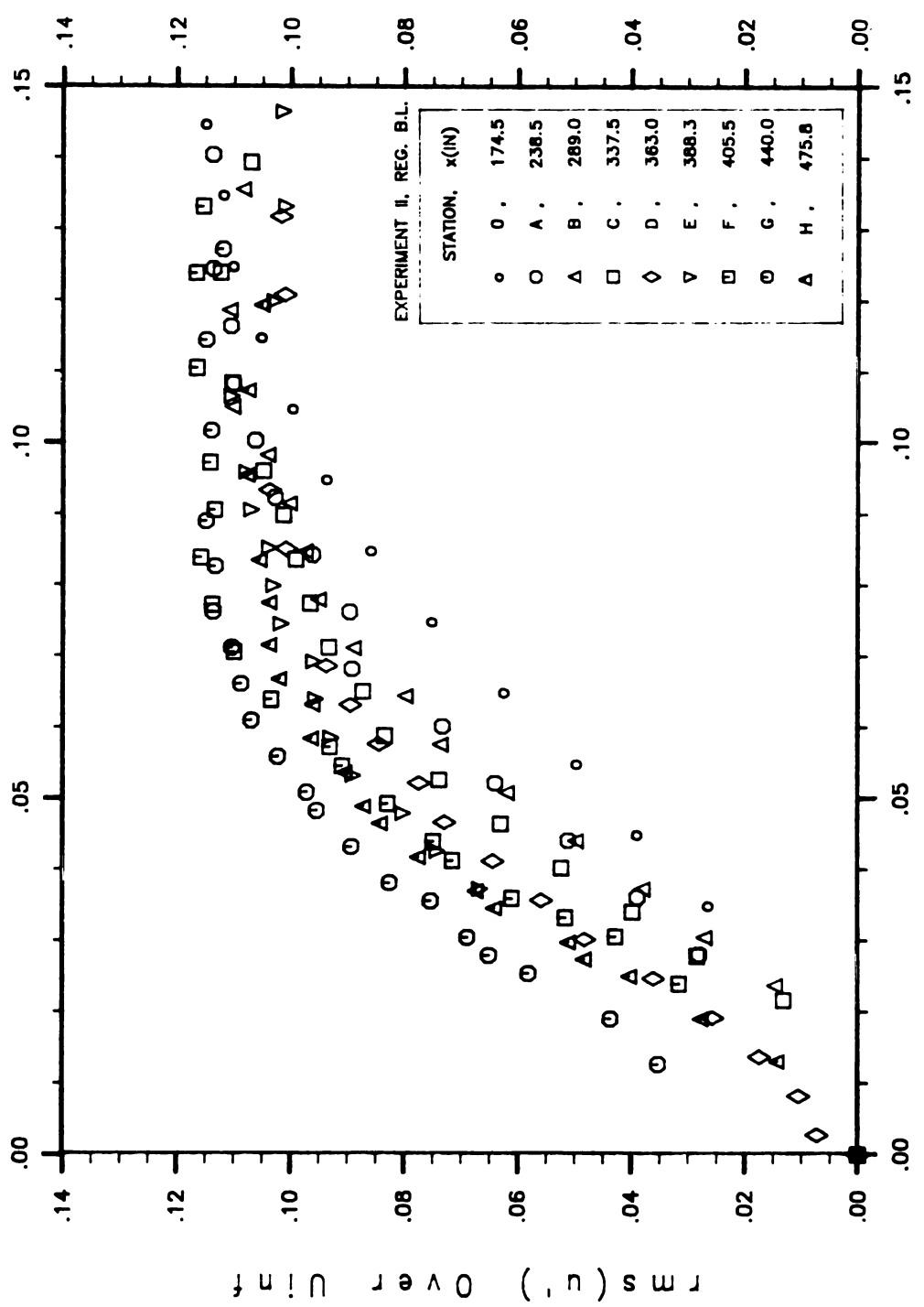

Figure 3.25 Near wall variation of rms(u')/U_∞ vs y/θ at various streamwise stations in regular boundary layer from experiment II.

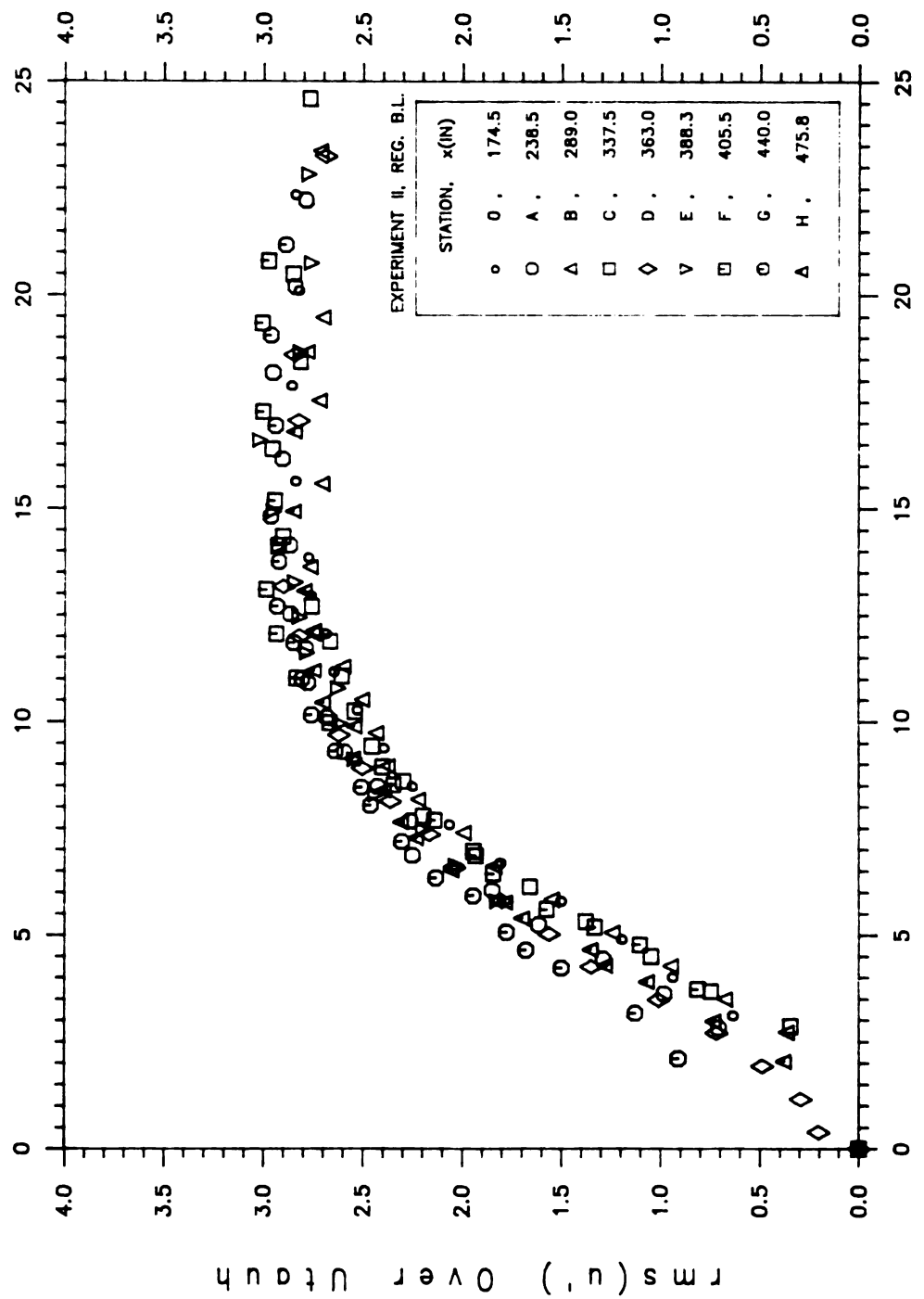

Figure 3.26 Near wall variation of $rms(u')/u_{\tau\theta}$ vs $\rho y u_{\tau\theta}/\mu$ at various streamwise stations in regular boundary layer from experiment II.

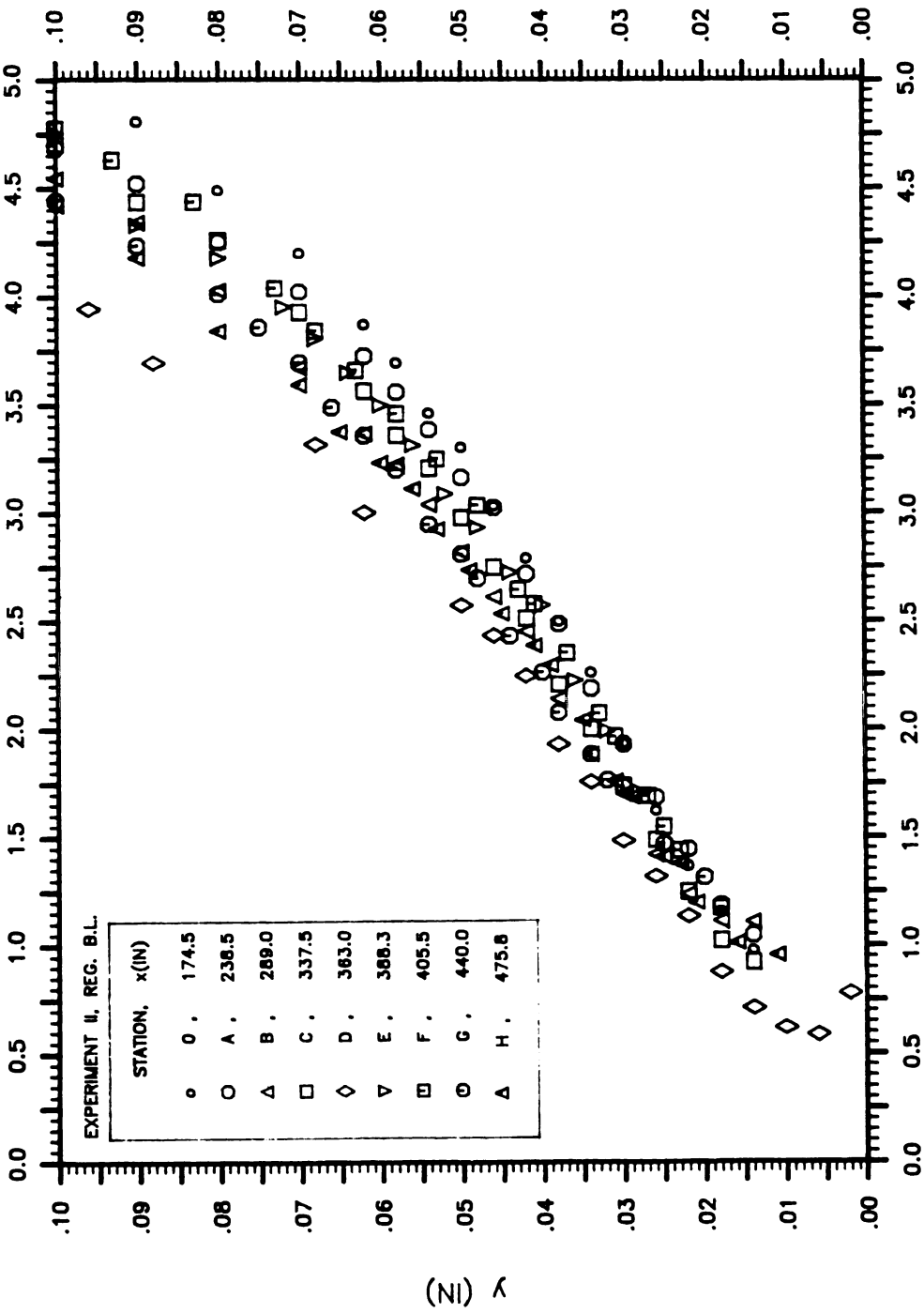

Figure 3.27 Near wall mean velocity profile (y vs $\bar{U}$) at various streamwise stations in regular boundary layer from experiment II.

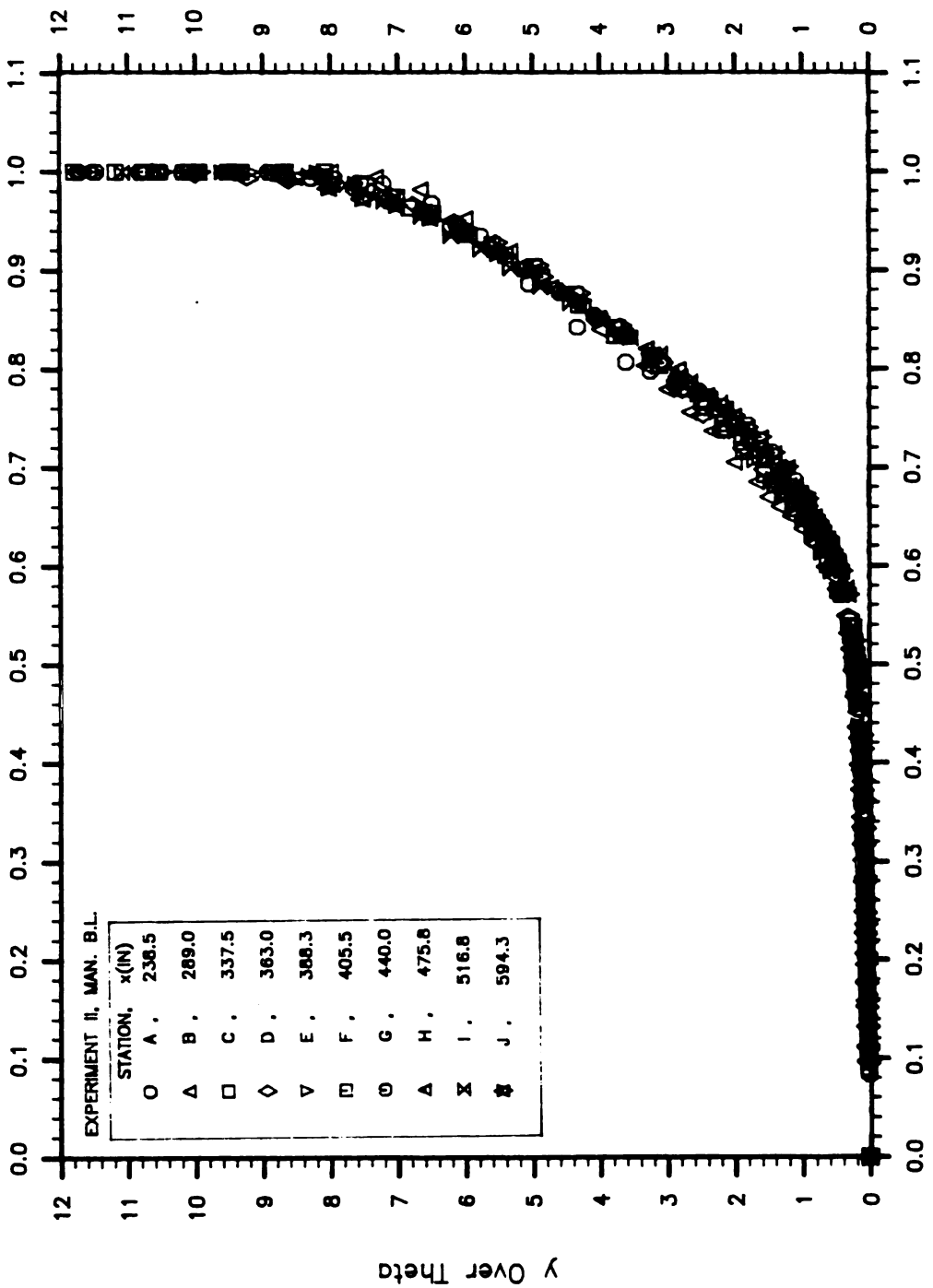

Figure 3.28 Non-dimensional mean velocity profiles (y/θ vs $\overline{U}/U_{\infty}$) at various streamwise stations in manipulated boundary layer from experiment II.

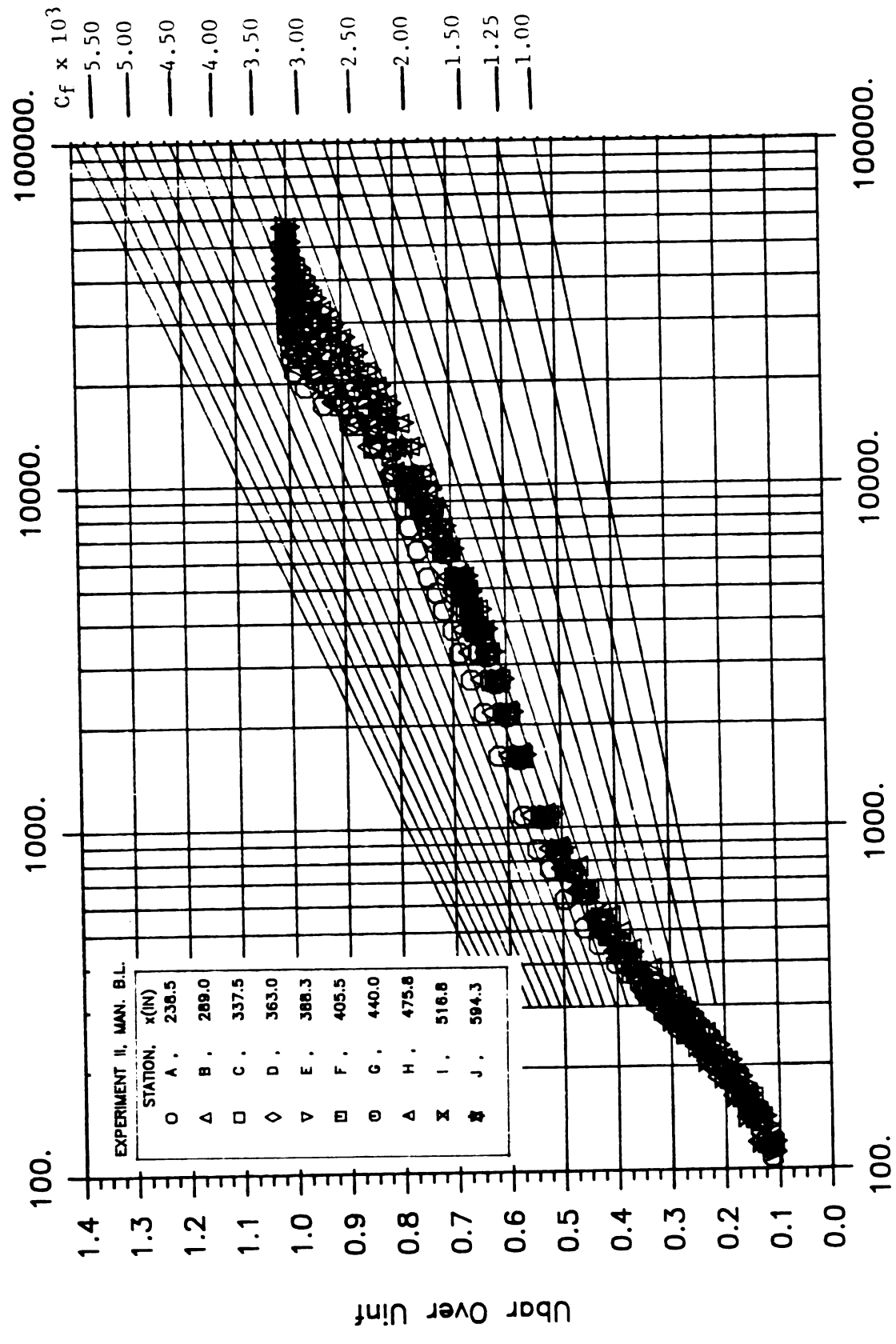

Figure 3.29 Clauser plot for mean velocity profiles ($\bar{U}/U_\infty$ vs $\rho U_\infty y/\mu$) at various streamwise stations in manipulated boundary layer from experiment II.

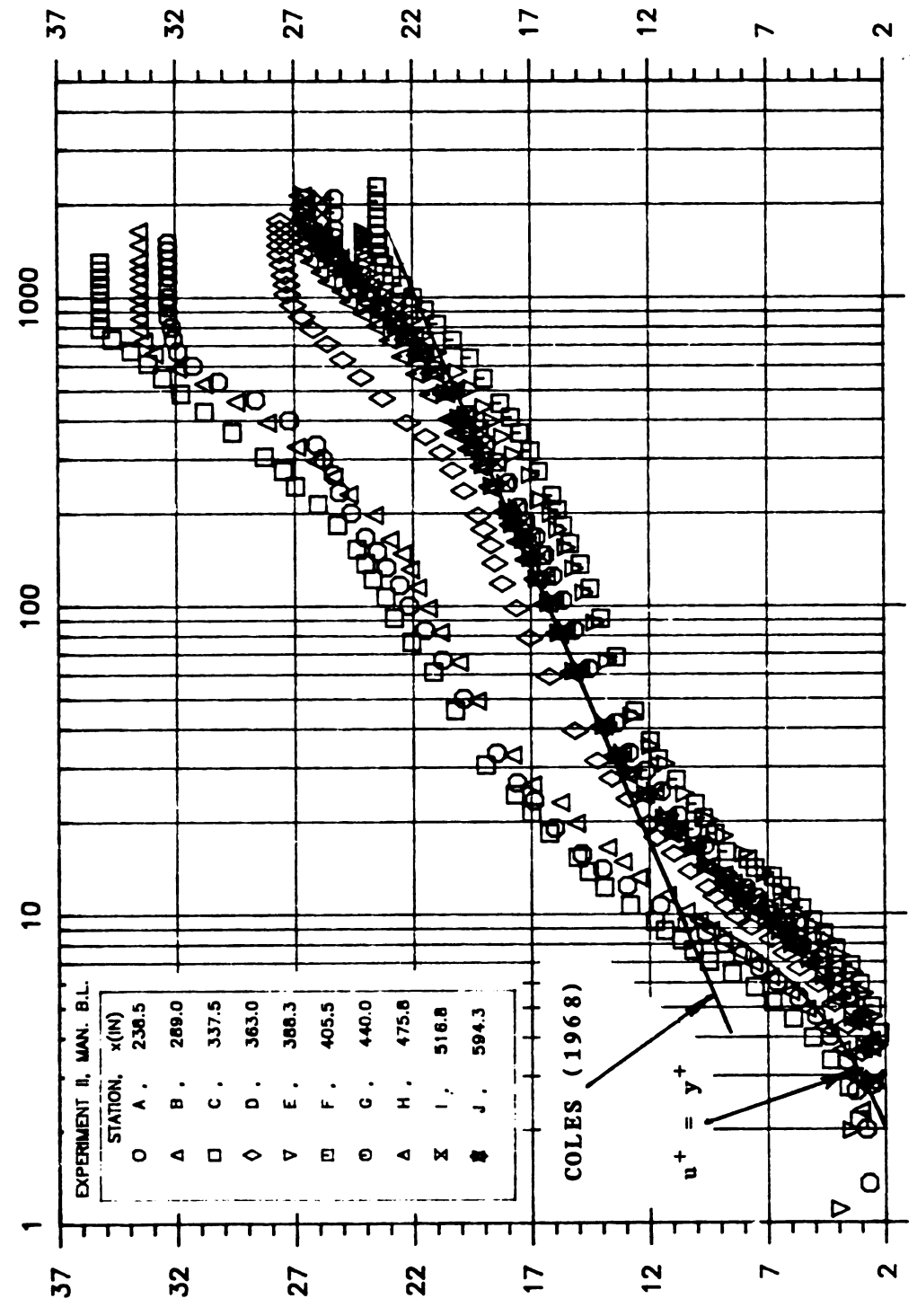

Figure 3.30 Wall-unit non-dimensionalized mean velocity profiles ($\bar{U}/u_\tau\theta$ vs $\rho y u_\tau\theta/\mu$) at various streamwise stations in manipulated boundary layer from experiment II.

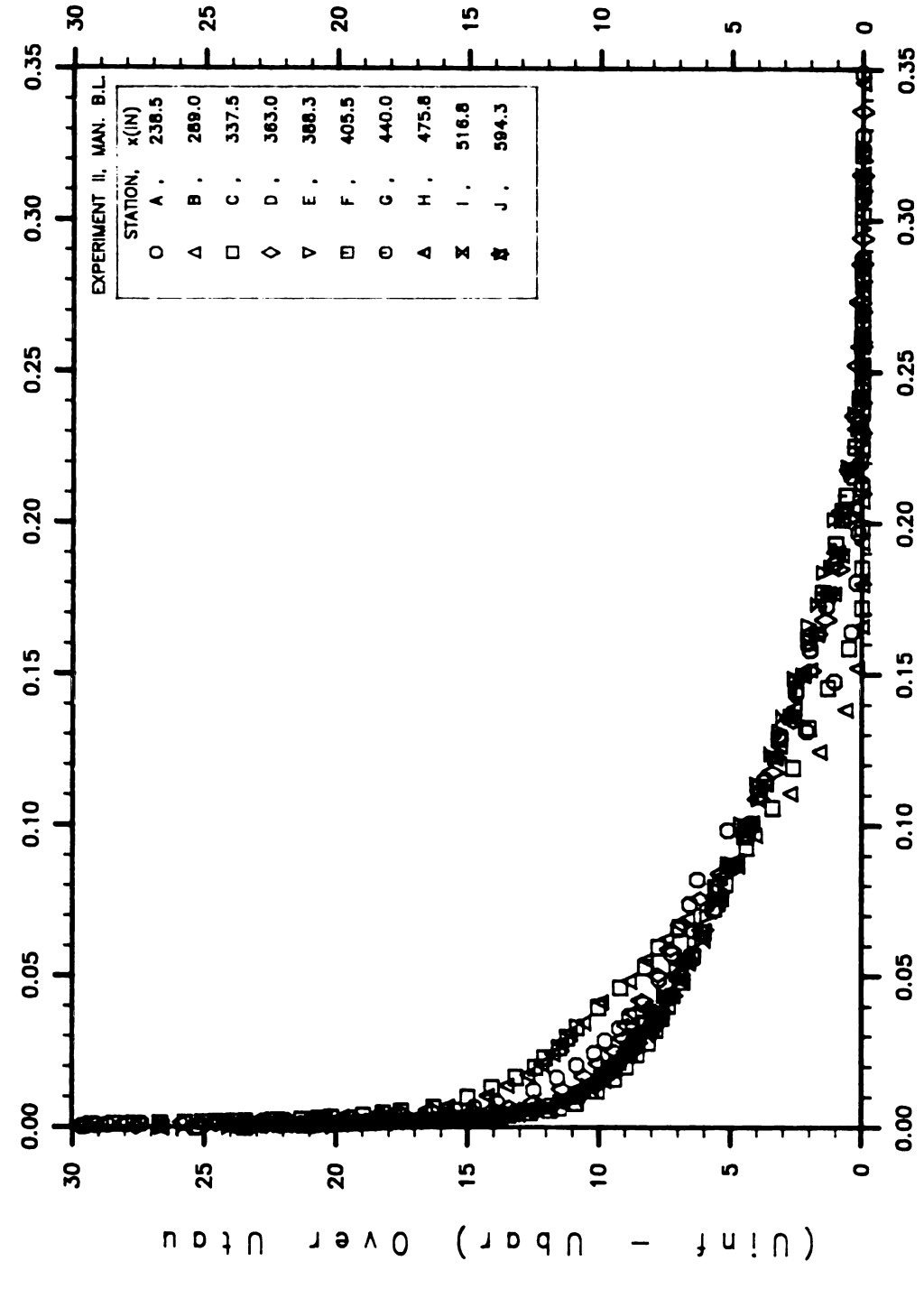

Figure 3.31 Variation of $(U_\infty - \bar{U})/u_{\tau\theta}$ vs $(yu_{\tau\theta}/\delta_d U_\infty)$ at various streamwise stations in manipulated boundary layer from experiment II.

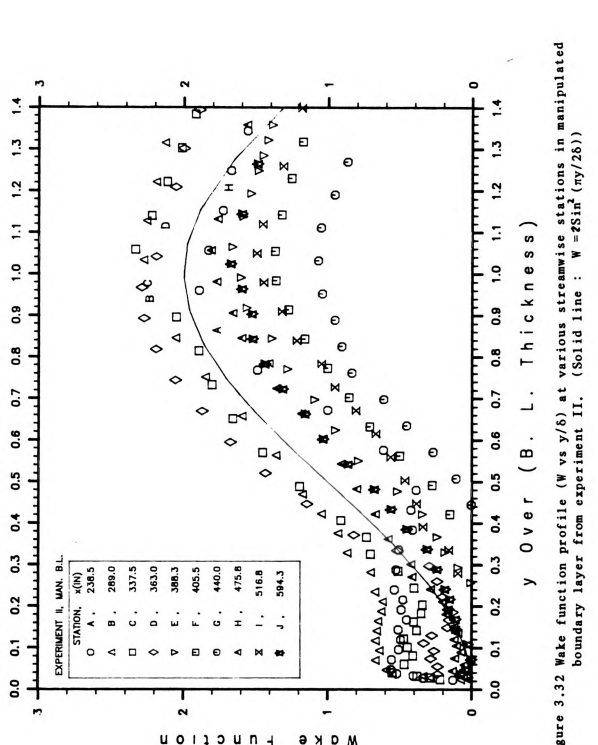

Figure 3.32 Wake function profile (W vs y/δ) at various streamwise stations in manipulated boundary layer from experiment II. (Solid line : $W = \beta \sin^2(\pi y/2\delta)$)

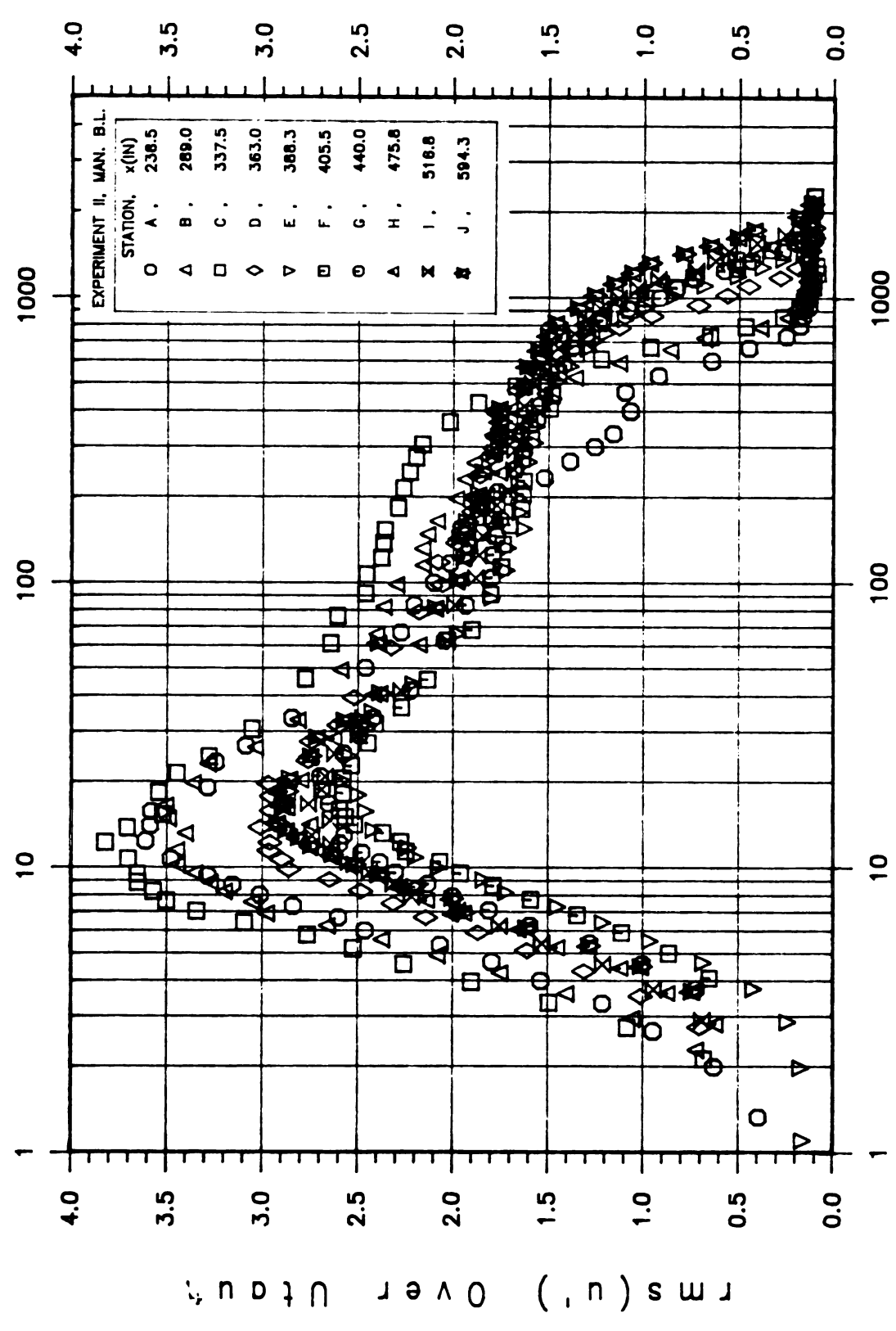

Figure 3.33 Wall-unit non-dimensionalized fluctuating velocity profile (rms(u')/$u_{\tau\theta}$ vs $\rho y u_{\tau\theta}/\mu$) at various streamwise stations in manipulated boundary layer from experiment II.

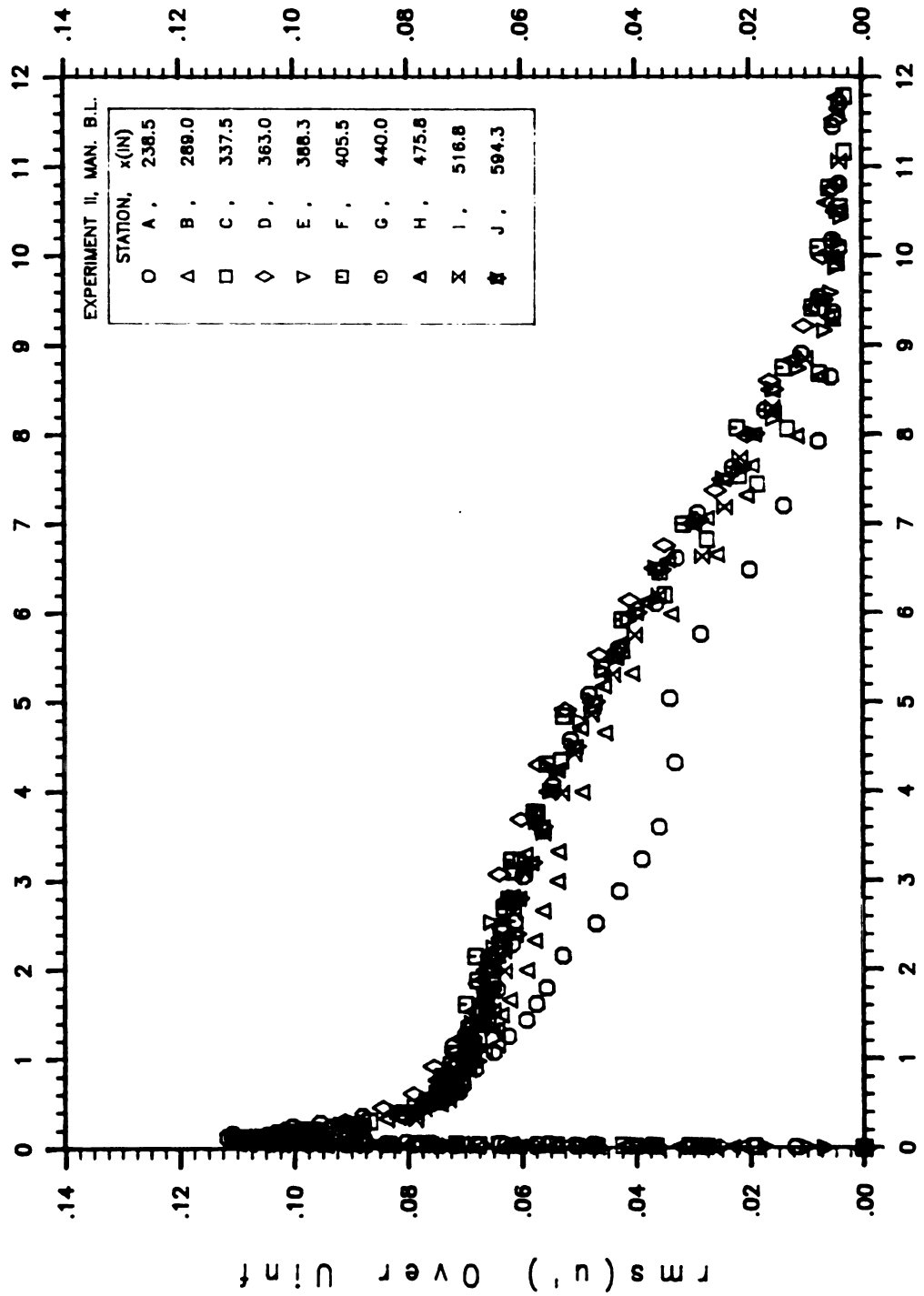

Figure 3.34 Variation of rms(u')/U_∞ vs y/θ at various streamwise stations in manipulated boundary layer from experiment II.

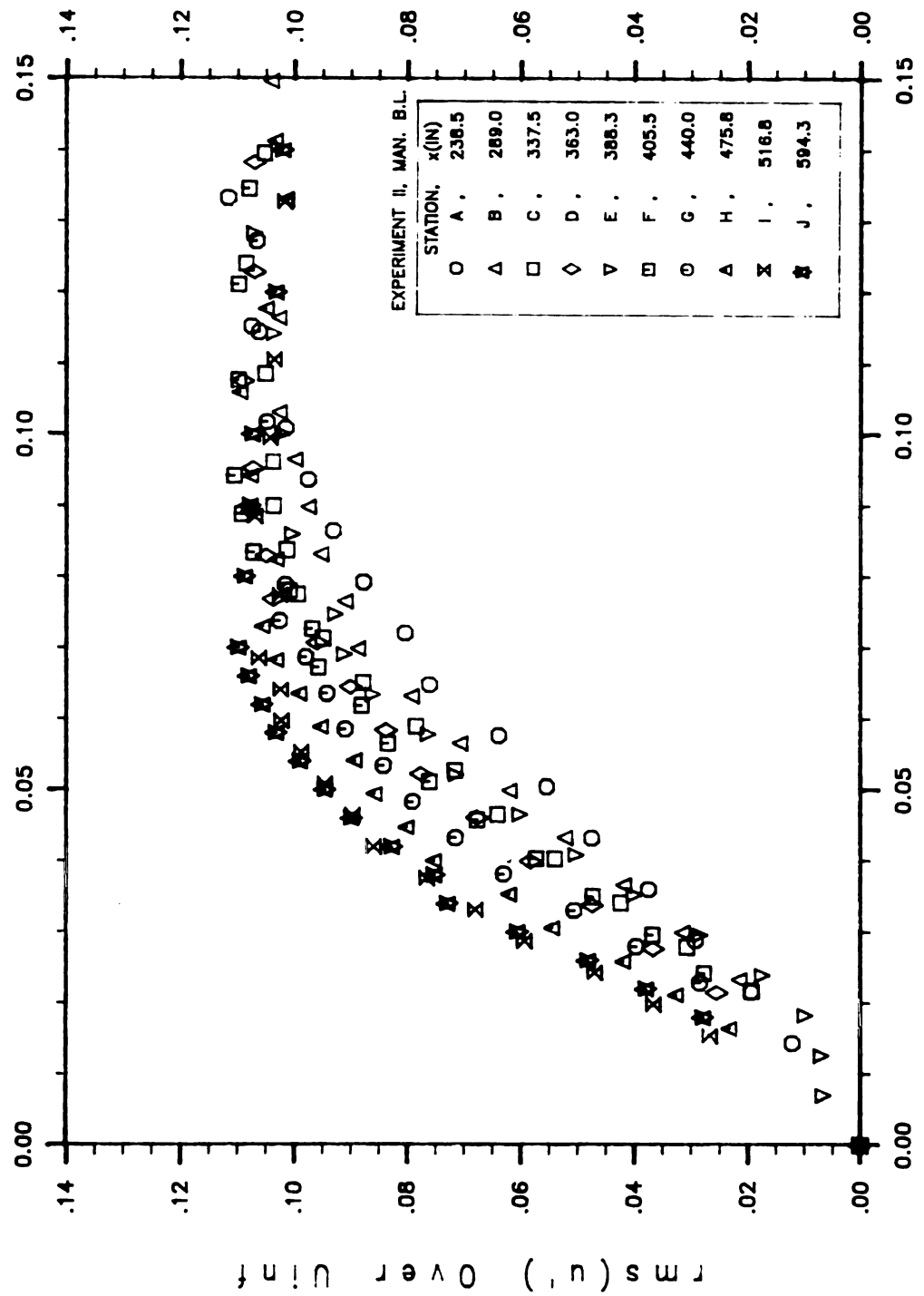

Figure 3.35 Near wall variation of rms(u')/U_∞ vs y/θ at various streamwise stations in manipulated boundary layer from experiment II.

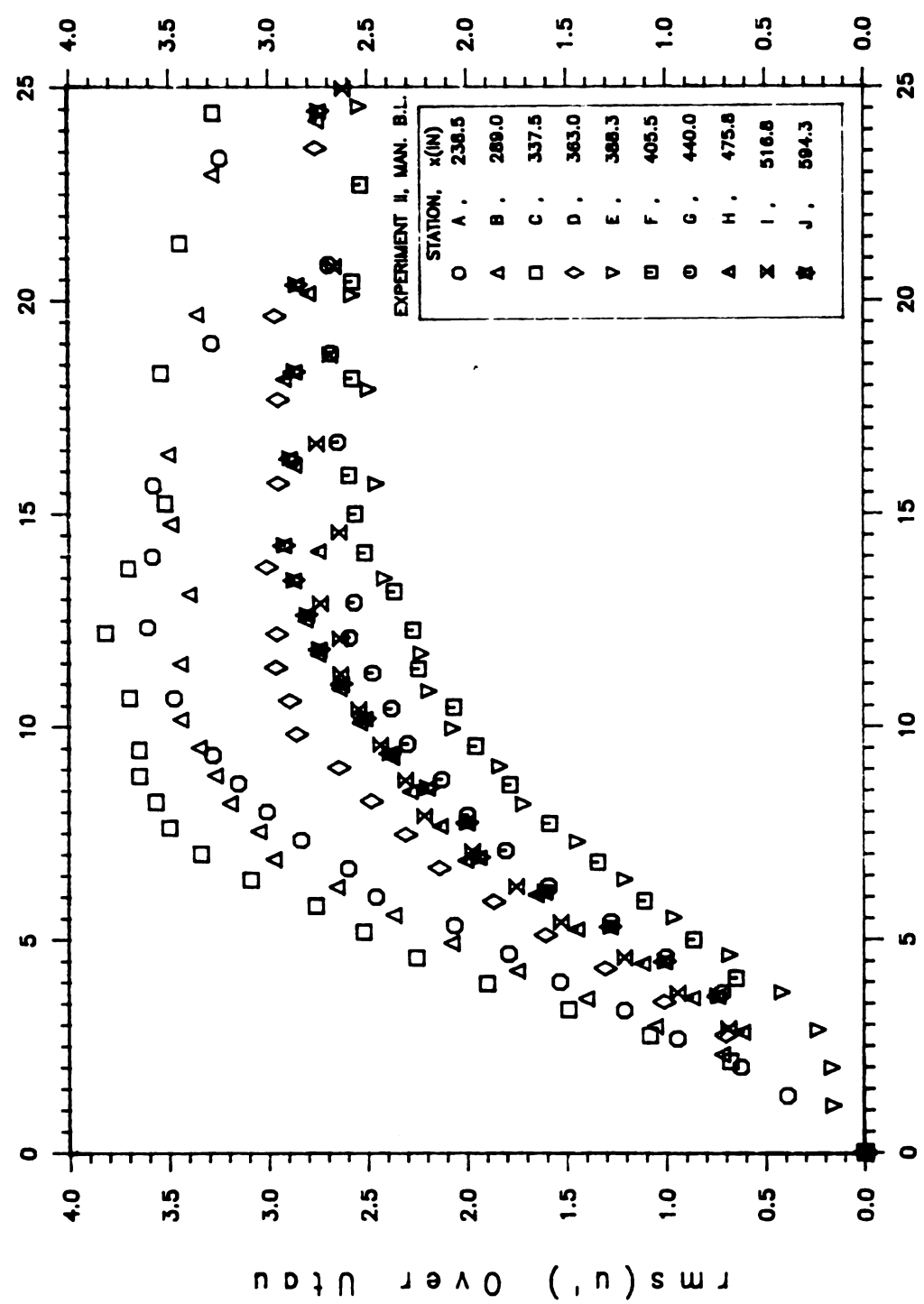

Figure 3.36 Near wall variation of rms(u')/$u_{\tau\theta}$ vs $\rho y u_{\tau\theta}/\mu$ at various streamwise stations in manipulated boundary layer from experiment II.

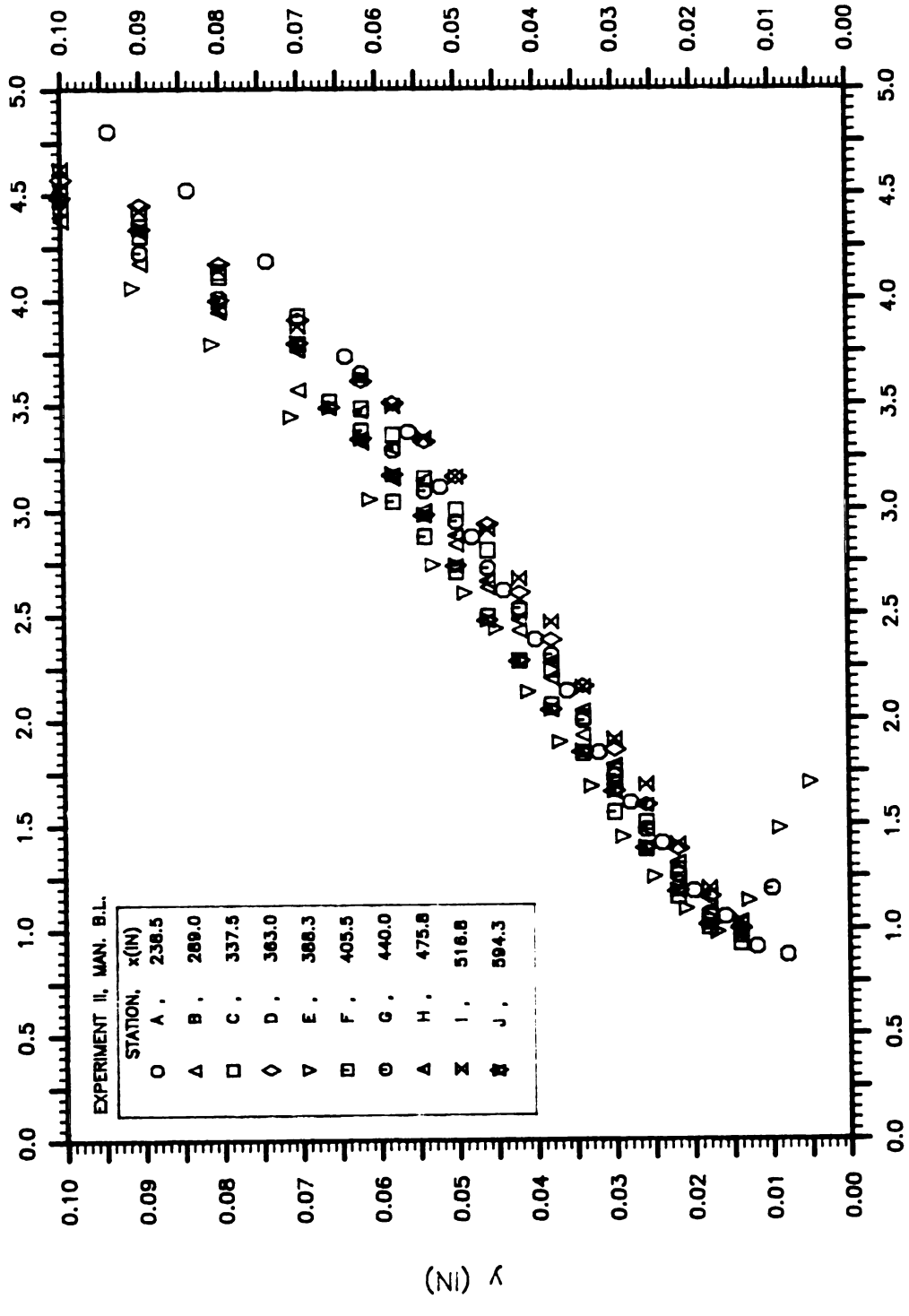

Figure 3.37 Near wall mean velocity profiles (y vs $\bar{U}$) at various streamwise stations in manipulated boundary layer from experiment II.

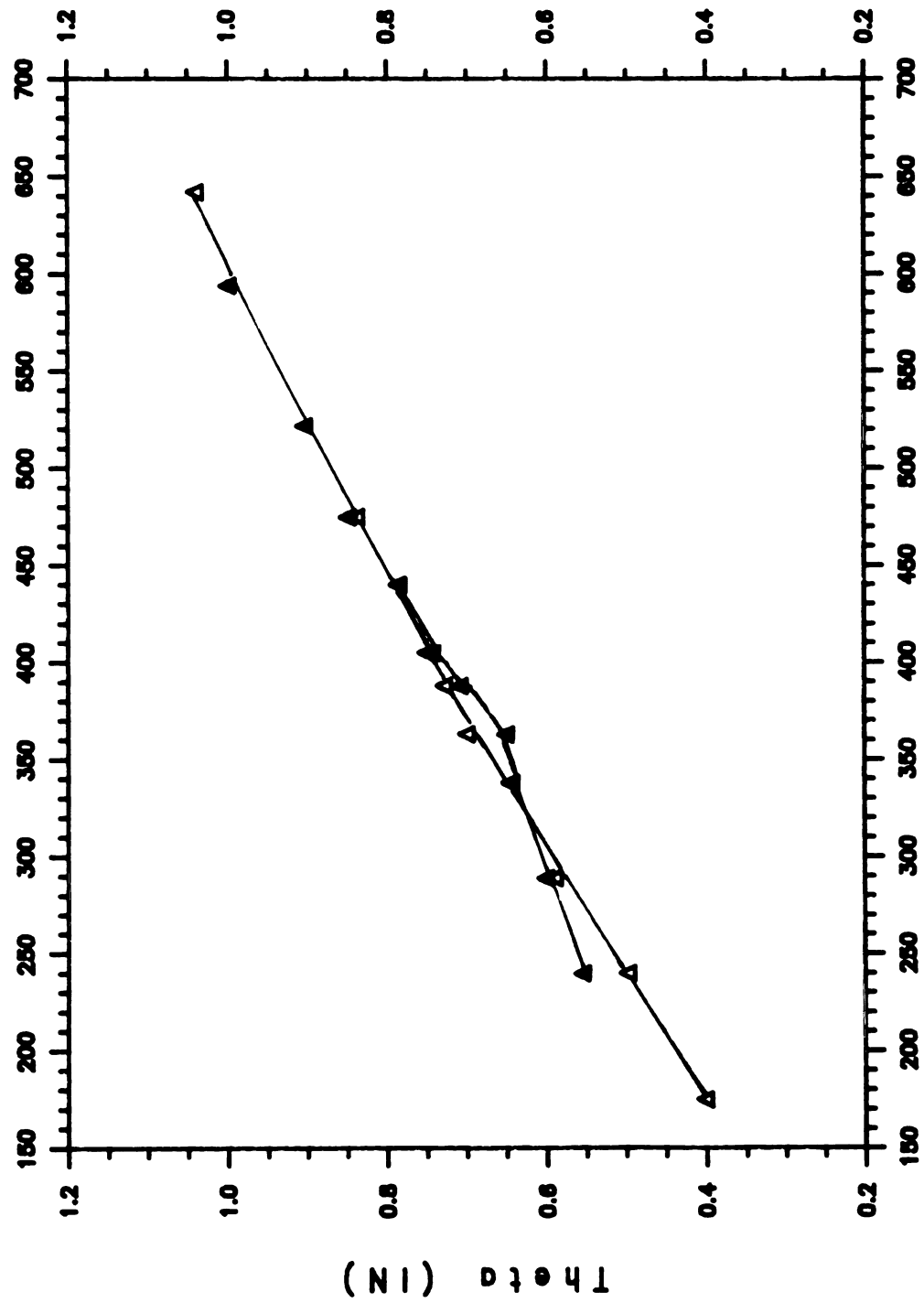

Figure 3.38 Comparison of streamwise momentum thickness distributions (θ vs x) for regular (open) and manipulated (filled) boundary layers from experiment II.

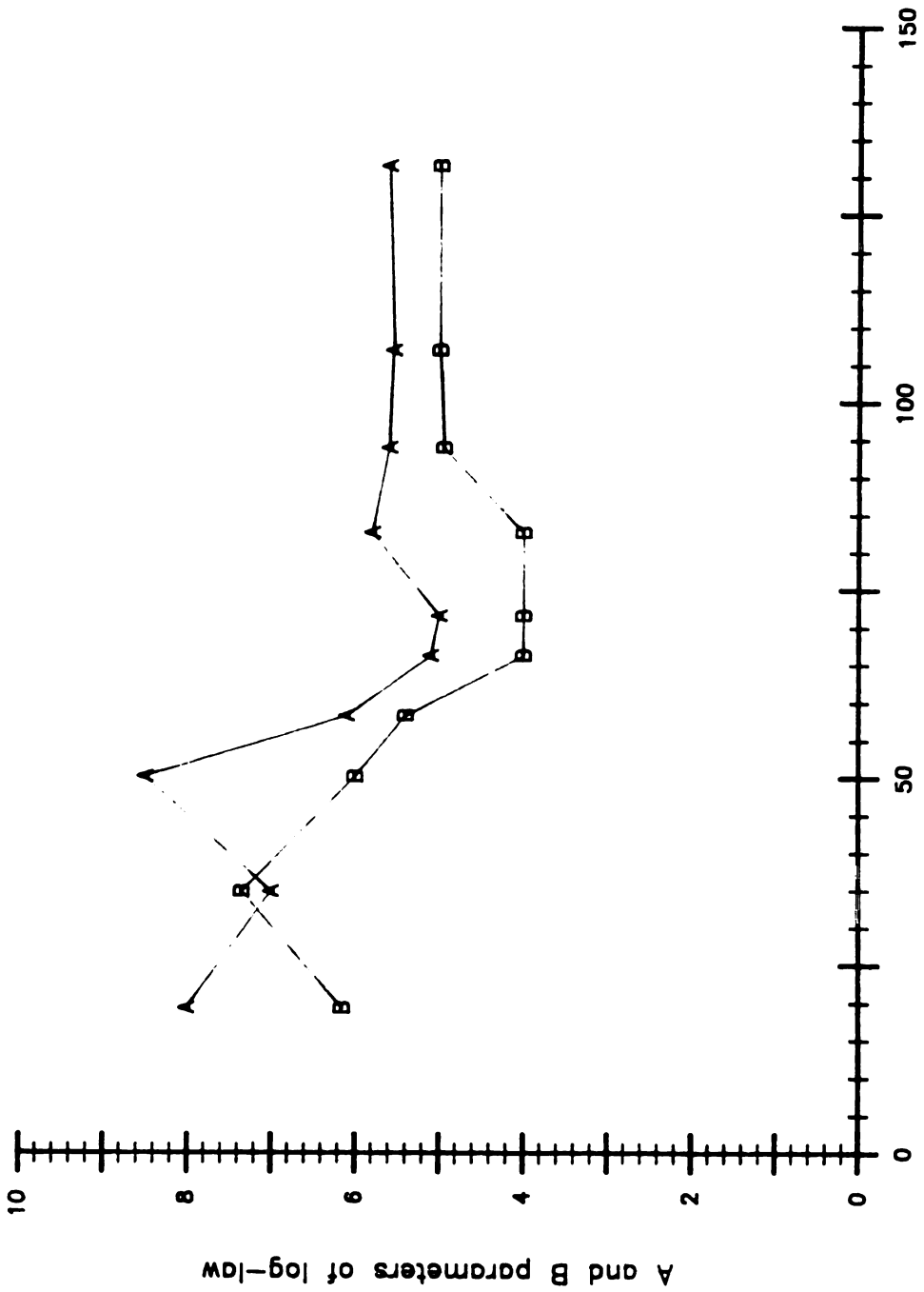

Figure 3.39 Streamwise variation of "law of the wall" ($u^+ = A\log_{10}(y^+) + B$) parameters (A and B) in manipulated boundary layers from experiment II.

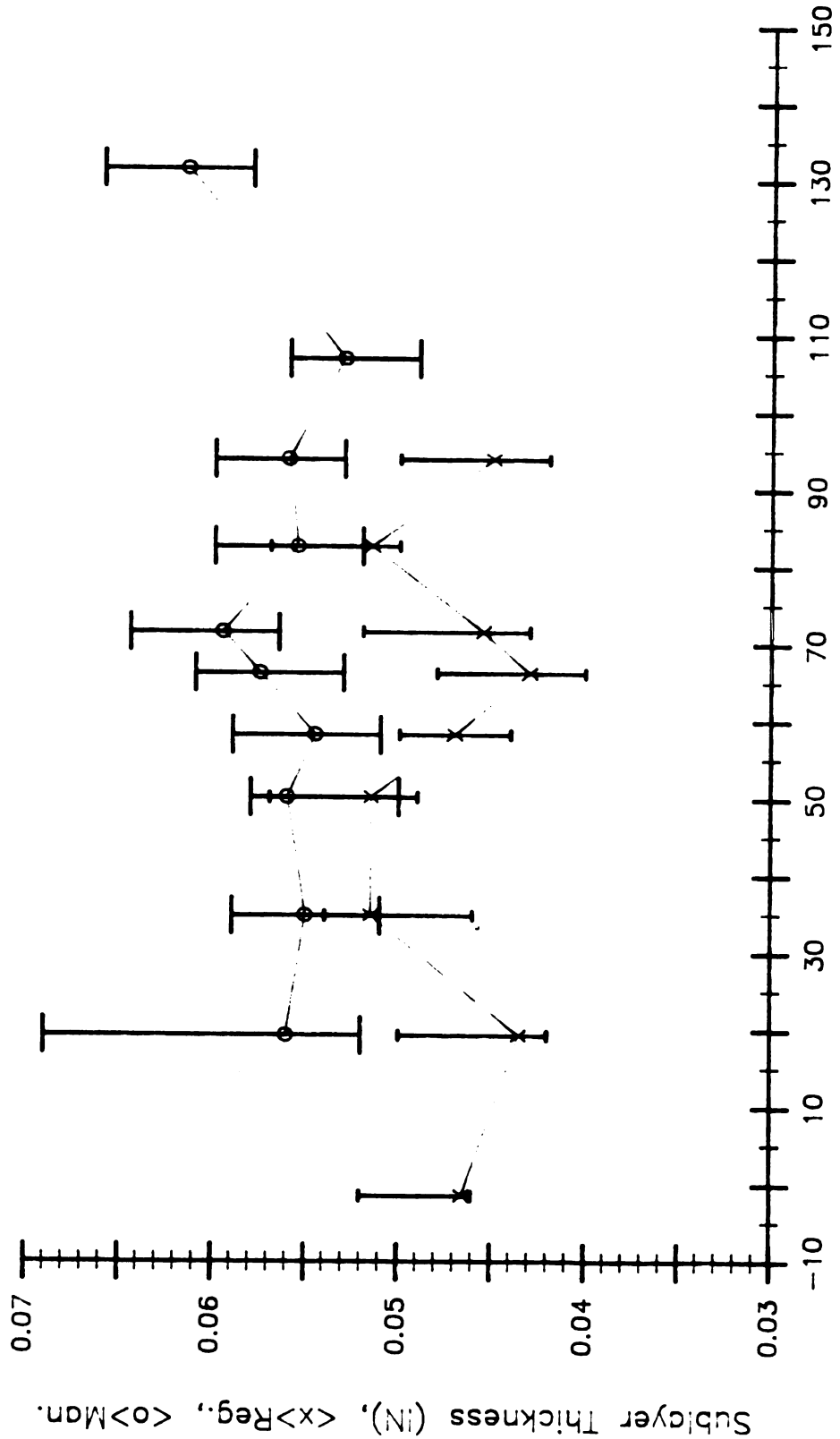

Figure 3.40 Comparison of streamwise sublayer thickness distribution (δ_{s1} vs ξ) in regular (x), and manipulated (o) boundary layers. (The ends of error bars represent distances of the data points below and above the chosen sublayer thickness shown in the figure).

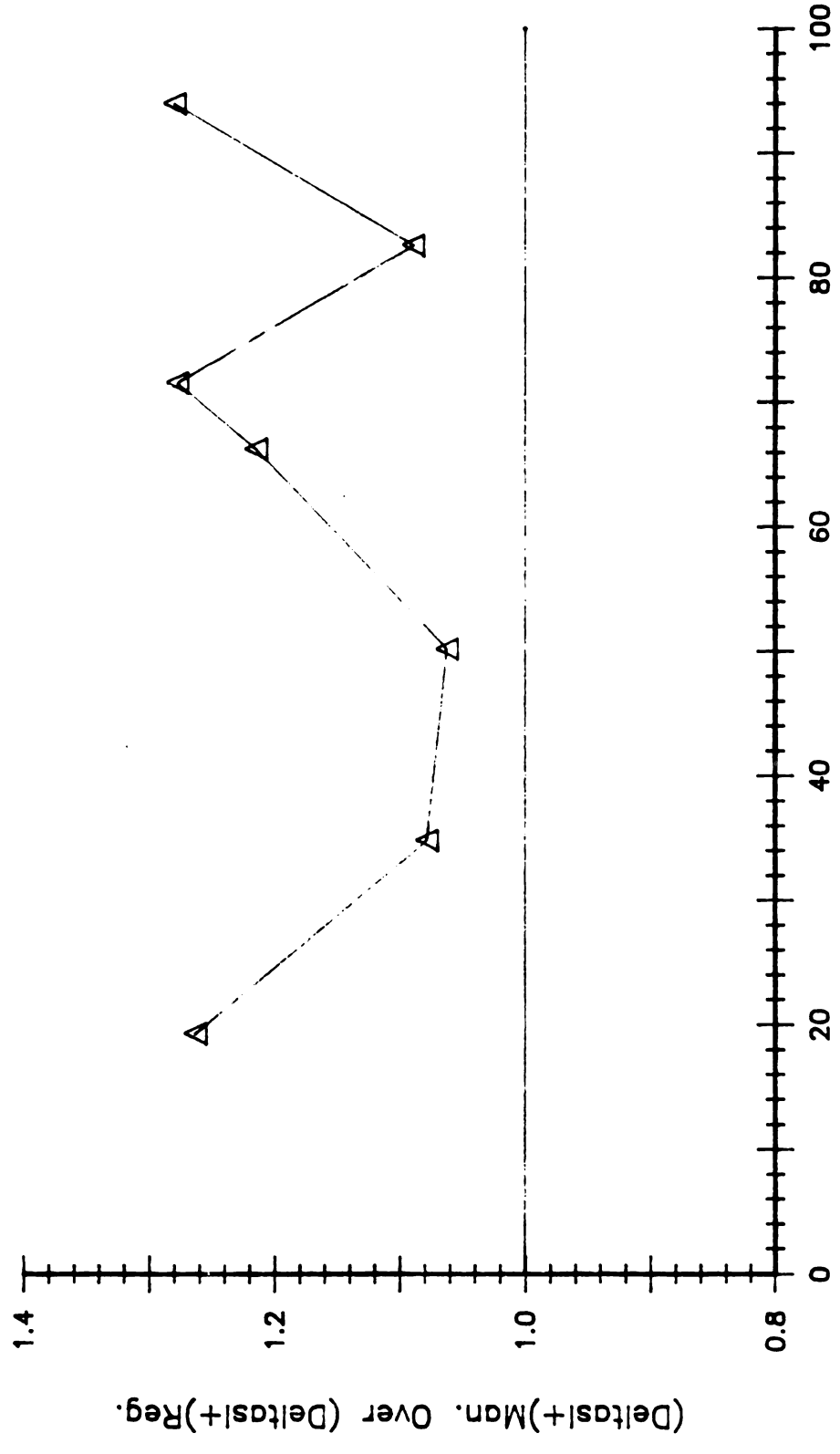

Figure 3.41 Wall-unit non-dimensionalized ratio of sublayer thickness $[\rho\delta_{sl}u_{\tau n}/\mu]_{man.}/[\rho\delta_{sl}u_{\tau n}/\mu]_{reg.}$ vs ξ.

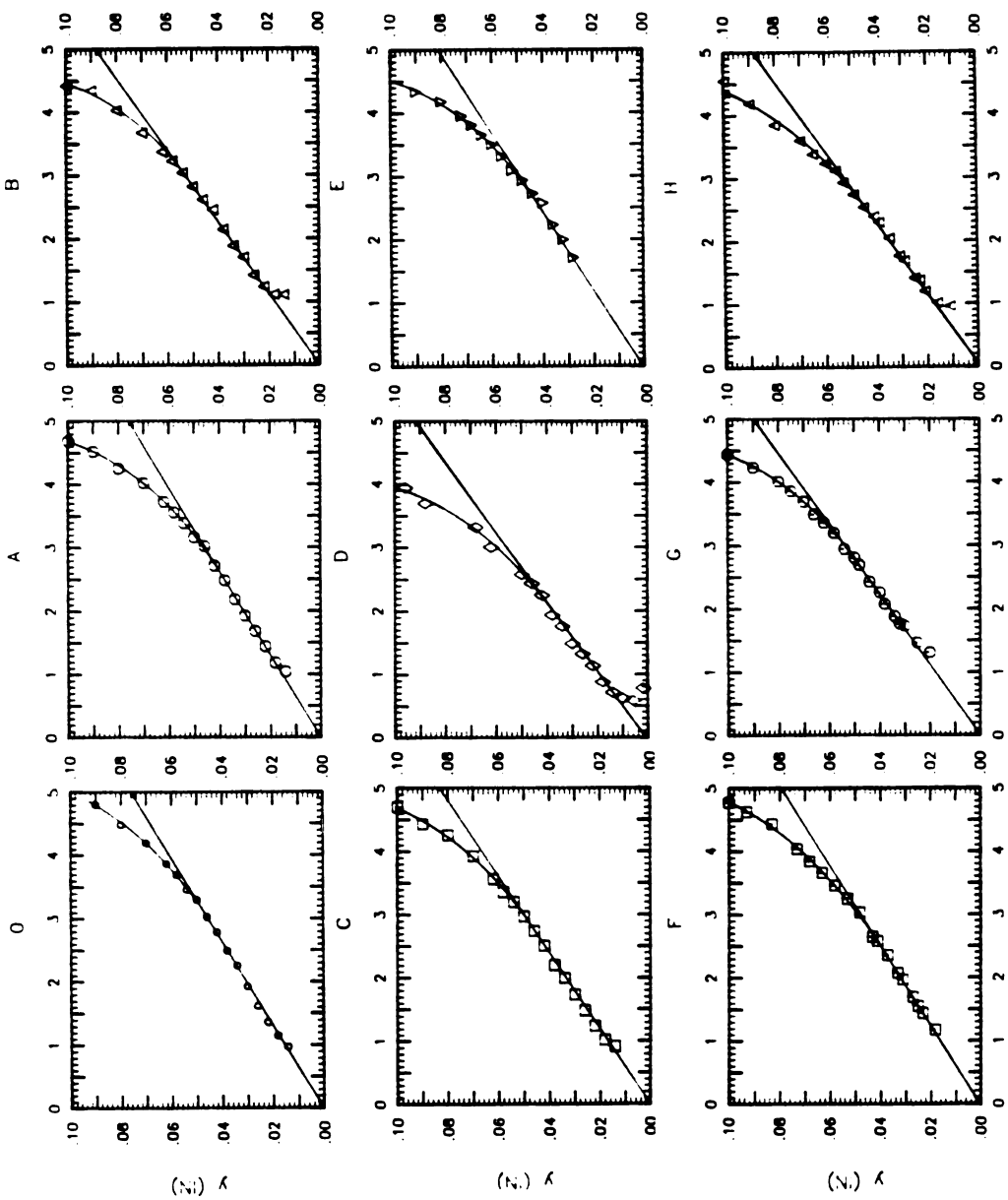

Figure 3.42 Near wall mean velocity profile (y vs $\bar{U}$) at various streamwise stations (O, A-H) used to measure the $d\bar{U}/dy_w$ and the sublayer thickness in regular boundary layer from experiment II.

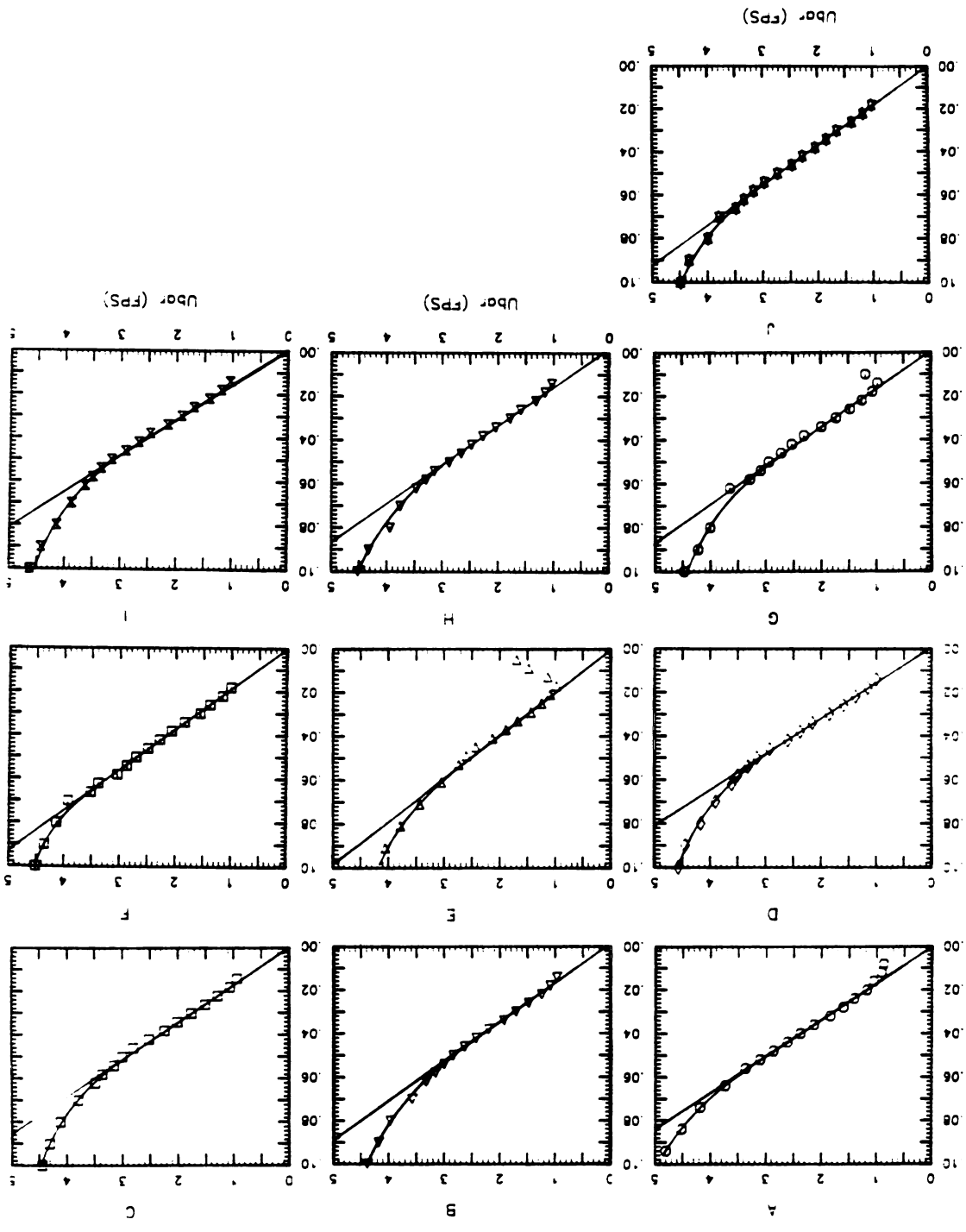

Figure 3.43 Near wall mean velocity profile (y (In.) vs $\bar{U}$) at various streamwise stations (A-J) used to measure the $d\bar{U}/dy_w$ and the sublayer thicknees in manipulated boundary layer from experiment II.

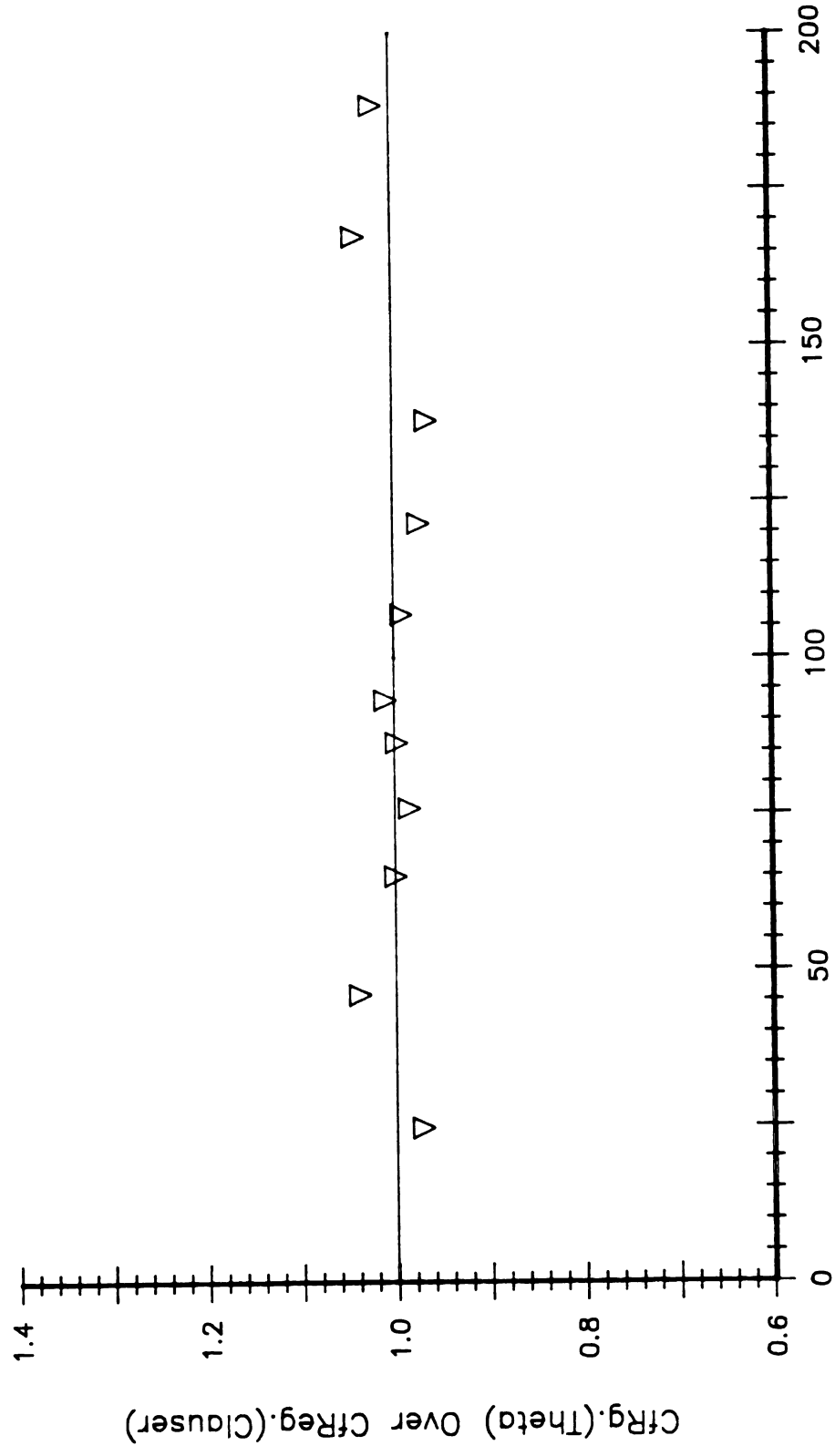

Figure 3.44 Streamwise variation of the $C_{f\theta}/C_{fc}$ in regular boundary layer for experiment I.

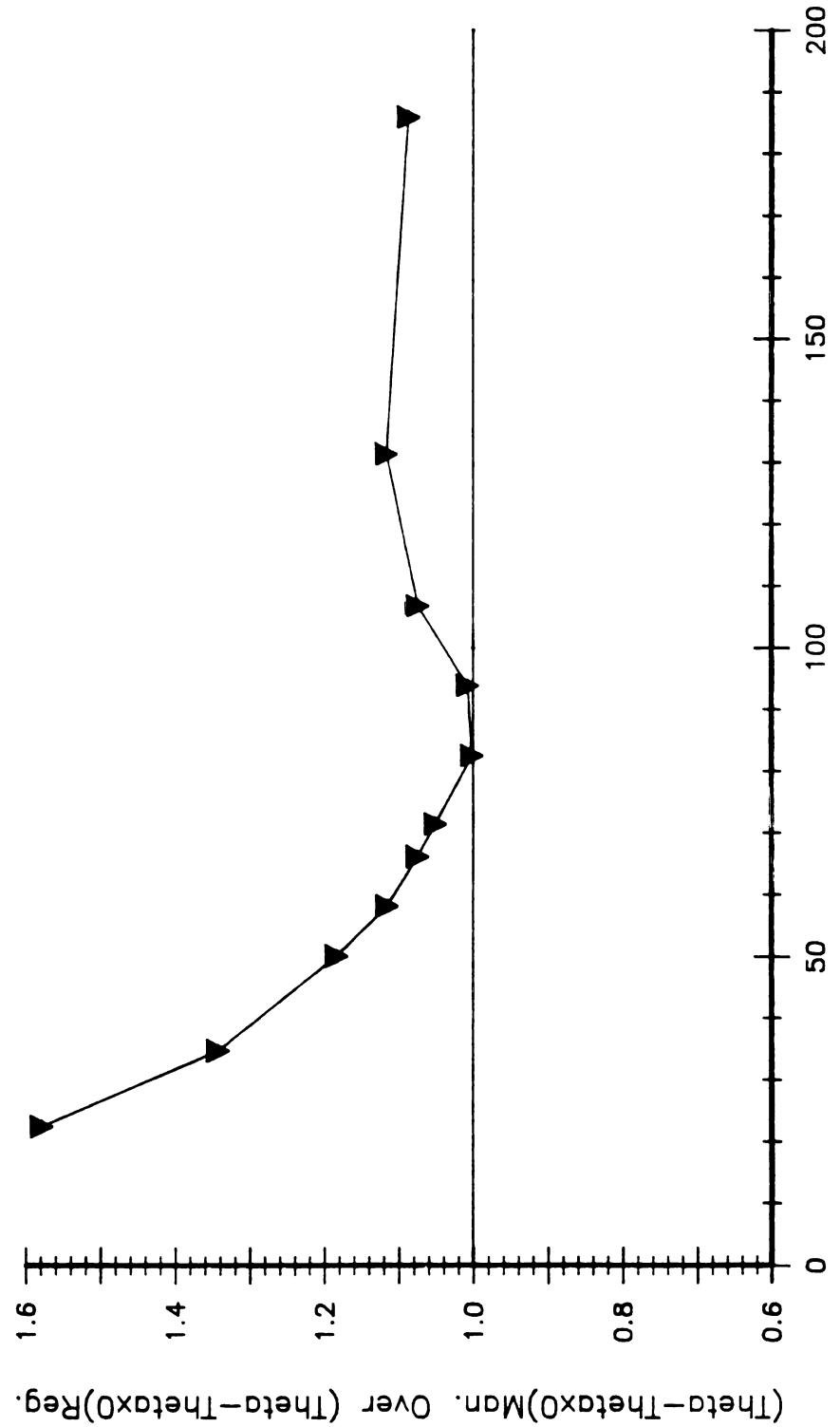

Figure 3.45 Streamwise variation of the non-dimensional net drag ratio (NDR) $(\theta - \theta_o)_{Man.}/(\theta - \theta_o)_{Reg.}$ for experiment I.

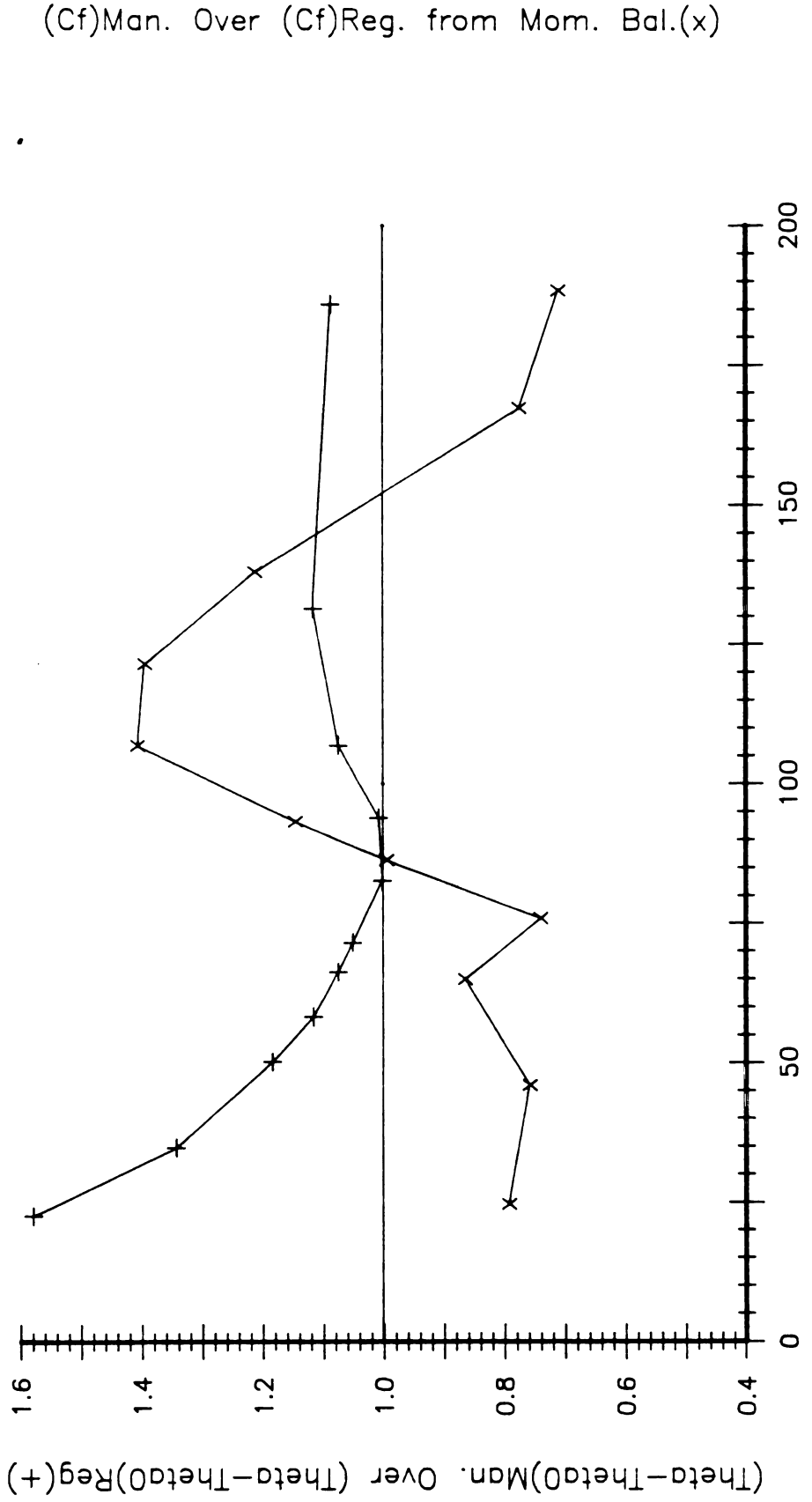

Figure 3.46 Comparison between streamwise variation of the non-dimensional net drag ratio (NDR) $(\theta - \theta_0)_{Man.}/(\theta - \theta_0)_{Reg.}$ (+), and the local skin friction ratio $(C_{f\theta})_{Man.}/(C_{f\theta})_{Reg.}$ (x) both obtained from momentum balance in experiment I.

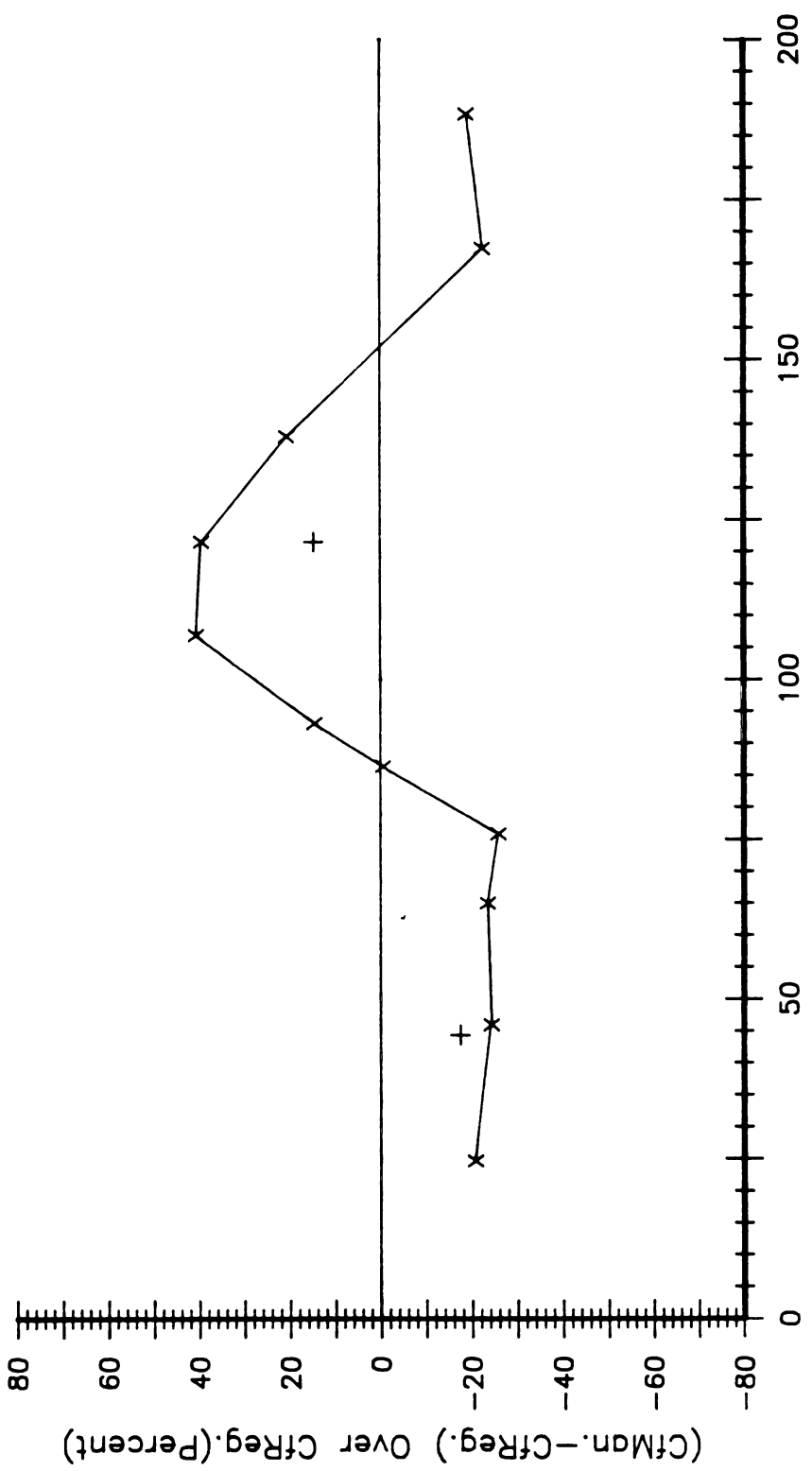

Figure 3.47 Comparison between streamwise percent variation of $(C_{fMan.} - C_{fReg.}) / C_{fReg.}$ from momentum balance (x), and from slope of mean velocity profile at the wall $(d\bar{U}/dy_w)$ (+) in experiment I.

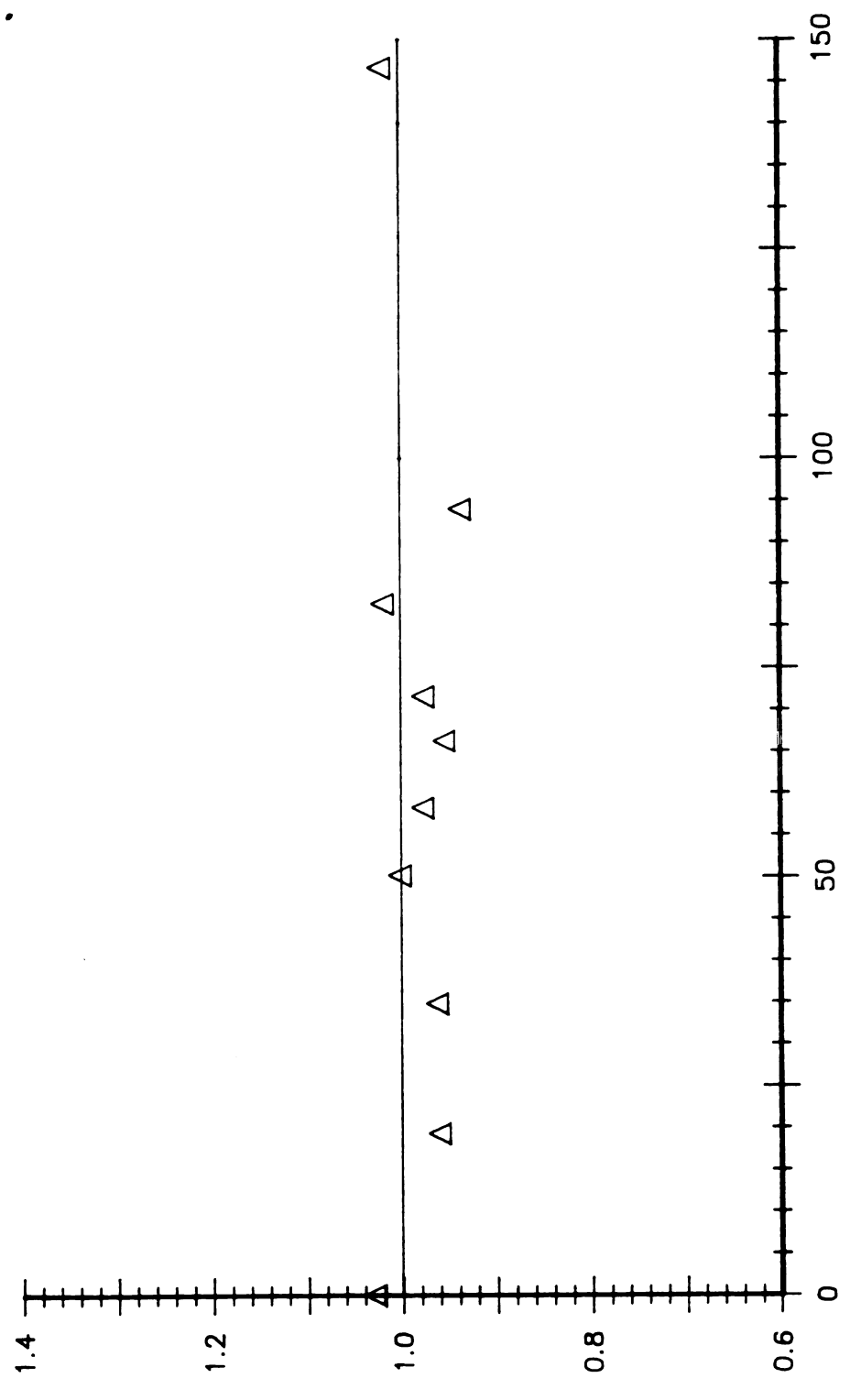

Figure 3.48 Streamwise variation of the $C_{f\theta}/C_{fc}$ in regular boundary layer for experiment II.

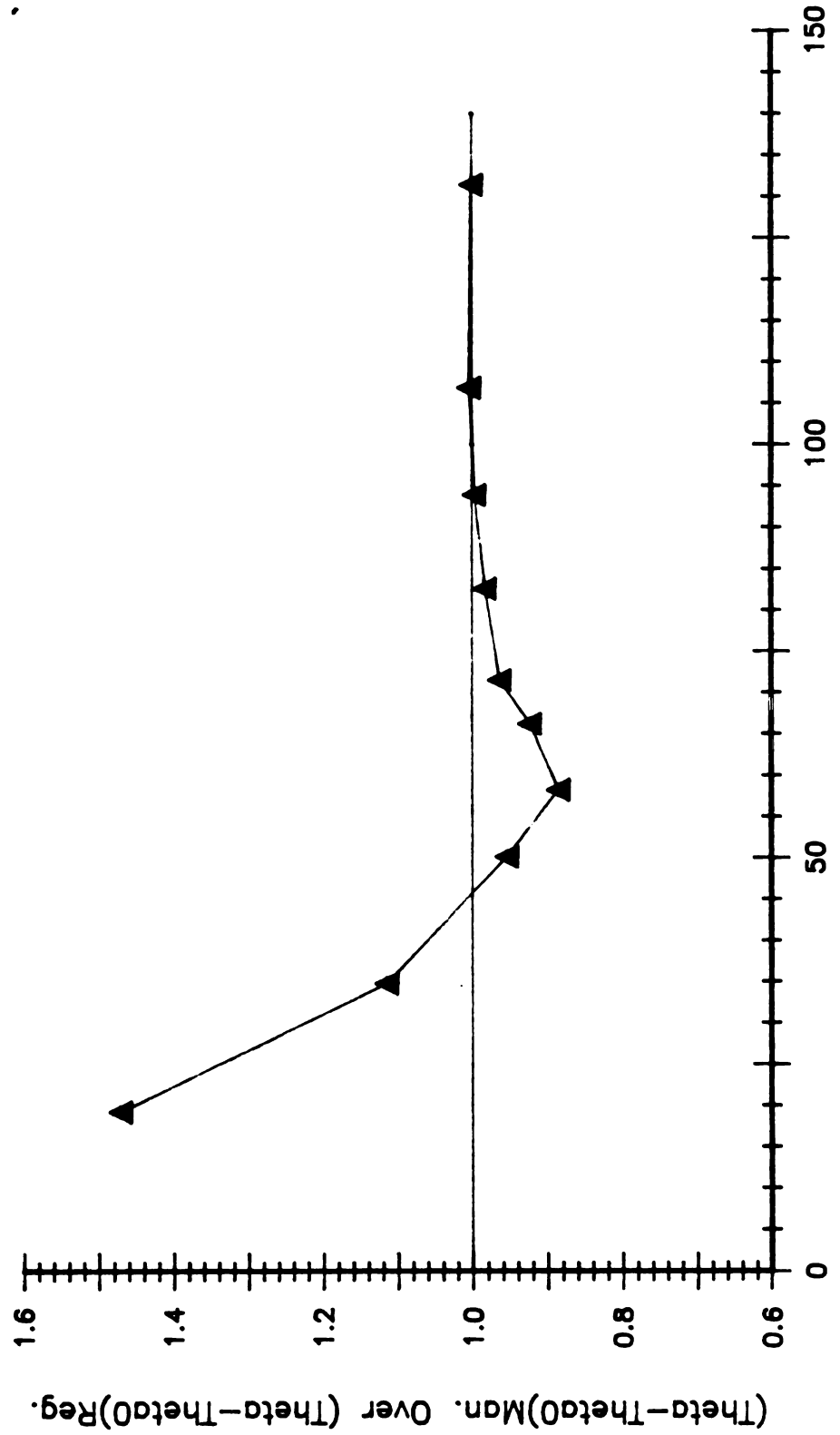

Figure 3.49 Streamwise variation of the non-dimensional net drag ratio (NDR) $(\theta - \theta_e)_{Man.}/(\theta - \theta_e)_{Reg.}$ for experiment II.

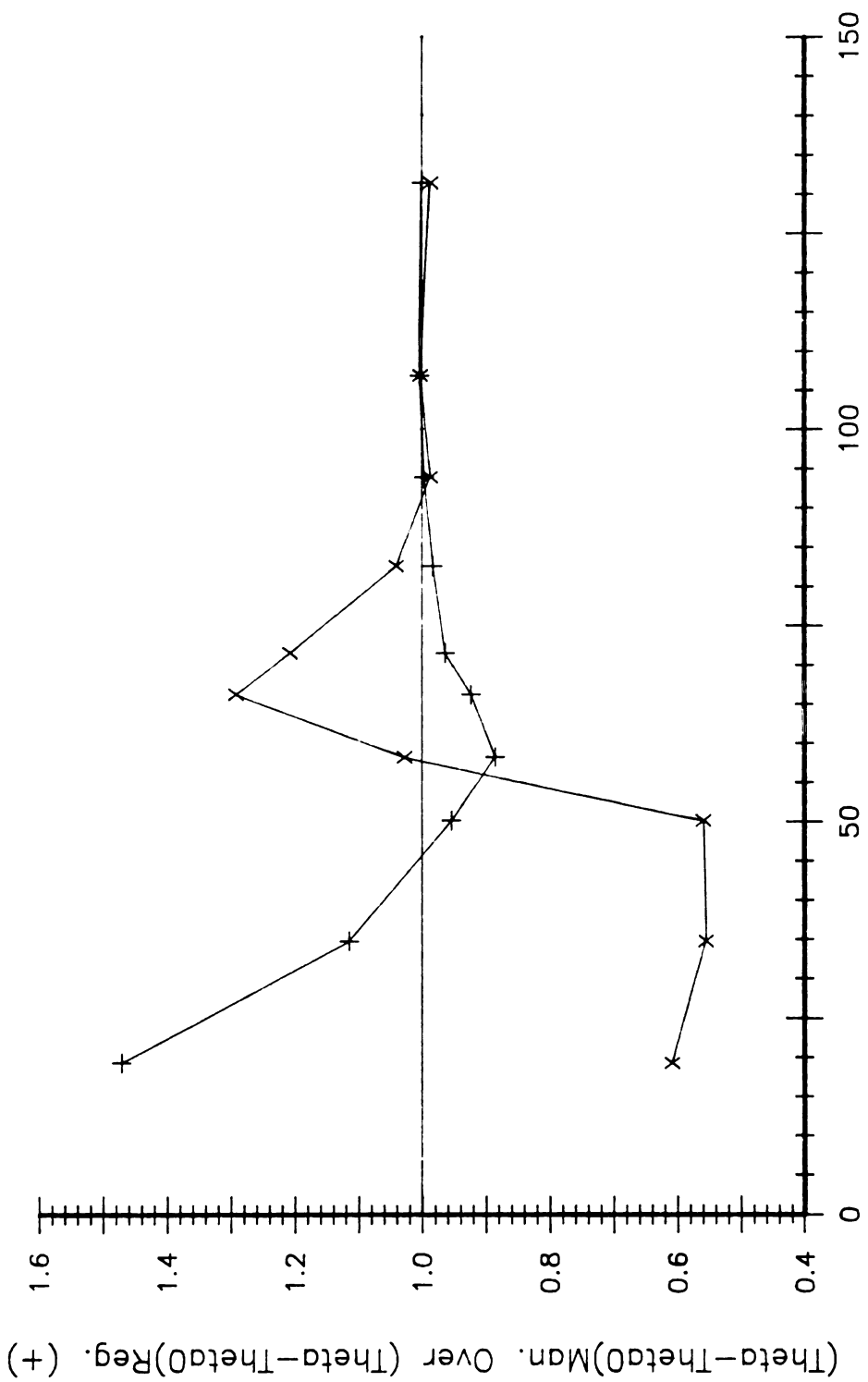

Figure 3.50 Comparison between streamwise variation of the non-dimensional net drag ratio (NDR) $(\theta - \theta_o)_{Man.}/(\theta - \theta_o)_{Reg.}$ (+), and the local skin friction ratio $(C_{f\theta})_{Man.}/(C_{f\theta})_{Reg.}$ (x) both obtained from momentum balance in experiment II.

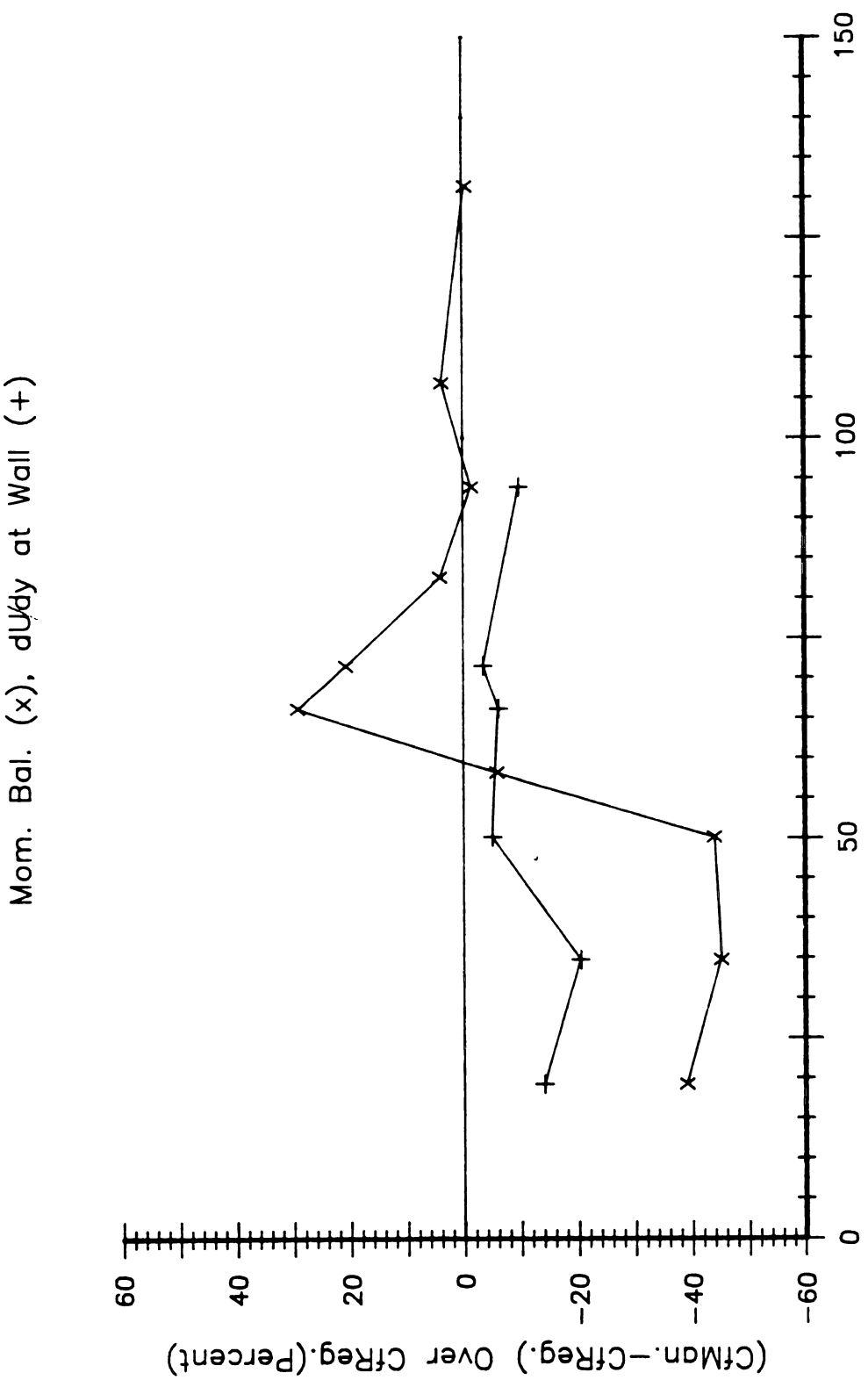

Figure 3.51 Comparison between streamwise percent variation of $(C_{fMan.} - C_{fReg.}) / C_{fReg.}$ from momentum balance (x), and from slope of mean velocity at the wall $(d\bar{U}/dy_w)$ (+) in experiment II.

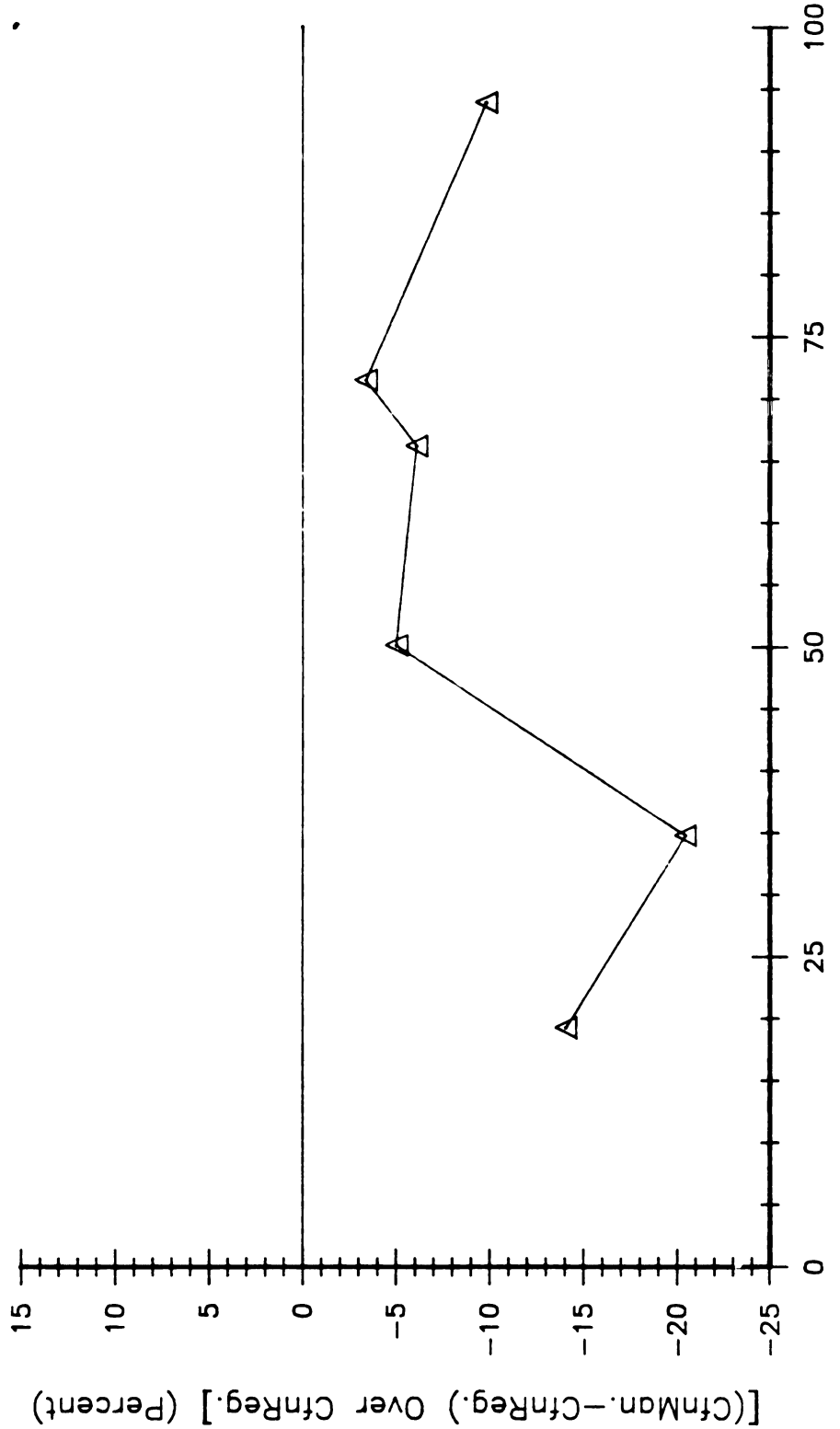

Figure 3.52 Streamwise percent variation of $(C_{fnMan.} - C_{fnReg.}) / C_{fnReg.}$ obtained from slope of mean velocity at the wall $(d\bar{U}/dy_w)$ in experiment II.

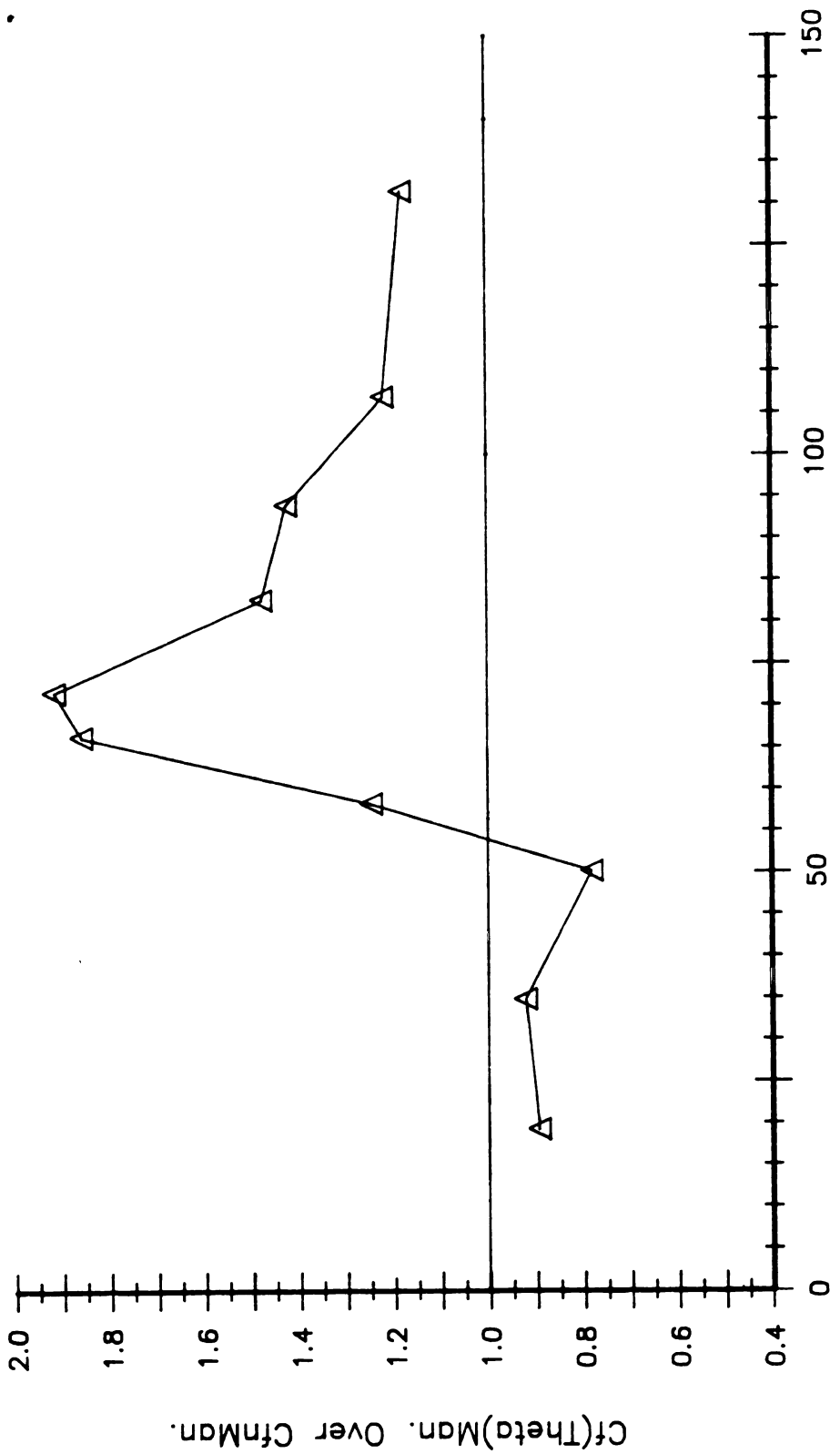

Figure 3.53 Streamwise variation of ratio ($C_{f\theta}$)Man. / C_{fn})Man.) obtained in manipulated boundary layer in experiment II.

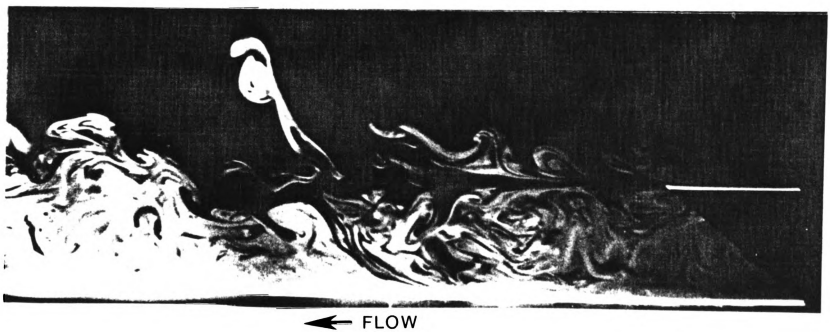

Figure 3.54 A snap-shot of the turbulent boundary layer downstream of the second manipulator plate. (Flow is from right to left).

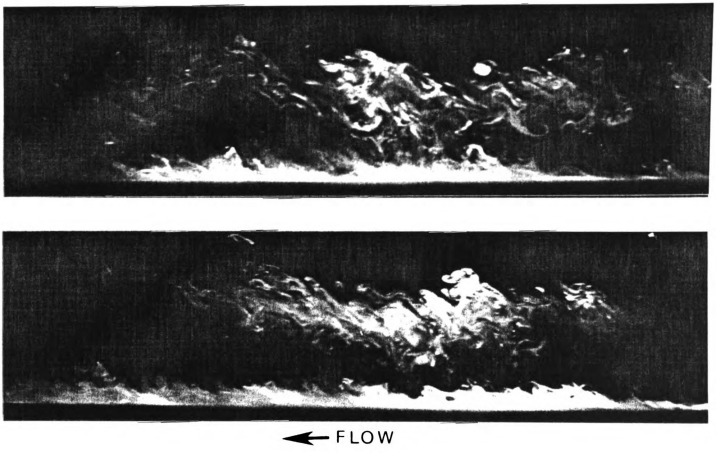

Figure 3.55 Snap-shots of manipulators wake interaction with wall-layer fluid upstream plate in place (top), and both plates in place (bottom) at $\xi = 20$ (center of the pictures).

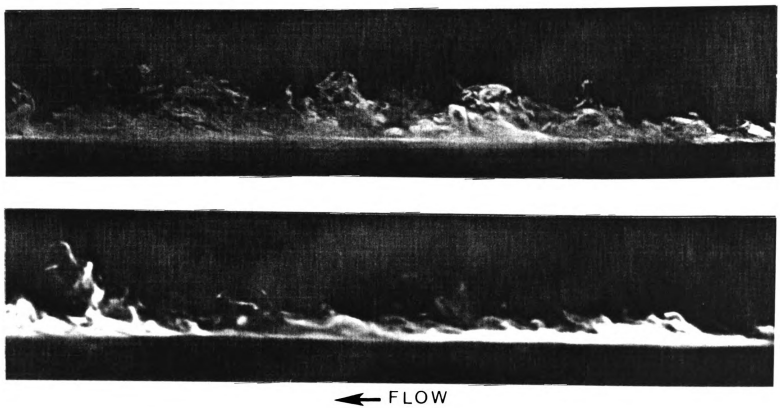

Figure 3.56 Snap-shots of wall-layer normal transport of fluid marker ($TiCl_4$) into outer region at ξ = 20 (center of the pictures), regular (top), and manipulated (bottom) boundary layers.

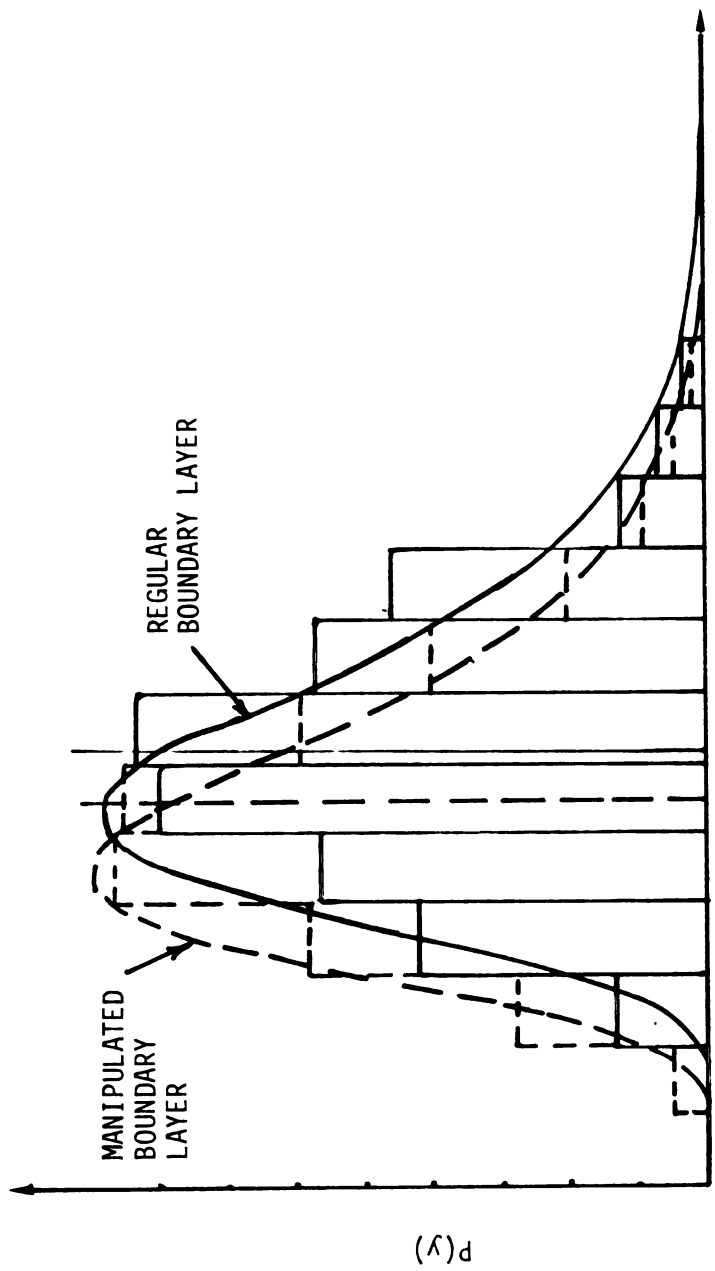

Figure 3.57 Probability distribution of normal transfer of flow marker ($TiCl_4$) into the wall region measured over $\pm 3.3\delta_o$ around $\xi = 20$ for regular and manipulated boundary layers.

Figure 3.58 Plan view of smoke-filled turbulent sublayer showing the "pocket" flow modules, which result from the interaction of outer layer typical eddies with the sublayer region.

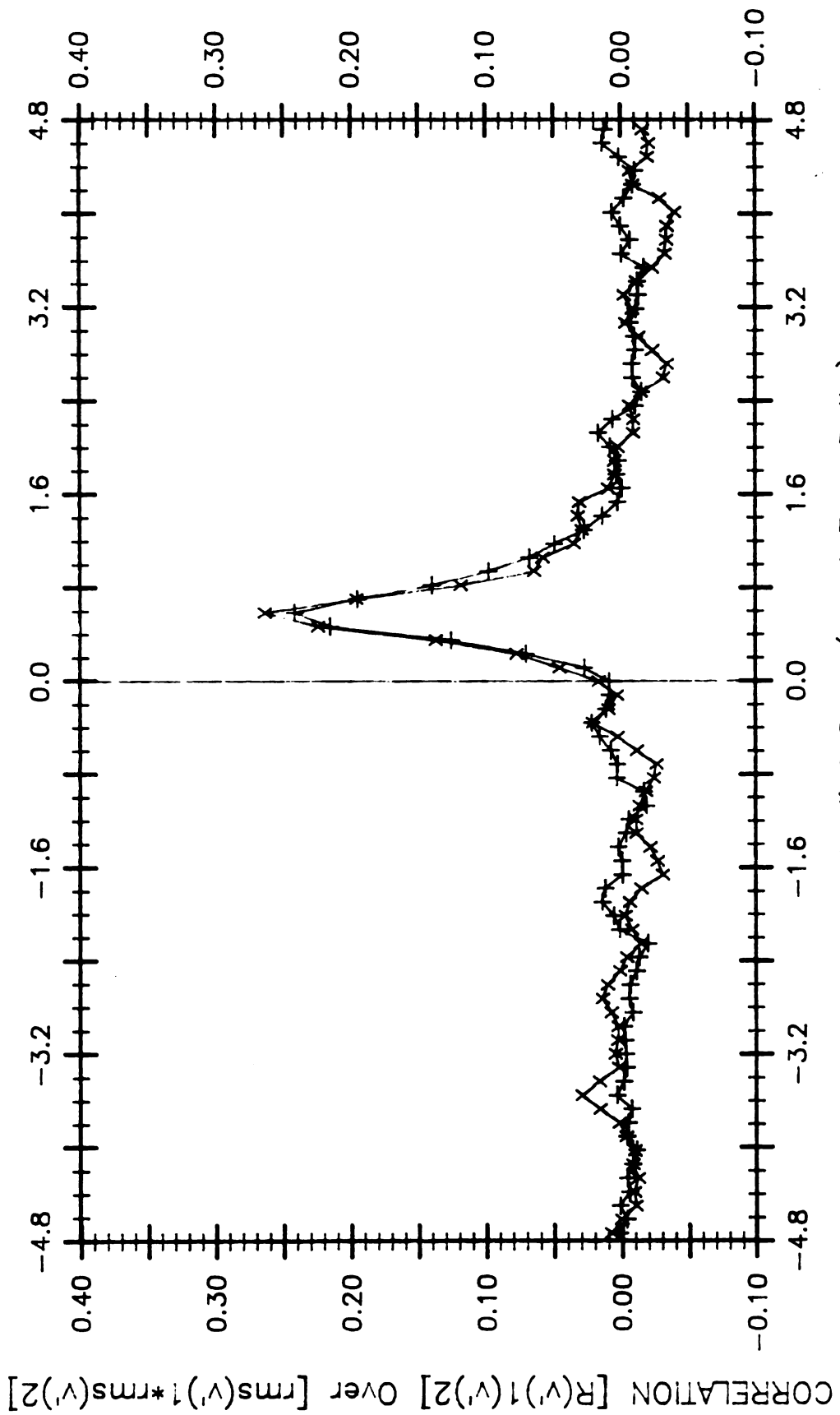

Figure 3.59 Variation of $R_{v'_1 v'_2}/rms(v'_1)rms(v'_2)$ versus τ for regular (x), and manipulated ($\dagger\dagger$) ^{2}boundary layers at ξ = 51.

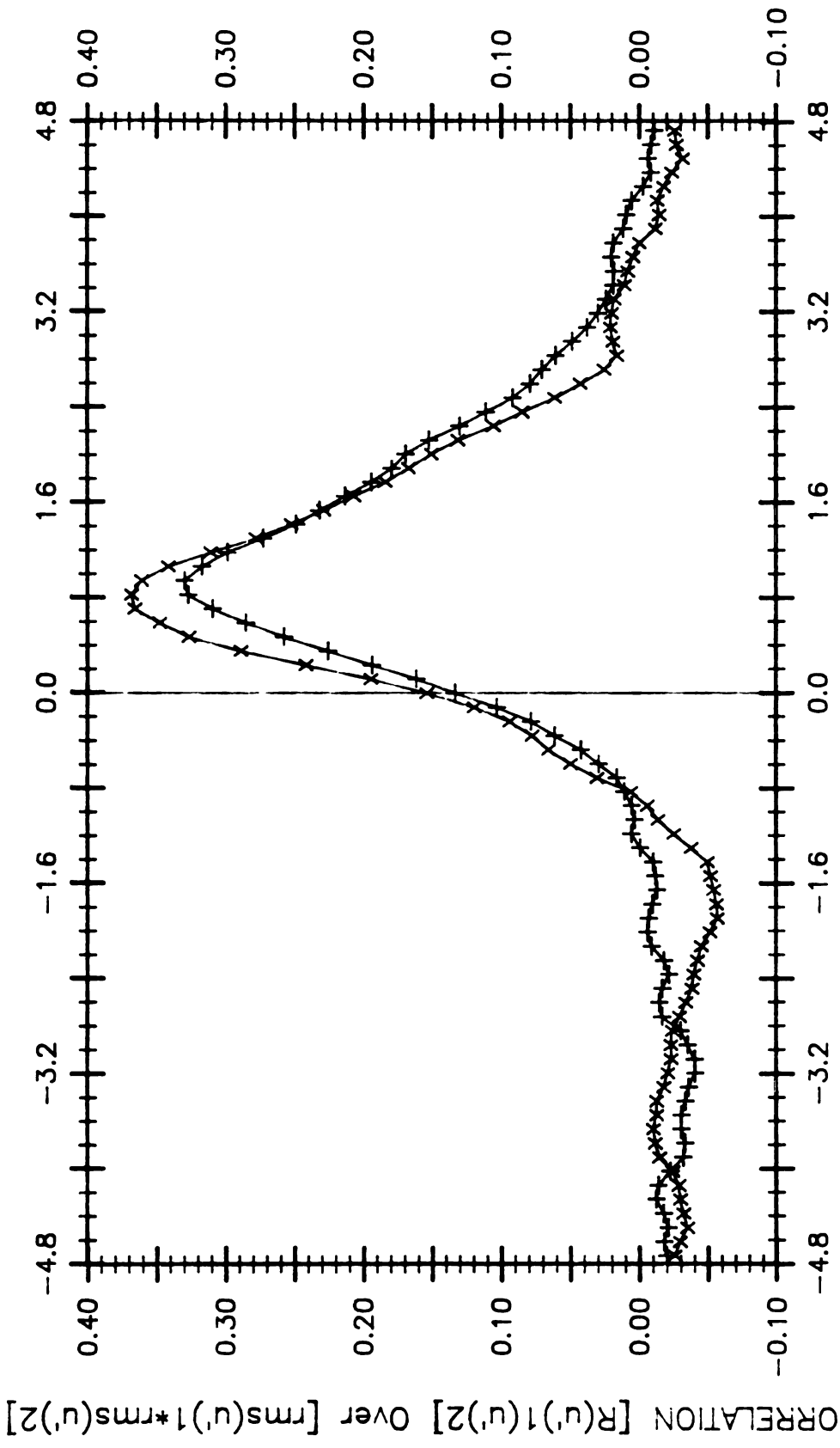

Figure 3.60 Variation of $R_{y'_1 y'_2}/rms(u'_1)rms(u'_2)$ versus τ for regular (x), and manipulated (+) boundary layers at $\xi = 51$.

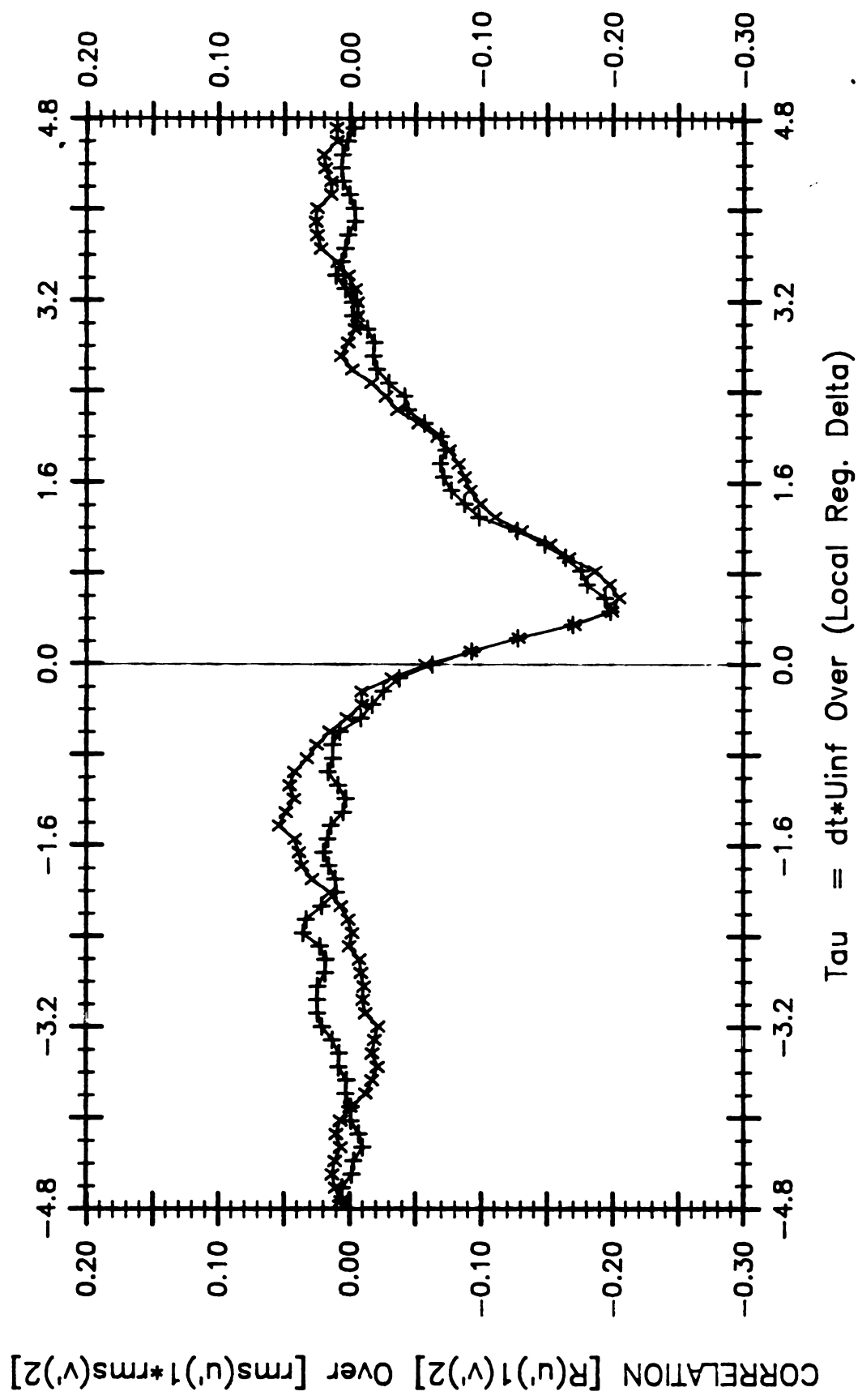

Figure 3.61 Variation of $R_{u'v'}/rms(u'_1)rms(v'_2)$ versus τ for regular (x), and manipulated (+) boundary layers at ξ = 51.

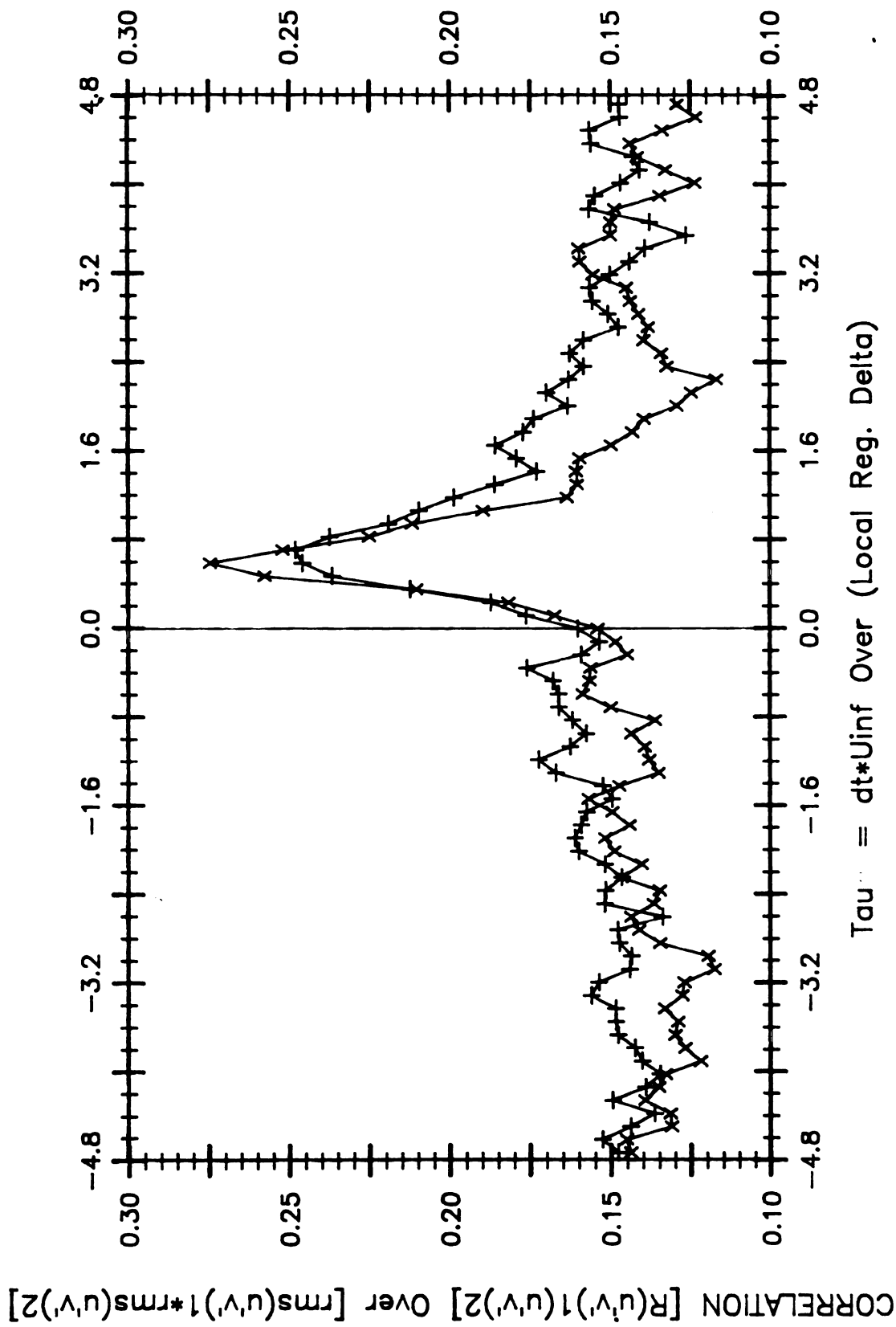

Figure 3.62 Variation of $R_{(u'v')_1(u'v')_2}/rms((u'v')_1)rms((u'v')_2)$ versus τ for regular (x), and manipulated (+) boundary layers at ξ = 51.

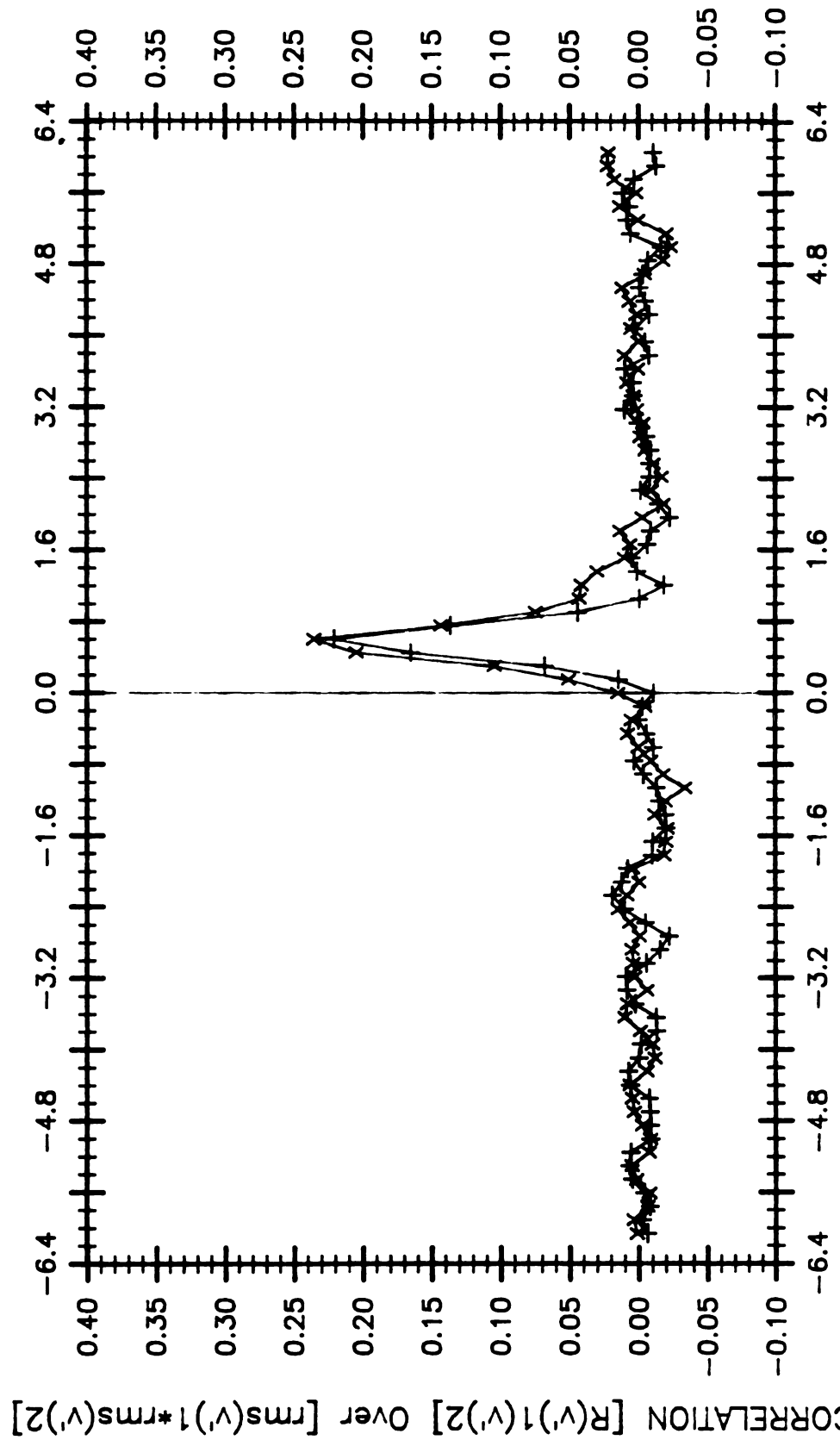

Figure 3.63 Variation of $R_{v',v'}/rms(v'_1)rms(v'_2)$ versus τ for regular (x), and manipulated (+) boundary layers at $\xi = 20$.

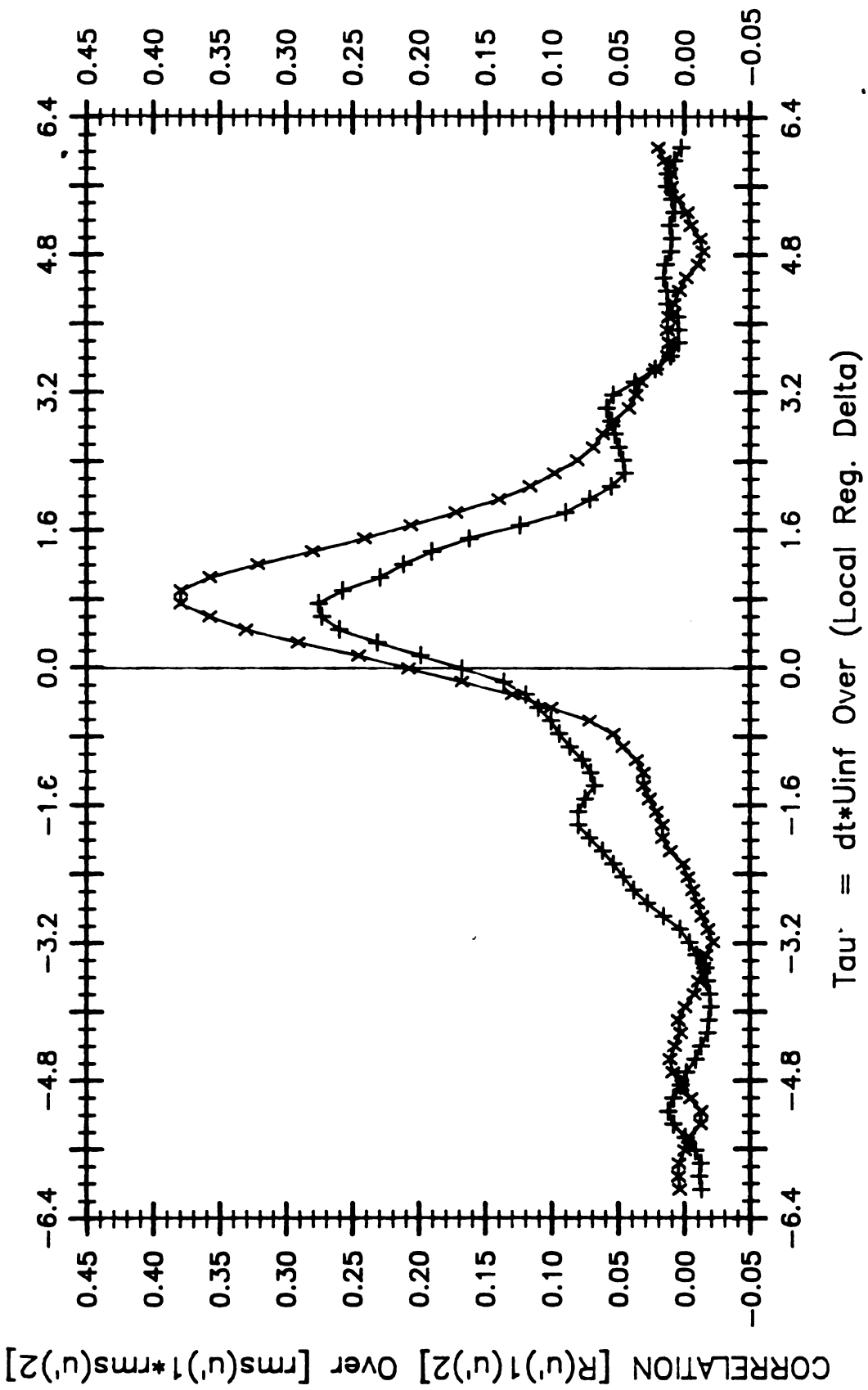

Figure 3.64 Variation of $R_{u'_1 u'_2}/rms(u'_1)rms(u'_2)$ versus τ for regular (x), and manipulated (+) boundary layers at ξ = 20.

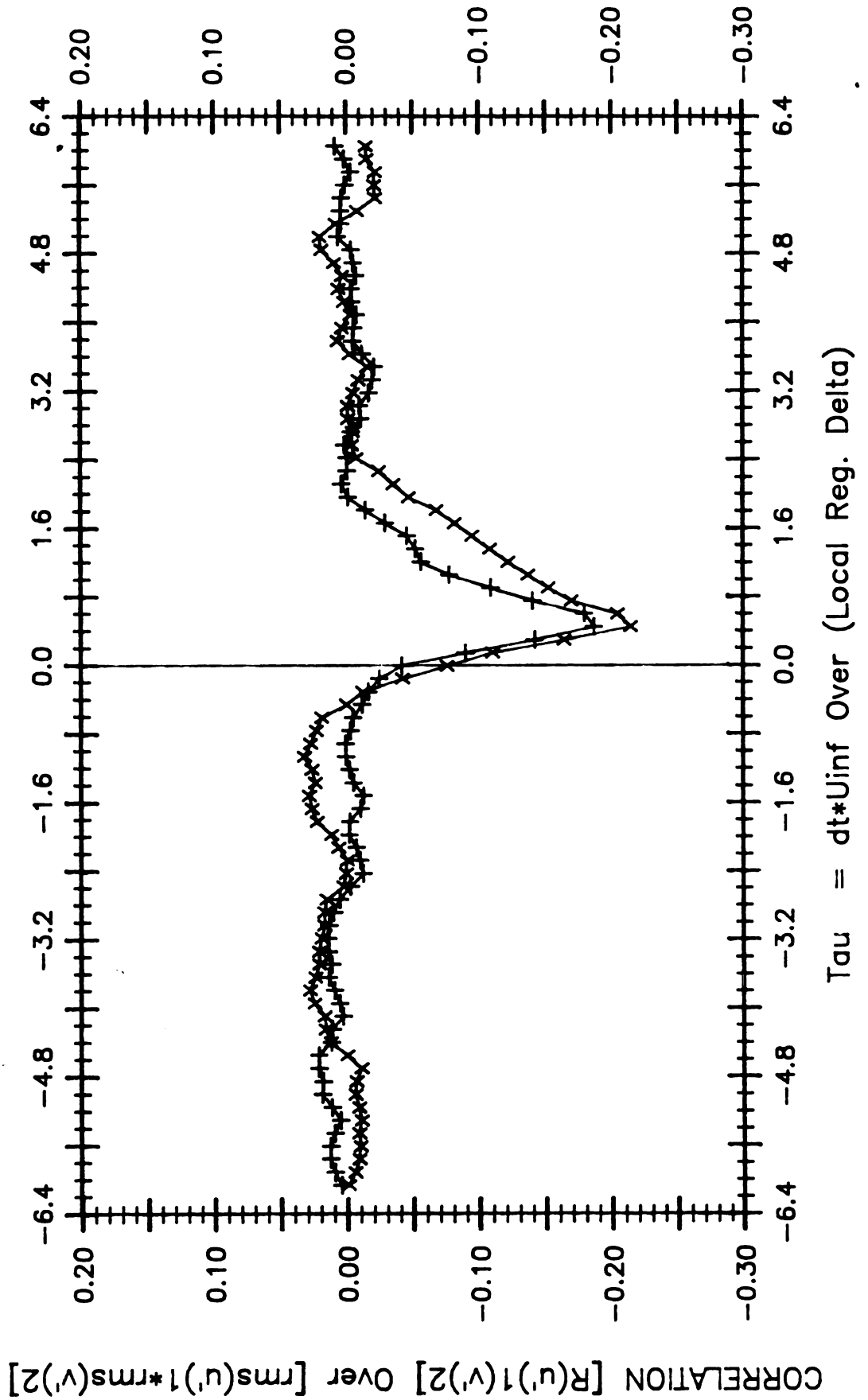

Figure 3.65 Variation of $R_{u'_1 v'_2}/rms(u'_1)rms(v'_2)$ versus τ for regular (x), and manipulated (+) boundary layers at $\xi = 20$.

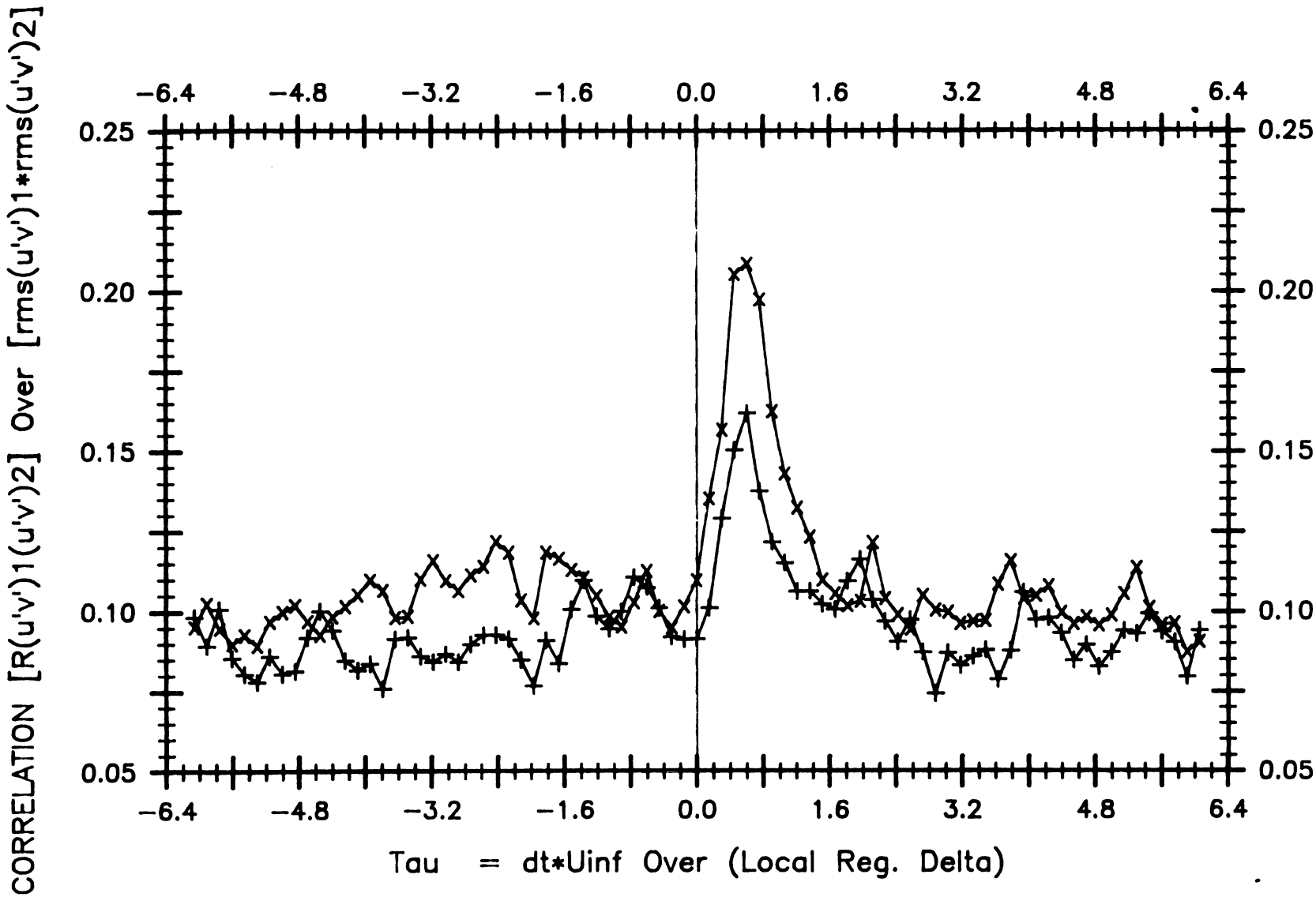

Figure 3.66 Variation of $R_{(u'v')_1(u'v')_2}/rms((u'v')_1)rms((u'v')_2)$ versus τ for regular (x), and manipulated (+) boundary layers at ξ = 20.

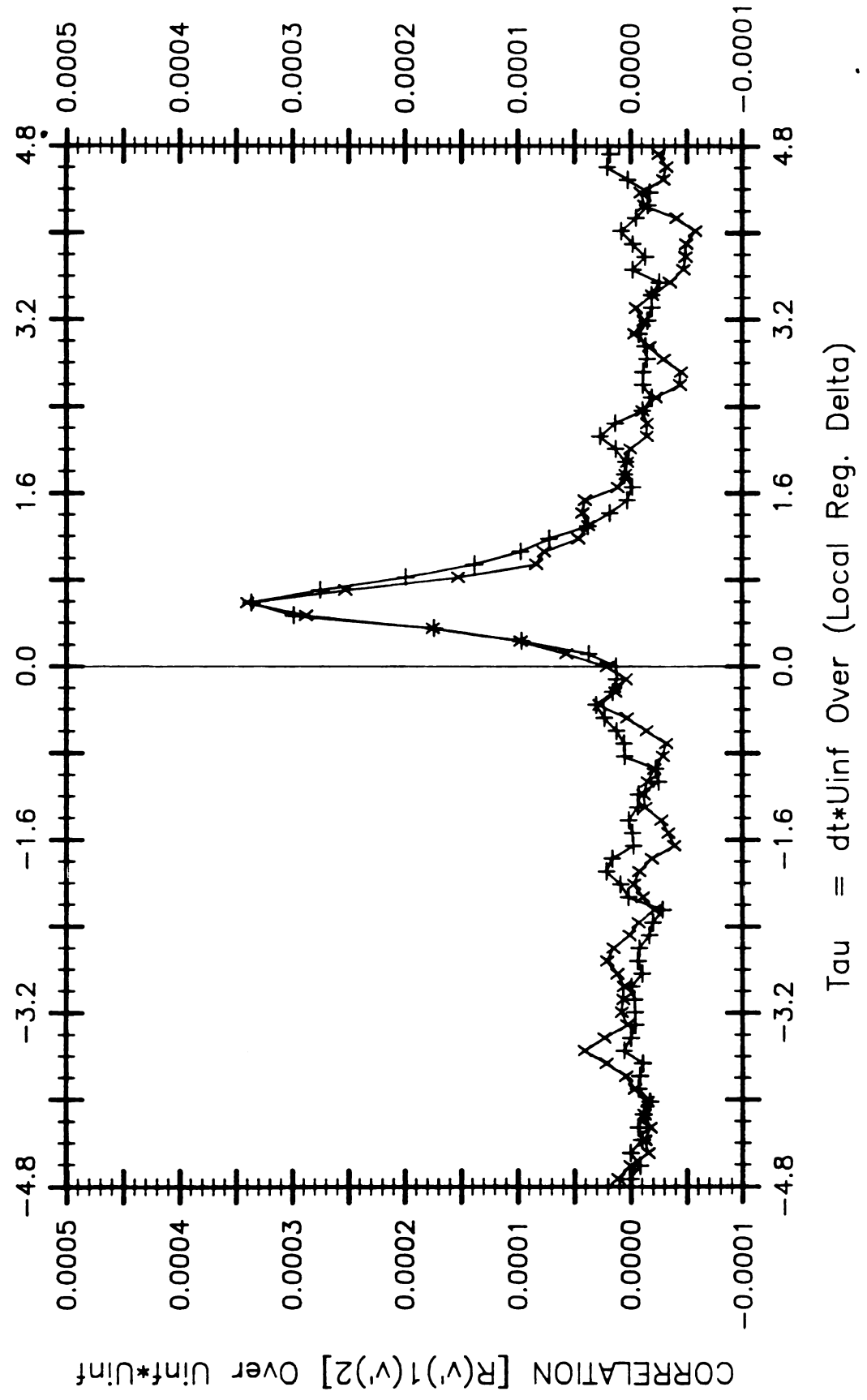

Figure 3.67 Variation of $R_{v'_1 v'_2}/U_\infty^2$ versus τ for regular (x), and manipulated (+) boundary layers at ζ = 51.

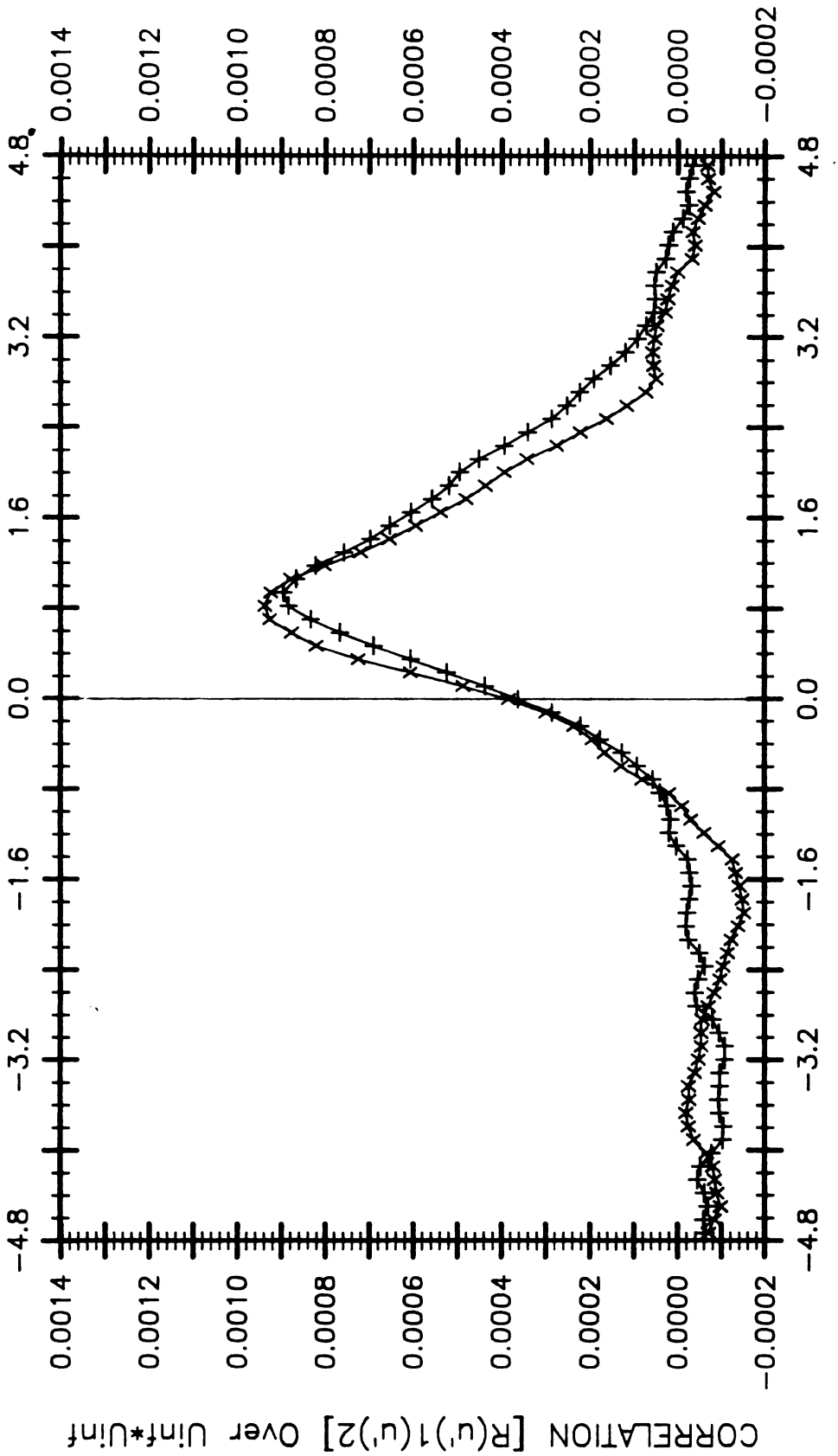

Figure 3.68 Variation of $R_{u'_1 u'_2}/U_e^2$ versus τ for regular (x), and manipulated (+) boundary layers at ζ = 51.

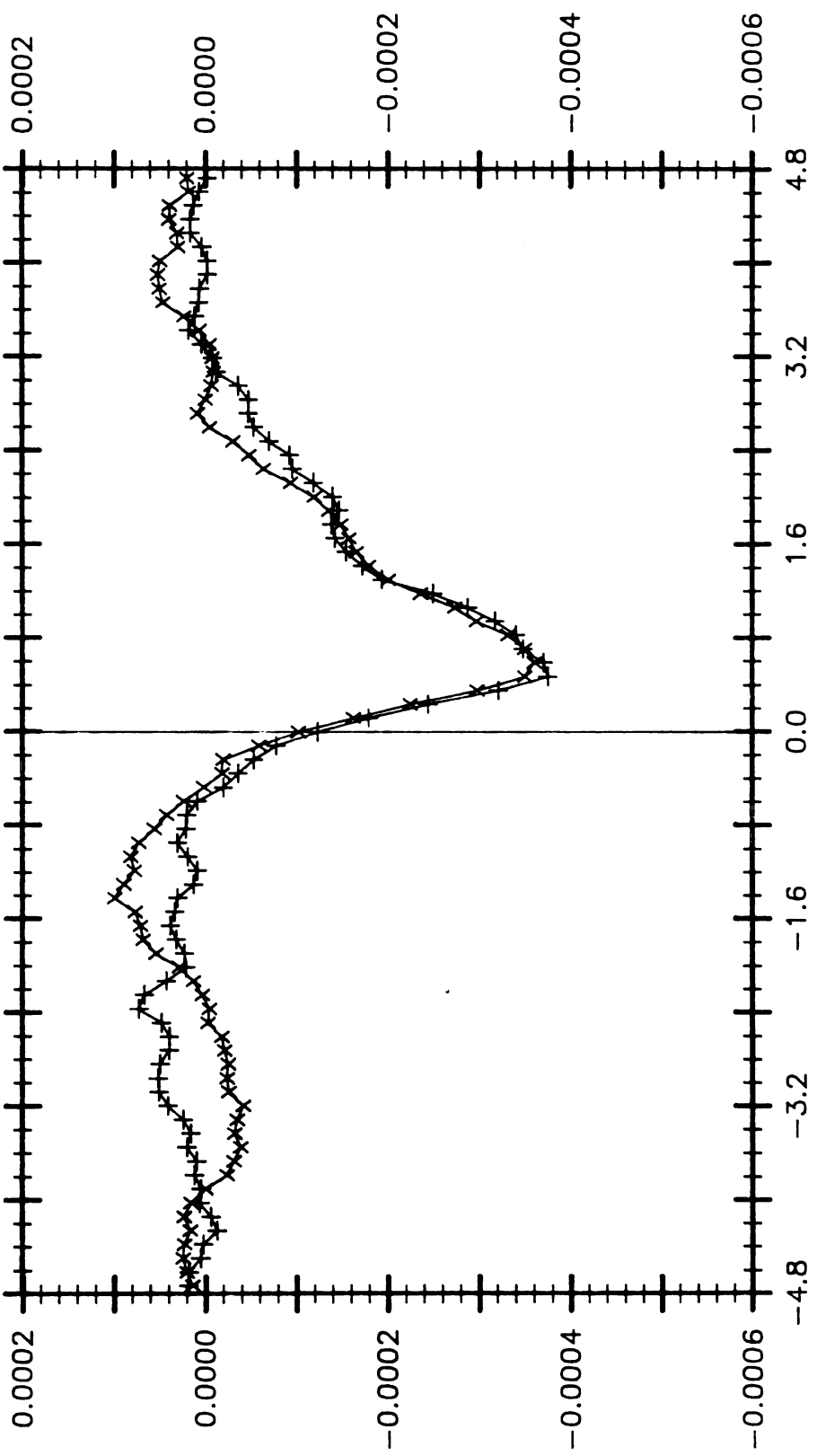

Figure 3.69 Variation of $R_{u'v'}/U_\infty^2$ versus τ for regular (x), and manipulated (+) boundary layers at ξ = 51.

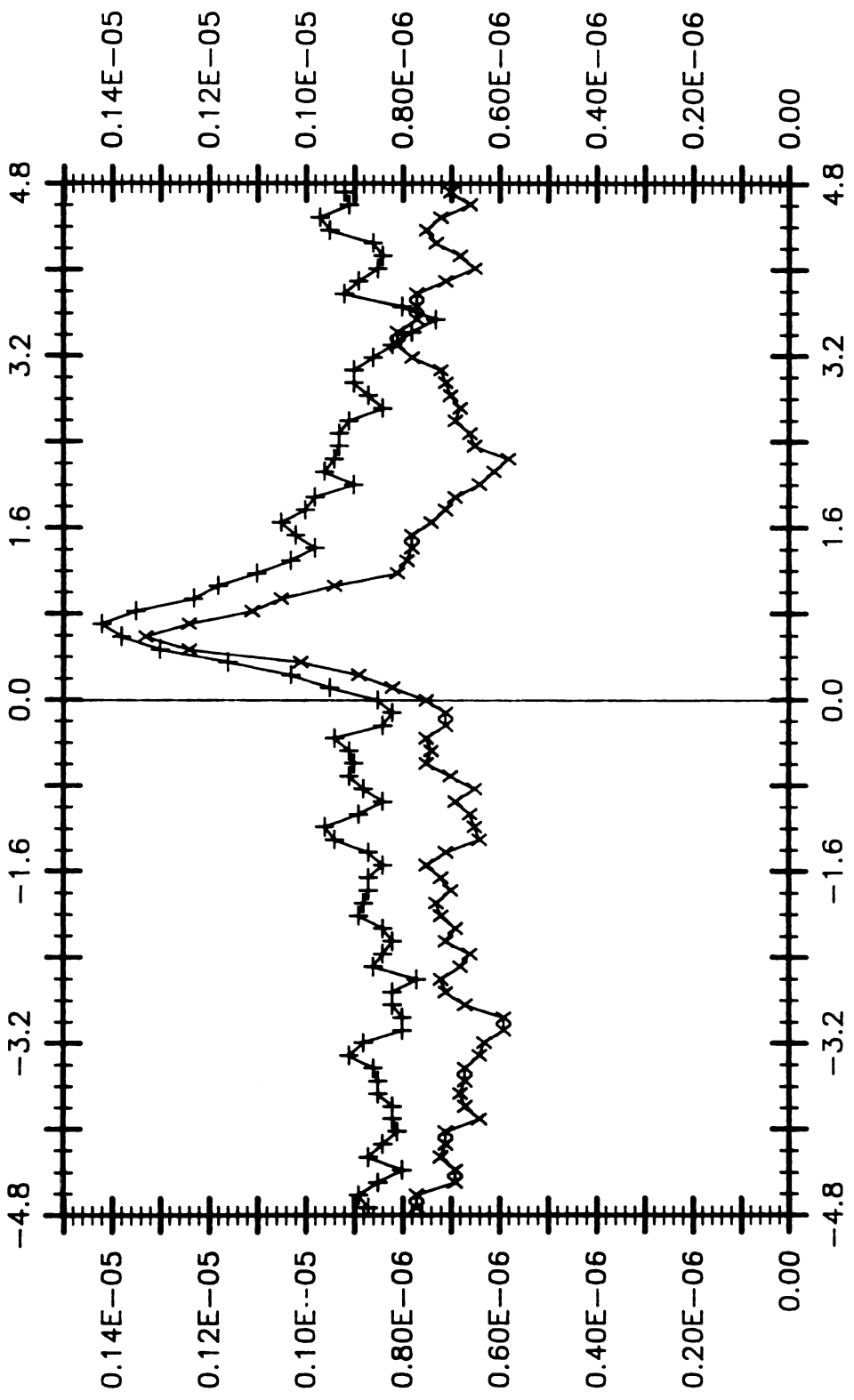

Figure 3.70 Variation of $R_{(u'v')_1(u'v')_2}/U_\infty^4$ versus τ for regular (x), and manipulated (+) boundary layers at ξ = 51.

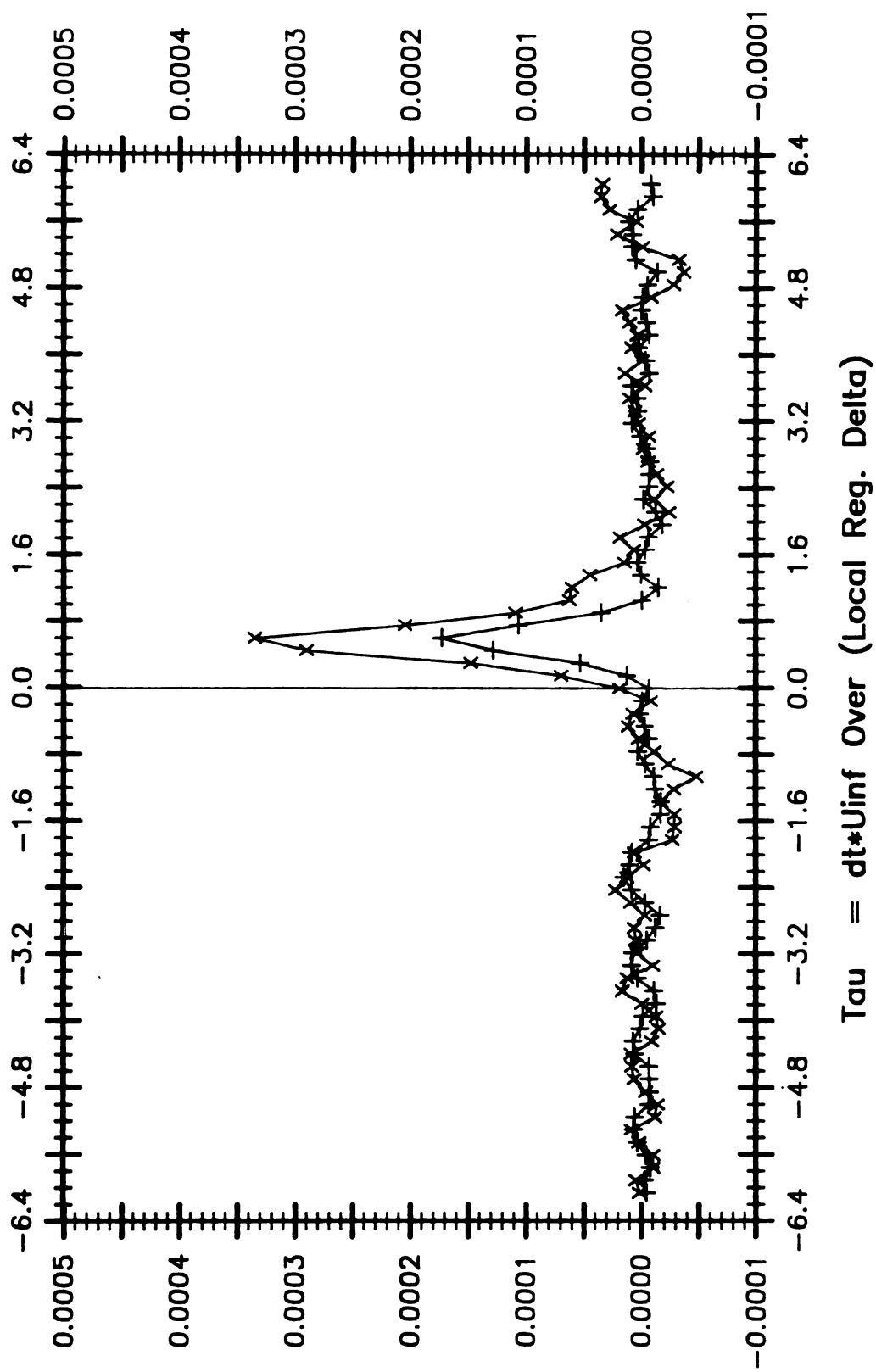

Figure 3.71 Variation of $R_{v'_1 v'_2}/U_\infty^2$ versus τ for regular (x), and manipulated (+) boundary layers at ξ = 20.

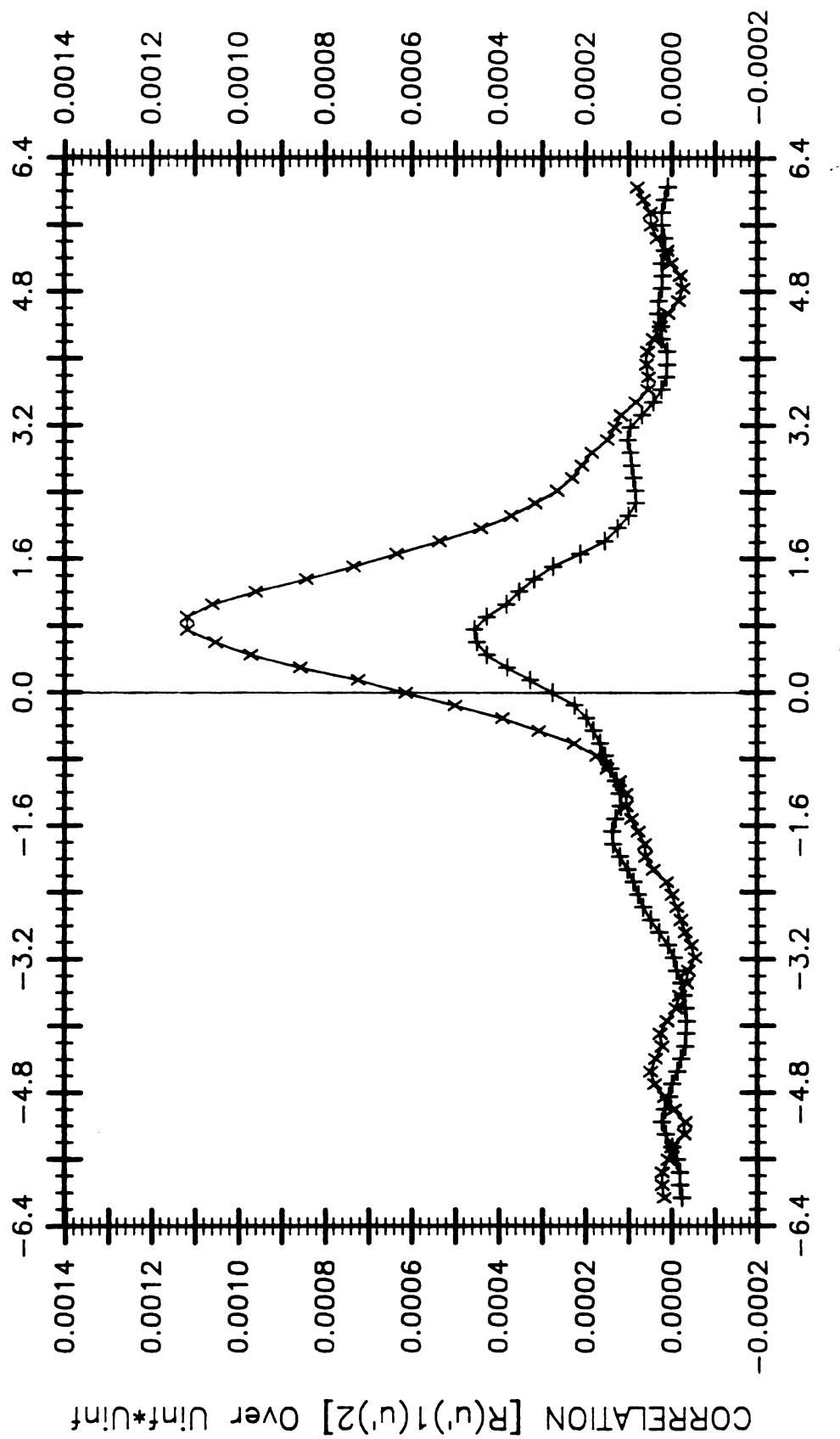

Figure 3.72 Variation of $R_{u'_1 u'_2}/U_\infty^2$ versus τ for regular (x), and manipulated (+) boundary layers at ξ = 20.

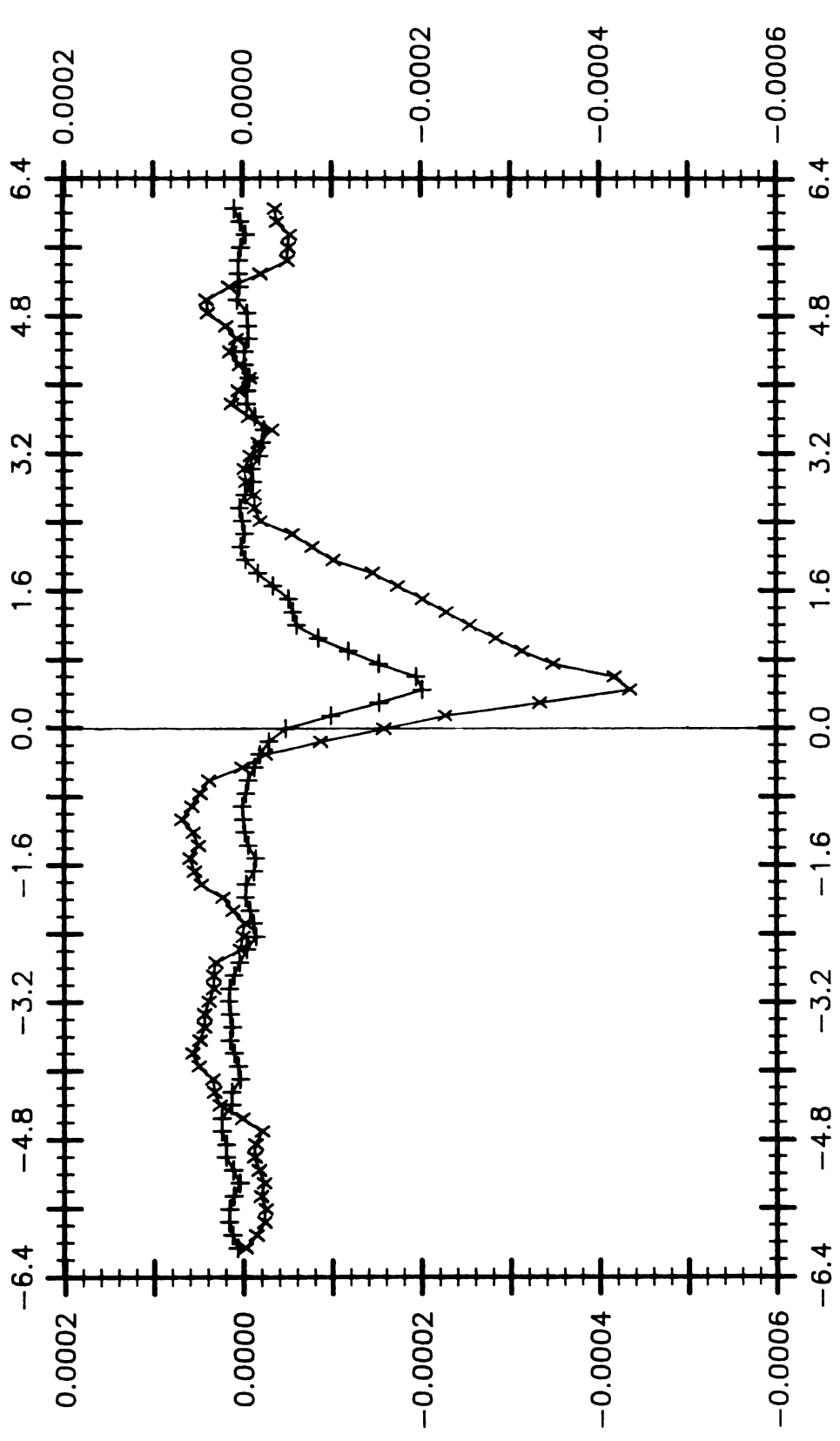

Figure 3.73 Variation of $R_{u',v'}/U_\infty^2$ versus τ for regular (x), and manipulated (+) boundary layers at ξ = 20.

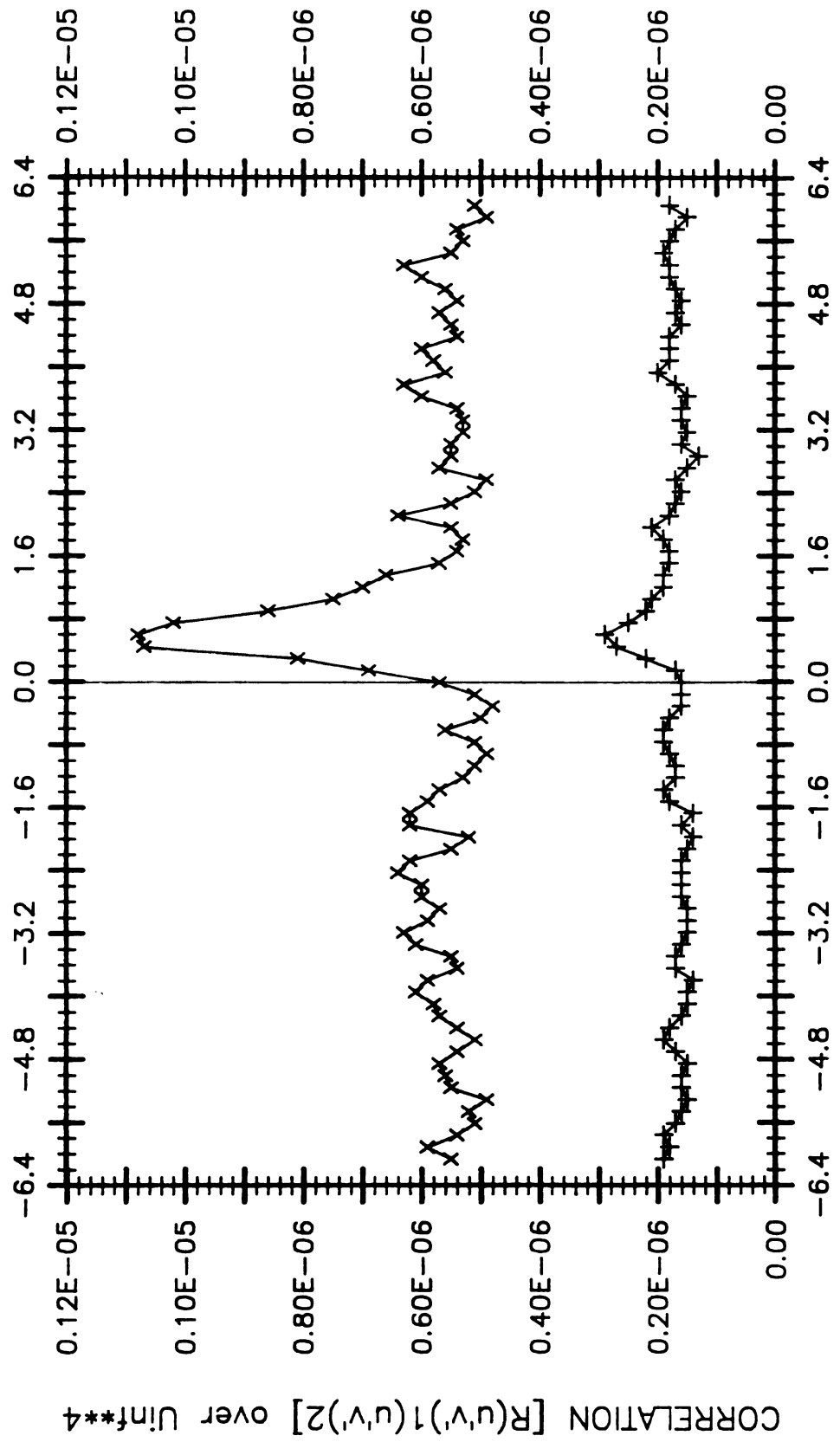

Figure 3.74 Variation of $R_{(u'v')_1(u'v')_2}/U_\infty^4$ versus τ for regular (x), and manipulated (+) boundary layers at ξ = 20.

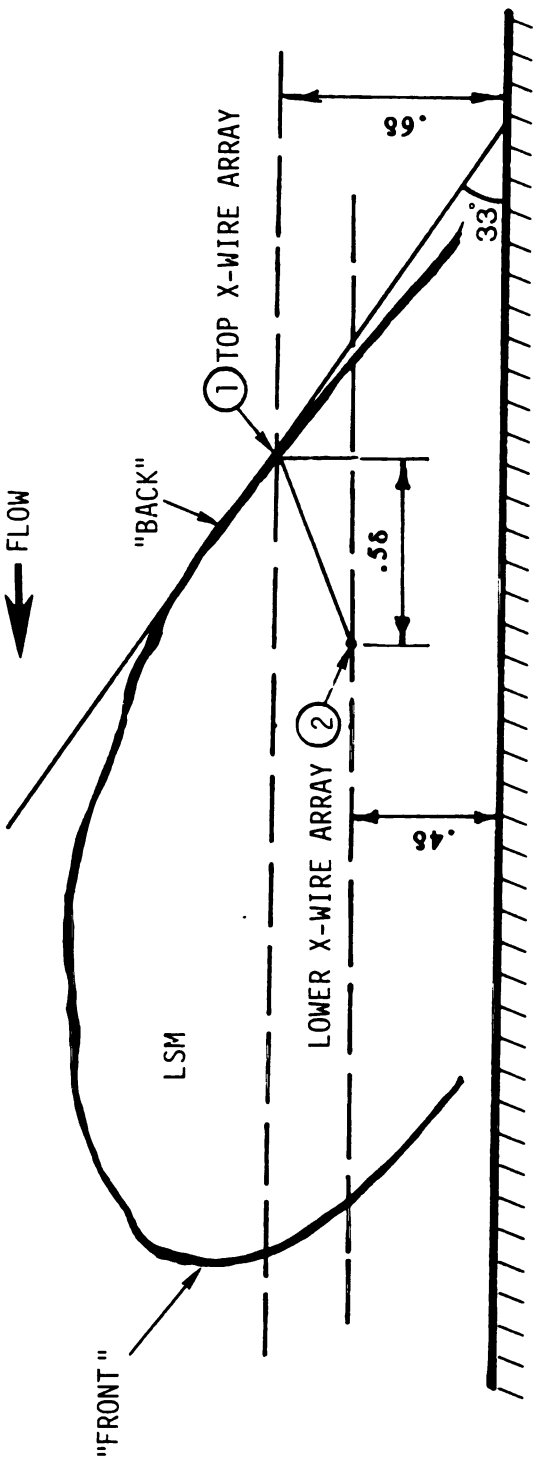

Figure 3.75 Schematic of an ideal large-scale motion in turbulent boundary layer used to estimate the position of the lower x-wire array signals with respect to 'front' and 'back' of the structure in the ensemble average results. The dashed lines indicate the y location of x-wire arrays.

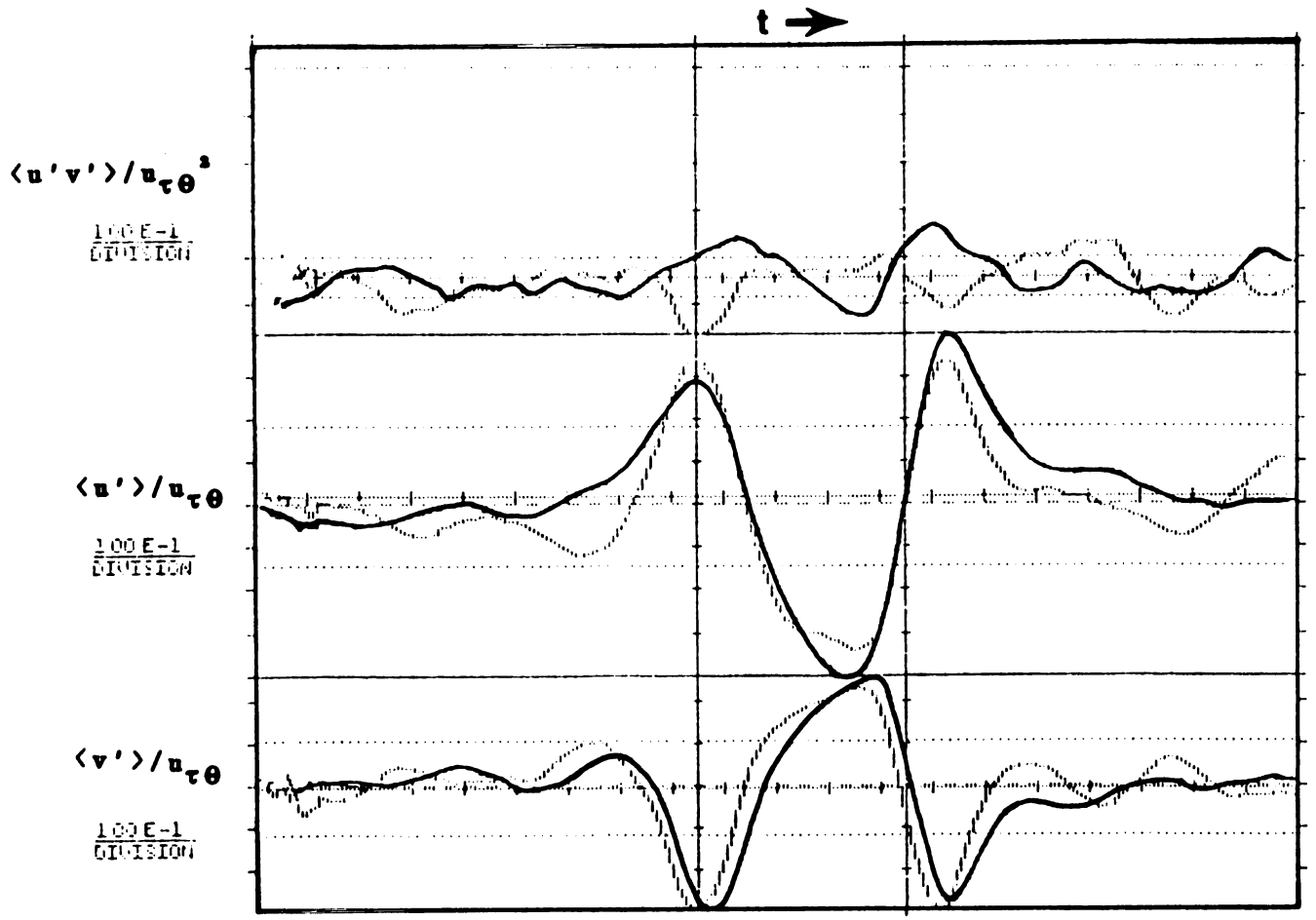

Figure 3.76 Ensemble averaged v', u', and u'v' signals conditionally sampled to large scale motions and normalized by $u_{\tau\theta}$ in regular (solid line signals) and manipulated (light dashed line signals) boundary layers at $y = .65\delta_{local}$.
The vertical axes correspond to the normalized large eddy smoke boundaries. Zero lines are represented by three dots with a space between them (... ...). The average of the signals are shown by very close dotted lines, and the standard deviation of the normal boundary layers are shown by two lines with rather spaced dots. This convention is same for the following ensemble average signals in next seven figures.

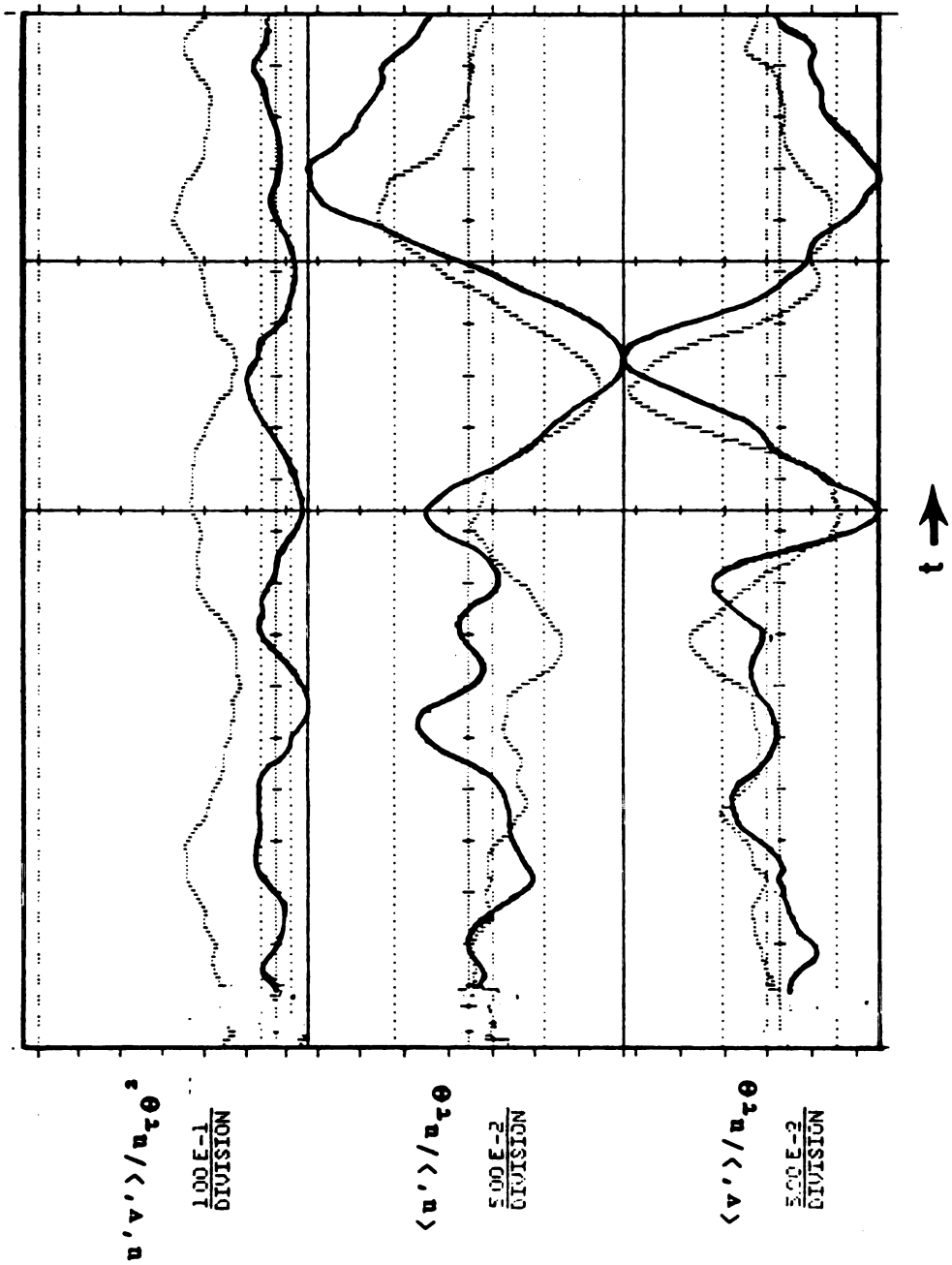

Figure 3.77 Ensemble averaged v', u', and u'v' signals conditionally sampled to large scale motions and normalized by $u_\tau\theta$ in regular (solid line signals) and manipulated (light dashed line signals) boundary layers at y = .46.

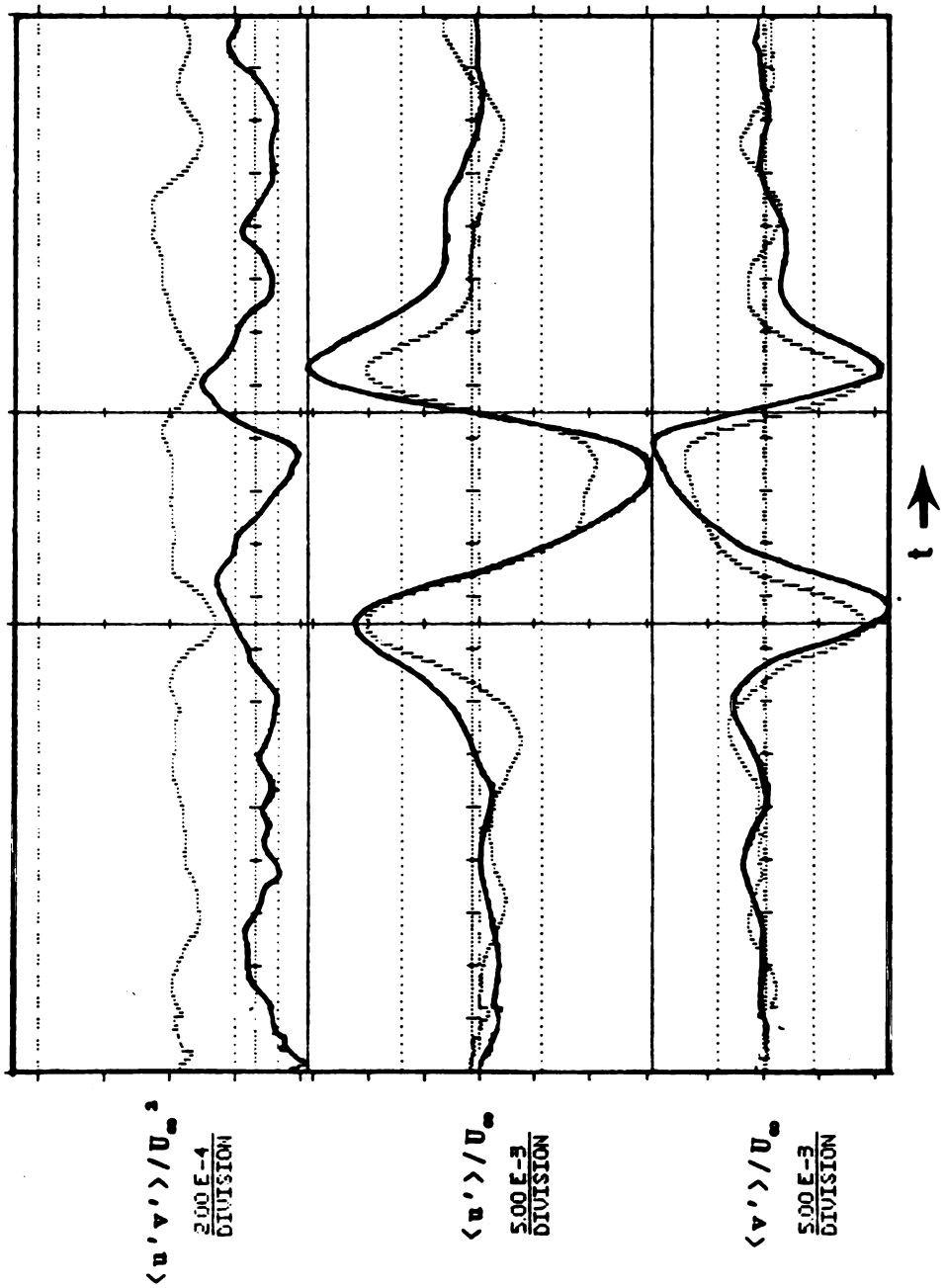

Figure 3.78 Ensemble averaged v', u', and u'v' signals conditionally sampled to large scale motions and normalized by U_∞ in regular (solid line signals) and manipulated (light dashed line signals) boundary layers at y = .66.

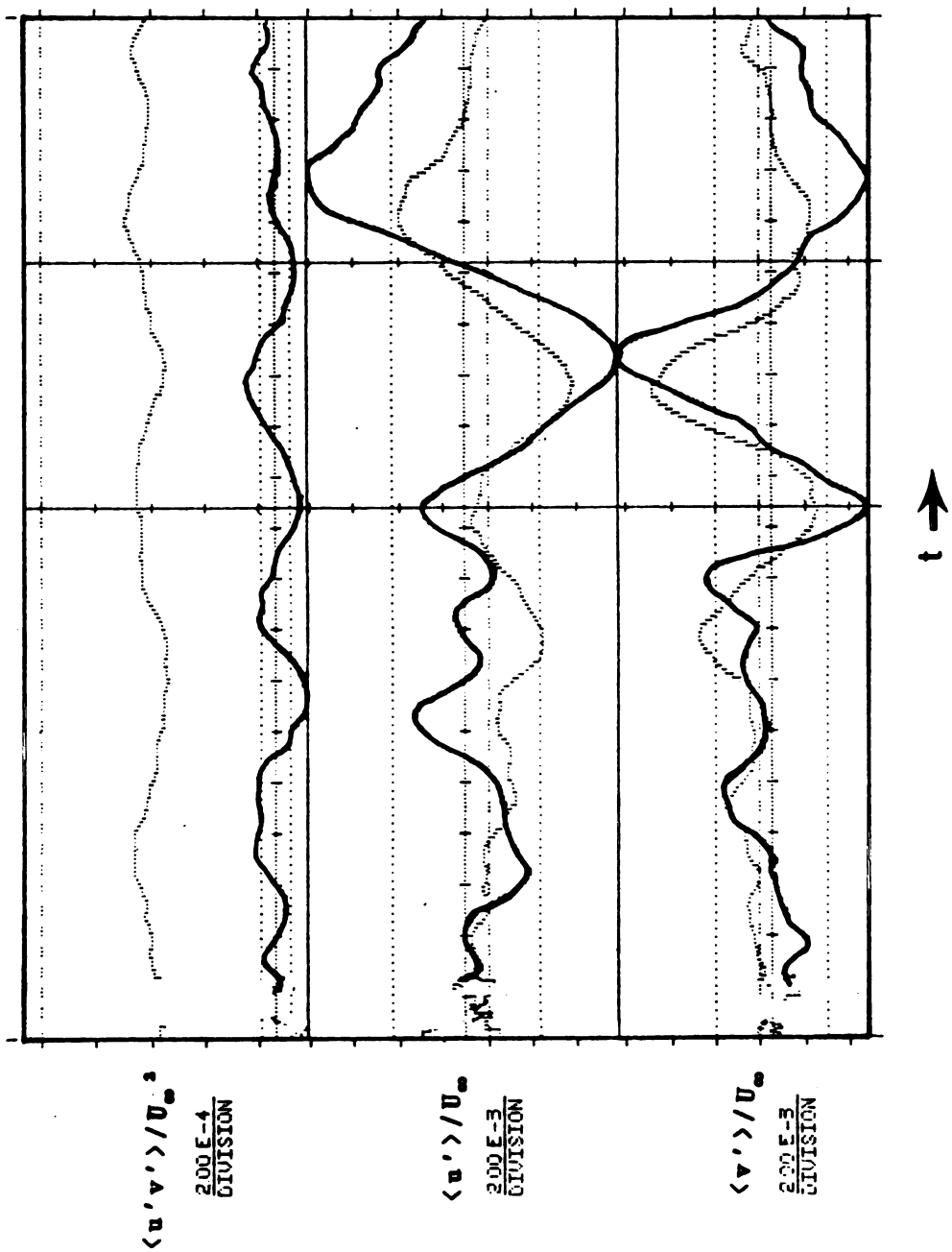

Figure 3.79 Ensemble averaged v', u', and u'v' signals conditionally sampled to large scale motions and normalized by U_∞ in regular (solid line signals) and manipulated (light dashed line signals) boundary layers at y = .46.

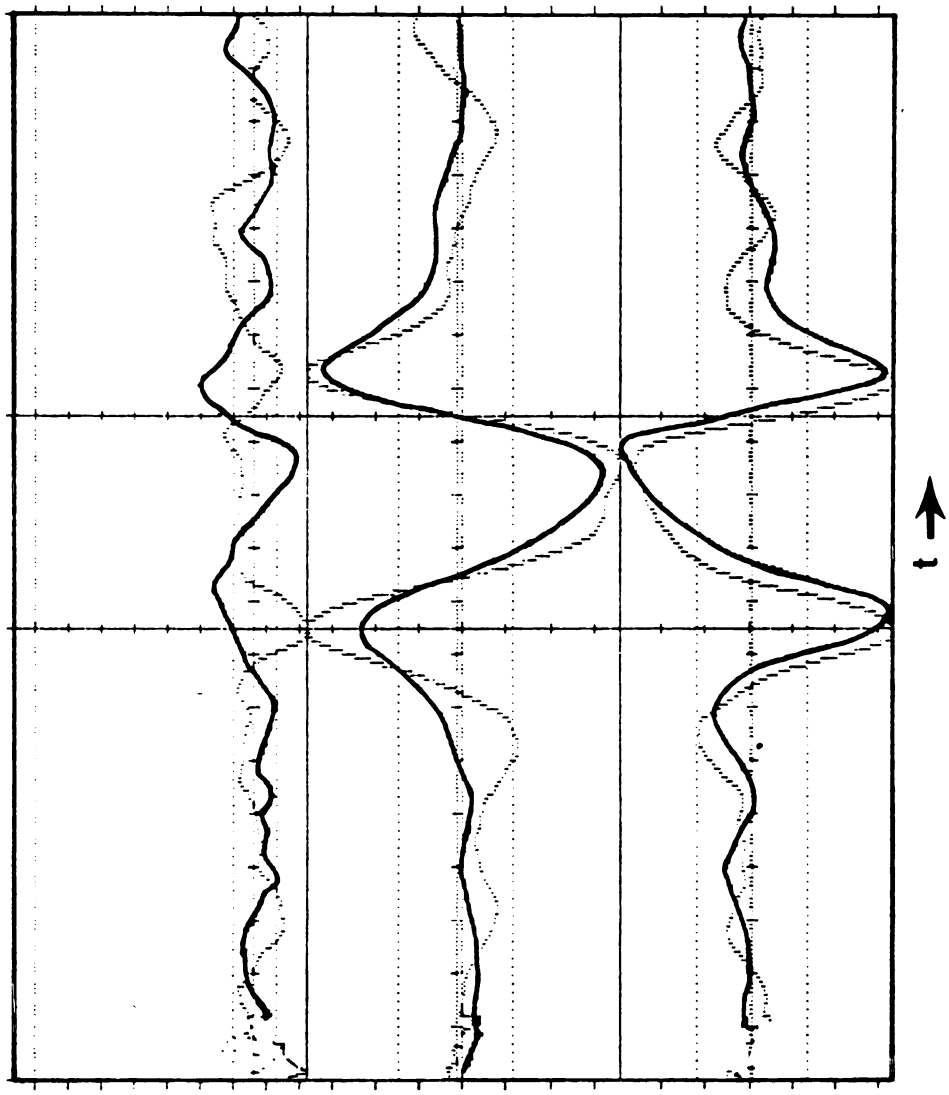

Figure 3.80 Ensemble averaged v', u', and u'v' signals conditionally sampled to large scale motions and normalized by their respective rms values in regular (solid line signals) and manipulated (light dashed line signals) boundary layers at y = .66.

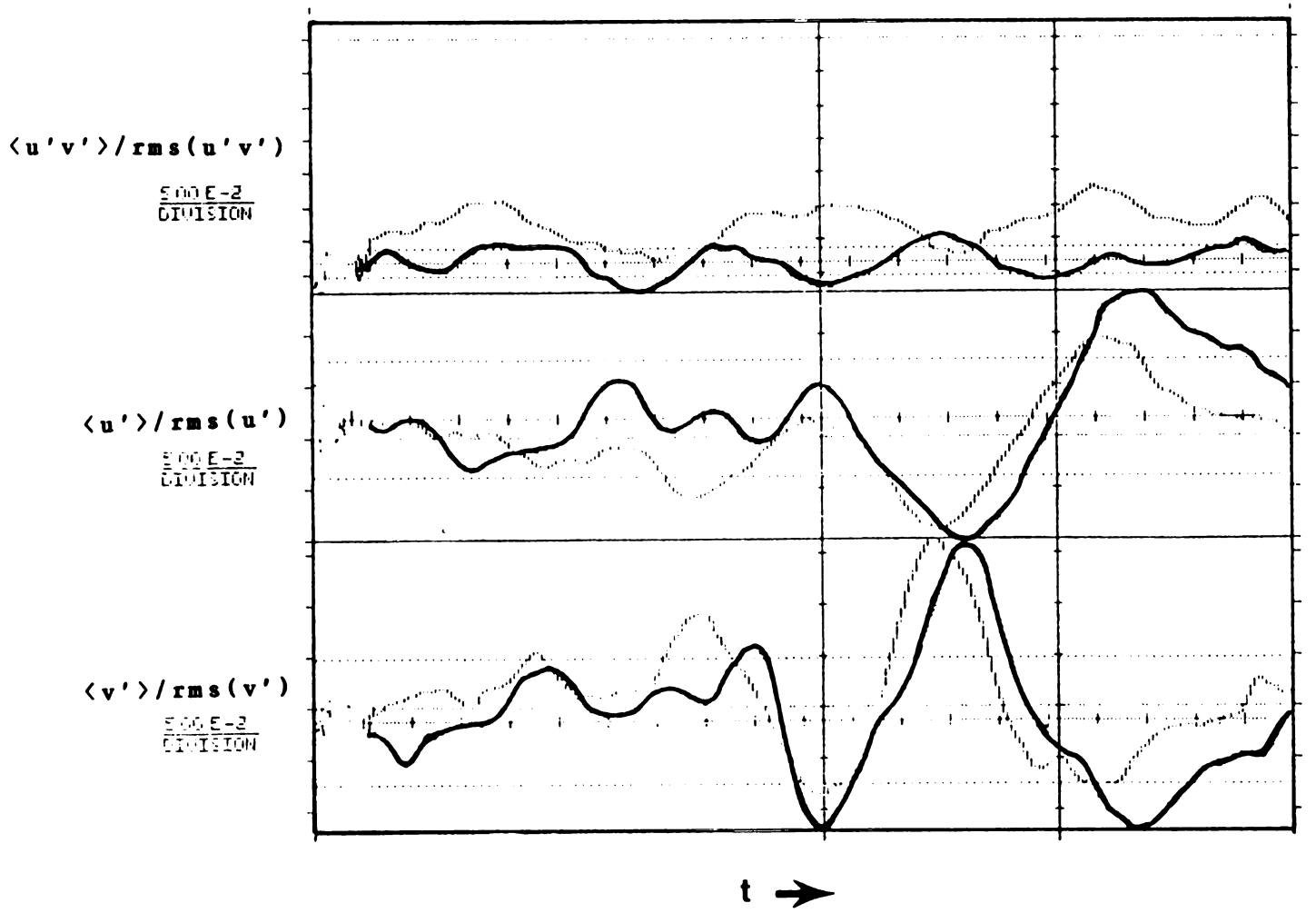

Figure 3.81 Ensemble averaged v', u', and u'v' signals conditionally sampled to large scale motions and normalized by their respective rms values in regular (solid line signals) and manipulated (light dashed line signals) boundary layers at y = .46.

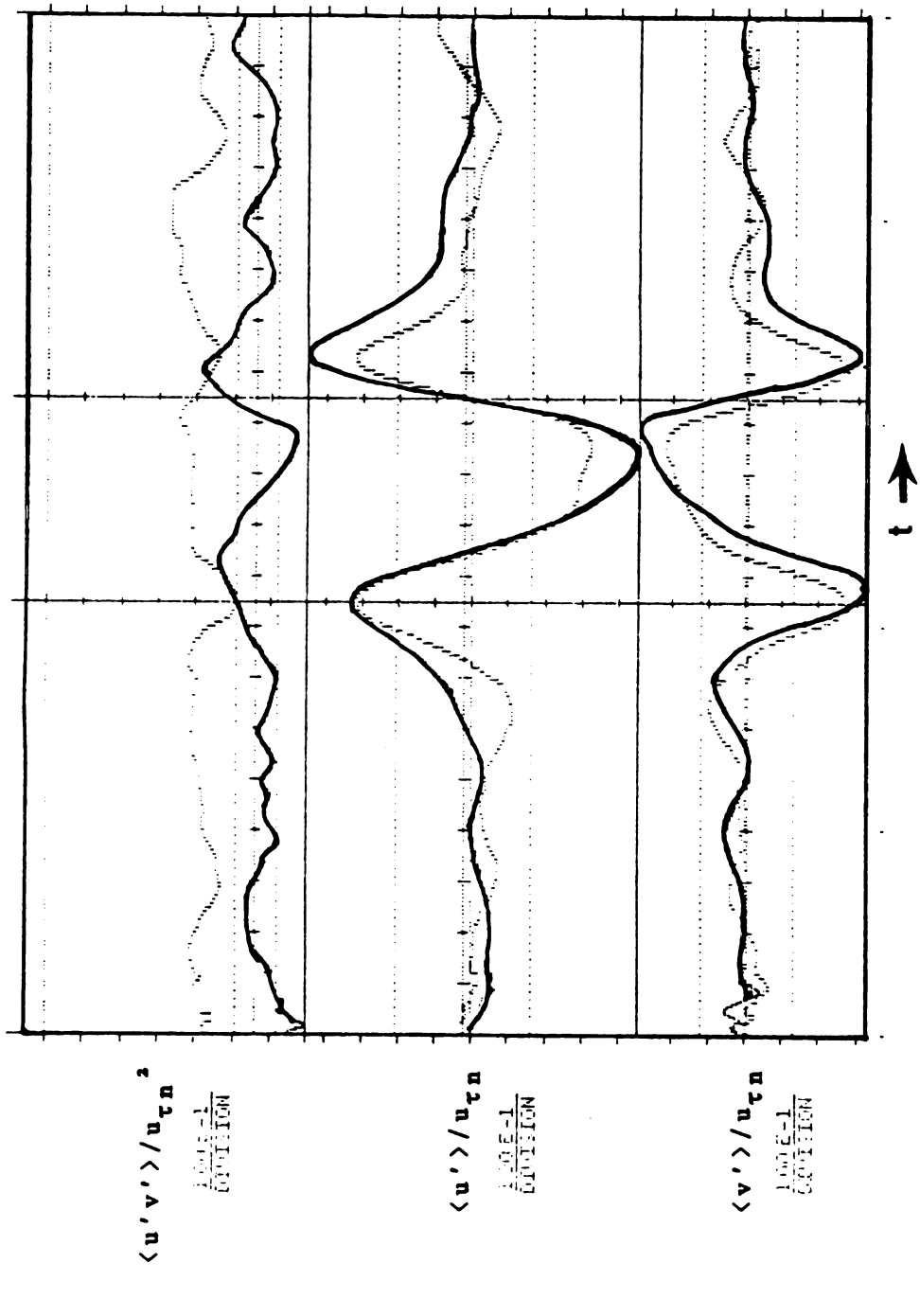

Figure 3.82 Ensemble averaged v', u', and u'v' signals conditionally sampled to large scale motions and normalized by $u_{\tau n}$ in regular (solid line signals) and manipulated (light dashed line signals) boundary layers at y = .66.

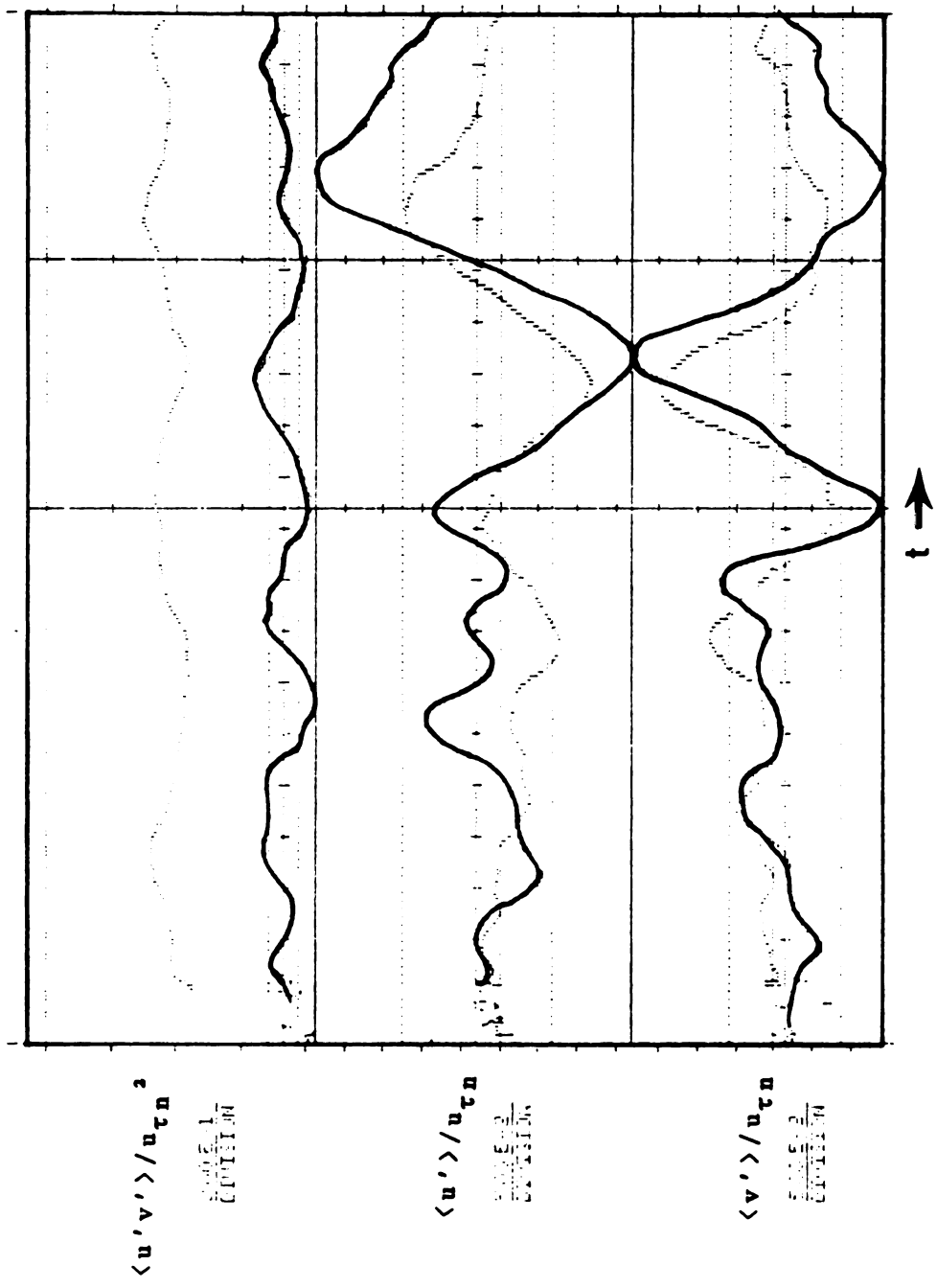

Figure 3.83 Ensemble averaged v', u', and u'v' signals conditionally sampled to large scale motions and normalized by $u_{\tau n}$ in regular (solid line signals) and manipulated (light dashed line signals) boundary layers at y = .46.

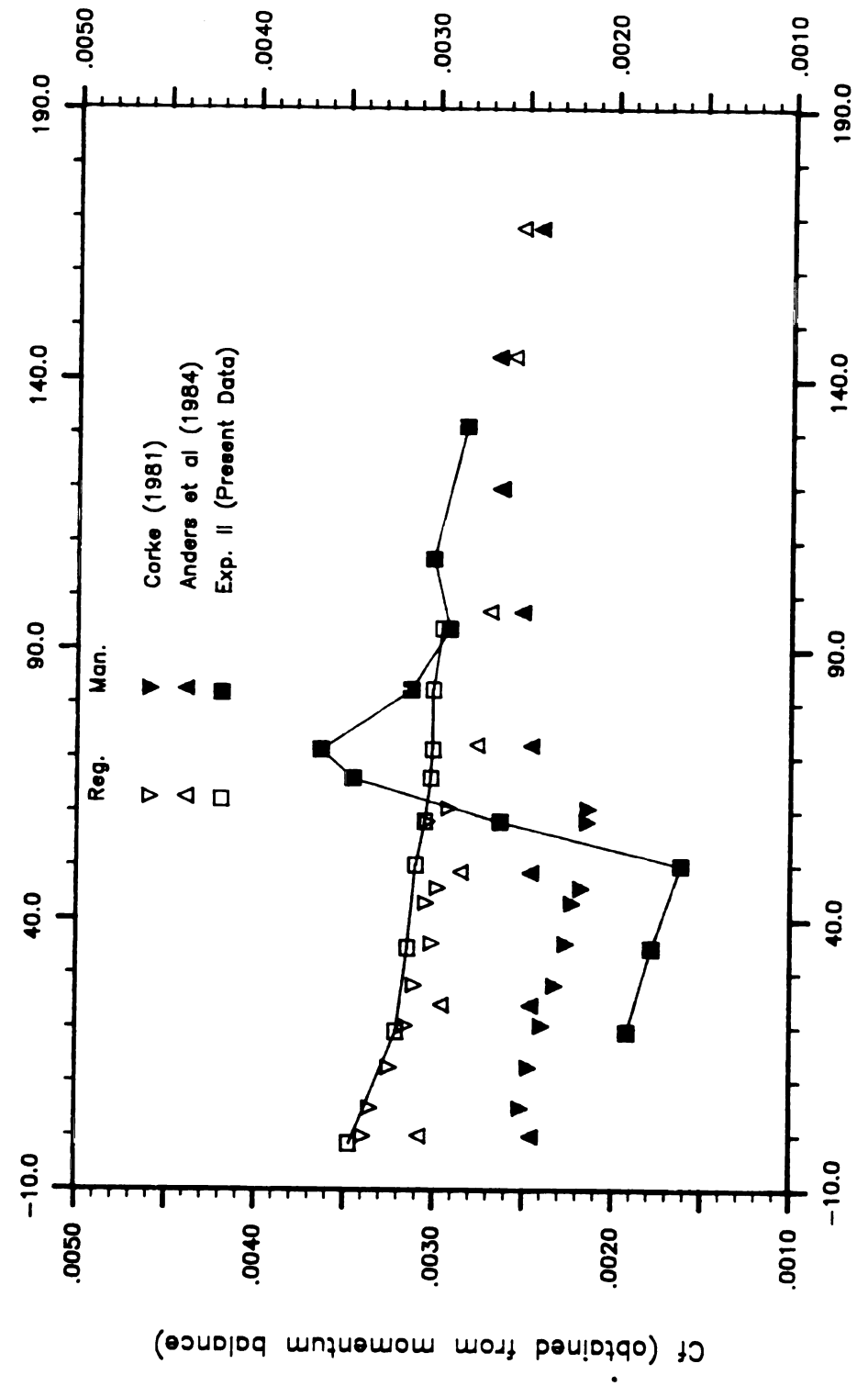

Figure 4.1 Variation of $C_{f\theta}$ versus $(x-x_0)/x_0$ for regular and manipulated boundary layers and comparison with other investigators' results.

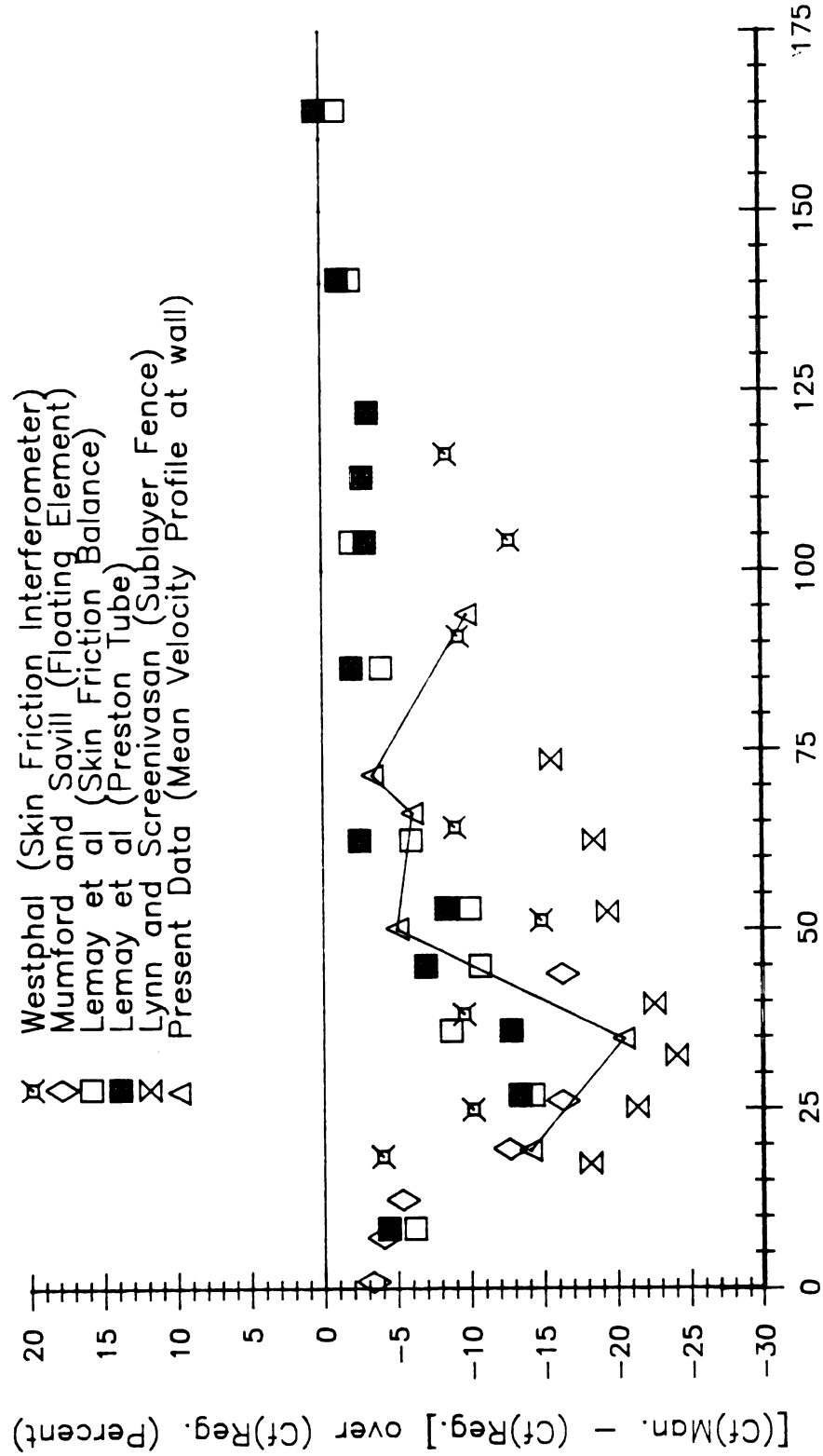

Figure 4.2 Variation of $[C_{fMan.} - C_{fReg.}]/C_{fReg.}$ versus $(x-x_o)/x_o$ obtained via different techniques.

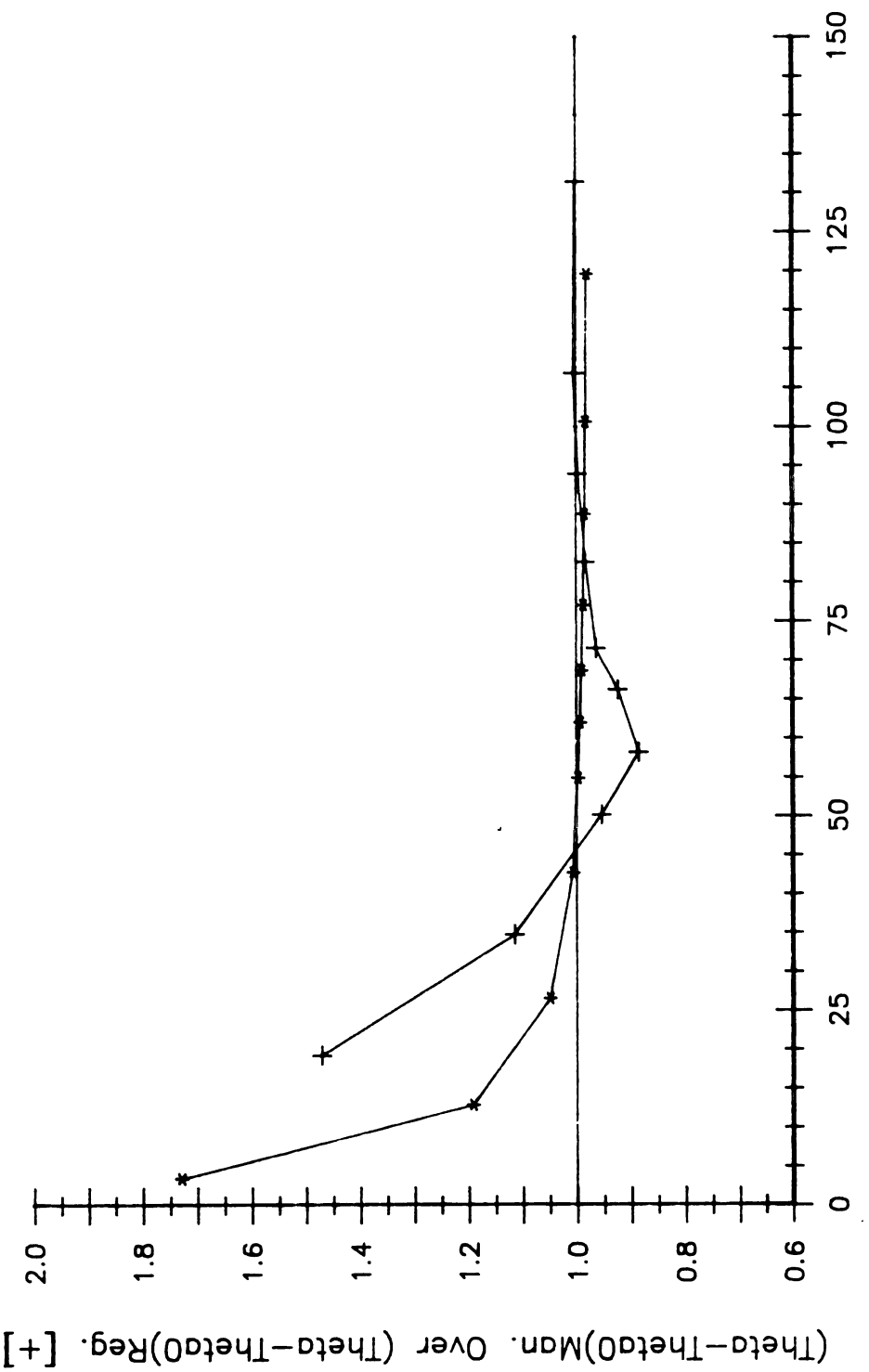

Figure 4.3 Streamwise comparison between non-dimensional net drag ratio (NDR) $(\theta_x - \theta_o)_{Man.}/(\theta_x - \theta_o)_{Reg.}$ obtained from momentum balance, and direct measurement of $d\bar{U}/dy_w$ in experiment II.

TABLES

Table 3.1 Mean boundary layer characteristics and wall-layer statistical information of visualization experiment at ξ = 20.

B. L. Parameters	Regular	Manipulated
δ (IN)	4.16	4.17
θ (IN)	0.4988	0.5550
H	1.4116	1.3594
R_θ	2542	2991
$C_{f\theta}$	0.003144	0.001914
C_{fn}	0.002473	0.002125

Statistical information of outward normal travel (y^+) of fluid corresponding to the figure 3.56.

Mean (y^+)	240.3	179.1
Std. Dev. (y^+)	72.4	62.1
Skewness Factor	0.2525	0.5517
Flatness Factor	2.9477	3.3372

Table 3.2 Mean Boundary Layer Integral Characteristics

	STATION	O	A	B	C	D	E	F	G	H
REGULAR	δ (IN)	3.16	4.16	5.16	5.33	5.52	5.79	6.11	6.65	7.46
	δ_d (IN)	0.5494	0.7166	0.8102	0.7864	0.9640	1.0718	1.0409	1.0904	1.1491
	θ (IN)	0.4011	0.4986	0.5905	0.6459	0.7286	0.7509	0.7511	0.7867	0.8382
	H	1.3698	1.4373	1.3722	1.2175	1.3230	1.4274	1.3859	1.3860	1.3709
	R_θ	2152.50	2540.42	2872.19	3484.51	3946.77	4263.80	4028.71	4296.31	4143.06
	$C_{f\theta}$	0.003467	0.003144	0.003206	0.002887	0.002560	0.002672	0.003008	0.003007	0.002855
	C_{fn}	.002421	.002413	.002370	.002169	.001964	.001998	.002266	.001884	.002267

	STATION	A	B	C	D	E	F	G	H	I	J
MANIPULATED	δ (IN)	4.17	4.26	4.91	5.38	5.45	5.69	6.30	6.62	7.15	8.31
	δ_d (IN)	0.7544	0.8630	0.8591	0.8630	0.9496	1.0596	1.1007	1.1886	1.2541	1.3818
	θ (IN)	0.5550	0.6011	0.6445	0.6507	0.7088	0.7429	0.7858	0.8490	0.9037	0.9996
	H	1.3594	1.4357	1.3328	1.3262	1.3399	1.4264	1.4008	1.4000	1.3877	1.3823
	R_θ	2991.30	3305.84	3460.18	3525.61	3773.07	3958.86	4141.76	4564.90	4848.87	5415.91
	$C_{f\theta}$	0.001914	0.001779	0.001615	0.002631	0.003456	0.003636	0.003130	0.002818	0.003011	0.002828
	C_{fn}	.002125	.001884	.002059	.002105	.001875	.002188	.002064	.002044	.001759	.001893

APPENDICES

APPENDIX A: Computer Programs

In addition to the general TSL programs (not listet here), the following programs were specifically used to process the data in the experiment.

```
      PROGRAM CAL1WIRE
C-----------------------------------------------------------------------
C     CAL1WIRE.FTN
C-----------------------------------------------------------------------
C     This program calculates the constants in the Collis and
C     Williams expression which relates hot-wire voltage to
C     flow velocity.
C     The expression is Voltage**2 = A + B*Velocity**.45.
C
C     The constants are obtained by first converting the voltages
C     and velocities to Collis and Williams variables; i.e.
C     Voltage**2 and velocity**.45.
C     Then a least squares curve fitting routine is used to fit a
C     straight line through the variables.
C     The constants  A and B are output.
C
C     The programs also computes the standard error of the
C     estimate of the velocity.
C
C     Other quantites calculated are:
C
C     Variable names:
C
C     VOLTHW(I) = Input hot-wire voltages in volts
C     VOLTPR(I) = Input voltage from the Barotron pressure
C                 transducer, volts
C     VEL(I) = Velocity calculated fromthe pressure transducer ft/s
C     X(I) = Hot-wire voltage squared
C     Y(I) = Velocity VEL(I) squared
C     YEST(I) = the estimate of the velocity**.45 using the curve fit
C     VELEST(I) = the estimate of the velocity from the curve fit
C     EY(I) = the deviation of the estimated velocity (curve fit of hot-wire
C     data) from the real value of the velocity(from pressure).
C     SCALE(J) = least squares curve fit estimates
C
C     The program interactively requests the Temperature, Barometric
C     pressure and number of data pairs in the datafile.
C
C     INPUT IS READ FROM A DATA FILE WHICH CONTAINS
C     pairs of hot wire voltages(VOLTHW), and pressure transducer
C     voltages(VOLTPR).
C     Example:
C     RD   3.456,9.878
C     The FORMAT is (2X,F8.3,1X,F8.3)
C
C     This program is linked as follows:
```

```
C     LINK/CODE:FPP CALIWIRE
C
C     Output is sent to the line printer and to output files
C     OUTPUT.DAT and CWRAW.DAT
C
C     ****************************************************************
C
      DIMENSION X(50),Y(50),EY(50),DY(50),DX(50),YEST(50)
      DIMENSION VOLTHW(50), VEL(50), VELEST(50),VOLTPR(50),SCALE(200)
      LOGICAL*1 FNAME(17)
      OPEN(UNIT=2,NAME='OUTPUT.DAT',TYPE='NEW',DISP='PRINT')
      TYPE *, 'ENTER DATA FILE NAME'
      ACCEPT 20, FNAME
C     TYPE *, 'ENTER NAME OF OUTPUT FILE WITH CURVE FIT'
C     ACCEPT 20,FOUT
20    FORMAT(17A1)
      OPEN(UNIT=1,NAME=FNAME,TYPE='OLD',ACCESS='SEQUENTIAL')
      TYPE *, ' NO OF DATA PAIRS'
      ACCEPT 11, N
11    FORMAT(I2)
      TYPE *,' ENTER BAROMETRIC PRESSURE IN INCHES OF HG'
      ACCEPT 1002, BARO
      TYPE *, ' ENTER TEMPERATURE IN DEGREES F '
      ACCEPT 1002, TEMP
1002  FORMAT(F10.3)
      XTIME=SECNDS(0.0)
      XN=N
      DO 777 I = 1,N
888   READ(1,10) F,VOLTHW(I),VOLTPR(I)
10    FORMAT(1A1,1X,F8.3,1X,F8.3)
      IF(F.NE.';') GO TO 777
666   READ(1,778) F
778   FORMAT(1A1)
      IF(F.EQ.';') GO TO 888
      GO TO 666
777   CONTINUE
      CLOSE(UNIT=1)
      WRITE(2,201)
201   FORMAT(25X, 'OUTPUT OF CAL1WIRE.FTN')
      WRITE(2,202) FNAME
202   FORMAT('0',2X, 'DATA FILE USED IS---  ',17A1)
      WRITE(2,749) N
749   FORMAT('0',2X,'NO OF DATA POINTS = ',I3)
      WRITE(2,1008)
1008  FORMAT('0',20X, ' INPUT DATA ')
      WRITE(2,1009)
1009  FORMAT(2X, ' VOLTHW(I) IN VOLTS--VOLTPR(I) IN VOLTS ')
      DO 1010 I = 1, N
      WRITE(2,1011) VOLTHW(I),VOLTPR(I)
1011  FORMAT(2X, 2F14.3)
1010  CONTINUE
      DO 1001 I = 1, N
C     COVERSION FACTOR IN EQUATION BELOW GOOD ONLY IF
```

```
C     VOLTPR(I) 1 VOLT/MM HG
C     CONVERT MILLIVOLTS TO VOLTS
      VOLTHW(I) = VOLTHW(I)/1000.0
      VOLTPR(I) = VOLTPR(I)/1000.0
      VEL(I) = 15.9*SQRT(((TEMP+459.7)*(VOLTPR(I)*.00535774))/(BARO))
1001  CONTINUE
      WRITE(2,1012)
1012  FORMAT('0',20X, 'OUTPUT')
      WRITE(2,133)
133   FORMAT('0',2X, '  VOLTHW(I) IN VOLTS--VEL(I) IN F/S')
      DO 12 I=1,N
12    WRITE(2,134) VOLTHW(I),VEL(I)
134   FORMAT(2X, 2F14.3)
C     CALCULATE THE COLLIS AND WILLIAMS VARIABLES
C     AND PERFORM A LEAST SQUARES FIT OF A STRAIGHT LINE TO
C     THEM
C     THE FORM OF THE EQUATION IS ----VOLTS**2 = A + B*VEL**.45
      DO 100 I = 1,N
      X(I) = VOLTHW(I)*VOLTHW(I)
100   Y(I) = VEL(I)**.45
      SUMX = 0.
      SUMY = 0.
      SUMXY = 0.
      SUMX2 = 0.
      SUMY2 = 0.
      SUMDY2 = 0.
      SUMDX2 = 0.
      SUMEY2 = 0.
      SMDXDY = 0.
      DO 1 I = 1,N
1     EY(I) = 0.
      DO 2 I = 1,N
      SUMX =SUMX + X(I)
      SUMX2 = SUMX2 + X(I)*X(I)
      SUMY = SUMY + Y(I)
      SUMY2 = SUMY2 + Y(I)*Y(I)
2       SUMXY = SUMXY + X(I)*Y(I)
      B1 = (XN*SUMXY - SUMX*SUMY)/(XN*SUMX2-SUMX**2)
      AVEY = SUMY/XN
      AVEX = SUMX/XN
      B0 = AVEY - B1*AVEX

C     The fit in terms of Velocity**.45
C     Q**.45 = B1*VOLTS**2 + B0
      A = -B0/B1
      B = 1./B1
C     VOLTS**2 = A + B*Q**.45
C     DETERMINE THE STANDARD ERROR OF THE ESTIMATE OF VELOCITY
      DO 3 I = 1,N
C     YEST(I) = the estimate of the velocity**.45 using the curve fit
3       YEST(I) = B1*X(I) + B0
C     CONVERTING TO AN EQUATION FOR VELOCITY
      DO 4 I = 1,N
```

```
      VELEST(I) = YEST(I)**(1./.45)
C     Calculate the deviations of Y(I), X(I),
C     from their average values, and the estimated velocity from the
C     curve fit
      DY(I) = Y(I) - AVEY
      DX(I) = X(I) -AVEX
4             EY(I) = VEL(I) - VELEST(I)
C     VARIANCE OF  THE ERROR OF ESTIMATE OF THE VELOCITY
      DO 5 I = 1,N
      SMDXDY = SMDXDY + DX(I)*DY(I)
      SUMDY2 = SUMDY2 + DY(I)*DY(I)
      SUMDX2 = SUMDX2 + DX(I)*DX(I)
5             SUMEY2 = SUMEY2 + EY(I)*EY(I)
      XN1 = N - 1
      SY = SQRT(SUMDY2/XN1)
      SX = SQRT(SUMDX2/XN1)
      RXY = SMDXDY/(SQRT(SUMDX2*SUMDY2))
      SE = SQRT(SUMEY2/XN1)
      WRITE(2,3001)
3001  FORMAT('0',2X,'VELOCITY(PRESS)---VELEST(I)---ERROR')
      WRITE(2,3002) (VEL(I),VELEST(I),EY(I),I=1,N)
3002  FORMAT(2X,3F14.3)
C     CALCULATION OF THE STANDARD ERROR OF THE VEL**.45
C     USING THE CORRELATION RXY
      SEBACK = SY*SQRT(1. - RXY*RXY)
C     Write voltage**2 and velocity**.45 to an output file, for
C     later plotting by MULPLT
      OPEN(UNIT=3,TYPE='NEW',NAME='CWRAW.DAT')
      WRITE(3,1130)
1130  FORMAT(';',/' CWRAW.DAT',/' OUTPUT FILE IN MULPLT FORMAT')
      WRITE(3,1123) N,TEMP,BARO
1123  FORMAT(/' N = ',I3,' TEMP = ',F7.3,'  BARO = ',F7.3)
      WRITE(3,1125) A,B
1125  FORMAT('VOLTS**2 = ',F7.3,' + ',F7.3,'*VELEST**.45')
      WRITE(3,1127)
1127  FORMAT(1X,'VOLTS**2--VEL**.45')
      WRITE(3,1126)
1126  FORMAT(';')
      WRITE(3,1124)(X(I),Y(I),I=1,N)
1124  FORMAT('RD',F8.3,',',F8.3)
      CLOSE(UNIT=3)
      WRITE(2,95)
95    FORMAT('0',2X, 'QUALITY OF FIT IN COLLIS AND WILLIAMS VARIABLES')
      WRITE(2,91)
91    FORMAT('0',2X,'VEL**.45     VELEST**.45      ERROR')
      WRITE(2,9) (Y(I), YEST(I), EY(I), I=1,N)
9     FORMAT(2X, 3F11.3)
      WRITE(2,70)
70    FORMAT('0',2X,'VELEST**.45 = B1*VOLTS**2 + B0')
      WRITE(2,747) B0,B1
747   FORMAT('0',2X,'VELEST**.45 = ',F7.3,' + ',F7.3,'*VOLTS**2')
      WRITE(2,748)
748   FORMAT('0',2X,'VOLTS**2 = A + B*VELEST**.45')
```

```
      WRITE(2,345) A,B
345   FORMAT('0',2X,'VOLTS**2 = ',F7.3,' + ',F7.3,'*VELEST**.45')
      WRITE(2,71) SEBACK
71    FORMAT('0',2X,'STAN ERROR OF THE EST OF VEL**.45 (USING RXY)',F7.3)
      WRITE(2,62)
62    FORMAT('0',2X, 'STAN DEV OF VEL**.45, SD OF VOLTS**2, CORR RXY')
      WRITE(2,61) SY, SX, RXY
61    FORMAT(10X, 3F7.3)
      WRITE(2,6) SE
6     FORMAT('0',2X,'STANDARD ERROR OF THE ESTIMATE OF VEL = ',F7.3,' F/S')
      WRITE(2,7) SECNDS(XTIME)
7     FORMAT('0',2X,'ELASPED EXECUTION TIME',F10.4,'SEC')
      CLOSE(UNIT=2,DISPOSE='PRINT')
C
C     Output file for MULPLT
C
      OPEN(UNIT=3,TYPE='NEW',NAME='LEASTSQ.DAT')
      RTHETA = Y(1)-.5
      DO 4999 J = 1,100
      RTHETA = RTHETA + .05
      SCALE(J) = A + B*RTHETA
      WRITE(3,5000) SCALE(J),RTHETA
5000  FORMAT('RD',F8.3,',',F8.3)
4999  CONTINUE
      CLOSE(UNIT=3)
      TYPE *, ' PROGRAM HAS FINISHED, SEE CWRAW.DAT, OUTPUT.DAT, LEASTSQ.DAT'
      CALL EXIT
      ENd



C-------------------------------------------------------------------
C COMMAND PROGRAM CALANL.CMD
C-------------------------------------------------------------------
.ENABLE SUBSTITUTION
.ENABLE DECIMAL
.ASK [:3S] DEBUG
.5:
      ;Welcome to HOT WIRE CALABRATION ANALYSIS
      ;This command file creates many plot to help analize velocity
      ;profile data
      .ASKS USERNM Please enter your name
      .ASKS COMNT Please enter a comment describing run
      .ASKS FILNM1 Please enter the NAME of the raw data file
      .GOSUB INDEX FILNM1,PERIOD
      .SETS REDNM1 FILNM1[1:PERIOD]+"RED"
      .SETS VPONM1 FILNM1[1:PERIOD]+"VPO"
      .SETS VP3NM1 FILNM1[1:PERIOD]+"VP3"
      .GOSUB MESQST
      .GOSUB VELQST
      COPY 'FILNM1' 'REDNM1'
      .SETS SLPFIL "'REDNM1'/-AU='REDNM1'"
```

```
        .GOSUB VELSLP
        .GOSUB VELSUB
.50:    .ASK ANS Do you want to process another file
        .IFT ANS .GOTO 5
        PURGE *.*
        PRINT 'VP3NM1'
        .EXIT
.VELSLP:
        .OPEN DATRED.SLP
        .DATA 'SLPFIL'
        .DATA <'B0'
        .DATA 'B1'
        .DATA 'BARO'
        .DATA 'TEMP'
        .DATA 'KVISC'
        .DATA 'VPONM1'
        .DATA ;
        .GOSUB GENANS
        .GOSUB MESANS
        .GOSUB VELANS
        .IFT LBUSTS .GOSUB LBUANS
        .DATA ;
        .DATA /
        .SETS FILNAM FILNM1
        .SETS SLPFIL "VELNERWAL.CAL/-AU=VELNERWAL.CAL"
        .GOSUB PDLSLP
        .SETS SLPFIL "FALCOVELX.CAL/-AU=FALCOVELX.CAL"
        .GOSUB PDLSLP
        .SETS SLPFIL "VELBIG.CAL/-AU=VELBIG.CAL"
        .GOSUB PDLSLP
        .SETS SLPFIL "CLAUSERC.CAL/-AU=CLAUSERC.CAL"
        .GOSUB PDLSLP
        .SETS SLPFIL "CLAUSERP.CAL/-AU=CLAUSERP.CAL"
        .GOSUB PDLSLP
        .CLOSE
        MCR SLP JDATRED.SLP
;       DEL DATRED.SLP
        .RETURN
.VELSUB:
        RUN/COMM:"'REDNM1'" VELPRO
        COPY 'VPONM1' NDX.DAT
        MCR MUL VELNERWAL.CAL
        MCR RAS PTX
        MCR MUL FALCOVELX.CAL
        MCR RAS PTX
        MCR MUL VELBIG.CAL
        MCR RAS PTX
        MCR MUL CLAUSERC.CAL
        MCR RAS PTX
        MCR MUL CLAUSERP.CAL
        MCR RAS PTX
        ;Please find the following numbers from the plots on the printer
        .ASKS DUDYWL Please enter DUDY at the wall
```

```
      .ASKS CFCLR Please enter cf CLAUSER
      .SETS FILNAM VPONM1
      .OPEN DATRED.SLP
      .SETS SLPFIL VPONM1+"/-AU="+VPONM1
      .DATA 'SLPFIL'
      .DATA 'DUDYWL'
      .DATA 'CFCLR'
      .DATA 'KVISC'
      .DATA 'VP3NM1'
      .DATA /
      .SETS FILNAM FILNM1
      .SETS SLPFIL "YOTHVSUUI.CAL/-AU=YOTHVSUUI.CAL"
      .GOSUB PDLSLP
      .SETS SLPFIL "INNERLAW.CAL/-AU=INNERLAW.CAL"
      .GOSUB PDLSLP
      .SETS SLPFIL "YROTTA.CAL/-AU=YROTTA.CAL"
      .GOSUB PDLSLP
      .SETS SLPFIL "WAKE.CAL/-AU=WAKE.CAL"
      .GOSUB PDLSLP
      .SETS SLPFIL "INNERRMS.CAL/-AU=INNERRMS.CAL"
      .GOSUB PDLSLP
      .SETS SLPFIL "WALLRMS.CAL/-AU=WALLRMS.CAL"
      .GOSUB PDLSLP
      .SETS SLPFIL "OUTERRMS.CAL/-AU=OUTERRMS.CAL"
      .GOSUB PDLSLP
      .CLOSE
      MCR SLP JDATRED.SLP
;     DEL DATRED.SLP
      RUN/COMM:"'VPONM1'" VELPR3
      MCR MUL YOTHVSUUI.CAL
      MCR RAS PTX
      MCR MUL INNERLAW.CAL
      MCR RAS PTX
      MCR MUL YROTTA.CAL
      MCR RAS PTX
      MCR MUL WAKE.CAL
      MCR RAS PTX
      MCR MUL OUTERRMS.CAL
      MCR RAS PTX
      MCR MUL INNERRMS.CAL
      MCR RAS PTX
      MCR MUL WALLRMS.CAL
      MCR RAS PTX
      .RETURN
.
.MESQST:
.SETS S1 πN/Aπ
.SETS STRDEF π[1:30:S1:30S]π
      ;
      ; PLEASE ENTER THE MEASURED EXPERIMENTAL CONDITIONS
   .ASKS BARO BAROMETRIC pressure in inches of Hg?
   .ASKS 'STRDEF' BAROST BAROMETRIC movement (RISE:FALL:STEADY)?
   .ASKS TEMP TEMPERATURE (Degrees F)?
```

```
   .ASKS 'STRDEF' HUMID RELATIVE humidity (%)?
   .ASKS 'STRDEF' WNDSPD WIND speed (MPH)?
   .ASKS 'STRDEF' WNDDIR WIND direction (N:NE:E:SE:S:SW:W:NW)?
   .ASKS 'STRDEF' PTINTK number of SAMPLES taken at each data point?
      ;
      ; BARO PRESS :'BARO'
      ; BARO STATUS:'BAROST'
      ; TEMP       :'TEMP'
      ; HUMIDITY   :'HUMID'
      ; WIND SPEED :'WNDSPD'
      ; WIND DIRECT:'WNDDIR'
      ; SAMPLES per DATA POINT  :'PTINTK'
      ;
      .ASK ANS Are the answers above correct
      .IFF ANS .GOTO MESQST
      .RETURN
.CALQST:
      ;
      ; PLEASE ENTER INFORMATION ON THE TYPE OF PROBE USED
      .ASKS 'STRDEF' NWIRES enter number of wires on probe?
      ;
      ;NUMBER OF WIRES ON PROBE:'NWIRES'
      ;
      .ASK ANS Are the inputted answers above correct
      .IFF ANS .GOTO CALQST
      .RETURN
.VELQST:
      ;
      ; PLEASE ENTER THE FOLLOWING CALABRATION VALUES
   .ASKS B0 enter value for B0 from VEL FUNCT?
   .ASKS B1 enter value for B1 from VEL FUNCT?
   .ASKS KVISC enter the kin. viscocity?
      ;
      ; B0 from VEL FUNCT          :'B0'
      ; B1 from VEL FUNCT          :'B1'
      ; KIN. VISC.                 :'KVISC'
   .ASK ANS Are the inputted answers above correct
   .IFF ANS .GOTO VELQST
.VEL2:
      ;
      ; PLEASE ENTER THE DESCRIPTION OF THE EXPERIMENT
   .ASKS 'STRDEF' STDIST DIST of station from tunnel inlet (inches)?
   .ASKS 'STRDEF' TPDIST TRIP distance from tunnel inlet (inches)?
   .ASKS 'STRDEF' TPDESC description and size of trip (inches)?
   .ASKS 'STRDEF' FANSET TUNNEL fan setting?
   .ASKS 'STRDEF' ZROVOL zero velocity voltage (volts)?
   .ASKS 'STRDEF' ADRNGE A/D voltage range (lower/upper volts)?
      ; STATION DIST from inlet in :'STDIST'
      ; TRIP DIST from inlet    in :'TPDIST'
      ; TRIP DESCRIPTION, SIZE     :'TPDESC'
      ; TUNNEL FAN SETTING         :'FANSET'
      ; ZERO VELOCITY VOLTAGE      :'ZROVOL'
      ; A/D VOLTAGE RANGE          :'ADRNGE'
```

```
      ;
      .ASK ANS Are the inputted answers above correct
      .IFF ANS .GOTO VEL2
      ;
      ; PLEASE ENTER INFORMATION ON USE OF THE TAPPM
      .ASK LBUSTS Are you using TAPPM for this run
      .IFT LBUSTS .GOSUB LBUQST
      .RETURN
.LBUQST:
   .ASKS 'STRDEF' LBDIST enter dist of 1st TAPPM from tunnel inlet (inches)
   .ASKS 'STRDEF' LBPLAT enter dist between TAPPM plates (inches)
   .ASKS 'STRDEF' LBHIGH enter height of TAPPM above tunnel floor (inches)
      ;
      ; TAPPM DIST from inlet in  :'LBDIST'
      ; TAPPM HEIGHT          in  :'LBHIGH'
      ; TAPPM PLATE SEPERATION in :'LBPLAT'
      ;
      .ASK ANS Are the inputted answers above correct
      .IFF ANS .GOTO LBUQST
      .RETURN
.GENANS:
.ENABLE DATA
 DATE    :'<DATE>'
 TIME    :'<TIME>'
 RUN BY :'USERNM'
 COMMENT:'COMNT'
.DISABLE DATA
.RETURN
.MESANS:
.ENABLE DATA
 MEASURED EXPERIMENTAL CONDITIONS
 BARO PRESS :'BARO'
 BARO STATUS:'BAROST'
 TEMP       :'TEMP'
 KIN. VISC. :'KVISC'
 HUMIDITY   :'HUMID'
 WIND SPEED :'WNDSPD'
 WIND DIRECT:'WNDDIR'
.DISABLE DATA
.RETURN
.VELANS:
.ENABLE DATA
 EXPERIMENTAL VARIABLES
 B0 FROM VEL FUNCT        :'B0'
 B1 FROM VEL FUNCT        :'B1'
 SAMPLES per DATA POINT   :'PTINTK'
 STATION DIST from inlet :'STDIST'
 TRIP DIST from inlet     :'TPDIST'
 TRIP DESCRIPTION, SIZE   :'TPDESC'
 FAN SETTING              :'FANSET'
 ZERO VELOCITY VOLTAGE    :'ZROVOL'
 A/D VOLTAGE RANGE        :'ADRNGE'
.DISABLE DATA
```

```
.RETURN
.LBUANS:
.ENABLE DATA
 TAPPM DIST from inlet     :'LBDIST'
 TAPPM HEIGHT (inches)     :'LBHIGH'
 TAPPM PLATE SEPERATION in:'LBPLAT'
.DISABLE DATA
.RETURN
.CALANS:
.ENABLE DATA
   OF WIRES ON PROBE      :'NWIRES'
.DISABLE DATA
.RETURN
.PDLSLP:
      .DATA 'SLPFIL'
      .DATA -/TIT2....DAT/,.
      .DATA  TIT2RAW DATA FILE :'FILNAM'
      .DATA /
      .RETURN
.INDEX:
      .SETS S1 "'FILNM1'"
      .SETS S2 "."
      .SETN I 1
.BEGIN:
      .IF S2 <> S1[I:I] .GOTO ELSE
          .SETN PERIOD 'I'
          .RETURN
.ELSE:
          .INC I
          .GOTO BEGIN



C-----------------------------------------------------------------
      PROGRAM VELPRO
C-----------------------------------------------------------------
C LOCAL VARIABLES
C     HWAVG(I) = HOT-WIRE AVERAGE VOLTAGE (RMS)
C     HWRMS(I) = HOT-WIRE RMS VOLTAGE (RMS)
C     PRESS(I) = PRESSURE TRANSDUCER VOLTAGE
C     DIST(I) = DISTANCE above the wall of the hot-wire measurement
C     UBAR(I) = MEAN VELOCITY FROM HOT WIRE
C     URMS(I) = RMS VELOCITY FROM HOT WIRE
C     UINF(I) = VELOCITY FROM PRESSURE TRANSDUCER
C     AVGU    = AVERAGE UINF FOR DATA RUN
C     RMSU    = RMS UINF FOR DATA RUN
C
C     it asks for the datafilename and the number of points in the
C     data file, the barometric pressure and the temperature.
C     These are read in, manipulated, and written out to a file
C     with the format:
C
```

```
      PARAMETER ASIZE=100
      IMPLICIT REAL(A-Z)
      REAL B0,B1,TEMP,BARO,KVISC,EXPONT,RTEMP,SUM,SUMSQ
      REAL HWAVG(ASIZE),HWRMS(ASIZE),PRESS(ASIZE),DIST(ASIZE)
      REAL BCONST,UFINAL,UBAR(ASIZE),URMS(ASIZE),UINF(ASIZE)
      REAL UoUINF(ASIZE),CNT,AVGU,RMSU,REY(ASIZE),YOFF
      INTEGER ICOUNT,I
      CHARACTER INFIL*30, OUTFIL*30,TAG*1,COMNT*80,JDATE*9,JTIME*8
      LOGICAL*1 PROCES
      DATA ICOUNT,I/0,1/
C-----------------------------------------------------------------
C START MAIN PROGRAM
C-----------------------------------------------------------------
      CALL GETCMD(PROCES,INFIL)
      IF(PROCES)THEN
              READ *, B0
              READ *, B1
              READ *, BARO
              READ *, TEMP
              READ *, KVISC
              READ *, YOFF
              READ 700, INFIL
              READ 700, OUTFIL
      ELSE
              TYPE *, 'ENTER B0---FROM VEL**.45 = B0 + B1*VOLTS**2'
              ACCEPT *, B0
              TYPE *,'ENTER B1---FROM  VEL**.45 = B0 + B1*VOLTS**2'
              ACCEPT *, B1
              TYPE *,'ENTER BAROMETRIC PRESSURE'
              ACCEPT *, BARO
              TYPE *,'ENTER TEMPERATURE IN DEGREES F'
              ACCEPT *, TEMP
              TYPE *,'ENTER KINEMATIC VISCOSITY'
              ACCEPT *, KVISC
              TYPE *,'ENTER THE Y OFFSET'
              ACCEPT *, YOFF
8             TYPE *,'ENTER INPUT DATA FILE :'
              ACCEPT 700,INFIL
9             TYPE *,'ENTER OUTPUT DATA FILE :'
              ACCEPT 700, OUTFIL
      ENDIF
      OPEN(UNIT=1,NAME=INFIL,STATUS='OLD',ERR=520)
      OPEN(UNIT=2,NAME=OUTFIL,STATUS='NEW',ERR=530)
15    READ(1,950,ERR=20,END=30) TAG, HWAVG(I), HWRMS(I),
     +     PRESS(I), DIST(I)
      IF(TAG .EQ. ';') THEN
20       WRITE(2,960) TAG,COMNT
         READ(1,955) TAG,COMNT
         IF(TAG .NE. ';')GOTO 20
      ELSE
         I =I+1
      ENDIF
      GOTO 15
```

```
C     manipulation  ***********************************************
30    ICOUNT  = I-1
      RTEMP   = TEMP+459.7
      SUM     = 0.0
      SUMSQ   = 0.0
      BCONST  = 0.00535774
      UFINAL  = (B0 + B1*(HWAVG(ICOUNT)/1000.0)**2)**(1./.45)
      DO 100 I = ICOUNT,1,-1
      IF(HWAVG(I) .EQ. 0.0) GOTO 100          !zero is passed over
      HWAVG(I)  =HWAVG(I)/1000.0              !convert to millivolts
      PRESS(I)  =PRESS(I)/1000.0
      UBAR(I)   = (B0 + B1*HWAVG(I)**2)**(1./.45)
      SLOPE  = 2.0/.45*(B0+B1*HWAVG(I)**2)**((1./.45)-1)*B1*HWAVG(I)
      URMS(I)   = SLOPE * HWRMS(I)/1000.
      UINF(I)   = 15.9*SQRT(RTEMP*PRESS(I)*BCONST/BARO)
      SUM       = SUM   + UINF(I)
      SUMSQ     = SUMSQ + UINF(I)**2
100   CONTINUE
C this routine for calculating u infinity
C     DO WHILE
         USUM=0.0
         I=ICOUNT
70       UMEAN = (USUM+UBAR(I))/(ICOUNT-I+1)
         DIFF  = UMEAN-UBAR(I)
         IF (DIFF .GE. .01*UMEAN) GOTO 75
           USUM  =  USUM + UBAR(I)
           I=I-1
             GOTO   70
C        ELSE
C           DO WHILE LT ICOUNT
75            I=I+1
              UBAR(I)=UMEAN
              IF(I .LT. ICOUNT) GOTO 75
C        ENDIF
C continue with calculations
      DO 175 I=1,ICOUNT
         DIST(I)   = DIST(I) + YOFF
         REY(I)    = UFINAL*DIST(I)/(KVISC*12.0)
         UoUINF(I) = UBAR(I)/UFINAL
175   CONTINUE
      CNT     = FLOAT(ICOUNT)
      AVGU    = SUM/CNT
      RMSU    = SQRT(ABS(SUMSQ-SUM**2/CNT)/(CNT-1))
C     output  ***********************************************
      CALL TIME(JTIME)
      CALL DATE(JDATE)
      WRITE(2,900) JDATE,JTIME,INFIL,OUTFIL
      WRITE(2,905) B0,B1,TEMP,KVISC
      WRITE(2,910) ICOUNT,AVGU,RMSU
      WRITE(2,915)
      DO 150 I=1,ICOUNT
         WRITE(2,920) HWAVG(I),HWRMS(I),PRESS(I),DIST(I)
150   CONTINUE
```

```
      WRITE(2,925)
      WRITE(2,930)
      DO 200 I=1,ICOUNT
         WRITE(2,935) UBAR(I),URMS(I),UINF(I),DIST(I),REY(I),
     +                UoUINF(I)
200   CONTINUE
      CALL EXIT
C
C FORMAT STATEMENTS
C
700   FORMAT(A)
900   FORMAT('0',T5,'VELPRO OUTPUT -- JULY-1-84 VERSION'/
     +                ' ',T7,'DATE    :',A/
     +                ' ',T7,'TIME    :',A/
     +                ' ',T7,'INPUT  FILE NAME:',A/
     +                ' ',T7,'OUTPUT FILE NAME:',A)
905   FORMAT('0',T5,'VELPRO INPUTS'/
     +                ' ',T7,'B0 from VEL Fu. :',F10.5/
     +                ' ',T7,'B1 from VEL Fu. :',F10.5/
     +                ' ',T7  TEMPERTURE (F)  :',F5.2/
     +                ' ',T7,'KIN. VISC.      :',F10.7)
910   FORMAT('0',T5,'VELPRO OUTPUT'/
     +                ' ',T7,'POINTS IN FILE  :',I5/
     +                ' ',T7,'AVG UINF (PRESS):',F10.7/
     +                ' ',T7,'RMS UINF        :',F10.7)
915   FORMAT( '0',T5,'VELPRO INPUT DATA '/
     +                ' ',T7,' AVG-(V)  RMS-(MV)  PRES-(V)  DIST-(IN)')
920   FORMAT(T7,4(F8.3,2X))
925   FORMAT(' ','VELPRO OUTPUT DATA',/
     +               T7,'UBAR',T16,'URMS',T25,'UINF',T34,'DIST',
     +              T45,'REY',T52,'UoUINF')
930   FORMAT(' ',T7,'F/S',T16,'F/S',T25,'F/S',T34,'IN'/';')
935   FORMAT('RD', F8.3, ',' ,F8.5, ',' ,F8.3, ',' ,F8.3, ','
     +                   ,F10.2, ',' ,F8.3)
C15   READ(1,950,ERR=20,END=30) TAG, HWAVG(I), HWRMS(I), PRESS(I), DIST(I)
950   FORMAT(A1,4(1X,F8.3))
955   FORMAT(A1,A60)
960   FORMAT(' ',A1,A60)
C
C ERROR CONTROL
520   TYPE 522,INFIL
522   FORMAT(' ','ERROR OPENING FILE:',A,'PLEASE REENTER')
      GOTO 8
530   TYPE 522,OUTFIL
      GOTO 9
      END
      SUBROUTINE GETCMD(CMDFIL,INFIL)
C LOCAL VARIABLES
      CHARACTER*1 CMDLIN*40,INFIL*30
      LOGICAL*1 CMDFIL
      INTEGER IDS,LENGTH
      DATA CMDLIN/' '/
      CALL GETMCR(CMDLIN,IDS)
```

```
C SCAN COMMAND LINE FOR COMMAND FILE NAME
      LENGTH=INDEX(CMDLIN,'.')
C
      IF(LENGTH.NE.0)THEN
D        TYPE 100,CMDLIN(1:LENGTH+3)
         OPEN(UNIT=1,NAME=CMDLIN(1:LENGTH+3),STATUS='UNKNOWN',ERR=15)
         CMDFIL=.TRUE.
         INFIL=CMDLIN(1:LENGTH+3)
      ELSE
        CMDFIL=.FALSE.
15      TYPE *,'COMMAND FILE NOT FOUND REVERTING TO MANUAL CONTROL'
      ENDIF
      RETURN
      END



C-----------------------------------------------------------------------
      PROGRAM VELPR3
C-----------------------------------------------------------------------
C     CALCULATES:
C             DELTA
C             DISPLACEMENT THICKNESS
C             MOMENTUM THICKNESS  -  POINTS DO NOT HAVE TO BE
C                  EQUALLY SPACED - BUT THE NUMBER OF DATA POINTS (N)
C                MUST BE AN ODD NUMBER
C*            LOCAL SKIN FRICTION COEFFICIENT -- CfNTN
C*            FRICTIN VEL.(based on CLAUSER PLOT) --  UTAUCR
C             SHAPE FACTOR --   H
C             INTEGRAL     --   G  (BASED ON CLAUSER _DUDY)
C             COLES FACTOR --   PI ( B . O . CLAUSER _DUDY)
C
C
C             RESR    RESISTANCE RATIO USED FOR H.W ANEMOMETRY
C             TRPS    TRIP SIZE(OR GRIT OF SAND PAPER)
C             HLB     HEIGHT OF LEBU DEVICE FROM WALL(INCHES)
C             RHDLTA  RATIO OF HLB AND DELTA(B.L.Thickness at the 1st LEBU)
C             RZTAH   RATIO OF DITANCE FROM 2nd LEBU AND HLB
C             S       DISTANCE BETWEEN LEBU DEVICES(inches)
C             CfCLR   LOCCAL FRICTION COEFF. FROM CLASER VEL.-PLOT
C                FIN2.VPR changed to FIN2.LVP
C             UINF    FREE STREAM VELOCITY ABOVE THE B.L. (FT/SEC)
C**** *
C             N       THE NUMBER OF DATA POINTS (ODD INCLUDING 0.0,0.0)
C             NFNL    THE FIRST _THE LAST POINT   THAT DUDY IS
C                     ESTIMATED FROM
C             VEL     HOT-WIRE READING IN (FT/SEC)
C             Y       POSITION OF PROBE (DISTANCE FROM WALL INCHES)
C             DELT99  CHOSEN PERCENATGE VALUE FOR "EDGE" OF THE BDL.
C                     USUALLY .99 OR .995 (INPUT)
C             DELTA   CALCULATED B.L. THICKNESS BASED ON DELT99
C             UTAUNTN FRICTION VELOCITY(CLR:CLASER And NTN=NEWTONIAN,sub's)
```

```
C             XNU     KINEMATIC VISCOSITY--NU  (FT**2/SEC)
C             DISP    DISPLACEMENT THICKNESS
C             THETA   MOMENTUM THICKNESS
C             RTHETA  REYNOLDS NUMBER BASED ON THETA
C**** *               CfNTN   LOCAL SKIN FRICTION COEFF.(B.O. DUDY AT Y=0)
C* FOR USE IN QUAD:
C             VEL     1.0-(VEL/UINF)  AND    (VEL/UINF)*VEL
C             YDIST   POSITION OF PROBE
C
C     THE VELOCITIES MUST BE (FT/SEC), THE POSITIONS MUST BE (INCHES)
C
C
C***  NOMENCLATURE  ************************************************
C
C     GCLR = G based on UTAUC
C     ANU = Kinematic viscosity ft*2/sec
C     YPLUSC(I) = Y*UTAUCLAUSER/ANU
C     YPLUSN(I) = Y*UTAUN/ANU
C     UTAUN = utau Newton
C     UTAUC = utau Clauser
C     THETA = momentum thickness
C     YOTHET(I) = Y/THETHA
C     DELTAS = displacement thickness
C     YODSTR(I) = Y/DELTAS
C     DELT99 = 99% thickness
C     YOD99(I) = Y(I)/DELT99
C     UOUINF(I) = U/UINF
C     UOUTAN(I) = U/UTAUN
C     UOUTAC(I) = U/UTAUC
C     UMUOUN(I) = (UINF-UBAR)/UTAUN
C     UMUOUC(I) = (UINF-UBAR)/UTAUC
C     UPOUIN(I) = RMSU/UINF
C     UPOUTN(I) = RMSU/UTAUN
C     UPOUTC(I) = RMSU/UTAUC
C     YROTAC(I) = (Y*UTAUC)/(DELTAS*UINF)
C     YROTAN(I) = (Y*UTAUN)/(DELTAS*UINF)
C
C***  ************************************************************
C
      REAL DUDYWL,CfCLR,KVISC,UBAR(100),URMS(100),UPRES(100)
      REAL DIST(100),REY(100), UoUINF(100)
      REAL UINF,UTAUN,UTAUCR,CfNTN,SLOPE,X,DELTA,VEL(100)
      REAL YDIST(100),DISP,THETA,DELTA3,RTHETA,SHAPE,GDUDY
      REAL GCLR,PItemp,PI,PICLR,VEL99
      REAL YPLUSC(100),YPLUSN(100),YOTHET(100),YODSTR(100)
      REAL YOD99(100),UOUTAN(100),UOUTAC(100),UMUOUN(100)
      REAL UMUOUC(100),UPOUIN(100),UPOUTN(100),UPOUTC(100)
      REAL YROTAC(100),YROTAN(100),WAKET(100),WAKEC(100)
      REAL WAKEN(100)
      INTEGER ICOUNT,I,J
      CHARACTER OUTFIL*30,INFIL*30,TAG*1,COMNT*60,JTIME*8
      CHARACTER JDATE*9
      LOGICAL*1 PROCES
```

```
      COMMON /QPARM/ VEL,YDIST
      DATA COMNT /' '/
C-----------------------------------------------------------------
C START MAIN PROGRAM
C-----------------------------------------------------------------
      CALL GETCMD(PROCES,INFIL)
      IF(PROCES)THEN
              READ (1,*) DUDYWL
              READ (1,*) CfCLR
              READ (1,*) KVISC
              READ 700, OUTFIL
      ELSE
              TYPE *, 'ENTER DUDY AT THE WALL'
              ACCEPT *, DUDYWL
              TYPE *,'ENTER CfCLR'
              ACCEPT *, CfCLR
              TYPE *,'ENTER KINEMATIC VISCOSITY'
              ACCEPT *, KVISC
8             TYPE *,'ENTER INPUT DATA FILE :'
              ACCEPT 700,INFIL
9             TYPE *,'ENTER OUTPUT DATA FILE :'
              ACCEPT 700, OUTFIL
              OPEN(UNIT=1,NAME=INFIL,STATUS='OLD',ERR=520)
      ENDIF
      OPEN(UNIT=2,NAME=OUTFIL,STATUS='NEW',ERR=530)
      I=1
15    READ(1,702,ERR=20,END=30) TAG, UBAR(I), URMS(I), UPRES(I),
     +                                DIST(I), REY(I), UoUINF(I)
      IF(TAG .EQ. ';') THEN
20       WRITE (2,960) TAG,COMNT
         READ  (1,705) TAG,COMNT
         IF(TAG .NE. ';')GOTO 20
         WRITE (2,960) TAG,COMNT
      ELSE
         WRITE(2,965) UBAR(I), URMS(I), UPRES(I), DIST(I),
     +                                  REY(I), UoUINF(I)
         I =I+1
      ENDIF
      GOTO 15
C
C***  MANIPULATION ***********************************************
C
C Calc of velocity profile experimental quantities
30    ICOUNT = I-1
      VISC   = KVISC*12.0
      UINF   = UBAR(ICOUNT)           !fix to reflect average of final
c                                     points within 1% of delt99
      UTAUN  = SQRT(VISC*DUDYWL)
      UTAUCR = UINF*SQRT(CfCLR/2.0)
      CfNTN  = 2.*(UTAUN/UINF)**2
      I = ICOUNT+1
200           I = I-1
      IF(VEL99 .LT. UBAR(I)) GOTO 200
```

```
      SLOPE = (VEL99-UBAR(I)) / (UBAR(I+1)-UBAR(I))
      X     = DIST(I+1)-DIST(I)
      DELTA = SLOPE * X + DIST(I)
      VEL(1)   = 1.0
      YDIST(1) = 0.0
      DO 225 J=2,ICOUNT
         VEL(J)   = 1.0 - UBAR(J)/UINF
         YDIST(J) = DIST(J)
225   CONTINUE
      CALL QUAD(ICOUNT,DISP)
      VEL(1)   = 0.0
      DO 250 J=2,ICOUNT
         VEL(J)   = UBAR(J)*VEL(J)/UINF
250   CONTINUE
      CALL QUAD(ICOUNT,THETA)
      DO 275 J=2,ICOUNT
         VEL(J)   = 1.0 - (UBAR(J)/UINF)**2
275   CONTINUE
      CALL QUAD(ICOUNT,DELTA3)
      RTHETA = (UINF*THETA)/(VISC)
      SHAPE  = DISP/THETA
      GDUDY  = (SHAPE-1.0) * UINF/ (UTAUN  * SHAPE)
      GCLR   = (SHAPE-1.0) * UINF/ (UTAUCR * SHAPE)
      PItemp = 0.41*(UINF*DISP/VISC-65.0)
      PI     = (PItemp * VISC/ (DELTA * UTAUN))  -1.0
      PICLR  = (PItemp * VISC/ (DELTA * UTAUCR)) -1.0
C nondimensionalize the measured values using the calc values
      DO 300 I=1,ICOUNT
         YPLUSC(I) = DIST(I)*UTAUCR/VISC
         YPLUSN(I) = DIST(I)*UTAUN/VISC
         YOTHET(I) = DIST(I)/THETA
         YODSTR(I) = DIST(I)/DISP
         YOD99 (I) = DIST(I)/DELTA
         UOUINF(I) = UBAR(I)/UINF
         UOUTAN(I) = UBAR(I)/UTAUN
         UOUTAC(I) = UBAR(I)/UTAUCR
         UMUOUN(I) = (UINF-UBAR(I))/UTAUN
         UMUOUC(I) = (UINF-UBAR(I))/UTAUCR
         UPOUIN(I) = URMS(I)/UINF
         UPOUTN(I) = URMS(I)/UTAUN
         UPOUTC(I) = URMS(I)/UTAUCR
         YROTAC(I) = (DIST(I)*UTAUCR)/(DISP*UINF)
         YROTAN(I) = (DIST(I)*UTAUN)/(DISP*UINF)
         WAKEC(I) = (UOUTAC(I)-(5.61*ALOG10(YPLUSC(I)))-5.0)*.41/.6
         WAKEN(I) = (UOUTAN(I)-(5.61*ALOG10(YPLUSN(I)))-5.0)*.41/.6
         WAKET(I) = 2*(SIN((3.1416/2)*YOD99(I)))**2
300   CONTINUE
C     output  ***************************************************
      CALL TIME(JTIME)
      CALL DATE(JDATE)
      WRITE(2,900) JDATE,JTIME,INFIL,OUTFIL
      WRITE(2,905) DUDYWL,CfCLR,KVISC
      WRITE(2,910) ICOUNT
```

```
C------
      WRITE(2,920) VEL99,UINF,DELTA,DISP,THETA,DELTA3,RTHETA,
     +                 SHAPE,GDUDY,GCLR,PI,PICLR,CfNTN,UTAUCR,UTAUN
      WRITE (2,921)
      WRITE(2,922)
      DO 390 I=1,ICOUNT
         WRITE(2,925) YPLUSC(I), UOUTAC(I), UPOUTC(I),
     +                          YPLUSN(I), UOUTAN(I), UPOUTN(I),
     +                          UOUINF(I), YOTHET(I), UPOUIN(I)
390   CONTINUE
      WRITE(2,930)
      DO 400,I=1,ICOUNT
         WRITE(2,935) YROTAC(I), UMUOUC(I), YROTAN(I), UMUOUN(I),
     +                          YOD99(I),  WAKET(I),  WAKEC(I),  WAKEN(I)
400   CONTINUE
      WRITE(2,945)
      CLOSE (UNIT=2)
C OUTPUT MULPLT DATA FILES
C output YOTHVSUUI plot file
      OPEN(UNIT=3,NAME='YOTHV.DAT',STATUS='NEW')
         WRITE(3,941) ( UoUINF(I),YOTHET(I), I=1,ICOUNT)
      CLOSE (UNIT=3)
C output innerlaw plot file
      OPEN(UNIT=3,NAME='ILAWC.DAT',STATUS='NEW')
         WRITE(3,941) (YPLUSC(I), UOUTAC(I), I=1,ICOUNT)
      CLOSE (UNIT=3)
      OPEN(UNIT=3,NAME='ILAWN.DAT',STATUS='NEW')
         WRITE(3,941) (YPLUSN(I), UOUTANIRMSN(I), I=1,ICOUNT)
      CLOSE (UNIT=3)
C output YROTTA  plot files
      OPEN(UNIT=3,NAME='YROTC.DAT',STATUS='NEW')
         WRITE(3,941) (YROTAC(I), UMUOUC(I), I=1,ICOUNT)
      CLOSE (UNIT=3)
      OPEN(UNIT=3,NAME='YROTN.DAT',STATUS='NEW')
         WRITE(3,941) (YROTAN(I), UMUOUN(I), I=1,ICOUNT)
      CLOSE (UNIT=3)
C output WAKE plot files
      OPEN(UNIT=3,NAME='WAKEC.DAT',STATUS='NEW')
         WRITE(3,941) (YOD99(I),WAKEC(I), I=1,ICOUNT)
      CLOSE (UNIT=3)
      OPEN(UNIT=3,NAME='WAKEN.DAT',STATUS='NEW')
         WRITE(3,941) (YOD99(I),WAKEN(I), I=1,ICOUNT)
      CLOSE (UNIT=3)
      OPEN(UNIT=3,NAME='WAKET.DAT',STATUS='NEW')
         WRITE(3,941) (YOD99(I),WAKET(I), I=1,ICOUNT)
      CLOSE (UNIT=3)
C output OUTER RMS plot files
      OPEN(UNIT=3,NAME='ORMS.DAT',STATUS='NEW')
         WRITE(3,941) (YOTHET(I), UPOUIN(I), I=1,ICOUNT)
      CLOSE (UNIT=3)
C output INNER RMS  plot file
C output WALL RMS plot files
      OPEN(UNIT=3,NAME='IRMSC.DAT',STATUS='NEW')
```

```
         WRITE(3,941) (YPLUSC(I),UPOUTC(I),I=1,ICOUNT)
      CLOSE (UNIT=3)
      OPEN(UNIT=3,NAME='IRMSN.DAT',STATUS='NEW')
         WRITE(3,941) (YPLUSN(I),UPOUTN(I),I=1,ICOUNT)
      CLOSE (UNIT=3)
      TYPE *,'PROGRAM VELPR3 NORMAL TERMINATION'
      CALL EXIT
C
C FORMAT STATEMENTS
C
C read formats
700   FORMAT(A)
702   FORMAT(A,1X,F8.3,1X,F8.5,1X,F8.3,1X,F8.3,1X,F10.2,1X,F8.3)
705   FORMAT(2A)
C write formats
900   FORMAT(';'/'0',T5,'VELPR3 OUTPUT -- JULY-1-84 VERSION'/
     +                ' ',T7,'DATE    :',A/
     +                ' ',T7,'TIME    :',A/
     +                ' ',T7,'INPUT  FILE NAME:',A/
     +                ' ',T7,'OUTPUT FILE NAME:',A)
905   FORMAT('0',T5,'VELPR3 INPUTS'/
     +                ' ',T7,'DUDY at the wall:',F10.5/
     +                ' ',T7,'CfCLR           :',F10.5/
     +                ' ',T7,'KIN. VISC.      :',F10.7)
910   FORMAT('0',T5,'VELPR3 OUTPUT'/
     +                ' ',T7,'POINTS IN FILE  :',I5)
920   FORMAT('0',T5,'VELPR3 OUTPUT INFORMATION:'
     1  /,' ',T7,'  VEL99-------------------------=',F5.2,' FT/SEC'
     1  /,' ',T7,'  UINFINITY-----------------------=',F5.2,' FT/SEC'
     1  /,' ',T7,'  B.L.THICKNESS-- DELTA -----------=',F5.2,' INCHES'
     1  /,' ',T7,'  DISPLACEMENT THICKNESS-----------=',F7.4,' INCHES'
     2  /,' ',T7,'  MOMENTUM THICKNESS---------------=',F7.4,' INCHES'
     2  /,' ',T7,'  ENERGY   THICKNESS---------------=',F7.4,' INCHES'
     3  /,' ',T7,'  REYNOLDS NUMBER (RTHETA) --------=',F8.2
     4  /,' ',T7,'  SHAPE FACTOR  ------------ H ----=',F7.4
     5  /,' ',T7,'  INTEGRAL (B.O DUDY)  ----- G ----=',F12.8
     6        /,' ',T7,'  INTEGRAL(B.O CLAUSER)------GCLR--=',F12.8
     7  /,' ',T7,'  COLES FACTOR(B.O DUDY)   - PI ---=',F8.4
     8        /,' ',T7,'  COLES FACTOR(B.O CLAUSER)--PICLR =',F10.4
     9  /,' ',T7,'  LOCAL SKIN FRICTION COEFF. CfNTN =',F8.6
     +  /,' ',T7,'  FRC.VEL.(Clauser Plot) UTAUCR----=',F6.4,' FT/SEC'
     +        /,' ',T7,'  UTAUNTN(From DUDY)----------------=',F7.4,' FT/SEC')
921   FORMAT('0',T5,'NONDIMSIONALIZED VALUES')
922   FORMAT('0',
     +               T6,'Y+ C',T20,  'U',   T31, 'URMS', T41,'Y+ N',
     +        T57,  'U',   T68, 'URMS', T81, 'U',  T95,  'Y',  T108,'URMS'/
     +            '+',          T18,'___',T30,'___',
     +        T56,'___',T67,'___',T80,'__',T93,'__',T108,'__'/
     +            ' ',          T18,'UTAU C',T30,'UTAU C',
     +        T56,'UTAU N',T67,'UTAU N',T80,'UINF',T93,'THETA',T108,'UINF'//)
925   FORMAT(' ',2(F9.4,4X,F9.6,4X,F9.7,4X),F9.7,4X,F9.6,4X,F9.7)
930   FORMAT('0',
     +               ' Y*UTAUC',  T16,'UNIF-UBAR',T29,'Y*UTAUN',
```

```
     +        T42,'UNIF-UBAR' ,T55,'  Y',    T68,'WAKE T',
     +              T81,'WAKE C',T94,'WAKE N',/
     +      '+','____',  T16,'____', T29,'____',
     +              T42,'____',  T55,'__'/
     +           ' ','DISP*UINF', T16,' UTAU C',  T29,'DISP*UINF',
     +              T42,' UTAU N',   T55,'DEL99'/)
935   FORMAT(' ',2(F9.6,4X, F9.4,4X), F9.6,4X, 3(F9.5,4X))
941   FORMAT(<ICOUNT>('RD',2(G15.5)/))
945   FORMAT(';')
960   FORMAT(2A)
965   FORMAT('RD', F8.3, ',' ,F8.5, ',' ,F8.3, ',' ,F8.3, ','
     +                  ,F10.2, ',' ,F8.3)
C ERROR CONTROL
520   TYPE 522,INFIL
522   FORMAT(' ','ERROR OPENING FILE:',A,'PLEASE REENTER')
      GOTO 8
530   TYPE 522,OUTFIL
      GOTO 9
      END
      SUBROUTINE GETCMD(CMDFIL,INFIL)
C LOCAL VARIABLES
      CHARACTER*1 CMDLIN*40,INFIL*30
      LOGICAL*1 CMDFIL
      INTEGER IDS,LENGTH
      DATA CMDLIN/' '/
      CALL GETMCR(CMDLIN,IDS)
C SCAN COMMAND LINE FOR COMMAND FILE NAME
      LENGTH=INDEX(CMDLIN,'.')
C
      IF(LENGTH.NE.0)THEN
D        TYPE 100,CMDLIN(1:LENGTH+3)
         OPEN(UNIT=1,NAME=CMDLIN(1:LENGTH+3),STATUS='UNKNOWN',ERR=15)
         CMDFIL=.TRUE.
         INFIL=CMDLIN(1:LENGTH+3)
      ELSE
        CMDFIL=.FALSE.
15      TYPE *,'COMMAND FILE NOT FOUND REVERTING TO MANUAL CONTROL'
      ENDIF
      RETURN
      END
C
      SUBROUTINE QUAD(K,OUT)
      REAL DU(100),DU1(100)
      COMMON/QPARM/DU,DU1
      TOT=0.0
      K3=K-1
      DO 30 I=2,K3,2
              E1=DU(I+1)-DU(I-1)
              E2=DU(I)-DU(I-1)
              V1=DU1(I+1)**2.0-DU1(I)**2.0
              V2=DU1(I+1)-DU1(I-1)
              V3=DU1(I)**2.0-DU1(I-1)**2.0
              V4=DU1(I)-DU1(I-1)
```

```
            A=(V4*E1-V2*E2)/(V1*V4-V3*V2)
            B=(E2-A*V3)/V4
            C=DU(I)-A*DU1(I)**2.0-B*DU1(I)
            TOT=TOT+A*(DU1(I+1)**3.0-DU1(I-1)**3.0)/3.0+B*
     1      (DU1(I+1)**2.0-DU1(I-1)**2.0)/2.0+C*(DU1(I+1)-DU1(I-1))
30    CONTINUE
      OUT=TOT
      RETURN
      END



C-----------------------------------------------------------------------
      PROGRAM CALFIT
C***********************************************************************
C                     VERSION 5
C     CALFIT TAKES THE OUTPUT OF AVGVOL AND PRODUCES A U-WIRE
C     CALIBRATION CURVE BY PERFORMING A LEAST SQUARES FIT ON
C     THE DATA.
C     THE INPUT FILE IS CURVE.DAT
C     THE OUTPUT FILE IS CALCRV.DAT
C*    MODIFIED BY NASSER RASHIDNIA SPRING 1984
C     TO ELIMINATE MILLIVOLT TO VOLTS CONVERSION ERROR
C     AND TO ELIMINATE INCORRECT AREA RATIO
C     THE CURRENT VERSION USES A PRESSURE TRANDUCER OUTPUT
C     FOR THE VELOCITY REFERENCE.  THIS INPUT MUST BE FROM
C     THE MKS BARYTRON AND THE INPUT VOLTAGES EXPRESSED IN
C     MILLIVOLTS
C*    MODIFIED
C     TO PRODUCE A FILE CALLED CALPLT WHICH IS USED BY THE CALPLOT PROGRAM
C     WHICH ALLOWS THE USER TO INSPECT THE LINEARITY OF THE DATA
C*    MODIFIED 14-OCT-81 TO IMPROVE READIBILITY
C     EXPAND PROGRAM TO ALLOW UP TO 16 SENSORS, CORRECT FOR
C     STANDARD DEVIATION INACCURACY AND TO ALLOW THE USE OF
C     A CALIBRATED HOT WIRE AS A VELOCITY REFERENCE.
C
C*    MODIFIED 28-NOV-81
C       TO ALLOW THE FLUIDS LAB PRESSURE TRANSDUCER MILLIVOLTS
C       TO BE INPUT INTO THIS PROGRAM
C
C*    MODIFIED 5-DEC-81
C       TO ALLOW THE PROGRAM TO LOOK FOR EXPONENTS (N)
C       UP TO .64       THE PREVIOUS UPPER BOUND WAS  .54
C*    MODIFIED WED-16-DEC-81
C       TO ALLOW N TO BE UP TO .99
C*    MODIFIED SUN-3-JAN-82
C       TO OUTPUT THE PARAMETERS A,B,STD,N OF THE CHANNEL
C       TO BE PLOTTED TO THE LAST LINE OF FILE CALPLT.DAT.
C      *** ALSO, ALL WIRE VOLTAGES ARE NOW OUTPUT TO CALPLT.DAT
C             SO THAT CALDRW CAN BE RUN FOUR TIMES (ONE/WIRE)
C             FOR EACH RUN OF CALFIT
C     MODIFIED MON-4-JAN-82
```

```
C       TO OUTPUT ALL A, B, STD, N, FOR ALL WIRES AND ITERATIONS
C     MODIFIED TUE-26-JAN-82
C       REMOVED OLD CODE CONCERNING WHICH WIRE TO PLOT(SEE *** ABOVE)
C       IMPROVED READABILITY OF COMMENT STATEMENTS WITH ------
C       CORRECTED TEMP CONVERSION (NEW: TR=459.7+TF) (OLD: TR=459.3+TF)
C             THIS MODIFICATION CHANGED THE P.T. VELOCITIES
C             BY LESS THAN 0.01 FT/SEC
C*************************************************************************
      DIMENSION XN(4),EW(16,85),EP(85),QP(85),
     1  A(16),B(16)
      REAL NCOWIL
      COMMON /DEV/ STDEV(70),STD(16),QPXN(85),AITER(75),
     1  BITER(75),EWSQ(16,85),NVELS,J
C------
C     INPUT SECTION ACCEPTS NUMBER OF SENSORS, COMPUTES
C     NUMBER OF WIRES, TYPE OF VELOCITY REFERENCE,
C     (IF REFERENCE IS A HOT WIRE IT ACCEPTS THE
C     COLLIS AND WILLIAMS COEFFICIENTS A, B, AND N)
C     THE TEMPERATURE, BAROMETRIC PRESSURE
C     THE NUMBER OF SPEEDS AND A CHANNEL TO BE PLOTTED
C     ON A VOLTS SQUARED VERSUS VELOCITY TO THE N AXIS.
C------
      TYPE *, 'ENTER 1 FOR DEBUG EQUATIONS'
      ACCEPT *, DEBUG
      TYPE 10
10    FORMAT(1X,'ENTER NUMBER OF SENSORS')
      ACCEPT *,NSENSO
      NWIRES=NSENSO-1
      TYPE 12
12    FORMAT(1X,'IS VELOCITY REFERENCE A HOT WIRE Y/N ')
      ACCEPT 13,ANSWER
13    FORMAT(A1)
      IF(ANSWER.NE.'Y') GOTO 14
      TYPE *, 'INPUT A OF COLLIS AND WILLIAMS LAW FOR REFERENCE WIRE'
      ACCEPT *, ACOWIL
      TYPE *, 'INPUT B OF COLLIS AND WILLIAMS LAW FOR REFERENCE WIRE'
      ACCEPT *, BCOWIL
      TYPE *, 'INPUT N OF COLLIS AND WILLIAMS LAW FOR REFERENCE WIRE'
      ACCEPT *, NCOWIL
      GO TO 18
14    TYPE 15
15    FORMAT(1X,'ENTER TEMPERATURE IN DEGREES F')
      ACCEPT *,TEMP
      TYPE 17
17    FORMAT(1X,'ENTER BAROMETRIC PRESS IN INCHES OF HG')
      ACCEPT *,BARO
18    TYPE 20
20    FORMAT(1X,'ENTER NUMBER OF FAN SETTINGS')
      ACCEPT *,NVELS
C
      TYPE *,'IF THE BAROTRON PRESS. TRAN. WAS USED'
      TYPE *,'MAX VEL < 12.0 FT/SEC ,   ENTER 1'
      TYPE *,' IF FLUIDS LAB P.T. WAS USED'
```

```
      TYPE *,'1.0 INCH WATER = 5.0 VOLTS,    ENTER 2'
      ACCEPT *,PTRAN
C------
C     OPEN THE AVERAGE VOLTAGE FILE CURVE.DAT AND READ IN
C     THE AVERAGES FOR EACH CALIBRATION SPEED
C------
      OPEN(UNIT=1,NAME='CURVE.DAT',FORM='FORMATTED',
     1  TYPE='OLD',READONLY)
      DO 30 I=1,NVELS
              READ(1,*)(EW(J,I),J=1,NWIRES),EP(I)
D             WRITE(7,*)(EW(J,I),J=1,NWIRES),EP(I)
30    CONTINUE
C------
C     CONVERTS MILLIVOLTS AS OUTPUT BY CONVOL TO VOLTS
C------
      DO 31 I=1,NVELS
      EP(I)=EP(I)/1000.0
      DO 31 J=1,NWIRES
      EW(J,I)=EW(J,I)/1000.0
31    CONTINUE
D     TYPE *,'THE FOLLOWING IS EW,EP  VOLTS'
D     TYPE *,EW,EP
      CLOSE(UNIT=1)
C------
C     CALCULATE THE REFERENCE VELOCITY
C
C------
      IF(PTRAN.EQ.2.0)GOTO 50
      IF(PTRAN.EQ.1.0)GOTO 32
      IF(PTRAN.NE.1.0)TYPE *,'YOU DIDNOT ENTER PROPER P.TRAN. CONTROL'
      GOTO 18
C
32    DO 40 I=1,NVELS
              IF(ANSWER.EQ.'Y') GOTO 35
C-----
C             THE EQUATION BELOW IS GOOD ONLY IF EP(I)=1 VOLT/MM HG
C-----
              QP(I)=15.9*SQRT(((TEMP+459.7)*(EP(I)*.01*.53682))
     1  /(BARO))
      GO TO 40
35    CALL WIRCAL(QP(I),EP(I),ACOWIL,BCOWIL,NCOWIL)
40    CONTINUE
      GOTO 60
C
50    TYPE *,'ENTER SLOPE(SLOPE) AND Y-INTERCEPT(YINTER)'
      TYPE *,' OF FLUIDS LAB P.T. CALIBRATION'
      ACCEPT *,SLOPE,YINTER
      DO 55,K=1,NVELS
      EP(K) = (EP(K)-YINTER)/SLOPE
D     TYPE *,'THIS IS EP IN INCHES OF WATER'
D     TYPE *,EP
      QP(K)=15.9*SQRT(EP(K)*(TEMP+459.7)/BARO)
55    CONTINUE
```

```
D     TYPE *,'THIS IS THE VELOCITY BASED ON THE P.T.'
D     TYPE *,QP
C
C------
C     OUTPUT DATA FOR VELOCITY PROFILE PLOTFILE CALPLT.
C------
60    OPEN(UNIT=2,TYPE='NEW',NAME='CALPLT.DAT')
      DO 70 I=1,NVELS
      WRITE(2,*)(EW(J,I),J=1,NWIRES),QP(I)
70    CONTINUE
C------       CLOSE(UNIT=2,DISPOSE='SAVE')
C
C     CALCULATION OF COLLIS AND WILLIAMS COEFFICIENTS FOR
C     EACH WIRE USING STANDARD DEVIATION SUBROUTINE CALCAB TO FIND
C     THE TWO COEFFICIENTS A AND B WHILE N RANGES FROM .3 TO
C     .54 (.99) AND THEN USES SUBROUTINE SMALL TO SELECT THE THREE
C     COEFFICIENTS ASSOCIATED WITH THE SMALLEST STANDARD DEVIATION
C     THE COEFFICIENTS ARE THEN OUTPUT TO THE LIST DIRECTED FILE
C     CALCRV IN ASCENDING ORDER
C------
      OPEN(UNIT=1,NAME='CALCRV.DAT',FORM='FORMATTED',STATUS=
     +       'UNKNOWN')
      OPEN(UNIT=9,NAME='COEFF.DAT',FORM='FORMATTED',STATUS=
     +       'UNKNOWN')
      DO 300 J=1,NWIRES
             XN(J)=.29
             DO 200 ITER=1,70
                    XN(J)=XN(J)+.01
                    DO 100 K=1,NVELS
                           EWSQ(J,K)=EW(J,K)**2
                           QPXN(K)=QP(K)**XN(J)
100                 CONTINUE
                    CALL CALCAB(ITER,DEBUG)
      WRITE(9,150) J,ITER,AITER(ITER),BITER(ITER),STDEV(ITER),XN(J)
150   FORMAT(2X,'WIRE  ',I1,'  ITER ',I2,'  A=',F6.3,'  B=',F6.3,
     1   '  STD=',F8.6,'  N=',F4.2)
200          CONTINUE
             CALL ISMALL(INDEX)
             A(J)=AITER(INDEX)
             B(J)=BITER(INDEX)
             STD(J)=STDEV(INDEX)
             XN(J)=.29+(.01*INDEX)
             WRITE(1,*) A(J),B(J),STD(J),XN(J)
             WRITE(2,*) A(J),B(J),STD(J),XN(J)
300   CONTINUE
      CLOSE(UNIT=9)
      CLOSE(UNIT=1)
      CLOSE(UNIT=2,DISPOSE='SAVE')
      CALL EXIT
      END
      SUBROUTINE ISMALL(INDEX)
C------
C     SMALL DETERMINES WHICH OF THE 25 SETS OF COEFFICIENTS IS
```

```
C     ASSOCIATED WITH THE SMALLEST STANDARD DEVIATION AND THEN
C     PLACES THAT STANDARD DEVIATION IN THE AITER, BITER, STD AND
C     INDEX VARIABLES FOR TRANMISSION TO THE MAIN PROGRAM FOR
C     OUTPUT AS A, B, STD AND N
C------
      REAL STDEV,STD,SMALL
C------       COMMON /DEV/ STDEV(25),STD(16),QPXN(40),AITER(30),
C     1  BITER(30),EWSQ(16,40),NVELS,J
C------
      COMMON /DEV/ STDEV(70),STD(16),QPXN(85),AITER(75),
     1  BITER(75),EWSQ(16,85),NVELS,J
      SMALL=STDEV(1)
      INDEX=1
      DO 100 K=2,70
            IF(SMALL.LT.STDEV(K))GOTO 100
            SMALL=STDEV(K)
            INDEX=K
100   CONTINUE
      RETURN
      END
C
      SUBROUTINE CALCAB(K,DEBUG)
C------
C     CALCAB COMPUTES LEAST SQUARES FIT OF NVELS DATA POINTS
C     (QPXN,EWSQ) TO THE
C     EQUATION EWSQ=AITER+BITER*QPXN.
C     STANDARD DEVIATION OF FITTED EWSQ TO DATA IS RETURNED IN STDEV.
C
C     COMMON /DEV/ STDEV(25),STD(16),QPXN(40),AITER(30),
C     1  BITER(30),EWSQ(16,40),NVELS,J
C------
      COMMON /DEV/ STDEV(70),STD(16),QPXN(85),AITER(75),
     1  BITER(75),EWSQ(16,85),NVELS,J
C------
C     ZERO SUMMATION VARIABLES
C------
      SX=0.0
      SX2=0.0
      SY=0.0
      SXY=0.0
      SERR2=0.0
C------
C     MAKE SUMMATIONS OF QPXN,QPXN**2,EWSQ,QPXN*EWSQ
C------
      DO 10 I=1,NVELS
            XI=QPXN(I)
            YI=EWSQ(J,I)
            SX=SX+XI
            SX2=SX2+XI*XI
            SY=SY+YI
            SXY=SXY+XI*YI
10    CONTINUE
C------
```

```
C     COMPUTE AITER,BITER
C__
_     IF(DEBUG.EQ.1) GO TO 500
      BITER(K)=(SXY-SX*SY/NVELS)/(SX2-SX*SX/NVELS)
      AITER(K)=(SXY-BITER(K)*SX2)/SX
      GO TO 1000
500   BITER(K)=(SXY-SX*SY/NVELS)/(SX2-SX*SX/NVELS)
      AITER(K)=(SY/NVELS-BITER(K)*SX/NVELS)
1000  CONTINUE
C------
C     MAKE SUMMATIONS FOR ERROR TERMS
C------
      DO 20 I=1,NVELS
            ERR=EWSQ(J,I)-(AITER(K)+BITER(K)*QPXN(I))
            SERR2=SERR2+ERR*ERR
20    CONTINUE
C------
C     COMPUTE STANDARD DEVIATION
C------
      STDEV(K)=SQRT(SERR2/NVELS)
      RETURN
      END
C
      SUBROUTINE WIRCAL(QP,EP,I,ACOWIL,BCOWIL,NCOWIL)
C------
C     THIS SUBROUTINE IS USED IF A HOT WIRE IS TO BE USED
C     AS A REFERENCE FOR THE CALCULATION OF THE COEFFICIENTS
C------
      DIMENSION QP(I),EP(I)
      REAL NCOWIL
            QP(I)=(((EP(I)*EP(I))-ACOWIL)/BCOWIL)**(1.0/NCOWIL)
      RETURN
      END



C-------------------------------------------------------------
      PROGRAM CPCN
C-------------------------------------------------------------
C     THIS PROGRAM HAS BEEN MODIFIED BY NASSER RASHIDNIA TO RUN
C     ON  RSX SYSTEM, AND FIT THE NEEDS OF NEW X-WIRES 6-MAR-85
C
C     THIS PROGRAM MODIFIED BY DAVE SIGNOR. ORIGINAL USAGE
C     WAS AS A SUBROUTINE IN PROGRAM CONVEL WRITTEN BY
C     BRIAN LEARY
C         ADDITIONAL DESCRIPTIVE INFORMATION ADDED MON. 14 DEC 81
C
C     PROGRAM CPCN CALCULATES CORRECTION COEFFICIENTS FOR
C     SMALL ANGLE DEVIATIONS OF THE "X" WIRES FROM 45 DEGREES.
C     THE ANGLE DEVIATIONS SHOULD BE ABOUT 5 DEGREES (LESS THAN 10)
C
C     THE RESULT SHOULD BE: CP IS POSITIVE AND CLOSE TO  1.0
C                           CN IS NEGATIVE AND CLOSE TO -1.0
```

```
C       IF THESE RESULTS ARE NOT OBTAINED, CHECK TO SEE THAT
C            THE INPUT REFERENCE ANGLE IS OF CORRECT SIGN.
C
C     QREF    REFERENCE FREE STREAM VELOCITY USED TO DETERMINE "X"-WIRE
C     ANGLE MISSALIGNMENT CORRECTION (FROM THE PRESSURE TRANSDUCER).
C     REFANG  ANGLE "X"-WIRE IS ROTATED TO PERFORM MISSALIGNMENT
C             AN ANGLE OF GREATER THAN 90 ON THE OUTER SCALE OF THE
C             CALIBRATION STAND IS A NEGATIVE SMALL ANGLE.
C             SIMILARLY ANGLES LESS THAN 90 ARE POSITIVE SMALL
C             ANGLES.
C             IE. 80 ON THE OUTER SCALE MEANS: REFANG = +10. DEGREES
C                100 ON THE OUTER SCALE MEANS: REFANG = -10. DEGREES
C     EP1REF  VOLTAGE AT REF VEL CONDITION FROM WIRE 1 OF "X" ARRAY.
C     EN2REF  VOLTAGE AT REF VEL CONDITION FROM WIRE 2 OF "X" ARRAY.
C     AX--    FIRST COEFFICIENT OF THE COLLIS AND WILLIAMS EQUATION
C             FOR THE CASE OF V=0, QREF=U, AND GAMMA=0 (GAMMA IS THE
C             DIRECTED ANGLE MEASURED FROM +X DIRECTION TO Q VECTOR
C     BX--    SECOND COEFFICIENT OF COLLIS WILLIAMS EQ. SAME CONDITIONS
C     ANX--   EXPONENT IN THE COLLIS _WILLIAMS EQ.
C
C*    DELTBP  THE DEVIATION FROM 45(OR 35) DEGREES OF THE FORWARD FACING
C             (POSITIVE) X-WIRE.
C*
      OPEN(UNIT=2,TYPE='NEW',NAME='CPCNXWIRE.DAT')
C*
      TYPE 21
21    FORMAT(1X,'ENTER ANGLE OF THE SLANTED-X-WIRE IN DEGREES, BETA')
      ACCEPT *,BETA
      TYPE 5
5     FORMAT(1X,'ENTER REFERENCE ANGLE IN DEGREES(80=+10), REFAN')
      ACCEPT *,REFAN
      REFANG = REFAN * 3.1416/180.0
      TYPE 10
10    FORMAT(1X,'ENTER FREE STREAM VELOCITY (FT/S), QREF')
      ACCEPT *,QREF
      TYPE 11
11    FORMAT(1X,'ENTER VOLTS OF THE FORWARD SLANTING X, EP1REF'/)
      TYPE *, '  WIRE / <-----FLOW    UP'
      TYPE *, ' '
      ACCEPT *,EP1REF
      TYPE 12
12    FORMAT(1X,'ENTER VOLTS OF THE BACKWARD SLANTING X, EN2REF'/)
      TYPE *, '  WIRE *<-----FLOW    UP'
      TYPE *, ' '
      ACCEPT *,EN2REF
      TYPE *,'ENTER THE COLLIS AND WILLIAMS COEFFICIENTS IN THE '
        TYPE *,'  ORDER SHOWN (XP1=FOR-X,XN2=BAK-X):'
      TYPE *,'AXP1,BXP1,ANXP1,AXN2,BXN2,ANXN2'
      ACCEPT *,AXP1,BXP1,ANXP1,AXN2,BXN2,ANXN2
C
C     ECHO INPUT INFORMATION
C
      WRITE(2,13) REFANG,REFAN,QREF,EP1REF,EN2REP,BETA
```

```
13    FORMAT(2X,'REFANG=',F6.3,'  RADIANS',4X,F7.3,' DEGREES',
     1  /' ',1X,'QREF=',F7.3,'  FT/SEC',/' ',1X,'EP1REF=',F7.3,
     2  '  VOLTS',/' ',1X,'EN2REF=',F7.3,'  VOLTS',
     3  /' ',1X,'BETA=',F7.3,' DEGREES')
      WRITE(2,20)AXP1,BXP1,ANXP1,AXN2,BXN2,ANXN2
20    FORMAT(1X,'  AXP1=',F7.3,3X,'BXP1=',F7.3,3X,'ANXP1=',F5.2,/,
     1  '   AXN2=',F7.3,3X,'BXN2=',F7.3,3X,'ANXN2=',F5.2)
C
C     CALCULATION OF CORRECTION COEFFICIENTS CP AND CN
C*
C*  NEW X-WIRE WITH ANGLES OF BETA DEG.
C*
      BETA2= BETA*3.1416/180.0
      X = COS(BETA2)
      Y = SIN(BETA2)
C*
      UXREF=QREF*COS(REFANG)
      VXREF=QREF*SIN(REFANG)
      EPREFS=EP1REF*EP1REF
      ENREFS=EN2REF*EN2REF
      ANXP1 = 1./ANXP1
      ANXN2 = 1./ANXN2
      CP=(((EPREFS-AXP1)/BXP1)**(ANXP1)-UXREF)/VXREF
      CN=(((ENREFS-AXN2)/BXN2)**(ANXN2)-UXREF)/VXREF
C-------ANGLE DEVIATION CORRECTION CALCULATION
      DELTBP = ((X*CP-Y)/(X+Y*CP))*57.29577951
      DELTBN = ((Y+X*CN)/(X-Y*CN))*57.29577951
      WRITE(2,40) CP CN,DELTBP,DELTBN
40    FORMAT(1X,'  CP =',F15.3,1X,'CN =',F15.3,/' ',
     1  2X,'DELTBP=  ',F10.3,3X,'DELTBN=  ',F10.3)
C*
      CLOSE(UNIT=2)
      TYPE 99, CP,CN,DELTBP,DELTBN
99    FORMAT(1X,'  CP =',F15.10,1X,'CN =',F15.10,/' ',
     1  2X,'DELTBP=  ',F10.3,3X,'DELTBN=  ',F10.3)
      TYPE *,' I AM DONE. From  CPCN.FTN (N. Ra.), OUTPUT is: CPCNXWIRE.DAT'
C*
      CALL EXIT
      END



C-------------------------------------------------------------------
      PROGRAM CORRELATE3
C-------------------------------------------------------------------
C     PROGRAM NAME              :CORRELATE3 (ON VMS SYSTEM)
C     DATE OF LAST MODIFICATION:1-APR-85
C-------------------------------------------------------------------
C     VARIABLE DECLARATION
      LOGICAL*1 PROCES
      CHARACTER*30  INFILE,DOCFIL,DATARR*9,STRING*8
      CHARACTER*1   INFRM*1,OUTFRM*1
```

```
      REAL     DATA(20),COL1,COL2,SUMC1S,SUMC2S,CORREL
      REAL *8 XBAR,XSTDEV,XCNT,SUMX,SUMXSQ,XDAT
      VIRTUAL COL1(10000),COL2(10000)
      INTEGER NCOLMN,NCOLM1,NCOLM2,UPPER,LOWER,STEP,OFFSET,NPOINT
C-----------------------------------------------------------------
C     COMMON BLOCK
C-----------------------------------------------------------------
C     VARIABLE INITIALIZATIONS
C-----------------------------------------------------------------
C ASK USER FOR EXECUTION INFORMATION
C-----------------------------------------------------------------
      LUN=3
      CALL GETCMD(PROCES,CMDFIL,LUN)
C  GET FILE INFORMATION FROM USER
      IF(PROCES)THEN
         READ(LUN,*) NCOLMN
         READ(LUN,800) INFRM
         READ(LUN,*) LOWER,UPPER,STEP
      ELSE
         TYPE 22
22       FORMAT(' ','Is the INPUT file formatted (Y:N):',)
               ACCEPT  800,INFRM
         TYPE 20
20       FORMAT(' ','Please enter the number of input ',
     +                'columns in the files: ',)
         ACCEPT *, NCOLMN
        TYPE 26
26      FORMAT(' ','Enter LOWER,UPPER and STEP values for N delta T')
        ACCEPT *,LOWER,UPPER,STEP
      ENDIF
C begin main program
125   IF(PROCES)THEN
         READ(LUN,800,END=250)INFILE
         READ(LUN,800) DOCFIL
         READ(LUN,*)  NCOLM1,NCOLM2
      ELSE
         IF(NPOINT .NE. 0.0) THEN
            TYPE *,'Process another file (Y:N)'
            ACCEPT 800, ANS
            IF (ANS. NE. 'Y')GOTO 250
         ENDIF
         TYPE 48
48       FORMAT(' ','Please enter the INPUT file name : ',)
         ACCEPT 800,INFILE
         TYPE 24
24       FORMAT(' ','Please enter the doc file name :  ',)
         ACCEPT 800,DOCFIL
        TYPE 46
46      FORMAT(' ','Enter Column 1 and Column 2 to be corelated')
        ACCEPT *, NCOLM1,NCOLM2
      ENDIF
c open input file
      IF (INFRM .EQ. 'Y') THEN
```

```
         OPEN(UNIT=2,NAME=INFILE,TYPE='OLD',
     +            FORM='FORMATTED',READONLY,ERR=900)
      ELSE
           OPEN(UNIT=2,NAME=INFILE,TYPE='OLD',
     +            FORM='UNFORMATTED',READONLY,ERR=900)
      ENDIF
      OPEN(UNIT=4,NAME=DOCFIL,TYPE='NEW',FORM='FORMATTED',
     +  ERR=910)
C record user inputs in doc file
      CALL DATE(DATARR)
      CALL TIME(STRNG)
      WRITE(4,500)     DOCFIL,DATARR,STRNG
      IF(PROCES)WRITE(4,512) CMDFIL
      WRITE(4,514)     INFILE,INFRM,NCOLMN,NCOLM1,NCOLM2
      WRITE(4,516)     UPPER,LOWER,STEP
      WRITE(4,520)
C-----------------------------------------------------------------
C begin processing
C-----------------------------------------------------------------
C set constants
      NPOINT = 1
C input user data
100   IF(INFRM .EQ. 'Y')THEN
         READ(2,*,END=145)(DATA(I),I=1,NCOLMN)
      ELSE
         READ(2,  END=145)(DATA(I),I=1,NCOLMN)
      ENDIF
      COL1(NPOINT) = DATA(NCOLM1)
      COL2(NPOINT) = DATA(NCOLM2)
      NPOINT  = NPOINT + 1
      IF(MOD(NPOINT,100).EQ. 0) TYPE *,'Read up to record :',NPOINT
      GOTO 100
C continue with processing
145   CLOSE (UNIT=2)
      TYPE *,NPOINT, ' Points read from input file'
      DO 200 OFFSET = LOWER,UPPER,STEP
      TYPE *,'Beginning correlation with offset =',OFFSET
      SUMX   = 0.0
      SUMXSQ = 0.0
      XCNT   = 0.0
         DO 150 I = 1,NPOINT
            IF((OFFSET+I .GE. 1).AND.(OFFSET+I .LT. NPOINT))THEN
               XDAT   = COL1(I) * COL2(I+OFFSET)
               SUMX   = SUMX + XDAT
               SUMXSQ = SUMXSQ + XDAT**2
CN             SUMC1S = SUMC1S + COL1(I)**2
CN             SUMC2S = SUMC2S + COL2(I)**2
               XCNT   = XCNT + 1.0
            ENDIF
150   CONTINUE
CN-----------------------------------------------------------------
               SUMC1S = 0.0
               SUMC2S = 0.0
```

```
      DO 151 J=1,NPOINT
                  SUMC1S = SUMC1S + COL1(J)**2
                  SUMC2S = SUMC2S + COL2(J)**2
151   CONTINUE
CN-------------------------------------------------------------------
C calculate average and standard deviation of X
      XBAR   = SUMX/XCNT
      XSTDEV = SQRT((SUMXSQ-(SUMX**2/XCNT))/(XCNT-1))
      CORREL = XBAR/(SQRT(SUMC1S/XCNT)*SQRT(SUMC2S/XCNT))
      WRITE(4,540) FLOAT(OFFSET),CORREL,XSTDEV,XCNT,XBAR
200   CONTINUE
CN    CLOSE (UNIT=2)
      CLOSE (UNIT=4)
      GOTO 125
250   TYPE*, 'PROGRAM CORELATE FINISHED'
      CALL EXIT
C-------------------------------------------------------------------
C FORMAT STATEMENTS
C-------------------------------------------------------------------
500   FORMAT(';'/' ','PROGRAM CORELATE DOCUMENTATION FILE  :',A/
     +          ' ',T5,'DATE :',A/
     +               ' ',T5,'TIME :'A)
512   FORMAT(' ',T5,'Control file name :',A)
514   FORMAT(' ',T5,'INPUT DATA FILE NAME : ',A/
     +               ' ',T5,'Input data file form :',L/
     +          ' ',T5,'Number of Columns    :',I3/
     +               ' ',T5,'First selected col.  :',I3/
     +               ' ',T5,'Second selected col. :',I3)
516      FORMAT(' ',T5,'Upper value of t      : ',I6/
     +               ' ',T5,'Lower value of t      : ',I6/
     +               ' ',T5,'Step  value of t      : ',I6/)
520   FORMAT('0','OFFSET      CORRELATION   XSTDEV          XCNT',
     +         '     XBAR       '/';')
540   FORMAT('RD',F8.1,',',F9.6,',',F9.6,',',F9.1,',',F9.6)
800   FORMAT(A)
900   TYPE 905,INFILE
905   FORMAT(' ','ERR-during opening file  ',A,' skipping file')
      GOTO 125
910   TYPE 903,DOCFIL
903   FORMAT(' ','ERR-during opening file,'A', exiting prog')
      CALL EXIT
950   TYPE *,'ERR-during writing of output file, exiting program'
      CALL EXIT
165   TYPE *, 'ERROR in proc. file skipping to next'
CN    CLOSE (UNIT=2)
CN    CLOSE (UNIT=4)
      GOTO 125
      END
C
      SUBROUTINE GETCMD(CMDFIL,INFIL,LUN)
C LOCAL VARIABLES
      CHARACTER*1 CMDLIN*40,INFIL*30
      LOGICAL*1 CMDFIL
```

```
      INTEGER IDS,LENGTH
      DATA CMDLIN/' '/
      CALL GETMCR(CMDLIN,IDS)
C SCAN COMMAND LINE FOR COMMAND FILE NAME
      LENGTH=INDEX(CMDLIN,'.')
C
      IF(LENGTH.NE.0)THEN
         OPEN(UNIT=LUN,NAME=CMDLIN(1:LENGTH+3),STATUS='UNKNOWN',ERR=15)
         CMDFIL=.TRUE.
         INFIL=CMDLIN(1:LENGTH+3)
      ELSE
        CMDFIL=.FALSE.
15      TYPE *,'COMMAND FILE NOT FOUND REVERTING TO MANUAL CONTROL'
      ENDIF
      RETURN
      END




C-----------------------------------------------------------------
      PROGRAM NORMALIZE
C-----------------------------------------------------------------
C       17-oct-85
C-----------------------------------------------------------------
      CHARACTER*30 FILNAM,OUTFIL,FORM*3,YN*1
      REAL RDATA(16),CONST(16)
      INTEGER IDATA(16),NCOLMN
      LOGICAL CMDFIL
      CALL GETCMD(LUN,CMDFIL)
15    ICOUNT=1
      IF(CMDFIL) THEN
              READ(LUN,5,END=97) FILNAM
              READ(LUN,5) OUTFIL
              READ(LUN,*) NCOLMN
              READ(LUN,5) FORM
              DO 119 IC=1,NCOLMN
              READ(LUN,5) YN
              IF(YN.EQ.'Y') THEN
              READ(LUN,*) CONST(IC)
              CONST(IC)=1./CONST(IC)
              ELSE
              CONST(IC)=1.
              ENDIF
119           CONTINUE
      ELSE
              TYPE*,'ENTER INPUT FILE NAME'
              ACCEPT 5,FILNAM
              TYPE*,'ENTER OUTPUT FILE NAME'
              ACCEPT 5,OUTFIL
              TYPE*,'ENTER NUMBER OF DATA COLUMNS IN FILE'
              ACCEPT*,NCOLMN
```

```
              TYPE*, 'ENTER FORMAT OF INPUT FILE  (FM/UFM)'
              ACCEPT 5,FORM
              DO 998 IC=1,NCOLMN
              TYPE*,'column:',IC,'  to be normalized ?  (Y/N)'
              ACCEPT 5,YN
              IF(YN.EQ.'Y') THEN
              TYPE*,'ENTER THE NORMALIZATION FACTOR'
              ACCEPT*,CONST(IC)
              CONST(IC)=1./CONST(IC)
              ELSE
              CONST(IC)=1.
              ENDIF
998           CONTINUE
      ENDIF
      IF(FORM.EQ.'FM') THEN
      OPEN(UNIT=1,NAME=FILNAM,FORM='FORMATTED',STATUS='OLD')
      OPEN(UNIT=2,NAME=OUTFIL,FORM='FORMATTED',STATUS='NEW')
      ELSE
      OPEN(UNIT=1,NAME=FILNAM,FORM='UNFORMATTED',STATUS='OLD')
      OPEN(UNIT=2,NAME=OUTFIL,FORM='UNFORMATTED',STATUS='NEW')
      ENDIF
      TYPE*, 'Begin normalization...'
10    IF(FORM.EQ.'FM') THEN
      READ(1,*,END=100)(RDATA(I),I=1,NCOLMN)
      ELSE
      READ(1,END=100)(RDATA(I),I=1,NCOLMN)
      ENDIF
      DO 13 I=1,NCOLMN
              RDATA(I)=RDATA(I)*CONST(I)
13    CONTINUE
      IF(FORM.EQ.'FM') THEN
      WRITE(2,*)(RDATA(I),I=1,NCOLMN)
      ELSE
      WRITE(2) (RDATA(I),I=1,NCOLMN)
      ENDIF
      ICOUNT=ICOUNT+1
      IF(MOD(ICOUNT,100).EQ.0)  TYPE*,'Rec = ',ICOUNT
      GOTO 10
100   CLOSE(UNIT=1)
      CLOSE(UNIT=2)
      TYPE*, 'Program ending. The output file is... ',OUTFIL
      IF(CMDFIL) GOTO 15
      GOTO 99
97    CLOSE (UNIT=LUN)
99    CALL EXIT
5     FORMAT(A)
      END
C-----------------------------------------------------------------
      SUBROUTINE GETCMD(LUN,CMDFIL)
C-----------------------------------------------------------------
      LOGICAL CMDFIL
      CHARACTER*40 CMDLIN
      DATA CMDLIN/' '/
```

```
      LUN = 3
      CMDFIL=.FALSE.
      CALL GETMCR(CMDLIN)
      LEN=INDEX(CMDLIN,'.')
      IF(LEN.NE.0)CMDFIL=.TRUE.
      IF(CMDFIL)THEN
      OPEN(UNIT=LUN,NAME=CMDLIN(1:LEN+3),STATUS='OLD',ERR=15)
      TYPE*,'Now is command file control mode...'
      ELSE
15    TYPE *,'Now is manual control mode...'
      CMDFIL=.FALSE.
      ENDIF
      RETURN
      END
```

APPENDIX B

Formulation of Direct Net Skin Drag Calculation

In order to calculate the net skin drag ratio of manipulated to regular turbulent boundary layers, the following formulation was used: When the manipluator was present in the boundary layer, the device drag D (neglecting pressure drag) was obtained. Assuming a two-dimentional incompressible flow, a control volume is drawn as shown in the following figure.

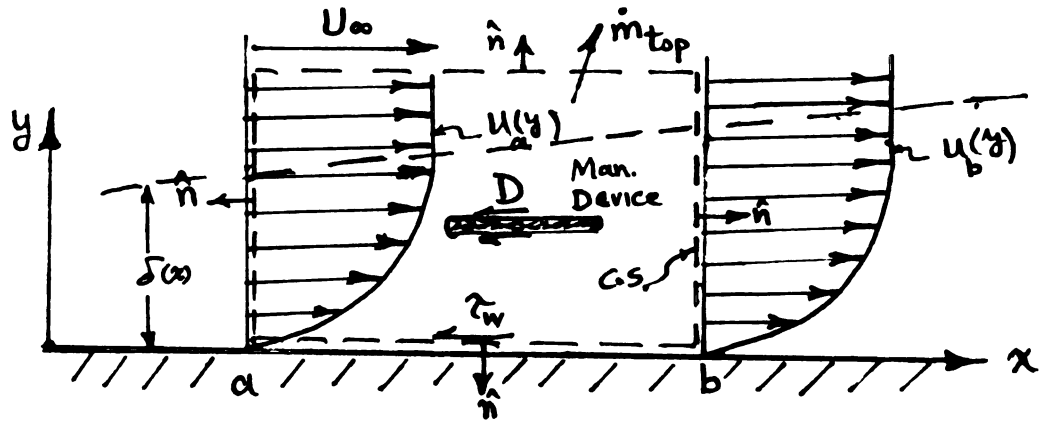

Using the control volume (surface) concept, one may write:

$$-\int_a^b \tau_w dx - D = \int_{front} \rho V_x \vec{V}.\hat{n} dA + \int_{rear} \rho V_x \vec{V}.\hat{n} dA + \int_{top} \rho V_x \vec{V}.\hat{n} dA + \int_{bottom} \rho V_x \vec{V}.\hat{n} dA$$

where τ_w = Wall shear stress
ρ = air density
V_x = streamwise component of the velocity vector $\vec{V}$
$\vec{V}$ = velocity vector
$\hat{n}$ = normal unit vector.

Substituting for the velocity, rearranging and assuming a unit width for the flow, one may simplify the above equation to:

$$(1) \qquad -\int_a^b \tau_w dx - D = -\int_0^\infty \rho u_a^2 dy + \int_0^\infty \rho u_b^2 dy + U_\infty \dot{m}_{top}$$

where $\dot{m}$ is mass flux from the top surface of the control volume and $1dy = dA$

Continuity equation is written as

$$\int_{C.S.} \rho \vec{V}.\hat{n} dA = 0$$

or

$$(2) \qquad \int_0^{\delta} \rho u_a dy - \int_0^{\delta} \rho u_b dy = \dot{m}_{top}$$

Substitute (2) into (1) and rearrange:

$$D = -\int_0^{\delta} \rho u_a (U_\infty - u_a) dy + \int_0^{\delta} \rho u_b (U_\infty - u_b) dy - \int_a^b \tau_w dx \quad (3)$$

Define $\theta = \int_0^{\delta} (u/U_\infty)[1 - u/U_\infty]dy$ and substitute into (2) to obtain the device drag:

$$(3) \qquad D = \rho U_\infty^2 (\theta_b - \theta_a) - \int_a^b \tau_w dx$$

The net drag ratio (NDR) at any station along the test wall can be calculated by substition of the wall shear stress (τ_w obtained from slope of mean velocity profile near wall) into the following equation:

$$(4) \qquad NDR = [D + (\int_{x_b}^{x} \tau_w dx)_{man.}]/(\int_{x_a}^{x} \tau_w dx)_{reg.}$$

BIBLIOGRAPHY

BIBLIOGRAPHY

Anders, J. B., Hefner, J. N. and Bushnell, D. M. 1984, "Performance of Large Eddy Breakup Devices at Post-Transitional Reynolds Numbers", Presented at the AIAA 22nd Aerospace Sciences Meeting, Reno, Nevda, AIAA-84-0345

Anders, J. B., and Watson, R. D., 1985, "Airfoil Large-Eddy Breakup Devices for Turbulent Drag Reduction", Presented at the AIAA Shear Flow Conference March 12-14, 1985/Boulder, Colorado, AIAA-84-0345

Bhatia, J.C., Durst, F., and Jovanovic, J., 1982, "Corrections of Hot-wire Anemometer Measurements Near Walls." J. Fluid Mechanics, Vol. 122, pp. 411-431.

Pertelrud, A., Troung, T. V., and Avellan, F., 1982, "Drag Reduction in Turbulent Boundary Layers Using Ribbons", AIAA Paper No. 82-1370.

Bradshaw, P. 1965, "The Effect of Wind Tunnel Screens on Nominally Two-Dimensional Boundary Layers", J. Fluid Mech. Vol. 27, p. 679.

Clauser, F.H., 1954, " Turbulent Boundary Layers in Adverse Pressure Gradients", J. Aeronautical Science, 21, 92, 108.

Coles, D. 1956, "The Law of the Wake in the Turbulent Boundary Layer", J. Fluid Mech. Vol. 1, pp. 191-226.

Coles, D. 1968, "Young Person's Guide to Data", Proceedings of Computation of Turbulent Boundary Layers, Stanford University, California.

Collis, D.C. and Williams, M.J., 1959, "Two-dimensional Convection from Heated Wires at Low Reynolds Numbers." J. Fluid Mechanics, Vol. 16, pp. 357-358.

Corke, T. C., Guezennec, Y., Nagib, H. M. 1980, "Modification in Drag of Turbulent Boundary Layers Resulting from Manipulation of Large-Scale Structures, Viscous Drag Reduction", G. R. Hough, Ed., Vol. 72. Progress in Astronautics and Aeronautics, pp. 128-143.

Corke, T. C., 1981, "A New View on Origin, Role and Manipulation of Large Scales in Turbulent Boundary Layers", Ph.D. Thesis, Illinois Institute of Technology, Chicago, Illinois, Dec. 1981.

Corke, T. C., Koga, D., Drubka, R. and Nagib, H. 1977, "A New Technique for Introducing Controlled Sheets of Smoke Streaklines in Wind Tunnels", IEEE Publication 77-CH 1251-8 AES.

de Bray, B. G., 1967, "Some Investigation Into the Spanwise Non-Uniformity of Nominally Two-Dimensional Incompressible Boundary Layers Downstream of Gauze Screens", Brithish Aeronautical Research Council, Report No. 29-271.

Falco, R. E. 1974, "Some Comments on Turbulent Boundary Layer Structure Inferred from the Movements of a Passive Contaminant", AIAA Paper No. 74-99.

Falco, R. E. 1977, "Coherent Motions in the Outer Region of Turbulent Boundary Layers", Phys. Fluids. Vol. 20, No. 10, Part II., pp. S124-S132.

Falco, R. E. 1980, "Combined Simultaneous Flow Visualization/Hot-wire Anemometry for the Study of Turbulent flows", J. of Fluid Engr. Vol. 102, pp. 174-183.

Falco, R. E. 1982, "A Synthesis and Model of Wall Region Turbulence Structure", in The Structure of Turbulence, Heat and Mass Transfer, ed. by Z. Zoric, pp. 124-135, Hemisphere Press.

Falco, R. E. 1983, "New Results, a Review and Synthesis of the Mechanism of Turbulence Production in Boundary Layer and its Modification", AIAA Paper No. 83-0377.

Favre, A. J. , 1965; "Review of Space-Time Correlations in Turbulent Fluids", J. Applied Mech., June 1965, p. 241.

Freymuth, P., Bank, W. and Palmer, M. 1983, "Use of titanium tetrachloride for visualization of accelerating flow around airfoils", presented at Third International Symposium on Flow Visualization, Ann Arbor, USA, September 6-9, 1983.

Guezennec, Y. G. and Nagib, H. M. 1985, "Documentation of Mechanisms Leading to Net Drag Reduction in Manipulated Turbulent Boundary Layers", AIAA Paper No. 85-0519.

Hefner, J. N., Weinstein, L. M. and Bushnell, C. M. 1980, "Large-Eddy Breakup Scheme for Turbulent Viscous Drag Reduction, Viscous Flow Drag Reduction", Progress in Astronautics and Aeronautics. Vol. 72, pp. 110-127, 1980.

Hefner, J. N., Anders, J. B. and Bushnell, C. M. 1983, "Alteration of Outer Flow Structures for Turbulent Drag Reduction", AIAA 21th Aerospace Science Meeting, Jan. 1983, AIAA Paper No. 83-0293.

Lemay, J., Provencal, D., Gourdeau, R., Nguyen, V. D., Dickinson, J., 1985, "More Detailed Measurements Behind Turbulence Manipulators Including Tandem Devices Using Servo-Controlled Balances", Presented at the AIAA Shear Flow Control Conference, March 12-14, 1985, Boulder, Colorado. Paper AIAA-85-0521

Liang, S. 1984, "Vortex Ring Moving Wall Interactions", M.S. Thesis, Department of Mechanical Engineering, Michigan State University.

Loehrke, R. I. and Nagib, H. M., 1977, "Experiments on Management of Free Stream Turbulence", AGARD Report, R-598, AD-749-891.

Lovett, J. A. 1982, "The Flow Fields Responsible for the Generation of Turbulence near the wall in Turbulent Shear Flows", M.S. Thesis, Department of Mechanical Engineering, Michigan State University.

Lynn, T. B. and Screenivasan K. R., 1985, "Correlation and Length Scale Measurements in Manipulated Boundary Layers", Report 85 FM 2, Department of Mechanical Engineering, April 1985.

Murlis, John, 1975, "The Structure of a Turbulent Boundary Layer at Low Reynolds Number", Ph. D. Thesis, Dept. of Aero., Imperial College of Science and Tech.

Mumford, J. C., and Savill, A. M., 1984, "Parametric Studies of Flat Plate Turbulence Manipulators Including Direct Drag Results and Laser Flow Visualization", Presented at the ASME symposium on turbulent and laminar boundary layers, their control and flow over compliant and other surfaces. ETCE New Orleans, Feb. 11-17, 1984.

Nagib, H. M., Guezennec, Y. and Corke, T. C. 1978, "Applications of a Smoke-Wire Visualization Technique to Turbulent Boundary Layers", Workshop on Coherent Structure of Turbulent Boundary Layers. Lehigh University, Pennsylvania.

Nagib, H. M., Guezennec, Y. and Plesniak, M., 1984, "Management of Turbulent Flow Structures in Boundary Layers Aimed at Drag Reduction", Progress report to NASA Grant Nsg-1591, Chicago, Illinois.

Patel, V.C., 1965, "Calibration of the Preston Tube and Limitations on its Use in Pressure Gradients" J. Fluid Mechanics, Vol. 23, part 1, pp. 185-208.

Patel, V.C., and Head, M.R., 1968, "Some Observations on Skin Friction and Velocity Profiles in Fully Developed Pipe and Channel Flows", J. Fluid Mechanics, Vol. 38, part 1, pp. 181-201.

Plesniak, M. W. , 1984, "Optimized Manipulation of Turbulent Boundary Layers Aimed at Net Drag Reduction", M.S. Thesis, Illinois Institute of Technology, Chicago, Illinois, Dec. 1984.

Preston, J. H., 1958, "The Minimum Reynolds Number for a Turbulent Boundary Layer and The Selection of a Transition Device." J. Fluid Mechanics, Vol. 3?, pp. 373-384.

Rao, K., Narasimha, R. and Narayanan, M. A. 1971, "The Bursting Phenomenon in a Turbulent Boundary Layer", J. Fluid Mech. Vol. 48, Part 2, pp. 339-352.

Rashidnia, N., Falco, R. E., 1983, "Effects of Outer Layer Flow Manipulators on Turbulent Boundary Layer Structures", Bull. Am. Phy. Soc., Series II, Vol. 28, pp. 1387.

Rotta, J. C. 1962, "Turbulence Boundary Layers in Incompressible Flow", Vol. 2. Pergamon, Oxford.

Schlichting, H. 1979, Boundary-Layer Theory. McGraw-Hill Book Company, New York.

Shaw, R., 1960, "The Influence of Hole Dimensions on Static Pressure Measurements", J. Fluid Mechanics, Vol. 7, part 2, pp. 550-564.

Signor, D.B., 1982, "A Study of Intermediate Scale Coherent Motions in the Outer Region of Turbulent Boundary Layers", M.S. Thesis, Department of Mechanical Engineering, Michigan State University.

Smith, A.M.O., 1955, "On the Growth of Taylor-Görtler Vorticies Along Highly Concave Walls." Quarterly Applications of Math, Vol. XIII, No. 3, pp.233-262.

Tennekes, H. and Lumley, J. L. 1972, A First Course in Turbulence. The MIT Press, Cambridge, Massachusetts.

Walsh, M. J., 1980, "Drag Characteristics of V-Groove and Tranverse Curvature Riblets", G. R. Hough, Ed., Vol. 72. Progress in Astronautics and Aeronautics, pp. 168-184.

Walsh, M. J., "Turbulent Boundary Layer Drag Reduction Using Riblets", Presented at the AIAA 12th Aerospace Sciences Meeting, Orlando, Florida, Jan. 11-14, 1982.

Westphal, R. V, 1985, "Skin Friction and Reynolds Stress Measurements for a Turbulent Boundary Layer Following Manipulation Using Flat Plates", pesonal comunication, and to be presented at the AIAA 24th Aerospace Sciences Meeting, Reno, Nevada, January 6-8, 1986.

Yajnik, K. S. and Anchorya, M. 1977, "Non-equilibrium Effects in A Turbulent Boundary Layer Due to the Destruction of Large Eddies", National Aeronautical Lab, Bangalore, NAL-BL-7.

Yoda, Hiroaki, 1981, "Effects of Dilute Polymer Additives on the Turbulence Structure Near a Wall", M.S. Thesis, Department of Mechanical Engineering, Michigan State University.